LINKED PROGRAMS OF EPITHELIAL MORPHOGENESIS AND CELL FATE IN THE PANCREATIC ENDOCRINE PROGENITOR NICHE

By

Eric Daniel Bankaitis

Dissertation

Submitted to the Faculty of the

Graduate school of Vanderbilt University

in partial fulfillment of the requirements

for the degree of

DOCTOR OF PHILOSOPHY

in

Cell and Developmental Biology

August, 2016

Nashville, Tennessee

Christopher Wright, D. Phil.

Guoqiang Gu, Ph.D.

Alvin Powers, M.D.

Roland Stein, Ph.D.

To my parents Vytas and Lee Anne Bankaitis

To my wonderful wife Kate

and

To my sons Tyler and Jackson

ACKNOWLEDGEMENTS

My graduate studies were made possible through funds from NIH BCBC UO1 (1UO1DK089570-01), by multiple imaging scholarships provided by the VUMC DDRC, DRTC and VICC [supported by NIH grants CA68484, DK20593, DK58404, DK59637], by the Vanderbilt Cell Imaging Shared Resource, and by the Vanderbilt Transgenic Mouse ES Cell Shared Resource.

First and foremost, I want to thank my mentor Chris Wright for his outstanding mentorship. There is a long list of things that I would thank Chris for, and the following are just a few. Thanks for your infectious passion for research, and for giving me the freedom and support to pursue my scientific curiosities both as a technician and as a graduate student in your lab. Thanks for the program in developmental biology, which has been arguably one of the most valuable parts of my graduate education. Thanks for teaching me to speak and write in 'proper' English; I am not quite 'there' yet, but your incessant honing of these skills will be vital for my future success in science. Thank you for never compromising on the highest standards of research quality and conduct. Thanks for the multiple trips to D.C., Denmark, and to the Holy Land in Jerusalem. Finally, I would point out that I have spent roughly 2,500 days as a graduate in Chris' lab. That's a lot of days. And while I can point to any number of these days where I was tired or frustrated or annoyed by the difficulties of doing science, in all retrospect I am not able to point to a *single one* of these days where I was bored, where felt as if I was not growing as a trainee and an individual, or where I was not being challenged to the limit of my character. Not only does this reflect the effectiveness of Chris' style of mentorship and leadership, but it is also something that in all my days I will never be able to put a price on. Thank you for giving me the skills I need to pursue a career in science, a deeper understanding of my strengths and weaknesses, and the confidence to move forward in my pursuit a career in academic science.

There are three additional individuals in my professional life that have been central to my intellectual development, and were vital for the progression of my research studies. I would first like to thank Mike Ray, who as a lab manager and colleague has made it possible to be productive moment that I spent working in the lab. Mike is one of the most professional

individuals I have ever met. There was never any problem in the lab that he would not immediately devote his time and efforts toward addressing, and there was never any material that I asked him to get for the purposes of my research that he would not immediately acquire. If I am lucky enough in the future to find myself interviewing lab managers for my own lab, the first question for all applicants will be “let me tell you a little bit about a guy named Mike Ray.” Second, I would like to thank Matt Bechard for being a fantastic research teammate. Matt and I worked very closely as our related projects developed. Matt and I could always freely engage in discussions (and even butt heads sometimes) over the practical and scientific elements of our research, without getting our feelings hurt. That matters, a lot! I am very proud of what we have both accomplished together, and value the fact that we are publishing multiple papers together. Having Matt around in these and other respects made my time in graduate school more stimulating and enjoyable, and also helped me to achieve a higher level of success. Third, I would like to thank my co-mentor and committee chair Dr. Guoquiang Gu. It is both a blessing and a curse sometimes to have a co-mentor close by who has done such fantastic work on the developing pancreas, who I am convinced knows everything there is to know about endocrine cell differentiation, and who it seems thinks more deeply and broadly about questions in developmental biology than most. Gu always pushed me hard to similarly think deeply about every facet of my research and research aims, was always prepared to take the time to read and comment on my manuscript drafts, and who taught me a great deal about how to better connect my data and interpretations with research that has been done previously. In many respects, I was lucky to find myself studying pancreas development at the time and place where I did. My studies would not have been possible without the history of fantastic work that investigators such as Gu have accomplished previously. I also want to thank members of the Gu and Wright labs (especially Fong Cheng Pan and Sebastian Reick), and Anna Means for their helpful discussions.

I would also like to thank the number of individuals who have sat on my committee, as the advice and critiques I have received from these individuals has been of incalculable value. Alongside each name is a small phrase that each has spoken at one time or another, and that have left long lasting impressions that have guided my development as a scientist. These

include Trish Labosky (*Chris is never going to let you do that…*), Lance Prince (*keep pushing!*), David Piston (*FOCUS*), Roland Stein (*you still are not telling me what the heck it is you are doing*), and Al Powers (*tell us how <u>we</u> can help <u>you</u>*). Each of these committee members, each in their own respect, have been outstanding mentors and role models. There is a certain satisfaction that comes from discerning how one might become a successful scientist, not by being told directly, but by sitting back, day to day, and watching successful individuals do what they do.

Finally, I want to thank the members of my family. My Mom, Lee Anne, and Dad, Vyto, especially have been incredible parents and professionals from I have come to appreciate the important things in life. They have taught me by example the value of hard work, especially when the chips are down, and how to be passionate about life's many pursuits. I want to thank my wife Kate, who I met here at Vanderbilt, and who is the love of my life. I can't wait to spend our future together, because you are amazing in every way, and I can always depend on you for your support and understanding, and appreciation. Last, I want to thank my two wonderful sons, Tyler and Jackson, who are my motivation and my inspiration that drives everything I do. I hope you will both cherish the privilege of having such wonderful family members on whom you can rely, no matter what.

TABLE OF CONTENTS

Page

LIST OF FIGURES

LIST OF ABBREVIATIONS

ACD	Asymmetric Cell Division
AMY	Amylase
aPKC	Atypical Protein Kinase C
BAC	Bacterial Artificial Chromosome
BBS	Blebbistatin
BrdU	Bromodeoxyuridine
Cdc42	Cell Division Control Protein 42 Homolog
CFP	Cyan Fluorescent Protein
CK19	Cytokeratin 19
Cpa1	Carboxypeptidase A1
DAPT	N-[N-(3,5-Difluorophenacetyl)-L-analyl]-S-phenylglycine t-butyl ester
DB	Ductal Branch
DBA	Dolichos biflorus agglutinin
DBZ	Dibenzazepine
Dia	Diaphanous-related formin
E	Embryonic day
Ecad	Epithelial cadherin
ECM	Extracellular matrix
EdU	Ethynyldeoxyuridine
EGFP	Enhanced green fluorescent protein
EMT	Epithelial to mesenchymal transition
ER	Estrogen receptor
FACS	Fluorescence activated cell sorting
F-actin	Filamentous actin
GFP	Green fluorescent protein

Gluc	Glucagon
GTPase	Guanosine triphosphate activating protein
H2B	Histone 2B
Hes1	Hairy and enhancer of split-1
Hnf	Hepatic nuclear factor
Ins	Insulin
MF	Mitotic figure
MPC	Multipotent progenitor cell
Muc1	Mucin 1
Neo	Neomycin
Neurog	Neurogenin (Ngn)
NICD	Notch intra-cellular domain
NmMyoII	Non-muscle Myosin II
PCR	Polymerase chain reaction
Pdx1	Pancreatic and duodenal homeobox 1
pHH3	Phospo-Histone H3
PP	Pancreatic Polypeptide
Prox1	Prospero Homeobox 1
Ptf1a	Pancreas transcription factor 1 subunit alpha
Puro	Puromycin
Rac	Ras-related C3 botulinum toxin substrate
RBPJ	Recombination signal binding protein for immunoglobulin kappa J region
RhoA	Ras homolog gene family, member A
RMCE	Recombinase-mediated cassette exchange
ROCK	Rho-associated protein kinase
SEM	Standard error of the mean

Sox9	SRY (sex determining region Y)-Box 9
TAM	Tamoxifen
YFP	Yellow fluorescent protein
ZO	Zona occludens

CHAPTER I

INTRODUCTION

The Stem-Cell Niche Concept and its application in understanding Organ Development

Stem-cells have a theoretically unlimited capacity for self-renewal, and because of their broad lineage potency (multipotency) are able to give rise to all cell types of a particular organism or organ [1]. In a historical sense, the phrase “stem-cell niche” is used to refer to the specific location of a stem-cell, the cellular components of the microenvironment surrounding the stem-cell, and the regulatory signals emanating from ‘support’ cells [1]. Studies on the stem-cell niche in diverse systems have shown that stem-cell function is controlled by extracellular cues that are deployed within spatially constrained ‘niche’ environments, and that activate intrinsic genetic programs within the stem-cell. A widely held belief is that the biological form of a niche is tightly integrated with niche function, and vice versa. Thus, the proper construction and maintenance of a niche is thought to depend on a precise regulation of cell and tissue architecture, which is coupled to the regulated progression of differentiating cell types from the stem-cell pool, and to the maintenance of reserve stem-cells that will remain within the niche. While concepts on stem-cell niche structure and function are remarkably well developed in relatively simple systems such as the *Drosophila* ovary and testis [2,3,4,5,6], or in homeostatic mammalian systems such as the bone marrow [7,8], skin/hair follicle [9,10], and the intestinal crypt [11] very little is known about whether and how organ-specific progenitor populations are assembled, maintained, and regulated within niche environments to control organ formation.

It can be argued that the stem-cell niches that have been best characterized represent relatively stable, and stereotypically organized biological entities. The major gaps in our knowledge with respect to if and how niche environments guide organ formation can largely be attributed to the fact that organogenesis represents a relatively rapid, highly complex, and spatially dynamic process. During organ development, it is often more appropriate to refer to multipotent populations as organ-specific progenitor cells, rather than *bona fide* stem-cells. While it is still debated as to whether there is a strict distinction between stem and progenitor

cells, an organ-specific progenitor can be defined as a cell that, unlike a stem cell, has a more limited tendency to self-replicate, and also has a greater tendency to differentiate toward a "target" cell type, or a rather limited number of cell types [12] (Fig. 1.1A). Multipotentiality in progenitors is thus often confined to windows of time that exist only transiently during embryonic development, making investigations into the niches within which they reside technically and conceptually difficult. These collective points are especially important, because it is now thought that many organ systems, in their mature and functional final states, do not harbor a reserve pool of stem-like cells that drive appreciable self-renewing or regenerative capacity under normal or even injury-induced conditions. Therefore, understanding the mechanisms through which organ-specific progenitor cells become expanded in number versus lineage-committed during development, and whether these processes are controlled within discrete niche environments, will be critical in our ability to gain control over the cell-biological mechanisms that regulate tissue formation as a means toward therapeutic applications.

The 'Niche Framework Model' as a basis to understand complex organ formation

When I first began my research in the Wright Lab, we were trying to think in new ways about the question "how must organs form?" In trying to envision a solution, we conceived the process of organ formation as essentially an engineering problem. During organ formation there must be enough growth in the progenitor pool to ensure that the organ obtains the correct size, the right cell types must be formed to meet the functional requirements of the organ, and cells must be placed with respect to each other at the right place at the right time. In meeting these three requirements, an organ formation 'program' can accomplish the proper size, composition, and spatial arrangement of properly differentiated cell types necessary for mature organ function. The blueprints of a particular organogenesis process can thus conceivably be reduced to three principle programs that must be precisely coordinated during development: these are cell differentiation, progenitor maintenance, and tissue morphogenesis. But how might these programs be coordinated, or even mechanistically coupled? We proposed a model wherein there must be a highly integrated system of feedback-based controls, which are organized and deployed within structured units or cell groupings,

which links these individual developmental programs together to guide the formation of a complex multi-cellular organ. We called this model the "niche framework" (personal communication, Christopher V.E. Wright 2009) (Fig. 1.1B).

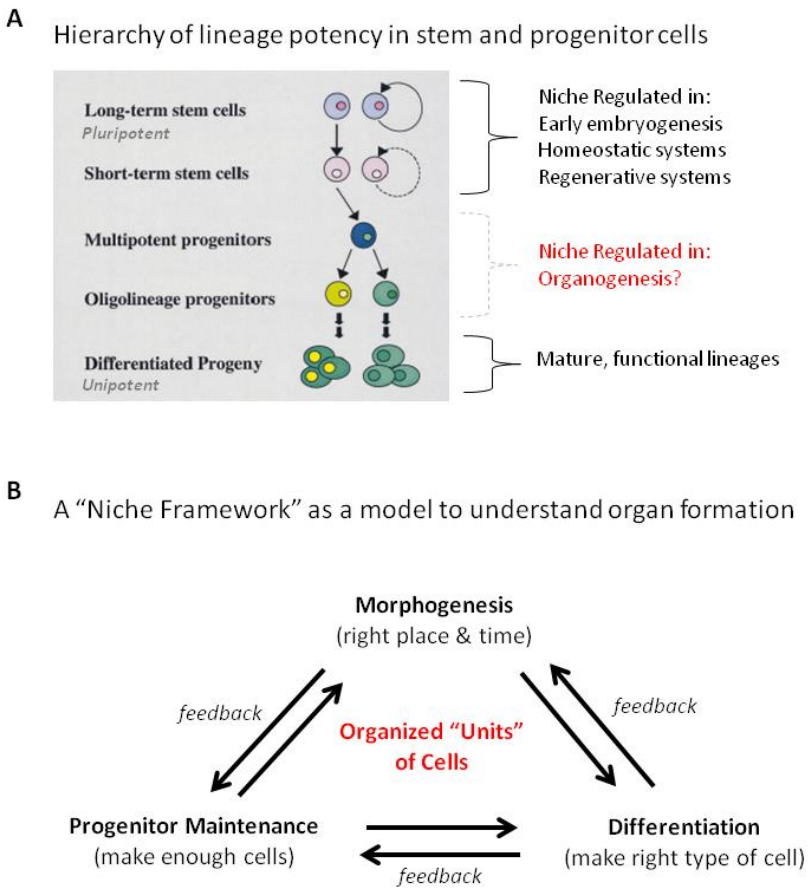

Figure 1.1. *The Niche Framework Model for the study of complex organ formation. (A) Schematic showing a typical hierarchy of lineage potency in stem and progenitor cells during development. The earliest embryonic stem-cells, and stem-cells reserved in homeostatic and regenerative systems, are assembled, maintained and regulated within discrete niche environments. As organs form during development, it is unclear whether similar niche environments regulate the functions of lineage-restricted progenitor types. (B) Our proposed "Niche Framework" model has three main features. First, there are three obligate developmental programs (morphogenesis, progenitor growth, and differentiation), which must be coordinated during organ formation. Second, there are feedback mechanisms in place that link each of the obligate developmental programs together in a closed circuit. Last, the feedback mechanisms linking morphogenesis, differentiation, and progenitor growth are organized and deployed within discrete 'unit' of cells. Altogether, these three features we propose represent the minimum requirements necessary to comprise a functional organ-specific niche. This figure was adapted from [12].*

Arguably, a niche-framework model, as a basis to understand how large and complex multi-cellular tissues arise, makes sense from a variety of perspectives. From the perspective of organ self-assembly, it is reasonable to presume that in order for organogenesis to proceed so precisely and reproducibly there must exist physiologically limited microenvironments wherein intracellular communication links individually wide-ranging cell behaviors (the inputs) together to ensure a stable and predictable large-scale outcome (the output). From the perspective of the acquisition of disease states, it follows that any detrimental perturbation to a morphogenetic, differentiation, or progenitor maintenance program has the potential to dismantle the coordinated organogenesis process, resulting in harmful consequences to the organism as a whole. Our niche-framework makes sense from the perspective of evolution, as it provides a limited set of 'principal components' that can be modified and elaborated upon over time to generate increasing complexity. Finally, by virtue of its non-linearity, our niche-framework model accommodates a structure-function tissue-building system that can be used reiteratively, in cycles that are tuned at some physiologically established rate, during organ formation. A major theme of this dissertation focuses on how we have built new and potentially and, potentially, increasingly unifying models for how organs are assembled during development using the "niche framework" as a guide, and the developing mouse pancreas as a model.

Pancreas development as a model to study organ-specific progenitor niches

The developing mouse pancreas provides a tractable model for beginning to ask questions about whether discrete niche environments coordinate progenitor growth, differentiation, and morphogenesis during organ formation. The pancreas is arguably one of the most thoroughly studied developing organ systems in mammals, and the lineage potency, marker-defined identity, and in some cases locations of various pancreatic progenitor pools have been described. Major themes have emerged over time regarding how various pancreatic progenitor populations behave as they contribute to differentiated lineages. In brief, these include, but are not limited to, the following:

- There are periods of development characterized by preferential replication and growth in an undifferentiated progenitor state, versus periods of preferential lineage-allocation from the progenitor pool [13].
- There is a gradual decrease in lineage potency over time, with early progenitors being multipotent, and later progenitors being bi-potent or even unipotent [14,15,16].
- Progenitor "domains" with specific lineage potencies become spatially segregated as the pancreas undergoes epithelial budding, tubulogenesis, and arborization [14,15].
- The size of the initial multipotent progenitor pool determines the ultimate size of the organ [17].
- There is little-to-no homeostatic regeneration of pancreatic lineages from "reserve" stem or progenitor pools in the adult organ [13,15,23].

While these themes will not necessarily apply to every developing organ system, they provide a framework to ask questions about the form and function of niche-microenvironments regulating organ-specific progenitor cells during development. The studies in this dissertation focus on whether and how a distinct niche regulates a relatively late-arising bipotent progenitor population wherein the final decision to become a pancreatic duct or hormone-secreting endocrine cell is made.

Early Specification and Growth of Multipotent Pancreatic Progenitors

The pancreas is an endodermally derived glandular organ consisting of two morphologically and functionally distinct exocrine and endocrine cell populations. The exocrine pancreas, which is comprised of the acinar and ductal lineages, represents the majority of the mature pancreatic cell mass. Acinar cells are arranged in numerous clusters that cap the terminal ends of the ductal tubes. Acinar cells secrete digestive enzymes into the ducts, which then empty these and other secretions into the duodenum to aid in digestion [18]. The endocrine pancreas, on the other hand, functions primarily in regulating nutrient metabolism and glucose homeostasis through the secretion and action of multiple hormones. Endocrine hormone-secreting cells

consist of five types: glucagon-secreting α-cells, insulin-secreting β-cells, somatostatin-secreting δ-cells, grehlin-secreting ξ-cells, and pancreatic polypeptide-secreting PP-cells [13]. In the mature organ, endocrine cells are arranged in spheroid-like aggregates known as islets of Langerhans, which are intimately linked to the vascular, neuronal, and mesenchymal organ constituents that altogether regulate glucose homeostasis throughout the body [20].

The Primary Transition of Pancreas Organogenesis

The beginning stages in pancreas organogenesis occur around embryonic day 9.0 (E9.0) as discrete dorsal and then ventral epithelial buds evaginate and begin to grow from a pre-patterned and pancreas-specified region of the foregut endoderm. This region of the foregut is located at the rostral end of the developing intestine and just caudal to the liver bud, and is marked by expression of the pancreatic transcriptional master regulator *Ptf1a* [21,22]. The pancreatic buds initially expand and grow substantially in a state that appears to be relatively devoid of branches or tubes. Around E10.5, however, groups of cells begin to become more structured and seem to form a pseudo-stratified epithelial bud [24] (Fig. 1.2A). Within the pseudo-stratified epithelial buds, cells begin to specify and establish apical and basal cell surfaces. This process is first evident with the formation of apically targeted vesicles within single cells, visible as puncta within the cell marked by the tight junctional marker Zona Occludens-1 (ZO1), and the apical lumen marker Mucin1 (Muc1). Around E10.5-11, these relatively isolated groups of polarized cells become oriented to form $Muc1^{+}$ apical microlumens [24,25,26]. These microlumens expand by recruiting more cells that develop an apical (future luminal) surface, coalesce with each other to form interconnected epithelial tubes, and grow rapidly and substantially in size, to generate a relatively continuous and interconnected network of polarized epithelial tubes by E12.5. The period that collectively spans these budding, growth, cell-polarization, and tubulogenesis processes is referred to as the “primary transition” [18] (Fig. 1.2A-D).

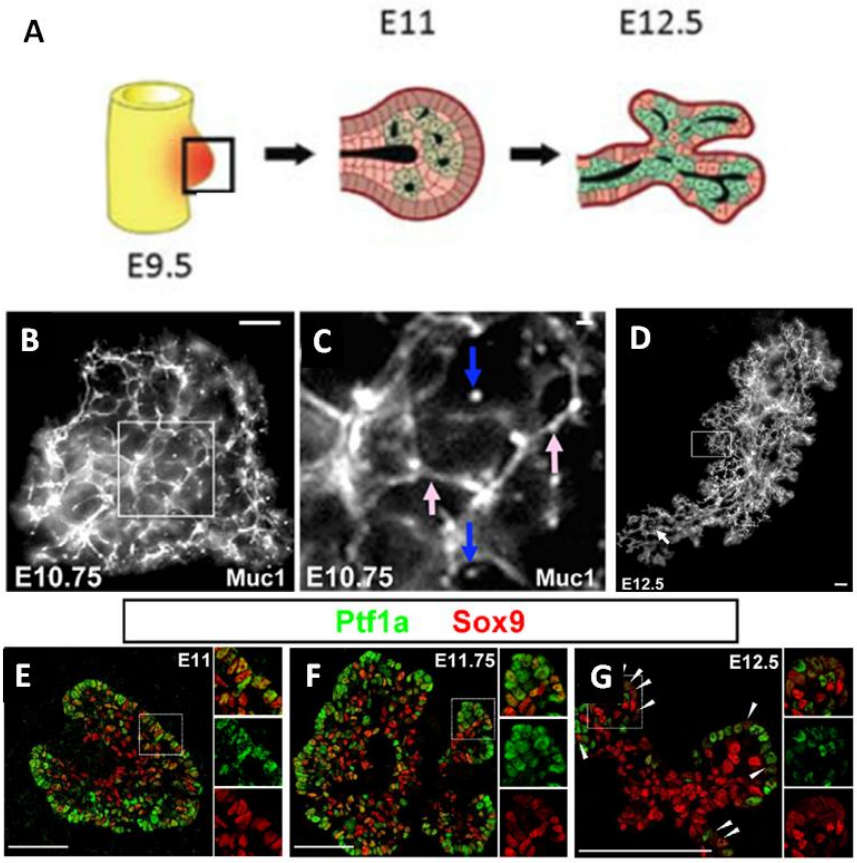

Figure 1.2. *Early specification and growth of the pancreatic anlagen during the primary transition. (A) schematic showing the initial transitions in pancreas formation comprised by budding outgrowth from the foregut endoderm, replicative expansion and microlumen formation, and progressive tubulogenesis and compartmentalization into 'tip' and 'trunk' domains. (B-D) Tubulogenesis (the apical surface of epithelial cells marked by Muc1) progresses from initial formation of microlumens in the bud, coalescence of microlumens into continuous tubes, resulting in the establishment of a web-like network, or plexus, of epithelial tubes. (E-F) Progression of the early bud into tip-trunk compartmentalization phases as marked by Ptf1a in the tip, and Sox9 in the trunk. This figure was adapted from [13, 23,24].*

Formation of Tip and Trunk Domains

During the primary transition, the pancreatic epithelium becomes increasingly segregated into morphologically and functionally distinct "tip" and "trunk" epithelial domains [14] (Fig. 1.2A). Discrete patterns of gene expression in the tip and trunk have been documented [13,14,23], and these have allowed for studies on the functional characteristics of cells therein using Cre-LoxP-based technologies [202]. Relatively early on in development (E9.5), pancreatic progenitors are thought to represent a relatively homogenous population in terms of both potency and gene expression, but there is evidence that spatial as well as transcriptional

heterogeneity is becoming established at this early stage. While there appears to be an appreciable degree of cell intermixing (i.e. there are no apparently abrupt boundaries between cell populations), gene expression pattern characterizations have shown that there are populations of $Cpa1^{+}Ptf1a^{+}Sox9^{+}$ cells located near the perimeter of the pancreatic bud, and populations of $Cpa1^{-}Ptf1a^{-}Sox9^{+}$ cells located interiorly [23] (Fig. 1.2E-G). Genetic lineage-tracing studies using *Cpa1*^{CreER} and *Ptf1a*^{CreER} mouse strains showed that $Cpa1^{+}Ptf1a^{+}$ cells of the primary transition are multipotent as a population, and able to give rise to all exocrine and endocrine lineages [14,23] (Fig. 1.3A). These cells were named primary multipotent progenitor cells (MPC), and close inspections on their localization showed that they are maintained within the tip domains throughout the primary transition. Moreover, pulse-chase lineage tracing analyses using low doses of tamoxifen to activate fluorescent tracer in only small numbers of *Cpa1*-expressiong MPC showed that early-labeled $Cpa1^{+}$ cells in the tip give rise to cells of the trunk domain, and eventually to differentiating endocrine cells [14]. The labeled cells that remain in the tip eventually differentiate into acinar cells. Finally, it was demonstrated that the multi-lineage allocation behavior of cells in the tip domain decrease dramatically over time, with essentially all cells being strongly biased toward a unipotent pro-acinar state by the end of the primary transition (Fig. 1.3B). Collectively, these experiments were repeated, independently confirmed, and quantified in detail in studies using the *Ptf1a*^{CreER} knock-in mouse line [23]. A model was proposed in which the so-called multipotent progenitor domain in the “tip” guides pancreas growth and lineage differentiation, at least during the early primary transition of development [14] (Fig. 1.3C).

Genetic Regulation of Pancreatic MPC

Studies in pancreas developmental biology have focused largely on identifying the transcriptional and signaling mechanisms that regulate endoderm specification into pancreas (rather than other nearby organ fates), MPC maintenance and survival, and commitment toward specific cell lineages. The proper coordination of each of these individual developmental processes is vital, because the initial numbers of MPC specified during the primary transition determines the final size of the pancreas. Comparing the developing mouse

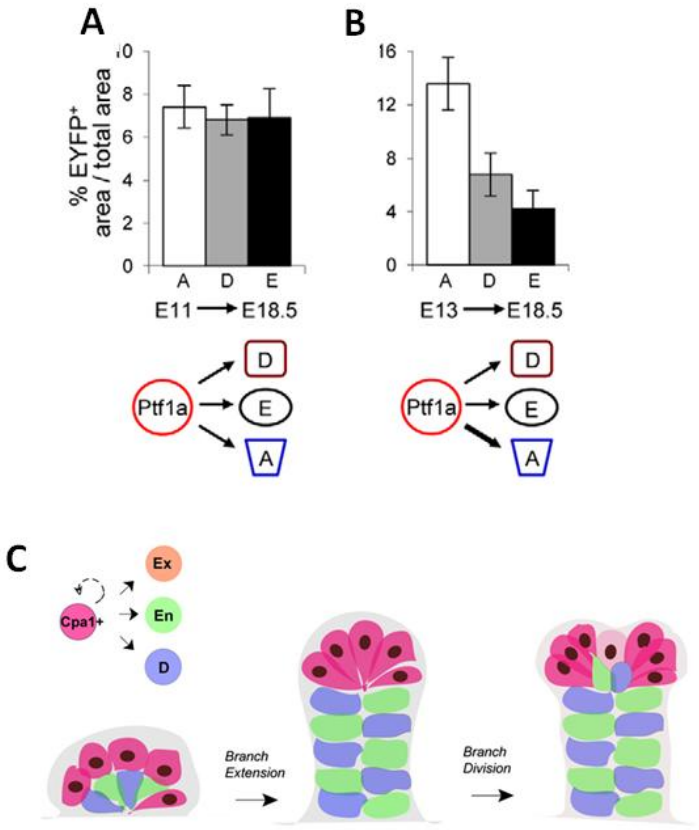

Figure 1.3. *Lineage potency becomes progressively restricted in the tip domain. (A) Results from a typical lineage tracing experiment following the progeny of tip populations via CreER-based methods. Early Ptf1a-expressing tip cells readily give rise to all lineages of the pancreas, whereas Ptf1a-expressing cells later become strongly biased toward a unipotent pro-acinar fate. (C) Proposed model for how the tip domain guides early pancreas formation. MPC in the tip replicate and grow while being maintained in the tip location. Progeny from these cells maintain the tip, but also give rise to trunk cells as the organ undergoes a proposed mechanism of branching outgrowth. This figure was adapted from [14,23].*

pancreas and liver as model systems, Stanger et al. [17] were able to manipulate, using inducible cell-death and blastocyst complementation experiments, the size of the initial pancreas or liver-specified progenitor pools. They could then ask whether the final size of each organ was pre-determined by the initial numbers of organ-specified progenitors, or whether there were compensatory growth mechanisms in place to ensure that a final "set point" in organ size could be achieved independent of the initial numbers of progenitors. The authors found that in the pancreas, but not the liver, final organ size was limited by the size of the initial progenitor pool, which suggested that at least in some organs, size is constrained by an intrinsic growth program established early in development. Therefore, in the pancreas there must be a

tightly coordinated regulation of the transcriptional and signaling events that drive specification of the appropriate number of initial MPC, and that control the balance between progenitor maintenance and cell differentiation throughout organogenesis. The introduction following will focus on selected transcriptional and signaling factors (as they relate to our studies on later developmental stages) that regulate pancreas specification, progenitor maintenance, and cell differentiation during primary transition.

Two of the most well studied transcriptional determinants of pancreatic fate are Pdx1 and Ptf1a. Both Pdx1 and Ptf1a are required for pancreas formation. Endodermal progenitors in the foregut that lack these transcription factors fail to become productively specified to the pancreatic lineage, and become incorporated early into adjacent tissues such as the bile duct and intestine [205, 206,207,208]. *Ptf1a*-expressing cells become localized within the 'tip' domain at early stages of primary transition where it marks and plays important functions in regulating, along with Pdx1, multipotent progenitor cell functions [13,14]. Later, Ptf1a becomes greatly upregulated in expression level as it becomes restricted to the pro-acinar lineage, where it functions as an important regulator in establishing acinar cell identity and function [209]. Pdx1 remains broadly expressed in essentially all undifferentiated cells of the pancreas during the primary transition [207,208] (Fig. 1.3C). Thus, Pdx1 and Ptf1a are used as functionally relevant markers of primary MPC in the early pancreatic bud and in the tip domain.

Sox9 is a member of the SRY/HMG box (Sox) family of transcription factors [19]. Sox9 functions in multiple respects to regulate the proliferation, survival and maintenance of progenitor cells in many systems including the neural crest, hair bulge, and intestinal epithelium [27, 28, 29]. A number of recent reports indicate similar roles in pancreatic MPC. High levels of Sox9 expression are first evident in the pancreatic buds at ~E10.5, and conditional lineage-tracing studies confirm that much like *Pdx1* and *Ptf1a*-expressing cells, Sox9 marks cell populations capable of giving rise to all three lineages of the pancreas [30]. Pancreas specific inactivation of *Sox9* results in a hypoplastic phenotype in both ventral and dorsal buds, and this effect can be attributed largely to increased cell death, decreased replication, precocious differentiation, and eventual depletion of the MPC pool [31]. Moreover, it was found that *Sox9* expression regulates

the transcriptional repressor *Hes1*, which represents a critical downstream effector of the Notch signaling pathway (introduced below). It is now thought that a potential genetic link between Sox9 and Notch plays a key role in blocking the activation of lineage-commitment factors to maintain MPC in an undifferentiated state [31, 32].

Notch pathway activity balances differentiation and progenitor maintenance

The Notch signaling pathway is well known as an important regulator of stem and progenitor cell maintenance, and binary fate decisions, in developing and homeostatic systems [33,34]. Canonical Notch signaling controls fate choice when a signal-sending cell upregulates membrane-bound Notch ligands (Delta/Serrate/Jagged) and engages Notch receptors in juxtaposed cells. This event transmits Notch signals to signal-receiving cells, resulting in the inhibition or induction of cell fate from within an otherwise "equivalent" group of progenitors [33]. Notch ligands including Delta-like 1 (Dll1), Dll3, Jagged1/2, and Serrate1/2 are expressed in the early pancreatic bud, as are Notch receptors Notch 1-4 [35,36,37], and transcriptional effectors of Notch such as RBPJ [44] and Hes1 [45, 46]. Although the exact locations and cell types involved in sending or receiving Notch signals remain ill defined, genetic lineage-tracing studies have shown that cells expressing *Hes1* during the primary transition represent MPC [46]. Early studies on Notch pathway function in the pancreas focused on genetic deletions of Notch ligands and receptors, the transcriptional mediator RBP-J, or the Notch effector Hes1. Mice genetically deficient for *RBPJ*, *Dll1*, and *Hes1* all display hypoplastic phenotypes in the early pancreatic bud, as well as a precocious differentiation of cells toward the endocrine lineage [36,37,38]. Conversely, overexpression of the Notch intracellular domain (NICD) in *Pdx1*-expressing MPC, which results in constitutive activation of the Notch pathway in these cells, blocks both endocrine and exocrine differentiation, and "traps" MPC in an undifferentiated state [39,40]. Thus, in the pancreas it appears that Notch maintains progenitor cells in an undifferentiated state, in part by blocking activation of lineage differentiation factors (Fig. 1.4A,B).

A

TABLE 1 | Mouse Models of Notch Signaling in Pancreas Development

Gene/Protein	Genetic Manipulation	Effect on Pancreas Development	Reference
Dll1	*Dll1*$^{-/-}$ *Foxa2*^{T2ACre};*Dll1*$^{f/f}$	Premature endocrine differentiation	16,25,26
Mib1	*Foxa2*^{T2ACre};*R26R*^{Mib1}	Loss of pro-endocrine/duct pancreatic progenitor cells	26
Jagged1	*Jag1*$^{f/f}$;*Foxa2*^{Cre} *Jag1*$^{f/f}$;*Pdx1*^{Cre}	Reduction of Ngn3 and endocrine cells in early pancreas; enhanced endocrine differentiation at postnatal stages	27
Notch1/2	*Ptf1a*$^{+/Cre(ex1)}$; *Notch1*$^{f/f}$;*Notch2*$^{f/f}$	Moderate reduction in pancreatic progenitor proliferation	28
Presenilin1/2	*Ngn3*^{Cre};*Ps1*$^{f/-}$;*Ps2*$^{-/-}$ *Ps1*$^{+/-}$;*Ps2*$^{-/-}$	Conversion of endocrine precursor cells to acinar fate upon reduction of gene dosage in Ngn3^{+} cells	29
NICD^{1}	*Pdx1*^{CreER};*R26R*^{NICD} *Ngn3*^{Cre};*R26R*^{NICD} *Pax4*^{Cre};*R26R*^{NICD} *Pdx1*^{NICD}	Impaired acinar and endocrine differentiation	30–32
MAML	*Pdx1*^{tTA};*pTRE*^{dnMAML1} *Foxa2*^{T2ACre};*R26R*^{dnMAML1}	Gain of pro-acinar progenitor fate at the expense of pro-endocrine/duct fate	26,33
Rbp-jk	*Pdx1*^{Cre};*Rbpj*$^{f/f}$ *Ptf1a*$^{+/Cre}$;*Rbpj*$^{f/f}$ *Ptf1a*$^{+/Cre(ex1)}$;*Rbpj*$^{f/f}$	Premature endocrine differentiation; pancreatic hypoplasia	28,34,35
Hes1	*Hes1*$^{-/-}$ *Foxa2*^{T2ACre};*Hes1*$^{f/f}$	Premature endocrine cell differentiation; pancreatic hypoplasia; loss of pro-endocrine/duct progenitor fate	25,26,36

B

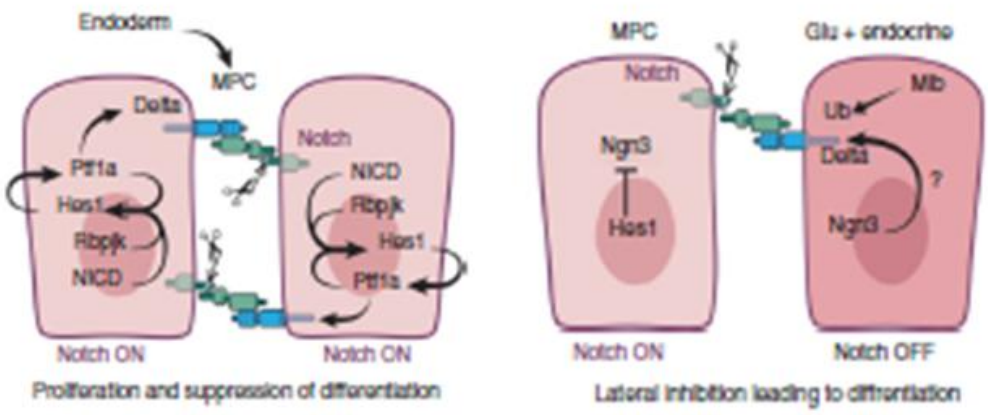

Figure 1.4. *Roles for Notch and Notch pathway components in pancreas development. (A) List of genetic manipulations and phenotypes from studies on Notch pathway function in foregut or pancreatic progenitors. (B) Proposed mode of Notch mediated repression of endocrine differentiation. In early pancreatogenesis, cells are broadly sending and receiving Notch signals. The net effect is that within the cellular environment, cells are held in a differentiation-suppressed and replicating state. At later stages, cells become differentiated into signal receiving and signal sending cells 9it is not known how this occurs). Signal receiving cells remain undifferentiated through Notch/Hes1-midated repression of Neurog3, while signal sending cells progress through Neurog3 activation and upregulation to commit to the endocrine lineage. The mechanism through which Neurog3-expressing cells suppress differentiation in surrounding epithelial progenitors through Notch is called lateral inhibition. This figure was adapted from [181].*

More recent advances in understanding the precise mechanisms through which Notch functions during pancreas organogenesis suggest that different levels of Notch may be involved in diversifying progenitor cell behaviors and/or fates [34]. Studies in the zebrafish pancreas

used Notch-reporter alleles, as well as genetic and pharmacological interference tests targeting Notch, to show that stepwise decreases in Notch activity regulate states of mitotic quiescence, replication in an MPC condition, or endocrine cell-fate allocation, respectively [41]. In addition, conditionally controlled and mosaic overexpression of a dominant-negative form of Mastermind, which functions as an obligatory transcriptional co-activator of NICD and RBPJ, resulted in "tip" versus "trunk" patterning defects in MPC prior to their terminal differentiation [42]. Here, Notch-suppressed MPC preferentially adopt a "tip" cell fate, and eventually differentiated into acinar cells. Conversely, wild-type cells in these same organs predominantly adopted a "trunk" fate, and thus differentiated into duct and endocrine cells. These data suggest that, in addition to primary functions in blocking individual terminal differentiation events, a tight spatiotemporal "tuning" of Notch levels within the progenitor pool may be important for regulating the progression of MPC toward different lineage-restricted populations. Lastly, recent studies are beginning to link Notch pathway components to the regulation of the expression or biochemical activity of transcription factors important for lineage specification [44,42]. Of particular relevance is a proposed transcriptional antagonism between *Ptf1a* and *Nkx6.1* that is important for controlling the patterning of tip ($Ptf1a^{+}$) versus trunk ($Nkx6.1^{+}$) domains during primary transition [43]. This effect on progenitor domain compartmentalization was suggested to be regulated by Notch via direct RBPJ binding sites on the *Nkx6.1* promoter [43], consistent with the idea that Notch in part directs the early specification of trunk progenitors at the expense of pro-acinar cells in the tip. In sum, the implications of these collective studies are that a precise and likely highly context-dependent regulation of the timing and levels of Notch pathway activity are important for diversifying lineage potential within the progenitor pool, for delaying precocious differentiation toward lineage-committed states, and for coordinating the balance between epithelial growth and cell-fate allocation in a manner that permits the developing pancreas to attain its predetermined size and cellular composition [13].

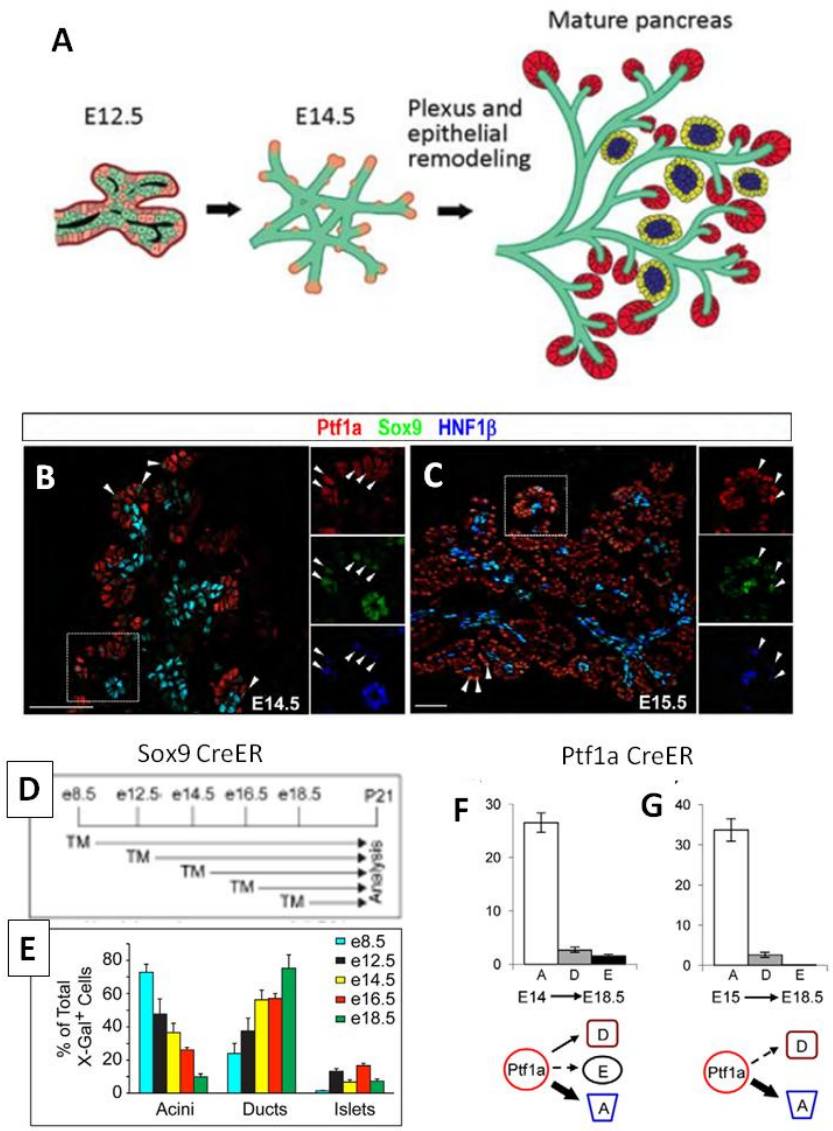

Figure 1.5. *Secondary transition epithelial remodeling and cell differentiation from the tip and trunk domains. The secondary transition comprises a period of roughly E12.5 to E18.5, where the pre-established pancreatic epithelium remodels from a branched web-like plexus into a hierarchically organized epithelial arbor. By birth, the pancreatic ductal epithelium is comprised of a relatively mature population of uni-potent duct cells, and new endocrine cells are no longer generated from the epithelium. (B,C) Ptf1a expression localizes to the pro-acinar tip domain, while high levels of Sox9 and Hnf1b expression mark the trunk domain. (D,E) Sox9^{CreER}-based lineage tracing at different time points of secondary transition shows a progressive restriction in lineage potency to favor duct and endocrine cells. (F,G) Ptf1a^{CreER}-based lineage tracing at different time points of secondary transition shows a progressive restriction in lineage potency in the tip to favor pro-acinar cells. This figure was adapted from [13,23,30].*

Duct and Endocrine Lineage Development from the Trunk Domain

It is now currently believed that the final binary fate decision to become a pancreatic duct cell versus a hormone-secreting endocrine cell is made within the confines of the trunk epithelial domain. The earliest entry points into the development of this model stem from studies describing the segregation of discrete transcription factor expression patterns into epithelial "tip" versus "trunk" domains at the end of the primary transition [14]. Initially, as described above, it was found that the potency of the *Ptf1a/Cpa1* expressing tip domain becomes progressively and then completely restricted to the pro-acinar lineage by around E13.5 [14,23]. This dynamic process of pro-acinar segregation from the duct/endocrine pool suggested that the trunk domain must be responsible for the further allocation of non-acinar pancreatic lineages from mid-to-late gestation. The implications of this are highlighted by the idea that the most significant contribution to formation of newly born endocrine cells is made during the mid-to-late gestation period [13], after the tip and trunk domains have separated, and during what has been categorized as a major wave of cellular differentiation termed the pancreatic secondary transition (E13.5-E17.5). Thus, a number of important studies were initiated to try to gain a better understanding of how duct versus endocrine lineage specification is regulated in the specific context of the trunk domain (Fig. 1.5A).

Two representative and functionally relevant transcription factors distinguishing tip and trunk domains are Ptf1a and Sox9, respectively. Early studies focusing on the expression patterns of these two transcription factors, among others, laid the groundwork for developing a model in which the trunk domain represents the embryonic tissue from which the bulk of the duct and endocrine lineages are derived. Concomitant with the end of the primary transition, Ptf1a and Sox9 expression are near completely exclusive, with the trunk being marked by $Sox9^{+}$ cells that are devoid of $Ptf1a^{+}$ cells [14,15,23] (Fig. 1.5B,C). Conditional lineage-tracing studies using a $Sox9^{CreER}$ transgenic mouse line showed that *Sox9*-expressing cells in the trunk were bipotent, and capable of giving rise to both duct and endocrine lineages throughout the secondary transition [15] (Fig. 1.5D,E). Further investigations found that in addition to Sox9, the trunk domain was selectively marked by the transcription factors Nkx6.1 [43], Hnf1b [47], and Hes1

[46]. Conditional lineage-tracing studies were performed using mouse lines where CreER recombinase was expressed under control of the regulatory elements of *Hnf1b* and *Hes1*, and were in essentially in complete agreement with the results obtained from studies using the *Sox9*^{CreER} line [46,47]. Interestingly, a feature of all of these genetic lineage-tracing studies was that, as the secondary transition progressed into late gestational stages, the trunk epithelium appeared to gradually restrict its lineage potential to favor the duct lineage over the endocrine lineage. These results implied that there was a time-dependent depletion of endocrine lineage competence within the trunk-resident population (i.e. the lineage bipotency of the trunk domain was not equivalent at all stages), reflecting a stage-limited and transient potential to derive endocrine cells from within an increasingly duct-lineage-biased epithelial pool.

The transcription factor Neurogenin3 regulates endocrine differentiation

The genetic program that leads to the production of an endocrine cell from bipotent Sox9^{+} trunk progenitors is initiated upon expression of the basic helix-loop-helix (bHLH) transcription factor and endocrine lineage determinant *Neurogenin3* (*Neurog3*). Neurog3 induces the downstream expression of a cascade of pro-endocrine transcription and maturation factors including, but not limited to, NeuroD1, Pax4, Arx, Rfx6, Nkx2.2, Myt1 and Insm1 [48,49,50,51,52,53,54]. Genetic inactivation of *Neurog3* in mice results in an almost complete blockade in the development of all of the cell types of the pancreatic endocrine lineage, and causes a severe diabetic phenotype in postnatal animals and eventual death [55]. Conversely, ectopic expression of Neurog3 can induce the differentiation of endocrine cells, both in the avian endoderm [56] and in an experimental mouse model where Neurog3 nuclear translocation (and thus function) is controlled via fusion to a tamoxifen-inducible estrogen receptor ligand-binding domain [57]. These studies have thus shown that *Neurog3* is both necessary and sufficient for the production of pancreatic endocrine cells.

Several studies suggest that the vast majority of *Neurog3*-expressing cells become post-mitotic as they undergo endocrine commitment [62,64,83]. Direct evidence to support this model comes from analyses of thymidine analog incorporation, clonal lineage tracing, and transcriptomic analyses of Neurog3^{+} populations. Neurog3 protein-positive cells that

incorporate BrdU during a three-hour pulse represent only a minor fraction (less than 5%) of the Neurog3-producing population as a whole, indicating that cells stop replicating their DNA shortly after Neurog3 becomes transcriptionally activated (this will be discussed in more detail below) [83]. Analyses of the expression of cell-cycle regulators in FACS-isolated *Neurog3*-expressing populations have shown that these cells express elevated levels (relative to non-*Neurog3*-expressing cells) of cell-cycle inhibitors such as Cdkn1a, Cdkn1b, Trp53, Rb1 and Rbl1, suggesting that cell-cycle progression is blocked as cells undergo endocrine commitment [83]. Evidence showing that Neurog3 binds to the regulatory regions of the Cdkn1a gene, moreover, suggested a direct role for Neurog3 in facilitating exit from the cell cycle. Consistent with this idea, exit from the cell cycle was shown to be *Neurog3*-dependent, because changes in the expression of cell-cycle regulators observed in normal *Neurog3*-expressing cells did not occur in these populations when Neurog3 protein was absent [83]. Finally, extensive and carefully quantified clonal analyses of the proliferation and differentiation properties of single *Neurog3*-expressing cells using Mosaic Analyses with Double Markers (MADM) showed that the vast majority of *Neurog3*-expressing cells represent the unipotent precursors of single hormone-producing endocrine cells [16]. Taken together, these collective studies suggest that *Neurog3* expression represents a triggering event in the production of an endocrine cell from within the pool of trunk epithelial progenitors, and that production of Neurog3 is associated with a rapid exit from the cell cycle upon endocrine commitment.

Cellular mechanisms underlying endocrine lineage allocation

While still a subject of much investigation and debate, the process whereby post-mitotic endocrine precursors become committed from the trunk appears to occur in association with a morphogenetic process of cell delamination from the epithelium [56,16,62,63,64]. The process of delamination is proposed to involve the *Neurog3*-dependent induction of an epithelial-to-mesenchymal transition (EMT) [65]. However, in order to classify endocrine birth as proceeding through a true EMT (as opposed to simply and epithelial-to-epithelial delamination process) we still need strong evidence supporting that each process in the EMT sequence actually occurs. These include: 1) breaking tight-junctional linkage with cell neighbors, 2) reduction in cell-cell

adherence, 3) acquisition of migratory characteristics, 4) breakdown of the basal lamina upon epithelial exit, and 5) reformation of tight junctions between adjacent cells to seal the epithelium across the region representing the previous location of the departed cell [66]. Nevertheless, several features of the EMT process, such as loss of cell-cell adherence via the downregulation of E-cadherin [56], and the acquisition of migratory characteristics prior to epithelial exit [65], have been relatively well described. Thus, it is widely held that concomitant with *Neurog3* activation, cells adopting the endocrine lineage physically delaminate from and exit the trunk epithelium. One additional model for endocrine cell birth, which is not mutually exclusive with a delamination or EMT-centric model, posits that endocrine cells are specified and committed via a process of asymmetric cell division (ACD). The common model for ACD depicts a process whereby there is an orthogonal-type division with respect to the plane of the epithelium to generate an apically localized daughter cell that retains progenitor characteristics, and a basally displaced daughter cell that exits the cell cycle to begin differentiation. Some evidence for this mechanism has indeed been described in the literature. Reporter-based single-cell live-imaging experiments indicate that a significant proportion of dividing trunk cells (approx 10% of Pdx1-reporting epithelial cells) acquire *Neurog3* expression and immune-reactivity shortly after a division event [67]. Retrospectively following the outcomes of these division events revealed that roughly half of all events result in the production of one *Neurog3*-expressing cell and one daughter retained in the epithelium, while the other half result in the production of two *Neurog3*-expressing daughters. Thus, it is possible that endocrine cells are allocated through various cellular mechanisms, some of which may depend on the processes of cell division and/or delamination themselves. Nonetheless, a working model derived from these collective studies posits that a general feature of endocrine birth and commitment from the trunk involves the generation of one or two quiescent, delaminating endocrine precursors, which will then exit the epithelium to populate the forming islets of Langerhans.

Endocrine-cell birth as a regulated progression through distinct Neurog3-expressing states

More recent studies suggest that endocrine-cell birth from the trunk epithelium does not occur via a simple *Neurog3* "ON-OFF" switch. Rather, it appears that there is likely to be a carefully regulated and step-wise progression of cells through different "states" of *Neurog3* activation on the way to generating a fully committed, mitotically quiescent, and delaminated hormone-producing endocrine cell. There is experimental evidence suggesting that cell populations in the trunk epithelium progress from a $Sox9^{+}Neurog3^{OFF}$ undifferentiated progenitor state, through to an initially endocrine-specified but perhaps reversible $Neurog3^{LO}$ state, and finally into a fully endocrine-committed $Neurog3^{HI}$ state, before finally down-regulating Neurog3 and acquiring a differentiated and hormone-producing status. The implication here is that the $Neurog3^{LO}$ state could represent a mitotic, stable, and endocrine-biased progenitor intermediate that represents a major and expandable source for the production of $Neurog3^{HI}$ endocrine committed cells. The idea that there could be a continuum of distinct, stable, and lineage-biased progenitor states existing during the development of the pancreas is of great relevance to understanding the regulatory mechanisms that both specify and commit endocrine cells from within the trunk epithelium. We focus this introductory section on laying out three major lines of indirect evidence that are consistent with the existence of a $Neurog3^{LO}$ endocrine progenitor intermediate.

There is a growing body of evidence suggesting that Neurog3 protein production does not mark all *Neurog3*-expressing cells existing within the trunk epithelium. In situ hybridization studies on the pattern of *Neurog3* transcripts within the trunk epithelium show a much more broad expression pattern of *Neurog3* expression when compared to directly detected Neurog3 protein [78]. At E15.5, Neurog3 protein is detected in what has been often described as a salt-and-pepper pattern, with the dominant state being characteristic of the nascent $Neurog3^{HI}$ cells that are undergoing delamination and commitment. *Neurog3* transcripts, on the other hand, are much more widely expressed in ostensibly non-endocrine-committed epithelial cells that appear to lie definitively within the trunk epithelium. Under experimental conditions where *Neurog3* has been genetically inactivated (i.e. Neurog3 protein is absent), and where *Neurog3*

transcriptional activity can be monitored via a *Neurog3*^{EGFP} knock in allele, there is a broadening of low-level *Neurog3* reporter expression in the trunk domain. This suggests that the signals that move cells into a Neurog3^{LO} condition are localized broadly within the epithelium, and that in the absence of Neurog3 protein-dependent Notch inhibition for instance, the 'default' state for many, if not all, epithelial cells is to adopt a Neurog3^{LO} condition [58,80]. Finally, preliminary studies in our lab have used immunolabeling and signal-amplification techniques to show that, in addition to the predominant Neurog3^{HI} state, there are in fact, under normal conditions, an appreciable number of readily detectable Neurog3^{LO} cells within the epithelium at mid gestation (unpublished observations, Matt Bechard, Wright Lab). While the quantitative overlap between *Neurog3*^{OFF} epithelial states, *Neurog3* transcriptionally active states, and Neurog3 protein LO and HI states remain to be fully established, these observations provide evidence that there are likely to be a diversity of functionally and transcriptionally distinct progenitor states existing in the trunk epithelium.

Recent genetic lineage tracing studies using BAC-transgenic *Neurog3* Cre and CreER mouse lines to indelibly label cell types derived from *Neurog3*-expressing populations have provided additional evidence for a *Neurog3* transcriptionally active and pre-endocrine committed state. In the Wright lab, we have utilized a highly sensitive BAC-transgenic *Neurog3*^{Cre} line, where Cre recombinase is controlled by a large portion of flanking upstream (~82 kb) and downstream (~102 kb) *cis*-regulatory elements [68] to achieve indelible and high-fidelity lineage tracing capability. With this tool we have preliminary analyses on the dynamic lineage allocation behaviors of *Neurog3*-expressing populations during pancreas organogenesis [Matt Bechard, Wright Lab, unpublished data]. Briefly, using this tool we have observed that many lineage-labeled cells are found in the pancreatic epithelium, even at late stages of development, which do not express detectable levels of Neurog3 protein, and do not exhibit the delaminating phenotype typical of cells undergoing endocrine lineage commitment. These results suggest that there exists an intermediate population of pre-endocrine-committed and Neurog3^{LO} cells that are long-lived within the trunk domain. Moreover, by postnatal time points the vast majority of lineage-labeled cells are found in the differentiated islets, suggesting that the Neurog3^{LO} population observed at earlier stages is only transiently maintained within the

epithelium, and that the overwhelming majority of these cells will eventually give rise to endocrine cells.

Additional experimental evidence for the Neurog3^{LO} endocrine-biasing model comes from studies where Neurog3 levels have been manipulated through the generation of a hypomorphic *Neurog3* allele [69,70]. Reducing Neurog3 dosage results in an increase in the proportion of low-level *Neurog3* expressing progenitors in the epithelium, and a reduction in the Neurog3^{HI} endocrine committed population. There is also a reduction in the mass of the endocrine pancreas at postnatal time points, consistent with the notion that acquisition of a high threshold of Neurog3 protein is required for full commitment toward the endocrine lineage. Finally, lineage tracing experiments carried out in these animals showed that Neurog3^{LO} progenitors were much more likely to adopt non-endocrine acinar and ductal lineages [69]. These results suggest that the transition from a Neurog3^{LO} to Neurog3^{HI} condition represents a distinct step in the progression through endocrine specification and commitment, and that if this transition is blocked, *Neurog3*-expressing populations can productively differentiate into non-endocrine lineages. While it can be argued that a genetic hypomorph for *Neurog3* (this animal only makes ~25% of the normal amount of protein) is an artificial representation of what might or might not be a 'normally' physiological distinct cell state, the behavior of cells in this condition, combined with the lineage tracing and *Neurog3* transcript localization studies, suggests that Neurog3^{LO} cells in the trunk epithelium could represent a transient, stable, and functionally distinct progenitor intermediate that acts as a 'source pool' for the generation of endocrine committed cells.

Notch Pathway Regulation of Cell Fate during Secondary Transition

There is an increasing body of evidence suggesting that the Notch pathway functions during the secondary transition, much as it does during the primary transition, to inhibit cell differentiation and to maintain undifferentiated progenitors. Similar to the difficulties encountered in working out the exact details of the proposed-context specific roles for various Notch ligands and effector molecules in regulating diverse processes at earlier stages of

development, however, a simple model for Notch-mediated control of cell fate during the secondary transition has also proved to be elusive. As a result, the genetic programs regulating *Neurog3* activation, and whether these are distinct from the mechanisms that activate *Neurog3* upregulation to high levels, remain poorly understood. This section on Notch pathway function during the secondary transition will focus on introducing results and conclusions from experimental manipulations that have been relatively simply designed and conservatively interpreted, shown to be reproducible, or that make specific connection(s) to regulatory influences that are relatively firmly established as essential in earlier stages of organogenesis.

To date, there has been no focused cell/tissue-specific manipulation to target Notch pathway activity within the secondary transition bipotent duct/endocrine progenitor population. Perhaps some of the most convincing evidence that Notch may suppress Neurog3 induction at this stage comes from biochemical evidence showing that Hes1, the expression of which appears to be largely Notch-dependent in the trunk [79], plays an important role in repressing *Neurog3* transcription [59]. Conditional *Hes1* lineage-tracing experiments following the lineage potency of Hes1-expressing epithelial cells during the secondary transition window of pancreatogenesis indicates that epithelial cells that maintain Notch pathway activity do not become endocrine cells, but rather are destined to contribute to the ductal lineage [46]. *Hes1*-expressing lineage-traced cells are capable of giving rise to endocrine cells and duct cells during the early stages of secondary transition (E12-E14.5), but their progeny become progressively duct-lineage-directed as development progresses (E15.5 and onward). Similar to models developed from studies during the primary transition, it is becoming apparent that specific levels of Notch pathway activity may be responsible for diversifying bipotent versus unipotent fates at later stages of pancreas formation. One study used titrated doses of a pharmacological inhibitor of Notch signal processing, DAPT, to build an argument that intermediate levels of Notch pathway activity cell-autonomously activate Sox9, which is in turn important for maintaining epithelial progenitors in an undifferentiated state [80]. Cells experiencing the highest levels of Notch will maintain both Hes1 and Sox9, eventually to give rise to the differentiated duct-cell lineage. Conversely, cells that receive the lowest dose of Notch pathway activity will rapidly adopt the endocrine lineage, via escape from Hes1-mediated repression of

Neurog3. While these studies collectively build upon the importance of Notch in diversifying lineage potency, or in executing binary fate decisions within an otherwise bipotent pool of

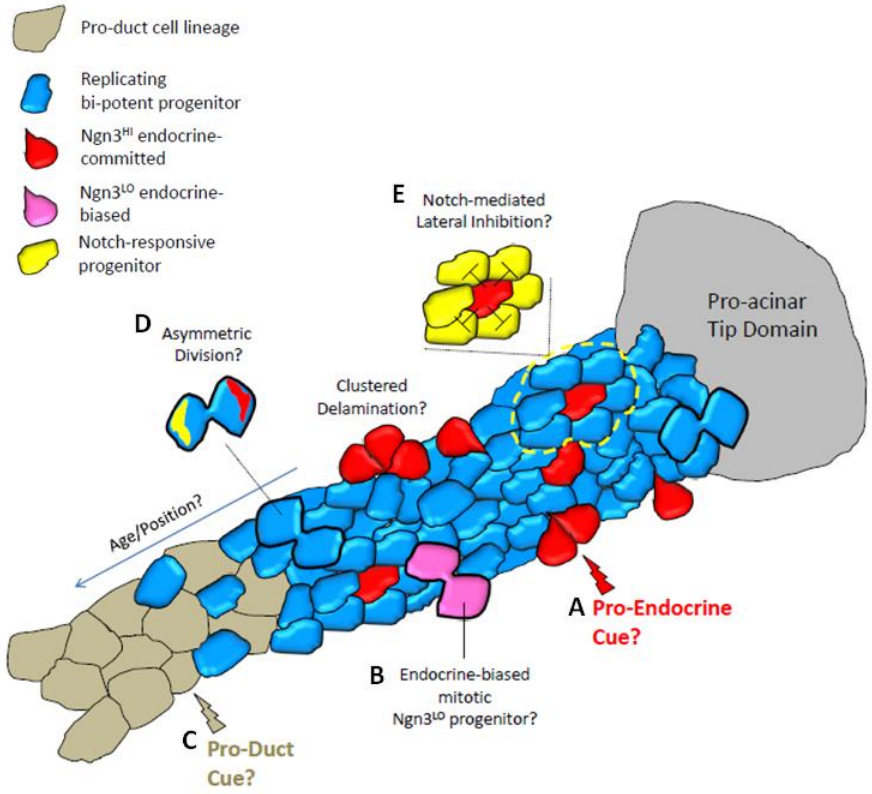

Figure 1.6. *Models for duct/endocrine progenitor dynamics during secondary transition. The duct and endocrine lineages are born from the trunk domain. Within the trunk, it is not known (A) how cells become committed to the endocrine lineage (Neurog3^{HI}), (B) whether there are stable, mitotic and pre-endocrine committed endocrine-biased progenitors (Neurog3^{LO}), (C) how and when cells become committed to the duct cell lineage, (D) whether cell fate is chosen during asymmetric division or otherwise, and (E) how Notch is deployed to regulate the balance between progenitor maintenance and cell fate allocation.*

epithelial progenitors, there remain major gaps in our understanding of when and how cells receive various Notch-pathway cues. Moreover, while numerous studies have shown important direct or indirect contributions of transcription factor activities such as Sox9, Hnf1b, Hnf6, Hnf3b, Foxa2 and Pdx1 [58,59,60,61] in regulating *Neurog3*, the event(s) that cause the initial activation of *Neurog3* in a given progenitor cell remain(s) obscure, and still not definitively linked to the mechanism of 'escape' from Notch. A large contingent of researchers in this field are working specifically toward developing a much deeper understanding of the cell biological and biochemical details of how extrinsic signaling pathways such as Notch act together with

transcription factors, or other currently unconnected factors, to orchestrate cell-fate allocation during pancreas development [81] (Fig. 1.6).

Integration of Epithelial Morphogenesis and Cell Fate in the Pancreas

When I started my graduate studies in 2009, there were a multitude of open questions remaining with regards to what are the developmental properties of cells within the trunk epithelium, how do they vary between cells within the population, and how do they change over time? We knew, for instance, that trunk cells as a population were capable of giving rise to both duct and endocrine lineages, but were there separate pools of duct progenitors and endocrine progenitors? How might their identities and functions be defined? Is the potency of each epithelial cell relatively equivalent over space and time? If there *is* appreciable heterogeneity among cell states, how is this heterogeneity developed, and how do cells of different types become patterned with respect to one another? Is patterning even important? It is worth taking a moment to reflect on these questions, because they were part of the beginnings of my thought process into trying to find ways to dissect the developmental complexity of the trunk domain to better understand how it 'works' to generate duct and endocrine tissues. Interestingly, a paper was published the same year I joined the lab, which showed that trunk domain morphogenesis, unlike the branching morphogenesis observed for example in the lung [175] and salivary gland [26] (and in the current depictions of the developing pancreas [14]), proceeds through asynchronous branching and remodeling of an irregular, web-like plexus intermediate, before yielding a typical arborized ductal system [24]. While the processes through which an epithelial plexus might become remodeled into a hierarchically organized ductal system were not understood, it was clear that the major wave of endocrine differentiation in the pancreas overlapped with this process of epithelial morphogenesis in a plexus state. This was interesting to us, and it forced us to begin to think about how different patterns of cell differentiation and growth might be driving, or perhaps even be driven by, patterns of epithelial morphogenesis. As my research studies evolved over

time, the concept that morphogenesis and cell fate could be integrated though precise mechanisms, regulated at both tissue and cellular scales, were to become a central themes.

One major unexplored territory in organ development regards if and how the cell-biological processes that regulate cell and tissue morphogenesis are linked to the activation of transcriptional determinants of cell fate. A central assumption of our "Niche Framework" model is that this must in fact be the case. The notion that morphogenesis and cell fate are linked in some fashion is supported by experimental evidence from numerous systems. For instance, a common phenotypic consequence of blocking cellular differentiation during organ formation, regardless of the type of experimental perturbation, is that tissue or organ morphology, at the micro and macro scale, becomes drastically altered. In the pancreas, blocking endocrine

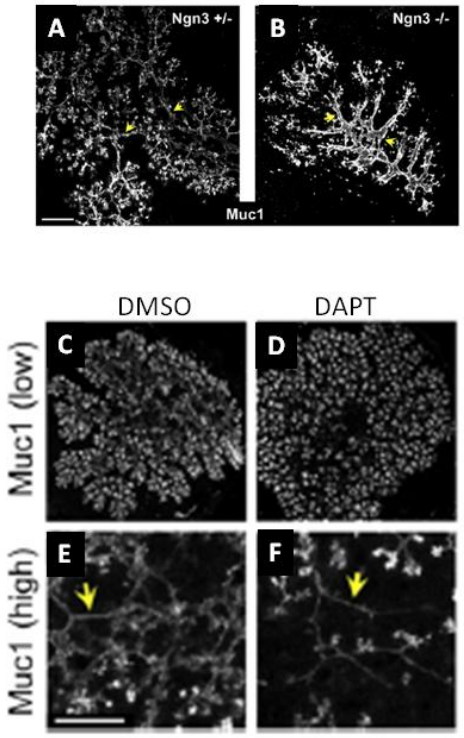

Figure 1.7. *Neurog3 regulates cell fate and epithelial morphogenesis. (A,B) Neurog3$^{+/-}$ and Neurog3$^{-/-}$ pancreatic epithelium labeled with Muc1 in whole mount. In the Neurog3$^{-/-}$, epithelia become fattened (yellow arrows) and branching is attenuated. (C,D) Neurog3-/+ or Neurog3-/- pancreatic explants treated with DMSO (vehicle) or DAPT (Notch inhibitor). (E,F) In the DAPT-treated condition, where endocrine differentiation is attenuated, epithelial lumens become more thin (yellow arrows). This effect of DAPT requires Neurog3. This figure was adapted from [72].*

differentiation by genetically ablating *Neurog3*, or accelerating endocrine differentiation by inhibiting Notch, causes opposite phenotypes with regards to epithelial morphology. In a *Neurog3*-deficient condition where there is no cell allocation toward the endocrine differentiation, the trunk epithelium becomes fattened (and probably 'over-stuffed' with cells), whereas in Notch-inhibited conditions in which endocrine differentiation is accelerated, the opposite happens - the epithelium becomes underpopulated or 'thinner' [72] (Fig. 1.7A-E).

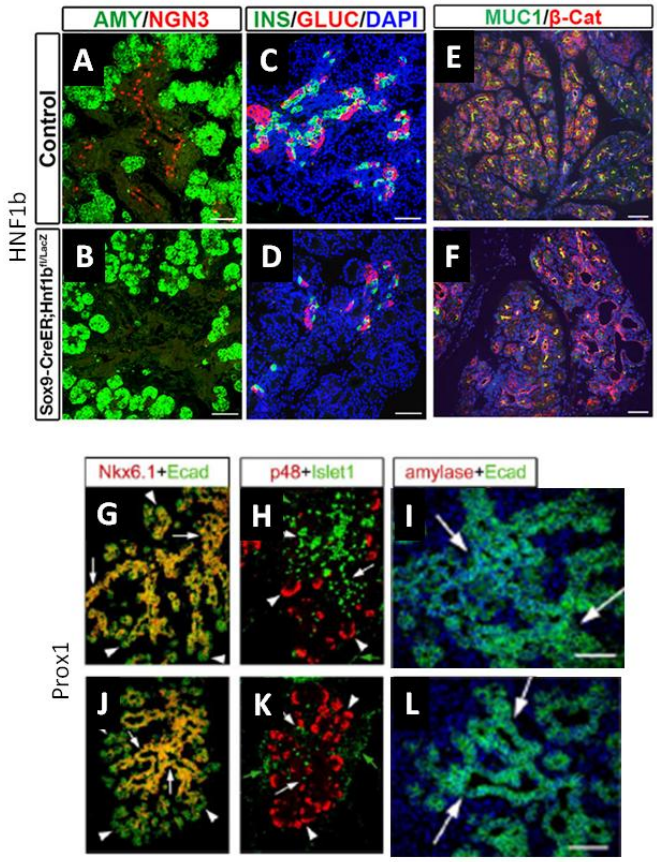

Figure 1.8. *Concurrent alterations to cell fate and epithelial morphogenesis. (A,B) Immunodetection of Neurog3 (newly born endocrine cells) and amylase (acinar cells) in control pancreas at E16.5, or in pancreas where HNF1b is deleted by Sox9^{CreER} (TAM injected at E12.5). (C,D) Immunodetection of insulin and glucagon in control or Sox9^{CreER};HNF1b$^{fl/LacZ}$ pancreas at E16.5 (TAM injected at E12.5). (E,F) Muc1 and beta-catenin detection at E18.5 in control and Sox9^{CreER};HNF1b$^{fl/LacZ}$ pancreas. Epithelial polarity is lost in the mutant condition, and epithelial lumens become dilated and cystic. (G,H) Immunodetection of Nkx6.1 (trunk marker) and Ecad in Prox1$^{+/-}$ and Prox1$^{-/-}$ pancreata at E15.5. Note the increase in diameter of the epithelial lumens in the mutant. (H,K) Ptf1a (p48; acinar cells) and Islet1 (differentiating endocrine cells) immunodetection in Prox1$^{+/-}$ and Prox1$^{-/-}$ pancreata at E15.5. Note the increase in acinar cells and decreased endocrine cells. (I,L) Ecad detection in Prox1$^{+/-}$ and Prox1$^{-/-}$ pancreata at E15.5. Note the increase in lumen diameter and alterations to cell shape in the Prox1$^{-/-}$. This figure was adapted from [74,75].*

Observations such as these are consistent with the idea that the progression of cells into differentiated states is important for shaping the morphological architecture of the tissues from which these cells arise. Moreover, tissue-specific inactivation of transcription factors expressed in the bipotent trunk domain, such as *HNF6* [73], *HNF1b* [74], and *Prox1* [75,76], result in malformed epithelia with concurrent defects in endocrine-lineage development (Fig. 1.8A-L). While these outcomes have traditionally been attributed to defects in transcriptional activation of *Neurog3* (some of the aforementioned factors bind to and activate the *Neurog3* promoter [74,77]), a number of them have roles in regulating epithelial morphology directly [256,257]. Thus, it is equally possible that mis-regulation of epithelial morphology in these mutants precludes, at least in part, efficient engagement of an endocrine differentiation program. In sum, while these phenomena show that mis-regulation of cell-fate allocation has consequences on epithelial morphogenesis, and possibly vice versa, they do not establish, nor rule out, that the two processes are mechanistically linked. Studies in the pancreas are beginning to shed light on an emerging paradigm that during organ formation, progenitor populations receive important inputs from morphogenetic determinants that are critical for mediating, or perhaps even initiating, cell fate determination.

As introduced previously, the transition from the early budding and progenitor growth phase (from E9-12.5) into the major cellular differentiation phase (from E12.5-birth) is marked by a complex reorganization of cells into polarized epithelial tubes. By mid-gestation, these tubes are thought to represent essentially a monolayered epithelium. Studies using Ecad (to mark cell-cell contacts), Muc1 (marking the apical surface), and laminin or collagen-IV (components of the basal ECM) have described how a seemingly unorganized mass of un-polarized epithelial cells (representing the founding MPC of the pancreatic buds) becomes remodeled at around E12-E13.5 until essentially every cell within the epithelium contacts both an apical and a basal surface [24,26]. Cells within the polarized monolayer maintain continuous contacts via $Ecad^{+}$ adherens junctions localized along the basolateral cell surface, and via subapical tight junctions as marked by ZO1. The apical domain of the epithelium is also marked, as expected for fully polarized cells, by the apical polarity determinants aPKC and Par3 [24,25]. The polarized architecture of the pancreatic epithelium is maintained, from the completion of tubulogenesis

and plexus formation, and into the later stages of cell differentiation, epithelial arborization, maturation, postnatal development, and adulthood [82].

If and how the morphological properties of cells within the developing pancreatic epithelium contribute to the regulation of endocrine cell-fate allocation has not been explored during the secondary transition. A seminal report carried out during the primary transition, however, has reported on the effect of genetic ablation of the RhoGTPase Cdc42 on the allocation of endocrine and exocrine lineages, and established the new concept that molecular regulators of cell morphology do indeed affect cell fate in the developing pancreas [71]. Cdc42 is a master regulator of cell polarity, and Cre-recombinase-mediated inactivation in pancreatic MPC causes mis-regulated apicobasal polarization. This defect in cell polarity causes an inability of MPC to initiate and expand an apical surface, and coordinate the process to form microlumens, which leads to a massive deficiency in the formation of polarized epithelial tubes. Coincident with this defect in tubulogenesis, there is a penetrant misallocation of progenitors toward the pro-acinar tip-domain fate, at the expense of the bipotent trunk domain fate, and a resultant deficiency in producing cells of the endocrine lineage (Fig. 1.9A-F). Surprisingly, experiments where the pancreatic mesenchyme was denuded from cultured Cdc42-deficient epithelia showed a substantial degree of restoration of endocrine differentiation competence, suggesting that Cdc42 is not cell-autonomously required for endocrine cell-fate allocation *per se*, but rather that Cdc42 normally functions cell non-autonomously to position and orient progenitor cells within micro-environments that are conducive for endocrine differentiation (that is, in this case, away from repressive mesenchymal components) (Fig. 1.9G-N). Thus, there appears to be a functional relationship between a cell's ability to incorporate into a properly polarized epithelial tube, and its ability to efficiently engage an endocrine differentiation program. Consistent with this notion, genetic interference with regulators of other morphogenetic pathways, such as planar cell polarity, causes reductions in the number of Neurog3-expressing cells that are born from the epithelium (specific effects on Neurog3^{HI} and Neurog3^{LO} states were not described) [85]. Together, these studies suggest that progenitor growth and differentiation programs do depend strongly upon, at least in part, the activity of regulators of tissue and cell polarity and morphogenesis. While the detailed mechanistic underpinnings that cause, for instance,

defective endocrine-lineage development in these cases remain unclear, the picture emerging is that insights into how endocrine progenitors and committed endocrine precursors are efficiently generated and maintained may be gleaned from characterizing, with increased spatiotemporal resolution, how cytoskeletal dynamics, cell polarity, actomyosin contractility, and/or the trafficking and distribution of receptors such as Notch, all are interconnected to

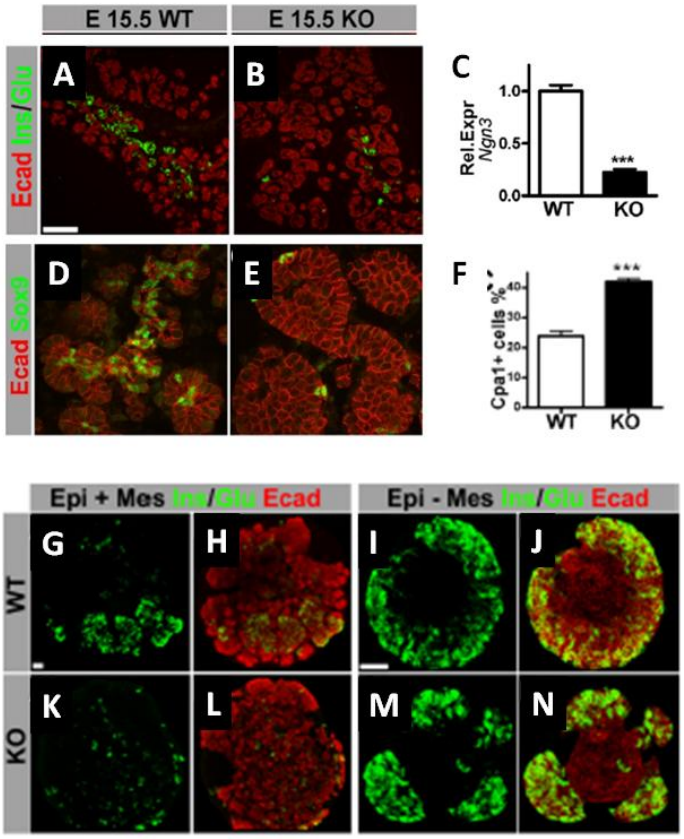

Figure 1.9. *Cell polarization and tubulogenesis mediate endocrine differentiation competence. (A-F) Genetic inactivation of the Rho-GTPase Cdc42 results in a failure in epithelial cell polarization and tubulogenesis, a loss of endocrine cells, Neurog3-expressing cells, Sox9^{+} trunk cells, and an increase in acinar differentiation (Cpa1^{+} cells). (A-D') Control and Cdc42-deficient pancreata were explanted at E11.5 and cultured on filters for 7 days in the presence or absence of mesenchyme, and harvested and labeled with Ecad, insulin, and glucagon. (A,B) In control explants with mesenchyme, endocrine cells are generated in normal numbers. In Cdc42-deficeint explants with mesenchyme (A',B'), endocrine cell generation is reduced. In the absence of mesenchyme (C,C',D,D'), both control and Cdc42-deficeint explants readily generate large numbers of endocrine cells. This figure was adapted from [25].*

provide functional links between cell and tissue morphogenesis processes and cell-fate determination [211].

Epithelial Morphogenesis during Development

Across metazoans, epithelial morphogenesis is a fundamental component of organ formation and function [87,88]. Sheets of embryonic epithelial cells undergo complex and coordinated movements during development to create diverse multicellular structures such as tubes, capsules, clefted branches, ingressions or egressions, and folds. There are many types of cell behaviors, both individualized and collective, that lead to the formation of such structures. These include, but are not limited to, directed cell movements and rearrangements, cell delamination and extrusion, proliferation, cell contractility, differential cell adhesion, and programmed cell death [87,88]. Over the past few decades the molecular mechanisms driving cell behaviors such as these have been intensively researched and in many respects have become quite well understood, especially for those mechanisms that are well conserved across species. The purpose of this brief introductory section on epithelial morphogenesis is to delve deeper into specific aspects of: 1) the morphological structure and cytoarchitectural organization of epithelia and 2) the molecular mechanisms controlling epithelial cell and tissue morphogenesis. With respect to the latter, we focus this introduction on actomyosin contractility and RhoGTPase signaling, which are most relevant to the themes of research reported in this dissertation.

Architectural properties of epithelial cells

An epithelium is defined as 'a laterally coherent sheet of cells with distinct apical-basal polarity' [88]. The apical surface of internal epithelia, such as those observed in tubular organs, faces the luminal space of an epithelial tube. The basolateral domain is subdivided into a basal surface that contacts, and mediates adhesion to, the extracellular matrix or basement membrane, and a lateral domain involved in cell-cell adhesion. Epithelial cells within an epithelial sheet are connected by adherens junctions and tight junctions that link them together. Adherens junctions are composed of cadherin proteins, such as E-cadherin (Ecad), that initiate and maintain intercellular contacts through *trans*-interactions with cadherins on opposing

basolateral cell surfaces [89,90]. Adherens junctions also involve catenin proteins, such as α [91,92] and β [93] and p120-catenin [94,95], which together play important roles in stabilizing adherens junctions and in linking them to the actin cytoskeleton [89,90]. Adherens junctions are localized circumferentially on the basolateral surface of epithelial cells, where they function in initializing and stabilizing cell-cell adhesions, regulating actin cytoskeletal dynamics, and mediating intracellular signaling and transcriptional regulation. Tight junctions are comprised primarily of claudin and occluden proteins, which are important in preventing the passage of membrane constituents between apical and basolateral membrane compartments, and in sealing the epithelium to gate the paracellular passage of ions and solutes across the apical and basal axis [89,96]. They are localized sub-apically (that is, just above the apical domain proper), and below the basolateral adherens junctions. Tight junction complexes, like adherens junctions, are connected to the filamentous actin (F-actin) cytoskeleton via various scaffold-like proteins. One of the most well studied families of such scaffold constituents represents the ZO (Zona Occludens) proteins. ZO-1, ZO-2 and ZO-3 are proposed to have both overlapping and non-redundant functions, and are found in close association with tight junction complexes and the juxtaposed circumferential bundles of cortical F-actin [89,97,98,99,100,101,102,103,104,105].

A core multi-protein complex component that is critical for the establishment and regulation of epithelial cell and tissue architecture is the F-actin cytoskeleton. The dynamic regulation of the F-actin cytoskeleton plays many important roles in numerous cell and tissue morphogenesis processes including, but not limited to, cell adhesion, cell migration, and cell division [106]. There are numerous actin-binding proteins that function to regulate F-actin assembly and organization in diverse cellular contexts. Typical configurations of the F-actin network structure are found in different regions of the cell, and individual F-actin based substrates are temporally regulated to mediate various cellular behaviors [107,108]. For each process, the F-actin cytoskeleton utilizes a distinct molecular composition and structure, which reflects that specific properties of these networks can be tuned towards mediating particular types of cell morphological transitions [106]. Widely documented examples include cellular protrusions important for directed cell migration and epithelial delamination, cortical F-actin bundles that

mediate the segregation of daughter cells during cytokinesis, and sub-apical bundles of F-actin that regulate epithelial cell shape change through processes such as apical constriction.

Rho-ROCK-myosin regulation of epithelial cell shape

Morphogenetic movements (such as the ones described above) in epithelia involve alterations in the relative sizes and shapes of apical, basolateral, and basal cell surfaces [109]. The shape and size of the polarized surfaces of epithelial cells are established and maintained, in large part, by Rho-GTPases that control the organization and dynamics of the actin cytoskeleton. The cell-shape changes that drive morphogenesis depend on, and can also in turn feed back on, the activity of Rho-GTPases. The net effect(s) of Rho-GTPase signaling in a given cell depends on a variety of complex and context-dependent factors, but the idea is that the relative sizes, shapes, and adhesive properties of the compartmentalized apical and basal domains of a cell can be modified to drive transient switches between relatively stable 'states' of epithelial cell morphology. In this manner, epithelial cells can be configured into columnar shapes (cells taller than they are wide), cuboidal shapes (cells as tall as they are wide), and squamous shapes (cells wider than they are tall) [89]. At the level of a multicellular tissue, localized or collective alterations to cell shape result in various types of tissue deformations. For instance, constriction of a cell's apical domain and a concomitant expansion of the basal domain will produce wedge or bottle-like shapes, which can be coordinated broadly across a field of epithelial cells to effect tissue folding or invagination [109,110]. These types of dynamic cellular deformations are associated with, and proposed to be driven by, Rho-pathway mediated regulation of force-generating actomyosin networks within the cell [109,111,112].

Myosin and actomyosin contractility

Contractile forces in cells results in large part from interactions between the F-actin cytoskeleton and the force generating molecular motor myosin II. Myosin is a large multi-subunit complex comprising a pair of heavy-chain motor domains, and two pairs of light chains. Myosin proteins oligomerize to form minifilaments in association with F-actin, and when such F-actin filaments are oriented in an anti-parallel manner with respect to each other, the molecular motor activity of myosin can move them in opposite directions, generating force.

This process is called actomyosin contraction [112]. Actomyosin contraction at the apical surface of epithelial cells represents a major effector of cell-shape change, and just as the actin cytoskeleton itself is arranged in specific ways to influence a wide variety of cell behaviors, the actomyosin network can be arranged and regulated in various ways to effect specific alterations in cell and tissue morphology [112]. In apical constriction, for instance, contractile forces generated by the actin-myosin cytoskeleton are exerted on the apical circumference of the cell, and these forces are in turn transmitted though sites of cell-cell adhesion. In the vertebrate neural tube, apical constriction is associated with a contraction of circumferential 'belts' of subapical cortical actomyosin [113,114], which results in the folding of the neural epithelium (Fig. 1.10A-C). Here, effectors of actomyosin contractility such as Shroom3 bind to subapical F-actin bundles, and recruit modulators of actomyosin contractility such as Rho-associated coiled-coil kinase (ROCK), to increase circumferential tension and constrict the apical domain of cells within the epithelial sheet [112,115, 116,117,118,119,120]. Apical constriction is also associated with extrusion of apoptotic cells from epithelia, epithelial cell delamination/EMT [121,122,123,124,125], and wound healing [126,127], indicating that apical constriction is a widely utilized mechanism that molds epithelial cells and tissues in various ways (Fig. 1.10C-E).

Actomyosin contractility is, along with many other aspects of epithelial morphogenesis potently influenced by regulators of cell polarity. One such regulator is the small GTPase RhoA, which functions as an important upstream regulator of a number of molecules in a signaling pathway that converges both on actomyosin contractility and actin remodeling dynamics [112,128]. For instance, RhoA signaling is shown in *Drosophila* to be required for efficient apical constriction [132,133], actin stress fiber formation in cultured cells [136], and contractile ring formation during cell division [137,138]. RhoA modulates myosin activity in large part through regulating its phosphorylation state [129,130]. RhoA activates ROCK, which stimulates myosin activity and actomyosin contractility through two mechanisms. ROCK inhibits dephosphorylation of myosin regulatory light chain, and also directly phosphorylates myosin regulatory light chain [131]. Activation of ROCK by RhoA in this manner has been shown to mediate apical constriction in several vertebrate and invertebrate systems [112]. Moreover, RhoA also regulates the activity of actin-filament nucleators such as the Diaphanous (Dia)-related formin proteins, which

facilitate the formation of new actin filaments [134]. It is though that a close cooperation between Dia and ROCK activities downstream of Rho provides for a major level of control over the form and function of the actin cytoskeleton and actomyosin machine. While there are many

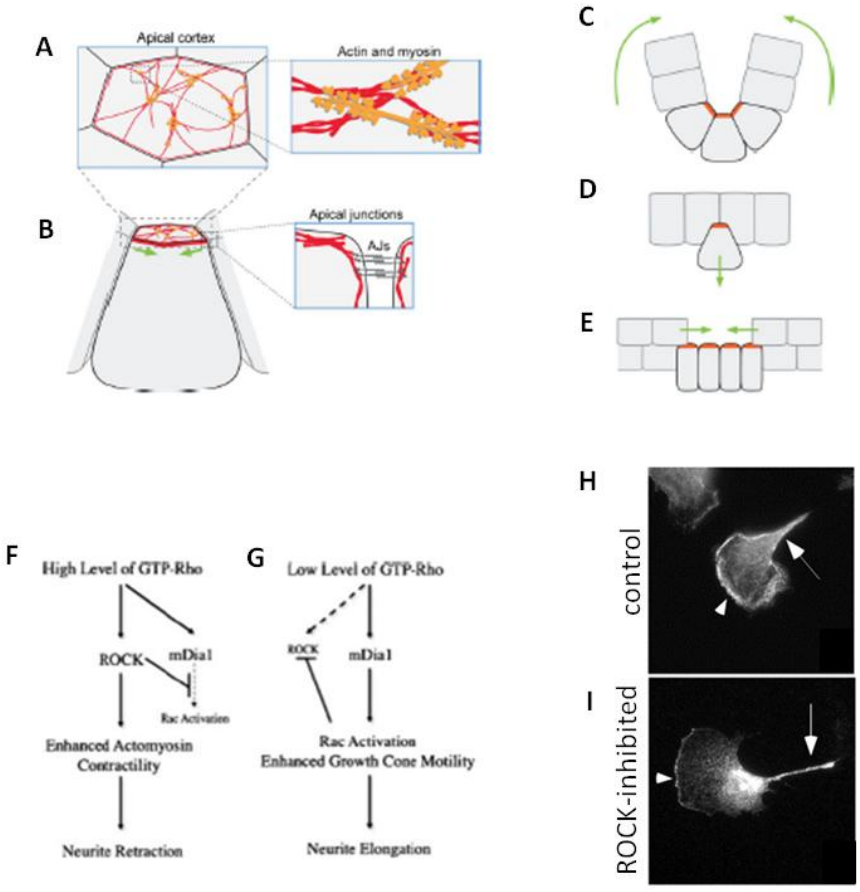

Figure 1.10. *The RhoA-ROCK-Myosin pathway regulates apical constriction and cell migration. (A) Contractile networks involved in apical constriction are comprised of F-actin (red) and myosin (orange), and can be organized into subapical contractile bundles and/or a two dimensional network underlying the apical membrane cortex. (B) Narrowing of the apical cell surface is driven by actomyosin contractions (green arrows). Cell-cell contacts at adherens junctions allow actomyosin contractions to shape tissues by folding (C), cell extrusion/delamination (D), or intercalation (E) [112], in addition to others. (F) High levels of Rho can block cell migration by enhancing actomyosin contractility and stress fiber formation through ROCK. (G) Lower levels of Rho permit migration by promoting the activity of the formin protein mDia, leading edge protrusivity, and upregulation of Rac (which is normally inhibited by high Rho activity). Note that Rac feeds back to inhibit ROCK, consistent with a mutual antagonism between Rho and Rac activities. (H,I) ROCK limits leading edge protrusivity in migrating cells (depending on the cell type, white arrowheads), and is required for cell rear retraction during directional movements (white arrows). This figure was adapted from [112,140,151].*

other known roles for RhoA in regulating processes such as endosome trafficking, adhesion, and migration [135], the power of RhoA-ROCK in stimulating, and responding to, actomyosin

contractility and actin filament assembly, clearly places the RhoA-ROCK-myosin pathway as a predominant mediator of cell-shape change.

Rho-ROCK-myosin control of cell migration

Cells migrate by polarizing in the direction of cell migration, extending protrusions at the leading edge of the cell, making adhesions to the ECM to stabilize protrusions and allow forward movement, and by finally dissembling adhesions and retracting the rear of the cell from the substrate surface [139]. Actin nucleation and polymerization drive membrane protrusion at the leading edge, and in association with integrin-mediated cell adhesion and actomyosin contractility, the cell body generates tension to pull the cell forward [140]. This sequence of events is controlled by a myriad of signaling molecules, but it has become increasingly appreciated that the Rho-GTPases Cdc42, Rac, and Rho play important roles in directing different and context-dependent aspects of the cell migration process [141,142]. Briefly, Cdc42 functions to establish and orient cell polarity through the Par6/aPKC pathway [143,144], Rac regulates membrane protrusion in the front of the cell by stimulating activation of the WAVE-Arp2/3 pathway [145], and Rho appears to be important for cell adhesion, cell contraction, and stress fiber formation through regulating ROCK-myosin [141]. Rho and Rac activities are known to antagonize one another in the cell, and the relative activities of these molecular regulators have been proposed to effect 'switch-like' transitions to drive or inhibit cell migration [140]. While the factors controlling upstream the activation of Rho-GTPases, and the molecular signaling cascades that lie downstream of Rho-GTPases, are miscellaneous and complex, the coordinated activities of Cdc42, Rac and Rho play a central role in cell motility, from neurite extension, to filopodia and lamellipodia formation, to cancer cell invasion [146,147]. For the purposes of this introductory section, I will focus primarily on those aspects of cell migration that are controlled by ROCK-myosin pathway activity, because it is most related to the studies that I will present in Chapter V.

Cell motility can be determined by the balance between the relative activities of the actin-nucleator mDia and the kinase ROCK [140]. mDia and ROCK act downstream of Rho to mediate remodeling of the actin cytoskeleton: mDia stimulates actin-filament nucleation and

polymerization, whereas ROCK activates myosin to induce cross-linking with the F-actin cytoskeleton, regulate actomyosin contractility, and modulate cell adhesion (Fig. 1.10E,F). ROCK also functions in remodeling of the actin cytoskeleton by indirectly inhibiting, through LIM kinases, the function of the actin-severing protein cofilin [146]. Many of ROCK's downstream target substrates are proposed to be involved in cell migration, and the specific role(s) for ROCK depends on the relative contributions of numerous pathway activities operating within a given cell type or during a given cellular process. For instance, ROCK activity can influence cell migration by limiting membrane protrusion at the leading edge of the cell, presumably through a function for ROCK in inhibiting Rac pathway activity [148,149] (Fig. 1.10E-H). A negative modulatory role for ROCK in cell migration was indeed shown to be important during delamination of neural crest cells [150], cell migration during wound healing [141,151], and the migration of fibroblasts [152]. ROCK activity is also vital for retraction of the rear of the cell during migration. Studies on trans-endothelial migration in monocytes and neutrophils have shown that Rho-ROCK is dispensable for cell attachment, spreading and crawling, but is essential for rear-surface retraction [153,154]. The effect of ROCK inhibition on perturbing rear retraction leads to highly abnormal elongation of the cell body along the axis of migration. Interestingly, defective rear retraction in ROCK-inhibited cells is not the result of reduced actomyosin contractility, but relates to the function of ROCK in disassembling integrin-mediated adhesions at the cell rear [153]. Finally, studies in tumor cells have shown that different types of cell migration can be influenced by ROCK, in coordination with other regulators of cell migration such as Rac. Tumor cells in 3D matrix show two types of movement: Rac-dependent mesenchymal movement and Rho/Rho-kinase-dependent amoeboid movement [154]. Inhibition of ROCK converts amoeboid morphology to mesenchymal morphology in a Rac-dependent manner, and silencing of Rac converts mesenchymal morphology back to an amoeboid state in a ROCK-dependent manner [147,154]. Together, these studies outline a number of typical functions for the ROCK-myosin pathway in regulating several critical aspects of cell migration, and highlight the notion that any effect of inhibiting or activating these molecules depends greatly on the cellular context. Notably, most studies on ROCK-myosin pathway activity have been performed in motile cells, with much less being known about how

these morphogenetic determinants influence, for example, cell delamination from an epithelium. This latter concept is a central focus of my research into the regulation of endocrine-cell specification and commitment. It relates directly to the delamination of nascent endocrine cells from the epithelium, and also to how the cell-biological processes that drive delamination are connected in turn to the deployment of *Neurog3*-dependent feedback mechanisms that non-autonomously regulate the growth, differentiation, and morphogenesis of epithelium progenitors from which new endocrine cells are born.

Dissertation Overview

If and how organ-specific progenitor populations are assembled, maintained, and regulated within niche environments to coordinate cell differentiation, growth, and morphogenesis processes during organ formation remains a largely unexplored yet central question in developmental biology. The challenges in addressing this question can largely be attributed to the fact that organ-specific progenitor populations exist, in many cases, only transiently during embryogenesis, and because they are regulated within extremely dynamic multicellular environments. Here, we use our proposed "Niche Framework" as a model to elucidate the biological form and mechanistic function of the niche that guides the genesis of the duct and endocrine pancreas from a pool of bipotent epithelial progenitors during development. These studies should greatly increase our understanding of how the therapeutically relevant hormone-secreting endocrine cells of the pancreas are formed. More importantly, however, insofar as any stem or progenitor cell niche, as a biological entity, represents a fundamental 'unit' of development, evolution, and regeneration [12], our studies should improve our understanding of how large and complex organs form and how they evolve. In addition, these studies should provide novel insight into how we might gain control over the cell biological processes that direct cell fate or progenitor maintenance programs, for use toward the artificial manufacture of organ-specific cell types, or even multi-cell-type tissues, to study and treat human disease. Our overarching hypothesis is that the signals controlling progenitor maintenance and cell fate allocation during pancreas development are both deployed within a

discrete and likely highly organized epithelium, and linked with the epithelial morphogenesis program.

In Chapter II, I present my parameterization of endocrine-progenitor growth and differentiation dynamics during the pancreatic secondary transition as a necessary step in establishing a new descriptive foundation for how progenitor maintenance is balanced quantitatively with endocrine cell differentiation. We characterize the relative distributions of Sox9 and Neurog3 producing cell states as a function of developmental time, and perform a series of EdU pulse-chase analyses to build a model that accounts for the developmental dynamics of the stage-specific flux of cells from the epithelial progenitor pool into the Neurog3-positive endocrine-committed state. We establish a new metric termed "endocrine yield", which can be used to define in spatiotemporal terms the relative magnitudes of endocrine flux that are occurring from the progenitor epithelium at any given stage. Finally, we use acute clonal-lineage tracing experiments to infer the cellular mechanisms, such as ACD or direct delamination, through which individual progenitors give rise to the endocrine lineage.

In Chapter III, I present how my studies led to experimental models that address the conditional control of progression of $Sox9^{+}$ progenitor cells into the endocrine lineage, as a basis to study how the process of endocrine differentiation non-cell-autonomously feeds back onto the trunk epithelium to regulate endocrine progenitor growth, differentiation, and morphogenesis during pancreatogenesis. We hypothesize that the obligate transcriptional co-regulator of Notch signaling, *RBPJ,* functions to regulate the balance between progenitor-cell maintenance and endocrine-cell differentiation during the secondary transition. A conditional genetic system comprised of a $Sox9^{CreER}$ transgene [30] and a floxed allele for *RBPJ* [86] was used to test this hypothesis. I then discuss our observations and interpretations of the experiments, their limitations, and the justification behind my proposal to discontinue these investigations. I also present an alternative experimental model for the conditional control of endocrine differentiation via the ectopic expression of Neurog3, and a $Neurog3^{BAC\text{-}CreER}$ model designed to interrogate even more deeply our newly proposed $Neurog3^{LO}$ condition. I discuss the potential

utility of these tools related to both the aims of this dissertation as well as the future goals that have emerged.

In Chapter IV, I address the hypothesis that endocrine-progenitor population growth, differentiation, and morphogenesis programs are coordinated by a discrete niche that guides the formation of the duct and endocrine pancreas. A three-dimensional (3D), spatiotemporally defined map of pancreas epithelium-remodeling patterns is developed, from which I discerned those characteristics of the pancreatic epithelium that are associated with its being the source of differentiating endocrine cells throughout secondary transition. I present the genetic and pharmacological interference tests that were designed to target Neurog3 and Notch, respectively, to lead to a model for how the formation of the duct and endocrine lineages are coordinated by feedback-control mechanisms operating within an 'epithelial plexus state' wherein endocrine progenitors are continually assembled and maintained, and their differentiation toward the endocrine lineage is regulated. These studies are the first to identify and begin to functionally characterize the pancreatic plexus-state epithelium as a candidate endocrine-progenitor niche.

Chapter V addresses the hypothesis that the signals controlling progenitor maintenance and cell fate allocation during pancreas development are deployed within a highly organized plexus epithelium, and are linked with the epithelial morphogenesis program of the plexus itself. We define the morphological and cyto-architectural properties of the plexus, and correlate changes in cell shape with cell-fate transitions. My findings suggest strongly that the morphogenetic program of the plexus instructs the earliest known step in the commitment of an endocrine cell from within the pancreatic epithelium. I build a model for how ROCK-nmMyoII pathway activity, Notch, and Neurog3 gene dosage are interconnected to link epithelial morphogenesis with cell-fate acquisition in the plexus niche.

CHAPTER II

ENDOCRINE PROGENITOR DYNAMICS DURING THE PANCREATIC SECONDARY TRANSITION

Introduction

Organogenesis relies on the proper spatiotemporal regulation and balance of cellular differentiation and replicative expansion of tissue-specific progenitors. In the developing mouse pancreas, numerous lineage tracing studies have shown that multipotent progenitors of the initial organ anlagen (E9.5-E12.5) give rise to all acinar, duct, and endocrine lineages. By E13.5, however, acinar potential becomes restricted to epithelial "tip" domains, while duct and endocrine lineages become diversified from *Sox9*-expressing bipotent progenitors residing in an epithelial "trunk" domain. While much is known about the transcription factors (such as Neurog3) and signaling pathways that maintain progenitors or direct cells toward different fates, the quantitative parameters that underlie and define a normal rate of cellular flux through various developmental processes, both at the tissue and cellular levels, are not well understood. Using gene expression pattern analyses, EdU pulse-chase, and acute mosaic lineage tracing, we describe and parameterize the lineage-allocation dynamics of Neurog3^{+} cells as they are born from replicating progenitors in the trunk.

Materials and Methods

Mice and Genotyping. Sox9^{CreER} mice were obtained from Maike Sander (UCSD). Primers used for genotyping were (5'HRsFr-ccttctcttccagagacttc and 5'HRsH-ctctggtcagagatacctgg; 780 bp) or (5'HRseqC- gcgatggatttccgtctctggtgtag and 5'HRseqD-gggtgctggacagaaatgtgtacact; 1080 bp).

Parts of this chapter have been published as Bankaitis ED, Bechard ME, and Wright CV. 2015. Feedback control of growth, differentiation, and morphogenesis of pancreatic endocrine progenitors in an epithelial plexus niche. *Genes and Development* **29**, 2203-2216 [211].

Immunodetection. Embryonic pancreas was paraformaldehyde-fixed (4%; 4^{o}C, 4-6 hours). For cryosectioning, samples were sucrose-equilibrated (30%; 4^{o}C overnight) and OCT-embedded (Tissue-Tek). Antibodies used include hamster anti-Muc1 (NeoMarkers, 1:1000), rabbit anti-Sox9 (Millipore, 1:5000), goat anti-Neurog3 (Gu Lab, 1:40,000), guinea pig anti-Neurog3 (Sander Lab, 1:2000), guinea pig anti-Pdx1 (Wright Lab, 1:1000), rat anti-Ecad (AbCam, 1:1000).

DBZ and EdU administration and quantification. DBZ (Cayman Chemical) was resuspended finely in ME4M slow-delivery vehicle (Methocell^{TM}) using a motorized pestle, and injected I.P. EdU (Life Technologies) was given I.P. (10 mg/kg). EdU was detected by the Click-iT Plus EdU Imaging Kit (Molecular Probes). S-phase indices and percent EdU incorporation were counted manually.

Mosaic lineage tracing. Pregnant dams were injected with a low dose of tamoxifen (0.03 mg) re-suspended in corn oil with a final injection volume of 0.1 mL. Embryonic pancreas was harvested 36 or 48 hours after injection, and samples were prepared for whole-mount immunolabeling as described [166]. Classification of different types of lineage allocation events were determined from regions of the pancreas where individual or paired cells were observed in relative isolation from other groups of cells (>30 μm) and were in direct contact with one another. All non-classifiable differentiation events were ignored, as is the cases where cells were found in clustered groups with other lineage labeled cells.

Image Acquisition. Confocal images were from a Zeiss LSM 510 META. Three-Dimensional reconstructions were rendered using Imaris Software.

Quantification and statistical analyses. All sectional analyses covered approximately 30% of the dorsal pancreas. For endocrine-yield measurements Sox9^{+} and Neurog3^{+} cells were counted manually. Statistical analyses were performed using GraphPad software.

Results

Patterns of Neurog3-expression vary during early stages of secondary transition

To understand how $Sox9^+$ progenitor cells progress through states of Neurog3 positivity during the process of endocrine cell birth and during various developmental stages, we analyzed the relative numbers and epithelial distribution patterns of $Sox9^+Neurog3^-$, $Sox9^+Neurog3^+$, and $Sox9^-Neurog3^+$ cell states by immunodetection. We initially targeted stages E12.5 and E14.5, as E12.5 represents the initial stages of secondary transition, and E14.5 is a time point representative of the major wave of cellular differentiation at mid-gestation. At E12.5, there were abundant $Sox9^+$ cells distributed continuously throughout the epithelium. Within the $Sox9^+$ population, there were numerous instances of Neurog3 co-expression. The vast majority of the $Sox9^+Neurog3^+$ cells expressed relatively low levels of Neurog3 protein, as compared to the $Sox9^-$ $Neurog3^{HI}$ cells undergoing delamination from the $Sox9^+$ epithelium. Visual inspection of typical sections at this stage indicated that the $Sox9^+Neurog3^-$ cell state was clearly the most abundant cell state in the epithelium. The numbers of $Sox9^+Neurog3^+$ and $Sox9^-Neurog3^+$ cells were fewer, but roughly equivalent with respect to one another (Fig. 2.1A-C). At E14.5, the $Sox9^+Neurog3^-$ cell state remained the most prevalent. There was, however, an apparent shift in the relative numbers of $Sox9^+Neurog3^+$ and $Sox9^-Nuerog3^+$ cell states to favor of the $Sox9^-$ $Nuerog3^+$ cell state (Fig. 2.1D-F). Quantifications by manual cell counting confirmed a shift from E12.5 to E14.5 in the distribution of $Sox9^+$ and $Sox9^-$ Neurog3-producing cell states (41.33 ± 4.93 % $Sox9^+Neurog3^+$ at E12.5 versus 14.67 ± 4.59 % at E14.5), suggesting that $Sox9^+Neurog3^+$ cells are relatively abundant at early secondary transition, but become progressively eliminated from the epithelium as development proceeds. Consistent with this notion, the proportional representation of $Neurog3^+$ cells in the $Sox9^+$ epithelium was measurably reduced between E12.5 and E14.5 (10.1 ± 2.46 % $Sox9^+Neurog3^+$ at E12.5 versus 3.77 ± 1.07 % at E14.5) (Fig. 2.1I,J). These results suggest that, as the developing pancreas enters the major wave of differentiation during secondary transition, fewer $Neurog3^+$ cells are found in the $Sox9^+$ epithelium (Fig. 2.1K).

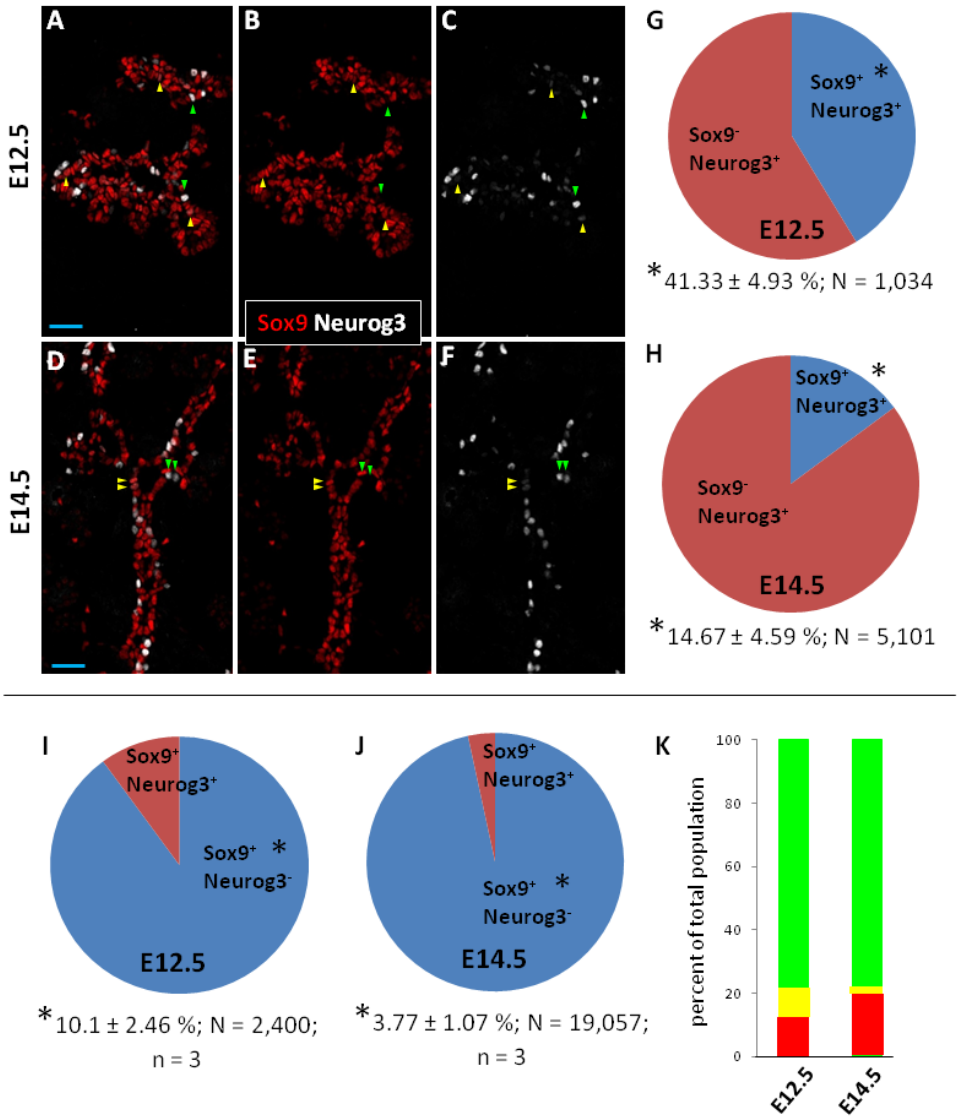

Figure 2.1. *Dynamic patterns of Neurog3 expression in the trunk domain. (A-F) Split channels from confocal images of immunodetection of Neurog3 protein in Sox9$^+$ trunk epithelial cells at E12.5 and E14.5.Yellow arrowheads indicate Sox9$^+$Neurog3$^+$ cells, green arrowheads indicate Sox9$^-$Neurog3$^+$ cells (G,H) Quantification of the total Neurog3$^+$ population that is also Sox9$^+$ (41.33 ± 4.93 %; N = 1,034; n = 3 at E12.5, 14.67 ± 4.59 %; N = 5,101; n = 3 at E14.5). (I,J) Quantification of the total Sox9$^+$ population that is Neurog3$^+$ (10.1 ± 2.46 %; N + 2,400; n = 3 at E12.5; 3.77 ± 1.07 %; N = 19,057; n = 3 at E14.5). (K) Graphical representation of the proportional distribution of Sox9$^+$Neurog3$^-$ (green), Sox9$^+$Neurog3$^+$ (yellow), and Sox9$^-$Neurog3$^+$ (red) cells states at E12.5 and E14.5, as calculated from G-J, when all cell states are summed. Scale bars are 40 μm. Error is S.E.M.*

Cells producing low levels of Neurog3 in the Sox9$^+$ epithelium replicate

To understand whether or not there could be functionally relevant distinctions between Sox9$^+$Neurog3$^-$, Sox9$^+$Neurog3$^+$, and Sox9$^+$Neurog3$^-$ cell states, we analyzed and compared replication behaviors in each state using thymidine analog incorporation (EdU) and phospho-histone H3 (pHH3) detection. Timed wild-type matings were set up, and pregnant dams bearing E12.5 or E14.5 embryos were pulse injected with EdU, and sacked after one hour. Embryos were immediately harvested, the pancreata isolated, fixed, sectioned, and labeled for Sox9, Neurog3, and EdU. Analysis of confocal section from these samples showed frequent EdU incorporation in the Sox9$^+$ epithelium (Fig. 2.2A). Quantification of the one-hour EdU incorporation index in the total Sox9$^+$ populations at each stage indicated that Sox9$^+$ epithelial cells are highly replicative at E12.5 (29.3 ± 1.03 %), and at E14.5, although the EdU incorporation index was significantly reduced at E14.5 (22 ± 2.7 %) (Fig. 2.2B). Analyses of the EdU incorporation index in Sox9$^+$Neurog3$^+$ cells showed a reduction in the number of cells incorporating EdU relative to the Sox9$^+$Neurog3$^-$ state at each stage (18 ± 0.0, n =1 at E12.5; 7.9 ± 2.5 % at E14.5) (Fig. 2.2C), suggesting that Sox9$^+$Neurog3$^+$ cells can synthesize DNA, but do so less frequently than Sox9$^+$Neurog3$^-$ cells. By E14.5, out of all Neurog3$^+$ observed only 1.63 ± 0.45 % exhibit EdU positivity, indicating that only a small fraction of all cells producing Neurog3 replicate DNA. Quantification of the distribution of EdU positive cells as a function of all Neurog3$^+$ cells exhibiting EdU positivity showed that the vast majority (85.3 ± 1.37 %) of Neurog3$^+$ cells replicating DNA are expressing Sox9 (Fig. 2.2D). These patterns of EdU incorporation, which reflect the relative mitotic behaviors between Sox9 and Neurog3$^+$ cell states, were confirmed by co-labeling analyses with the mitosis marker pHH3. At E12.5 and 14.5, we could readily detect, albeit relatively rarely as compared to the Neurog3$^-$ epithelial populations, instances where Neurog3$^+$ cells were co-labeled with pHH3. These cells were consistently closely apposed to the Muc1$^+$ lumen surface, and expressed the epithelial marker Ecad, confirming their localization within the epithelium proper (Fig. 2.2E-F, Matt Bechard, Wright Lab). Similar to the replication patterns shown by EdU, the numbers of Neurog3$^+$ cells positive for pHH3 were reduced from E12.5 to E14.5. Consistent with the notion that it is predominantly the Sox9$^+$Neurog3$^+$ population that exhibits proliferative behavior, there was an

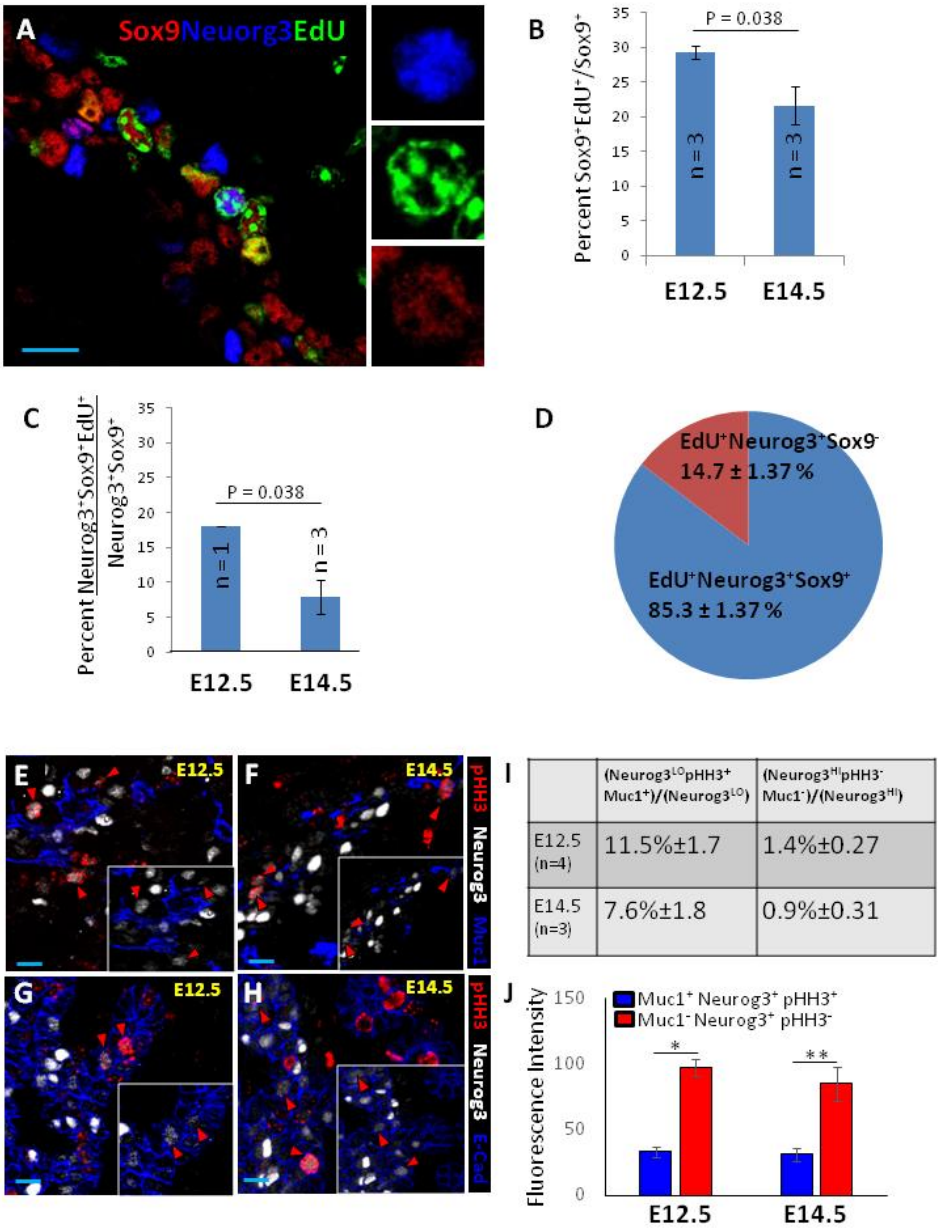

Figure 2.2. *Neurog3^{+}Sox9^{+} epithelial populations express low levels of Neurog3 and exhibit proliferative behavior. (A) Immunodetection of Sox9, Neurog3, and EdU at 100x magnification (0.6 μm optical slice) at E14.5 after 1 hour of EdU incorporation. Insets show split channels for a typical EdU^{+}Sox9^{+}Neurog3^{+} cell state. (B) One hour S-phase index in the total Sox9^{+} population at E12.5 and E14.5. (C) One hour S-phase index in the Sox9^{+}Neurog3^{+} population at E12.5 and E14.5. (D) Proportion of Neurog3^{+}EdU^{+} cells that are Sox9^{+} at E14.5. (E,F) Immunodetection of Muc1, Neurog3, and pHH3 at E12.5 and E14.5. Insets show split channels with pHH3 removed. (G,H) Immunodetection of ECad, Neurog3, and pHH3 at E12.5 and E14.5. (I)Quantification of pHH3 positivity in total Neurog3^{LO} versus Neurog3^{HI} populations. (J) Analysis of mean Neurog3 fluorescence intensities in Neurog3^{+}pHH3^{+}Muc1^{+} versus Neurog3^{+}pHH3^{-}Muc1^{-} populations. Scale bars are 10 μm. Error bars are S.E.M, (*) P=0.0010, (**) P=0.0175.*

8-fold difference between pHH3-positivity in the epithelium-resident (defined by Muc1 positivity) Neurog3^{LO} population, and the Neurog3^{HI} population that is undergoing epithelial delamination (Fig. 2.2I-J, Matt Bechard, Wright Lab). These results are consistent with previous work showing that Neurog3^{+} cells represent a largely post-mitotic and endocrine committed population of cells. However, these results also indicate a previously unappreciated mitotic potential in the Sox9^{+}Neurog3^{LO} condition, which is most readily apparent at early stages of secondary transition.

These preliminary analyses on the expression patterns and mitotic properties of the Sox9^{+}Neurog3^{-}, Sox9^{+}Neurog3^{+}, and Sox9^{-}Neurog3^{+} led us to conclude that there are likely to be a diversity of cell states existing within the trunk domain during secondary transition. Moreover, these cell states appear to have different replicative properties. We provided novel and direct evidence that cells expressing low levels of Neurog3 in the Sox9^{+} epithelium can replicate their DNA under normal developmental conditions. We also provided evidence that these cycling Neurog3^{+} cells are enriched at early stages of secondary transition, suggesting that a staging period of endocrine-biased progenitor amplification might presage the major lineage commitment stages observed later in gestation. While the behaviors observed within the Sox9^{+}Neurog3^{+} cell state were highly suggestive of a mitotic, possibly stable, and endocrine-biased progenitor intermediate, due to the relatively rare nature of these cells, especially as secondary transition progressed, we concluded that new tools and approaches were needed to study this prospectively novel progenitor population. Studies in this direction were carried forward in detail by Dr. Matt Bechard in the lab. The subsequent analyses of endocrine progenitor dynamics presented here will now shift focus toward understanding the dynamics of the endocrine commitment step in endocrine birth during the major mid-gestational wave of differentiation, and how endocrine commitment is balanced with growth and maintenance of the Sox9^{+} progenitor pool during secondary transition.

In vivo endocrine-progenitor dynamics and establishment of the Neurog3 to Sox9 ratio

In order to quantify and parameterize the balance between progenitor maintenance and endocrine differentiation during secondary transition, we devised a method, based on the ratio of [differentiating Neurog3$^+$ cells]:[Sox9$^+$ epithelial cells], to quantify the relative flux from the Sox9$^+$ trunk towards the Neurog3$^+$ endocrine lineage. Sox9 expression is lost upon upregulation of Neurog3 [30,31]. The transient upregulation of Neurog3, in turn, indicates commitment to a

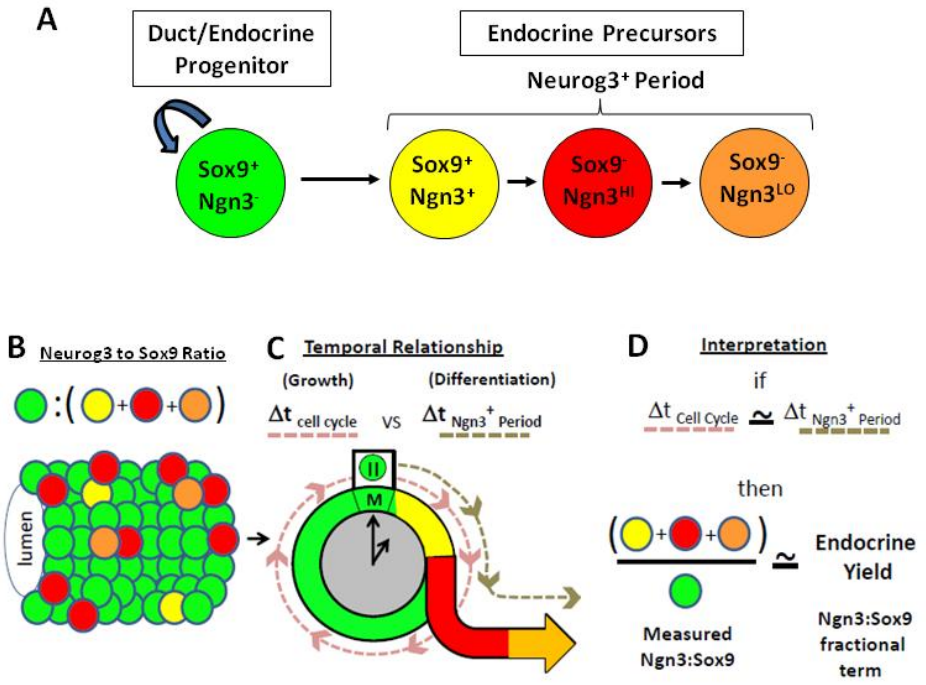

Figure 2.3. *The ratio of Neurog3$^+$ to Sox9$^+$ cells reflects the balance between endocrine differentiation and progenitor growth. (A) Lineage diagram showing the progression, from replicating Sox9$^+$ progenitor status, through sequential Neurog3$^+$ states during endocrine-lineage commitment. Neurog3 and Sox9 co-expression in the epithelium (Sox9$^+$Neurog3$^+$) defines the initial Neurog3$^+$ state, followed by high levels of Neurog3 during delamination (Sox9$^-$Neurog3^{HI}), and finally Neurog3 down-regulation (Sox9$^-$Neurog3^{LO}) in committed endocrine cells. (B-D) Derivation of endocrine yield, a quantitative descriptor of endocrine-lineage flux from the epithelium, based on a measured ratio of Neurog3$^+$ and Sox9$^+$ cell states. (B) Theoretical segment of the trunk-epithelium with a representative distribution of Sox9$^+$ and Neurog3$^+$ cell states. (C) The Neurog3:Sox9 ratio observed at a given sampling time is determined by the temporal relationship between the Sox9$^+$ cell-cycle period (growth parameter) and the duration of the Neurog3-positive period of endocrine commitment (differentiation parameter). (D) Provided comparable time-frames for these two parameters, endocrine yield can be determined by converting the Neurog3:Sox9 ratio into a fractional representation reflecting the number of cells maintaining replicative Sox9$^+$ cell status, versus differentiating Neurog3$^+$ status, in a defined epithelial segment at a given time. This figure was adapted from [211].*

post-mitotic endocrine-precursor state [16,83] (Fig. 2.3A). The Neurog3:Sox9 observed at a given time, therefore, is largely determined by the temporal relationship between 1) the average cell-cycle period of the $Sox9^+$ population (epithelial growth/maintenance), and 2) the average duration of the $Neurog3^+$ period of endocrine commitment (differentiation) (Fig. 2.3B,C). Provided the time frames for these parameters are comparable, the Neurog3:Sox9 ratio reflects the magnitude of endocrine differentiation (endocrine flux) from the trunk. To validate the Neurog3:Sox9 ratio, we adapted EdU pulse-chase methods [155] to measure and relate progenitor-replication and endocrine-differentiation parameters *in vivo* (Fig. 2.3D).

Dividing $Sox9^+$ populations progress continuously through an estimated 12-hour cell-cycle period

When $Sox9^+$ cells enter mitosis, we invariably observe sub-cellular segregation of Sox9 immunoreactivity away from condensed, $DAPI^+$ DNA. These $Sox9^+$ mitotic figures (MF) are EdU^+ in cells that have recently undergone S-phase (Fig. 2.4A-C). To quantify the average cell-cycle period, we timed the appearance and disappearance of pulse-administered EdU within the $DAPI^+$ DNA of $Sox9^+$ progenitors as they passed though rounds of mitosis (Fig. 2.4G) [156]. Because EdU bioavailability after single-pulse administration is short (distribution half-life 1.4 ± 1.7 min., elimination half-life 24 ± 2.9 min. at 100 mg/kg, [157]), and because the MF state represents a short, transient event during the cell-cycle, this method estimates cell-cycle periods at a population level.

In the $Sox9^+$ epithelium, S-phase indices determined after one-hour EdU-pulse are similar at E14.5, E16.5, and E18.5 (22 ± 2.7%, 16 ± 3.2%, and 16 ± 1.8%, respectively) (Fig. 2.4D-F). We chose stage E14.5 for a 24-hour EdU pulse-chase analysis of the $Sox9^+$ cell-cycle period. All $Sox9^+$ MF were EdU^- one hour after EdU pulse, (Fig. 2.4H), indicating that cells incorporating EdU at S-phase had not yet entered M-phase. At 2 hours, the percentage of $Sox9^+EdU^+$ MF remained unchanged, as did the S-phase index in the $Sox9^+$ population, consistent with a ≤ 1 hour bioavailability of EdU under these conditions. Between 2-3 hours after EdU pulse, essentially all of the detected $Sox9^+$ MF became EdU^+ (75.3 ± 2.7% at 2 hrs, 98.3 ± 2.5% at 3 hrs), consistent with an asynchronously cycling $Sox9^+$ population incorporating EdU at different periods along the duration of S-phase, then proceeding over time into mitosis. EdU saturation

in the Sox9$^+$ MF was maintained for approximately 5 hours, before decreasing essentially to 0% between the 8-13 hour period (6.3 ± 2.5% at 8 hrs, 0 ± 0% at 12 hrs, 1.7 ± 2.6% at 13 hrs), consistent with the EdU$^+$Sox9$^+$ population completing M-phase of the cell cycle. Subsequent time points (13-15 hrs) showed rapid and saturating re-entry of EdU$^+$ DNA in Sox9$^+$ MF. After this population passed through mitosis (indicated by a second reduction in EdU-positivity in Sox9$^+$ MF), a third M-phase was detected at 24 hours. At late time points, EdU saturation of the Sox9$^+$ MF population was shorter in duration, reflecting an expected DNA replication-dependent dilution of EdU-signal. These results demonstrate that EdU pulse-chase reproducibly detects a labeled portion of the Sox9$^+$ population moving through three consecutive and largely coherent cell-cycle periods with average ~11.3 ± 0.68 hr time intervals.

Endocrine-committing populations take an average of 12 hours to move through the Neurog3$^+$ state

To determine the average duration of the Neurog3$^+$ period of endocrine commitment, we used EdU pulse-chase to monitor EdU$^+$ DNA, from initial incorporation in the replicating Neurog3$^-$ Sox9$^+$ progenitors, through marker-defined, chronological stages of endocrine commitment (Fig. 2.5A-A'') [56]. These include the initial trunk-resident Sox9$^+$Neurog3$^+$ state, the post-delamination Sox9$^-$Neurog3^{HI} state, and the late Sox9$^-$Neurog3^{LO} state [30,31,32]. The baseline EdU$^+$ index in all Neurog3$^+$ states at one hour EdU pulse was ~1%, consistent with their largely post-mitotic status. At two hours EdU pulse, the percentage of Sox9$^+$Neurog3$^+$EdU$^+$ cells remained unchanged (Fig. 2.5F), indicating that Sox9$^+$Neurog3$^-$ cells incorporating EdU at S-phase had not yet progressed into the initial Sox9$^+$Neurog3$^+$ state. At three hours we observed an accumulation of EdU$^+$ DNA in the Sox9$^+$Neurog3$^+$ population. At 6 hours, the EdU$^+$ index in Sox9$^+$Neurog3$^+$ cells reached 22 ± 2.7%; as expected, because this quantity reflects the baseline EdU$^+$ index in Neurog3$^-$Sox9$^+$ progenitors from which Neurog3$^+$ cells arise. Similar accumulation of EdU in the Sox9$^-$Neurog3^{HI} state reached 22% at 10 hours, followed by the late Sox9$^-$ Neurog3^{LO} state at 15 hrs (Fig. 2.5B,C). Finally, at 17 hours, EdU$^+$ DNA was detected in Pdx1^{HI}Neurog3$^-$ cells, which represent a state (likely β-cell, the principle cell type produced at this stage) arising after downregulation of Neurog3 [52,55] (Fig. 2.5D,E; Fig. 2.6A-F). By

measuring the time difference (Δt) between the curves demarcating early and late Neurog3^{+} state (between Sox9^{+}Neurog3^{+} and Sox9^{-}Neurog3^{LO}), bounded within the range defining the minimum and maximum baselines for EdU-incorporation in the Neurog3^{-}Sox9^{+} and

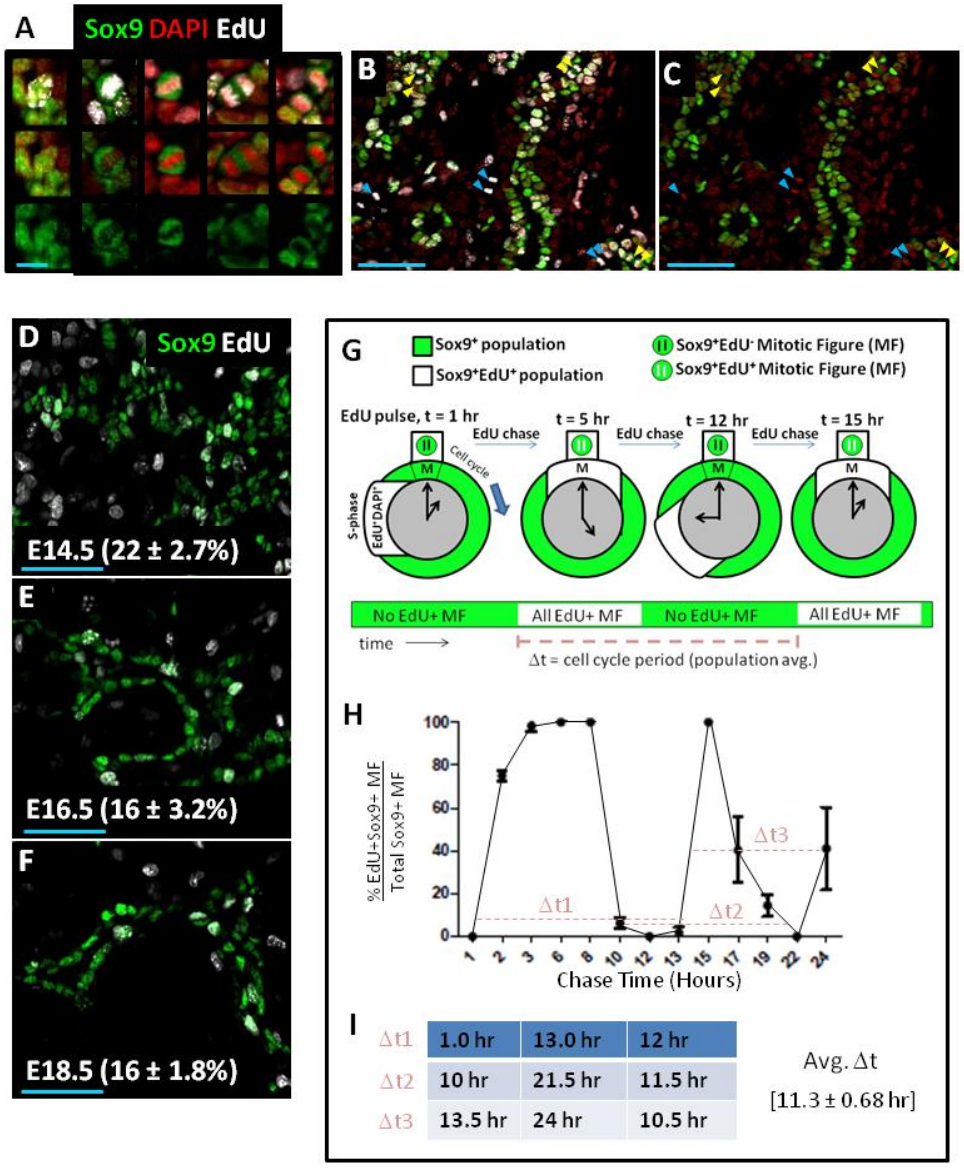

Figure 2.4. *EdU pulse-chase analysis measures average cell-cycle period in Sox9^{+} cells. (A) Individual Sox9^{+}EdU^{+} cells captured before and during mitosis (left to right; Sox9^{+} cell not in mitosis, mitotic figures (MF) in prophase, metaphase, anaphase, and cytokinesis). Scale bar 10 μm. (B,C) MF observed in representative 20x field at E14.5, 3 hours post-EdU injection. Sox9^{+}EdU^{+} MF (yellow arrowheads), Sox9^{-}EdU^{+} MF (cyan arrowheads), MF after DNA segregation into daughters (doublet arrowheads). Scale bars 50 μm. (D-F) One hour S-phase indices are similar from E14.5-E18.5. Scale bar 50 μm. (G) Diagram of EdU pulse-chase in replicating Sox9^{+} populations. Sox9^{+} cells undergoing S-phase are labeled by EdU. EdU^{+}Sox9^{+} populations (white) undergo and complete mitosis (t = 5 hrs), before undergoing subsequent round of mitosis (t = 12-15 hrs). Rounds of mitosis can be tracked by monitoring*

waves of EdU-positivity in the Sox9$^+$ MF states (green and white bar over time). Δt's are determined from intervals between waves of EdU+ MF. (H) 24 hour EdU pulse-chase analysis of cell-cycle period in Sox9$^+$ populations, with Δt's represented in dashed light red line. (I) Calculation of avg. Δt from pulse-chase measurements in H. Error bars are S.E.M. This figure was adapted from [211].

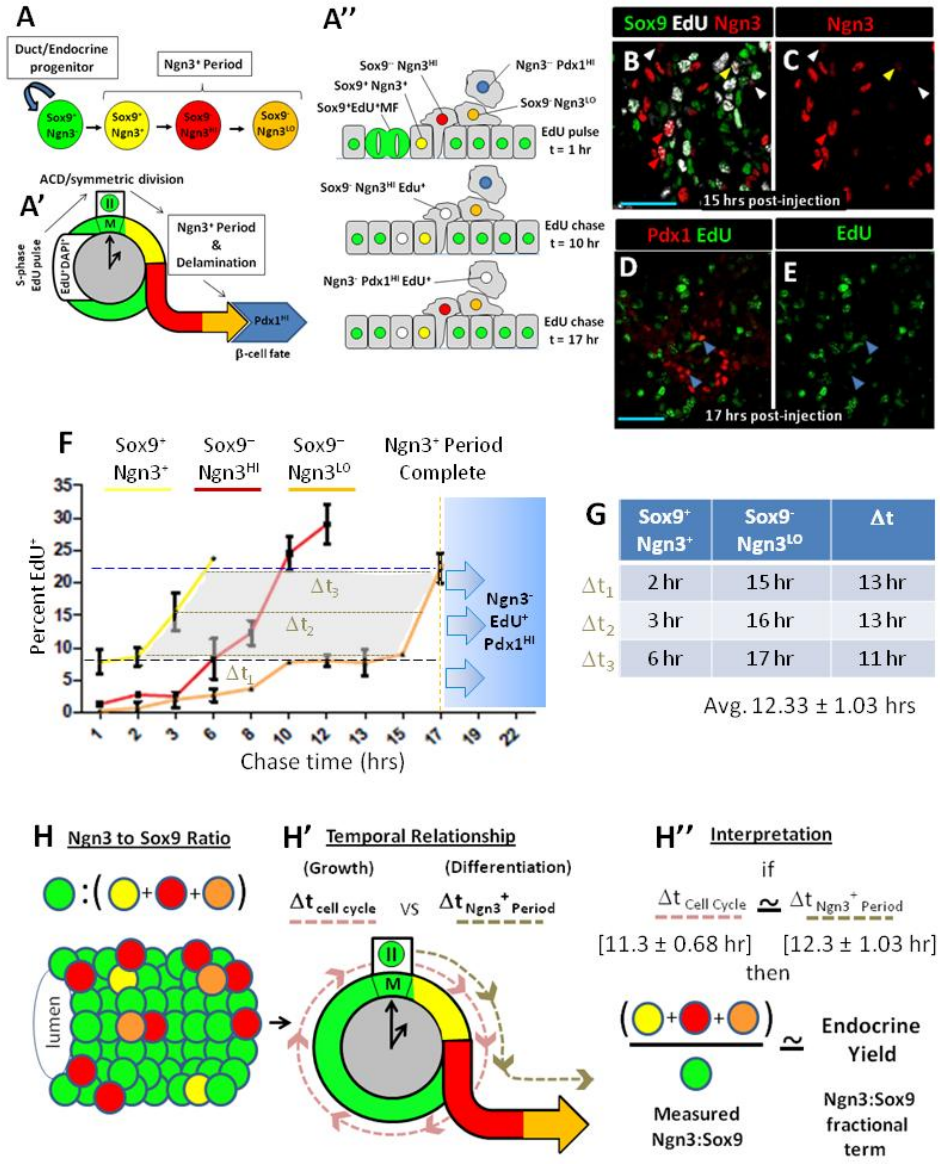

Figure 2.5. *EdU pulse-chase measures duration of the Nuerog3$^+$ period of endocrine commitment. (A-A'') Pulsed-EdU is incorporated in Sox9$^+$ cells at S-phase, and chased (EdU$^+$ DNA in white) through marker-defined stages of Neurog3-positivity. (B,C) EdU captured in cells of various Neurog3$^+$ states. Early Sox9$^+$Neurog3$^+$ cells (yellow arrowheads), Sox9$^-$Neurog3^{HI} cells (red arrowheads), late Sox9$^-$Neurog3^{LO} cells (white arrowheads). (D,E) EdU in Neurog3$^-$Pdx1^{HI} cells (blue arrowheads). (F) Time-course for EdU pulse-chase analysis of the Neurog3$^+$ period. Graph indicates percentage of EdU$^+$ cells in Sox9$^+$Neurog3$^+$ (yellow line), Sox9$^-$Neurog3^{HI} (red line), or Sox9$^-$*

Neurog3^{LO} (orange line) states at time points indicated. Blue dashed line shows one-hour EdU-incorporation baseline for Sox9^{+}Neurog3^{-} cells (22 ± 2.7%). Black dashed line, one-hour EdU-incorporation baseline for Sox9^{+}Neurog3^{+} cells (8.5 ± 2.8%). Blue shading with arrows indicates the period when EdU^{+} DNA becomes increasingly observed Neurog3^{-}Pdx1^{HI} populations (indicating end of Neurog3^{+} period). Grey shaded area, the domain and range of data points used to estimate the Neurog3^{+} period. (G) Calculation of ⊿t (brown dashed lines in F) from the lines demarcating Sox9^{+}Neurog3^{+} and Sox9^{-}Neurog3^{LO} cell states. Error bars, standard deviations (N=3 pancreata). (H-H'') Derivation of endocrine yield as a quantitative measure of the relative magnitude of endocrine differentiation from the trunk domain. This figure was adapted from [211].

Sox9^{+}Neurog3^{LO} cell states (Fig. 2.5F, grey shaded area, Sox9^{+}Neurog3^{+} ≤ y ≥ Neurog3^{-}Sox9^{+}), these data indicate an average duration of ~12.3 +/- 1.03 hrs (Fig. 2.5G) for the Neurog3^{+} period of endocrine commitment (Fig. 2.7).

These analyses indicate that the Sox9^{+} cell-cycle period and the duration of the Neurog3^{+} period of endocrine commitment are similar (11.3 ± 0.68 hrs and 12.3 +/- 1.03 hrs, respectively). Therefore, the Neurog3:Sox9 ratio estimates quantitatively the relative magnitude of endocrine differentiation occurring from the trunk at a given sampling time. For simplicity, we convert Neurog3:Sox9 hereafter to the fractional term "endocrine yield" (given as total Neurog3^{+} cells/total Sox9^{+} cells) (Fig. 2.5H-H'').

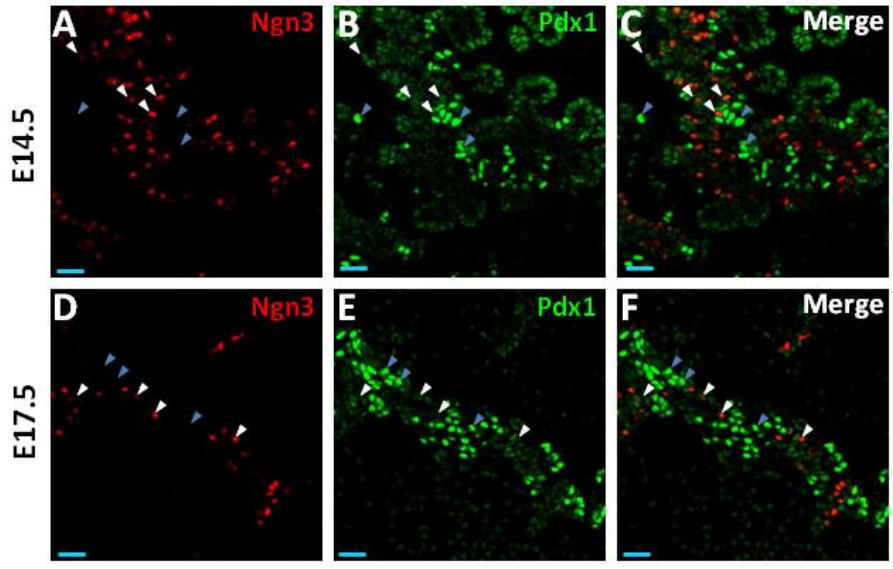

Figure 2.6. *Neuorg3 is down-regulated before acquisition of Pdx1^{HI} status. (A-F) Immuno-detection of Neurog3 and Pdx1 in cryosections at indicated stages. The vast majority of Neurog3^{+} cells co-express low levels of Pdx1 (white arrowheads). Low levels of Pdx1 are also observed in the Neurog3^{-} epithelium (yellow arrowheads in C,F). Pdx1^{HI} cells do not co-express Neurog3 (blue arrowheads). Scale bars are 20 μm. This figure was adapted from [211].*

	Sox9^{+} MF	Sox9^{+}Ngn3^{LO}	Sox9^{-}Ngn3^{HI}	Sox9^{-}Ngn3^{LO}
1 hour	76 (n=3)	307 (n=3)	462 (n=3)	227 (n=3)
2 hour	93 (n=3)	234 (n=3)	402 (n=3)	265 (n=3)
3 hour	71 (n=3)	181 (n=2)	259 (n=2)	189 (n=2)
6 hour	74 (n=3)	367 (n=3)	404 (n=3)	235 (n=3)
8 hour	105 (n=3)	445 (n=3)	469 (n=3)	340 (n=3)
10 hour	186 (n=3)	197 (n=2)	387 (n=3)	328 (n=2)
12 hour	90 (n=3)	232 (n=3)	452 (n=3)	216 (n=3)
13 hour	55 (n=3)	391 (n=3)	344 (n=3)	244 (n=3)
15 hour	190 (n=3)	510 (n=3)	719 (n=3)	602 (n=3)
17 hour	142 (n=3)	ND	535 (n=3)	507 (n=3)
19 hour	69 (n=2)	ND	ND	78 (n=2)
22 hour	25 (n =3)	ND	ND	151 (n=3)
24 hour	62 (n=3)	ND	ND	247 (n=3)

Figure 2.7. *Absolute numbers of Sox9^{+} mitotic figures and Neurog3^{+} cell states evaluated during EdU pulse-chase time-course analyses. "n" indicates the number of pancreata sampled for each time point. This figure was adapted from [211].*

Endocrine yield is robust throughout the secondary transition

Previous measurements from whole pancreas mRNA, or from limited quantifications of Neurog3^{+} cell numbers, suggest that endocrine birth peaks around E14.5-E15.5, and reduces thereafter [55,78,158]. However, these measurements do not take into account the direct relationship between cells undergoing endocrine-lineage commitment (Neurog3^{+}) versus maintenance and growth as Sox9^{+} progenitors. To address this, we quantified endocrine yield in sections representing ~33% of the dorsal pancreas, from E14.5-18.5 stages, as a bulk measure of endocrine differentiation dynamics. We detected essentially a constant endocrine yield throughout E14.5-17.5 stages; this trend reversed, relatively sharply, only at E18.5 (Fig. 2.8A-I). At all time points, we detected no significant change in the relative number of early (Neurog3^{+}Sox9^{+}) versus late (Neurog3^{+}Sox9^{-}) endocrine committing cell-states, indicating that new endocrine cells are being generated at all stages (Fig. 2.8J). These results show that Sox9^{+} trunk populations continuously allocate a large fraction of their progeny toward the endocrine lineage over essentially the entire mid-to-late gestational period.

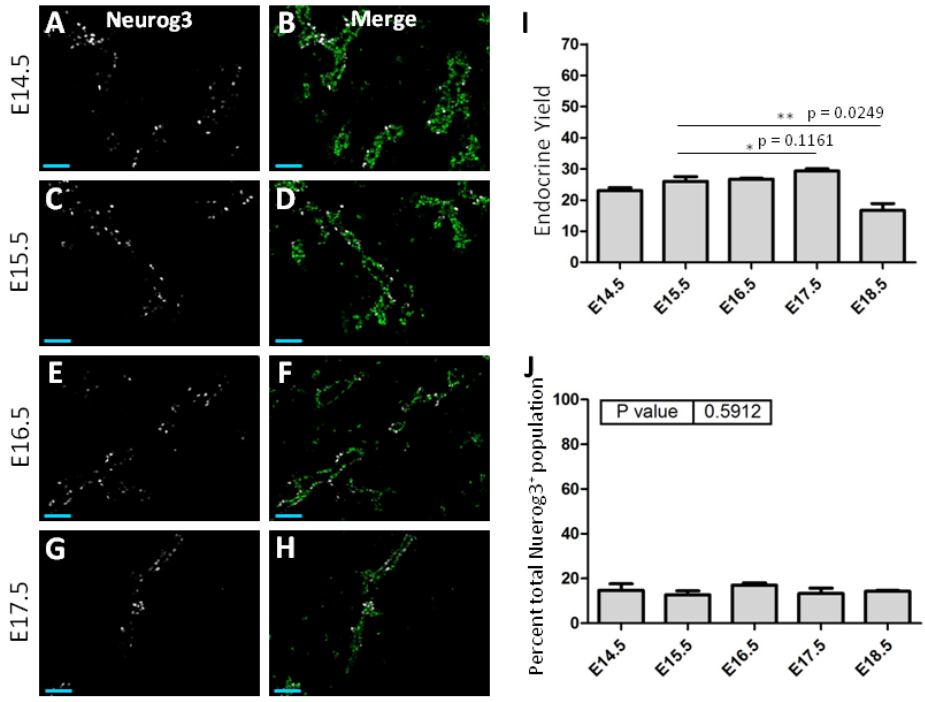

Figure 2.8. *Endocrine yield is robust at all stages of the secondary transition. (A-H) Representative images (E14-15.5) of Sox9^{+} and Neurog3^{+} populations at stages indicated. Later stage (E16-17.5) images focus on epithelium where Neurog3^{+} cells are being born in large numbers. Scale bars are 50 μm. (I) Bulk endocrine yield determined by sectional analysis of secondary transition stages. 33% of n = 3 dorsal pancreas analyzed at each stage. Error bars are S.E.M, (*) p=0.1161, (**) p=0.0249. Student's t-test. (J) Distribution of early (Sox9^{+}Neurog3^{LO}) and late (Sox9^{-} Neurog3^{+}) cell states among all Neurog3^{+} cells at indicated stages. Error bars are S.E.M for n = 3 pancreata at each stage, 30% of total pancreas analyzed. No statistical difference was detected at any stage (p = 0.5912, one-way Anova). This figure was adapted from [211].*

Evidence for asymmetric and terminal differentiation from individual trunk progenitors in vivo

Next, we wanted to understand how endocrine lineage allocation and progenitor maintenance might be regulated at the level of individual differentiation events. Our EdU-pulse chase data suggested that acquisition of the Neurog3^{+} state occurs shortly (2-4 hrs) after EdU incorporation in Sox9^{+} progenitors, suggesting the endocrine commitment occurs in close association with cell division. One interesting observation that we made was that, at 6 and 10 hour after EdU pulse-chase, we frequently observed EdU^{+}Sox9^{+}Neurog3^{+} and EdU^{+}Sox9^{-} Neurog3^{+} cells, respectively, differentiating as Neurog3^{+} neighboring cell-pairs. This suggested that one cellular mechanism for endocrine lineage allocation is to send both daughters, via

symmetric terminal differentiation, into the endocrine lineage after division (Fig. 2.9A-F). Consistent with this notion, we observed that the peak representation of EdU in the Sox9^{+}Neurog3^{+} state at 10 hr, and the Sox9^{-}Neurog3^{+} state at 17 hr, post pulse-chase approached double the baseline incorporation index observed in the Sox9^{+}Neurog3^{-} progenitor population from which these cells arise (40% for Sox9^{+}Neurog3^{+} at 6 hours, and 35% for Sox9^{-} Neurog3^{+} at 10 hours versus 22% of Sox9^{+}Neurog3^{-} progenitors at 1 hour; Fig. 2.9G). This quantitative relationship (% EdU in Neurog3^{+} populations is ~2x > % baseline EdU in Sox9^{+} progenitors) provides additional evidence that a prevalent lineage allocation behavior for Sox9^{+} progenitor cells is to generate more than one Neurog3^{+} daughter cell after division.

We next utilized an independent mosaic lineage tracing system to trace, in acute time frames, individual Sox9^{+} progenitors as they allocate Neurog3^{+} progeny. Using this method, we could provide evidence that neighboring pairs of Neurog3^{+} cells were indeed being derived from symmetric, terminal lineage allocation from a common Sox9^{+} trunk progenitor. We crossed *Rosa*26.RYFP mice [159] with mice bearing a *Sox9*$^{CreER(T2)}$ BAC-transgene [15], administered low doses of Tamoxifen (0.03 mg) to pregnant dams at E12.5 or E14.5, and harvested *Sox9*$^{CreER(T2)}$;*Rosa*26$^{RYFP/+}$ embryos 36-48 hours later. Samples were immuno-labeled for Sox9, Neurog3 and YFP, and confocal Z-stack volumes were acquired in regions of highly mosaic labeling patterns (Fig. 2.9H-I). Despite significant variations in the labeling frequency within and between samples, we observed evidence for three prevalent behaviors in YFP-labeled cells. The majority of YFP^{+} cells were maintained in the Sox9^{+} epithelium as dividing, Neurog3^{-} populations (not shown). We also observed frequent Neurog3^{+}YFP^{+} cells that were differentiating in isolation from other YFP^{+} cells, suggesting that Sox9^{+} cells can give rise to Neurog3-expressing progeny without undergoing a recent division event. We also frequently observed Neurog3^{+}YFP^{+} cells differentiating next to individual Neurog3^{-}YFP^{+} cells, suggesting that a cell had divided, and only one of the daughter cells had turned on Neurog3. Finally, we also observed frequent YFP^{+}Neurog3^{+} cells differentiating as neighboring cell pairs. Analysis of the percentage of total Neurog3^{+}YFP^{+} cells differentiating as neighboring cell-pairs suggests that a substantial portion (~60%, N=26 at E14.5, N = 157 at E16.5) of endocrine cells are allocated through symmetric terminal differentiation, while the remainder is allocated via direct

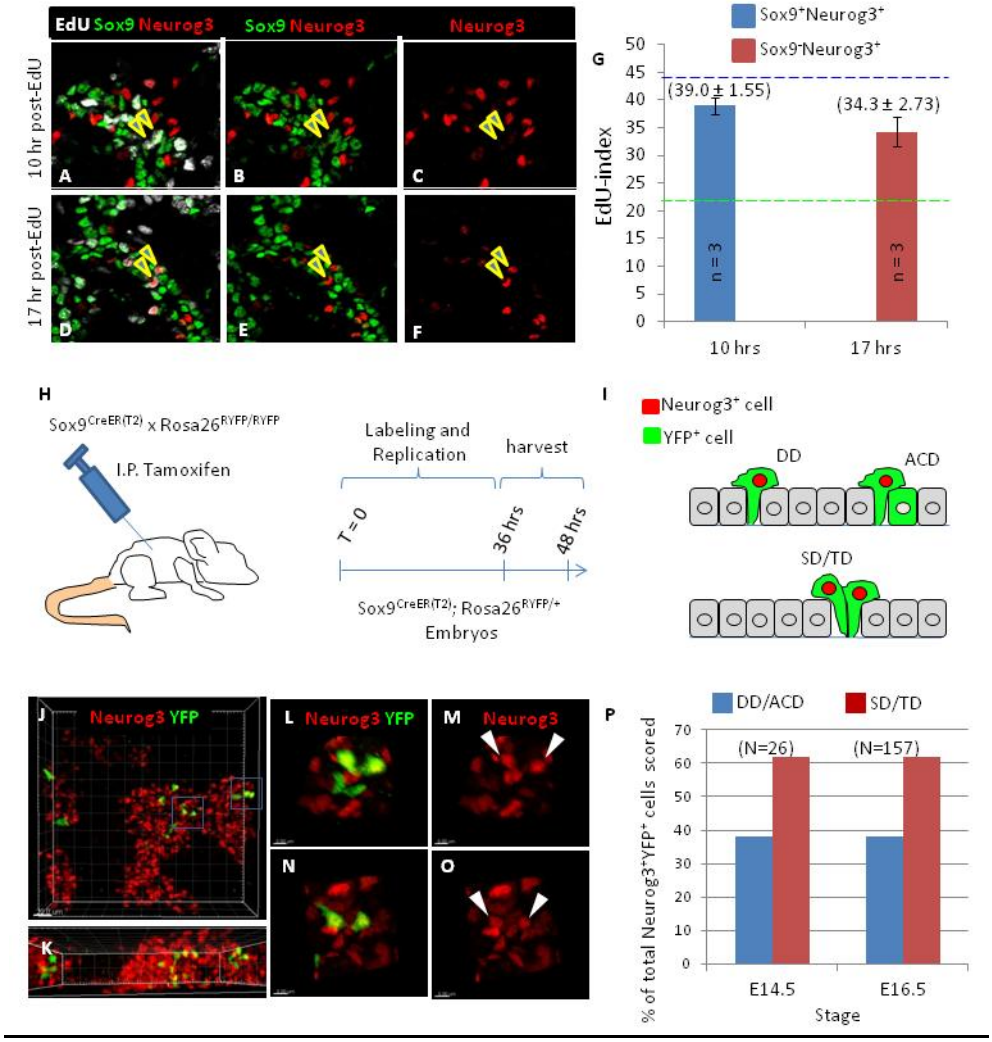

Figure 2.9. *Acute mosaic lineage tracing confirms prevalent asymmetric and terminal differentiation behavior in replicating Neurog3$^+$ populations. (A-F) Detection of paired EdU$^+$Neurog3$^+$ progeny during EdU pulse-chase time-course. (G) Quantification of the peak EdU-labeling index attained in the Sox9$^+$Neurog3$^+$ and Sox9$^-$Neurog3$^+$ cell states during EdU pulse-chase time-course. Green dashed line indicates the theoretical peak EdU-labeling index expected for an "isolated and direct terminal differentiation" model. Blue dashed line indicates the theoretical peak EdU-labeling index expected for a "paired terminal differentiation" model. (H) Genetic lineage tracing system and tamoxifen administration strategy for acute analysis of "isolated" and "paired" terminal differentiation of Neurog3$^+$ cells. (I) Diagrammatic representation of possible lineage tracing outcomes supporting direct terminal differentiation, asymmetric terminal differentiation (ACD), and paired terminal differentiation models of endocrine cell birth. (J-O) Typical acute mosaic lineage labeling patterns discerned in 3D volumes of pancreatic epithelium labeled with Neurog3. YFP, and Sox9 (Sox9 not shown). (P) Quantification of the incidence of isolated and paired differentiation events at time points representative of the secondary transition (E14.5 and E16.5, respectively).*

differentiation or asymmetric cell division. While there are a number of important caveats to these interpretations (namely, we do not know exactly when in reference to a cell division event a given cell became reporter^{+}), our collective observations suggest that while the individual lineage allocation behaviors of Sox9^{+} trunk progenitors appear to vary, two prevalent modes of endocrine lineage allocation occur during endocrine cell birth. These include a terminal, symmetric differentiation of both daughter cells, and asymmetric allocation of only one daughter cell, toward the Neurog3^{+} state, in close association with a cell division event.

Discussion

The genetic regulation of endocrine differentiation by the transcription factor Neurog3 and the signaling mechanisms (such as Notch) that balance differentiation with pancreatic progenitor maintenance have long been established. To date, however, there is little to know understanding of the physiological parameters that underlie the regulated progression of pancreatic progenitors into the endocrine lineage during the secondary transition. As a result, there are major gaps in our understanding of the diversity of possibly functionally distinct progenitor states existing in the epithelium, how cell-type heterogeneity and organization develop over time, and how in quantitative terms the flux toward differentiated lineages is balanced with an appropriate growth of the pancreatic progenitor pool. We describe a novel replicating cell state that expresses low levels of the endocrine lineage determinant Neurog3, that is enriched during early stages (E12.5) of trunk domain formation, and that represents a candidate endocrine-biased and replicating progenitor pool. Subsequently (E14.5 and after), endocrine lineage commitment is continually robust and surprisingly long-lived in the trunk, with an estimated one-quarter to one-third fraction of progenitors being allocated to the endocrine lineage (Neurog3^{HI}) every twelve hours. This endocrine lineage flux is balanced with an estimated 12-13 hour cell cycle in the Sox9^{+} cells that remain behind in the epithelium. Finally, we provide evidence that individual Sox9^{+} progenitors grow and differentiate through various cellular mechanisms; these include symmetric renewing divisions, asymmetric divisions, and symmetric terminal differentiation behaviors. These findings begin to parameterize the

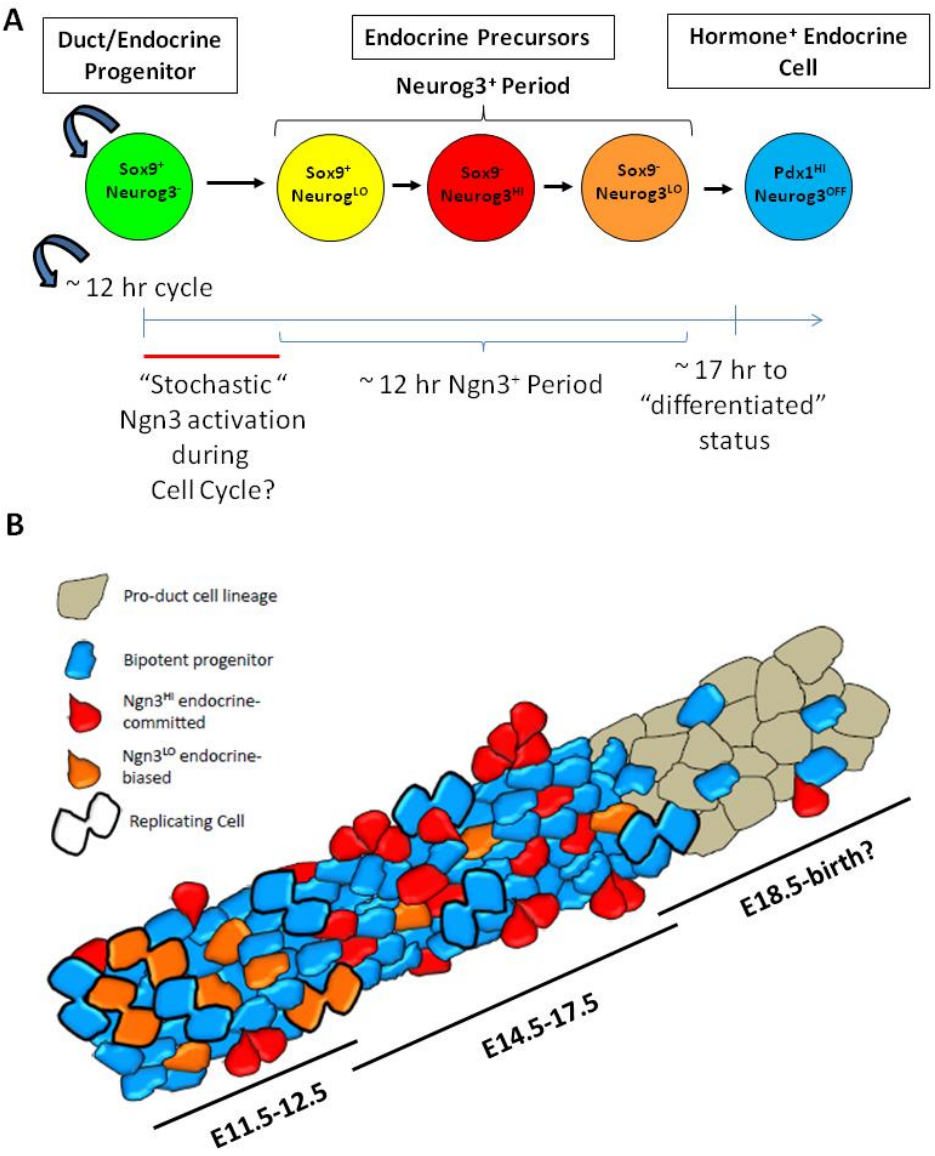

Figure 2.10. *Model for in vivo endocrine progenitor dynamics during the pancreatic secondary transition. (A) Lineage diagram on population averages of temporal parameters for progenitor replication and endocrine lineage allocation. Red line indicates the period of time between a progenitor cell's last division event and activation of Neurog3. This period appears to be short (2-6 hrs) in the majority of cells traced in our analyses. However, the appreciable mitotic index in Neurog3^{LO} cells (especially at E12.5) is suggestive of an inverse relationship between cell cycle rate and likelihood for Neurog3 activation. (B) Model for endocrine progenitor dynamics as a function of time. Various cell states analyzed and quantified are shown. Separate time-frames are indicated by black line and labeled accordingly. Each time frame is an independent "snapshot" of the prevalent progenitor behaviors representing prevalent progenitor behaviors occurring over a roughly ~12 hr time-frame.*

dynamic flux of endocrine cells from the trunk epithelium during the major wave of cellular differentiation in the pancreas (Fig. 2.10).

Our observations that Neurog3^{+} cells in the Sox9^{+} epithelium incorporate thymidine analogues at S-phase, and exhibit mitotic behavior as indicated pHH3 co-localization, puts forth several possibilities with respect to how the process of endocrine lineage allocation may progress during development. The observation that at E12.5 nearly half of the Neurog3^{+} population is found in the Sox9^{+} epithelium in a Neurog3^{LO} expressing state, suggests that at early stages of secondary transition, there may be maintained within the epithelium a replicating and "pre-endocrine-committed" Neurog3-expressing cell state. This idea is consistent with lineage tracing experiments utilizing a Nueorg3^{Cre} BAC transgene, which showed that a small but significant number of Nuerog3-expressing can adopt non-endocrine lineages during normal organogenesis [68]. Interestingly, this plasticity in the Neurog3-expressing lineage depends greatly on a cell's ability to upregulate Neurog3 to high levels [69], suggesting that there may be intrinsic or extrinsic mechanisms that regulate the progression of cells through OFF-LO-HI states of Neurog3 expression. The notion that the Neurog3^{LO} state maintains replicative potential suggests that they may represent a mitotic progenitor state that is amplifying an endocrine biased progenitor pool during early stages of pancreas formation. It remains possible that the analyses presented here, which focus on detection of Neurog3 protein in snapshot time frames, might in fact under-represent the size of this proposed endocrine-biased progenitor population. For instance, limitations in our ability to detect very low amounts of protein by immunodetection, or the idea that Neurog3 protein levels may oscillate in this pre-committed condition, might be addressed with the use of more sensitive lineage tracing tools and transciptional reporter alleles. Indeed, oscillations in Notch pathway effectors such as Hes7 [160] and Hes1 [161] are known to be important for regulating differentiation and progenitor maintenance in a number of biological systems, and in many respects act through repression of differentiation factors such a *Neurogenin* [162].

Previous analyses on the dynamics of endocrine lineage allocation during secondary transition have suggested that there exists a definitive peak in endocrine differentiation around E14.5-

E15.5 [55,78,158]. The analyses that have been performed, however, were not rigorously quantified, or have not been normalized in a way that allows for specific conclusions to be made as to when the highest absolute numbers of cells are being born, or when the highest period of flux from the epithelial progenitor pool occurs. We have established and validated a simple metric that estimates the proportion of epithelial progenitors adopting the endocrine committed state at a given sampling time. This metric, the Neurog3-to-Sox9 ratio, normalizes the number of endocrine cell being born to the number being left behind in the $Sox9^{+}$ epithelium, and in this manner can be used to quantify differentiation dynamics with increased precision, both in spatial and temporal terms. Here we have found that the magnitude of endocrine differentiation from the trunk domain is relatively constant over the course of secondary transition, and does not become reduced until E18.5. The idea that the trunk domain can stably and continually allocate a large fraction of its cellular mass toward the endocrine lineage could reflect that there are mechanisms in place that maintain a precisely balanced optimum flux of endocrine progenitors from the progenitor pool within this tissue. As such, future investigations should attempt to elucidate the feedback and/or feed-forward regulatory mechanisms that define this quantitative balance, and how they contribute to the regulation of organ size and cellular composition.

Cell labeling and lineage tracing approaches represent powerful approaches in studying the cellular mechanisms through which progenitor populations give rise to differentiated progeny, yet each method comes with its own advantages and limitations. With regards to Cre and CreER-based lineage tracing, for instance, the uncertainty regarding when an individual cell has activated a lineage label makes it difficult to interpret how a given cell moves through a process, which in the case of endocrine lineage allocation, appears to occur through various means. The use of reporter based knock-in alleles has overcome these difficulties to some extent, especially where a given developmental processes can be monitored in real-time *in vitro*. Relating parameters measured via *in vitro* live imaging to those occurring *in vivo,* however, remains a major limitation to this type of analysis. Finally, EdU pulse-chase analyses have been used to monitor the replication and cell-cycle properties of progenitor populations, both *in vivo* and *in vitro*, but are limited in their ability to quantify the timing and specific

behaviors underlying cellular differentiation behaviors due to the non-specificity of thymidine analog labeling (i.e. any replicating cell population will become labeled), and the requirement that scoring of labeled populations be done in fixed tissues. Thus, in order to gain quantitative insights into how progenitor growth and differentiation behaviors are balanced during organ formation *in vivo*, it is necessary to utilize and cross-reference different cell-tracing approaches in parallel. We have leveraged the high temporal resolution enabled by a short bioavailability of EdU [157], a known injection time, and a set of directly detected and marker defined states that arise during progenitor replication and endocrine commitment to carry out a population-based analysis of endocrine differentiation and progenitor growth dynamics during secondary transition. We estimate approximately 12 hours for both the cell-cycle period and Neurog3 expression period *in vivo*, and a time frame of roughly 17 hours for an average cell to undergo its last S-phase in the epithelium and then to acquire differentiated endocrine cell status. Consistent with recent reporter-based single-cell live-imaging analyses in explants [163], the rapid EdU acquisition in Neurog3^{+} populations indicates that a large portion of endocrine-committing cells acquire Neurog3-immunoreactivity shortly after a division event. The single-cell live-imaging experiments carried out previously in explants did, however, report an average cycling time of 24 hours (instead of 12 hours in our case), which we would propose is likely due to reduced replication rates for progenitor cells in explanted culture systems. Indeed, our unpublished observations suggest that the increase in organ size observed in explants in culture does not match that which is observed in the same time frame *in vivo*. Our estimate of the time it takes to give rise to hormone producing endocrine cells are also in line, but perhaps more precisely temporally resolved, with what has been shown using Neurog3 reporter and Neurog3^{CreER} alleles *in vivo* [164,165]. Our mosaic lineage tracing analyses are well in line with previous live imaging analyses in explants, which have shown that endocrine cells are born through a prevalent symmetric terminal differentiation process, asymmetric differentiation after division, and a less well characterized direct differentiation that does not appear to involve a cell fate acquisition during, or in close association with, a cell division event. These same studies also provided evidence for a rare population of Neurog3-expressing cells that are capable of undergoing cell division [163]. Thus, a bigger picture is emerging from these various

analyses that suggest that there are likely to be many complex mechanisms in place to guide the progression of cells from an undifferentiated progenitor state through to a differentiated endocrine cell. We propose that future studies on the genetic and signaling-based regulation of endocrine differentiation should undertake a cautious consideration that the outcome of a given experimental manipulation may reflect cell-type and context-specific effects depending on the developmental state of a cell within the progenitor epithelium.

Acknowledgements

We thank the Vanderbilt Cell Imaging Shared Resource for training and access to equipment and image-processing software. Imaging scholarships were from the VUMC DDRC, DRTC and VICC [supported by NIH grants CA68485, DK20593, DK58404, DK59637]. We thank Anna Means, Guoqiang Gu, and members of the Wright/Gu labs for discussions. This study was supported by the National Institutes of Health (1UO1DK089570-01).

CHAPTER III

EXPERIMENTAL MODELS FOR CONDTIONAL CONTROL OF ENDOCRINE DIFFERENTIATION

Introduction

While the genetic and signaling mechanisms that balance progenitor maintenance and cell fate allocation during development are relatively well studied, how progenitor growth, differentiation, and morphogenesis processes are coordinated during organ formation remain obscure. This gap in our knowledge can be attributed to the challenges inherent in investigating how cell autonomously controlled processes non-autonomously influence various cell behaviors within a field of cells. Our goal is to develop experimental system(s) where the progression of cells into the *Neurog3*-expressing endocrine lineage (a cell autonomous process) can be conditionally and precisely manipulated, as a means to address larger questions about how the process of endocrine differentiation itself influences (cell non-autonomously) morphogenesis, cellular differentiation, and progenitor maintenance programs within the trunk. Here, we interrogate the cell-autonomous and non-autonomous functions of RBPJ in limiting endocrine differentiation from the trunk domain using conditional mosaic ablation of *RBPJ* with *Sox9*^{CreER}. We report our findings and discuss technical limitations that preclude use of this genetic system for our research aims. We design and test an alternative genetic strategy for mosaic and inducible ectopic Neurog3 expression, and present data showing the utility of this model for studying the nature and scale of *Neurog3*-dependent non cell-autonomous feedback within the trunk domain. Finally, we present our design and manufacture of a *Neurog3*$^{BAC\text{-}CreER}$ construct for controlled manipulations on the previously proposed Neurog3^{LO} endocrine-biased intermediate progenitor state. In sum, we propose new approaches and generate new tools that should be useful for studies on the molecular and genetic mechanisms controlling progression through the cell autonomous process of endocrine cell birth, and also on the underlying mechanisms linking this process to progenitor growth, differentiation, and morphogenesis processes through non-autonomous feedback communication.

Materials and Methods

Mice and Genotyping. Sox9^{CreER} mice were obtained from Maike Sander (UCSD). Primers used for genotyping were (5'HRsFr-ccttctcttccagagacttc and 5'HRsH-ctctggtcagagatacctgg; 780 bp) or (5'HRseqC- gcgatggatttccgtctctggtgtag and 5'HRseqD-gggtgctggacagaaatgtgtacact; 1080 bp). *RBPJ* floxed mice were a kind gift from Tasuko Honjo (Kyoto University). Primers used for genotyping were RBPJNeo-gcaatccatcttgttcaatggcc, RBPJF1-gcgtgcctccccgcatcta, RBPJwt1-gttcttaacctgttggtcggaacc, RBPJwt2- gcttgaggcttgatgttctgtattgc as described [191]. The *Rosa*26.lox.STOP.lox.rtTA.ires.GFP line was a kind gift from Mark Magnuson (Vanderbilt). Primers used for genotyping were (Rosa3-cgaggcggatacaagcaata, Rosa5-gagttctctgctgcctcctg, and RosaRTTA-aagaccgcgaagagtttgtc; Rosa3 & 5 = (wt) 322 bp, Rosa3 & RTTA = (knock-in) 215 bp). The *Rosa*26.Neurog3.CFP allele was also a kind gift from Mark Magnuson, and was genotyped with (Rosa26.S1-AGACTTATCTACCTCATAGGTG and CFPF-CAGCACGACTTCTTCAAG; 1209bp).

Immunodetection. Embryonic pancreas was paraformaldehyde-fixed (4%, 4^{o}C, 4-6 hours). For cryosectioning, samples were sucrose-equilibrated (30%; 4^{o}C overnight) and OCT-embedded (Tissue-Tek). Thin (10 μm) and thick (35 μm) cryosections were obtained on a LEICA CM3050S cryostat. Antibodies used include hamster anti-Muc1 (NeoMarkers, 1:1000), rabbit anti-Sox9 (Millipore, 1:5000), goat anti-Neurog3 (Gu lab, 1:40,000), guinea pig anti-Neurog3 (1:2000), goat anti-RBPJk D-19 (Santa Cruz, titrated), mouse anti-RBPJk E-7 (Santa Cruz, titrated), rabbit anti-RBPJk (Protein Tech, titrated), DBA (Vector Labs, 1:500), guinea pig anti-PP (Linco, 1:500), rabbit anti-glucagon (Linco, 1:500), guinea pig anti-insulin (Dako, 1:1000), chicken anti-GFP (Aves, 1:2000).

Image Acquisition. Confocal images were from a Zeiss LSM 510 META. Images were also acquired on a ZIESS Observer.Z1 apotome.

Tamoxifen and Doxycycline administration. Doxycycline was dissolved in water (5.0 mg/mL) and administered intraperitoneally at 10.0 μg/g body weight. Embryos were harvested and fixed 12 hours after Dox injection. Tamoxifen was dissolved in pharmaceutical grade corn oil (Welch, Holme & Clark Co. Inc.) at 30 mg/mL, and 3.0 mg administered at each time point.

BAC transgene generation. pBACe3.6 RPCI-32-121F10 BAC bearing *Neurog3* genomic sequence was obtained from BAC-PAC resources. Plasmid PL451 [203] was modified by insertion of Puro^R-ΔTK upstream of Neo^R using BamHI and Nhe1 sites to generate PL451.Puro^R-ΔTK-em7-neo^R. The 5' homology region against the Neurog3 locus was a 40 bp region located immediately upstream of the *Neurog*3 start codon (5'HR: 5'-GCTGGCACACACACACCTTCCATTTTTTCCCAACCGCAGG-3') [68]. This 5'HR was synthesized into the forward primer used to amplify the CreER open reading frame (ORF) (Forward primer 5'HR1ay5: 5'–ctaaggggccc**gctggcacacacacaccttccatttttttcccaaccgcagg**atgtccaatttactgaccgtacacc-3'; Reverse primer 5'HR1brevy5: 5'-ctagagtcgaccagacatgataagatacattg-3'). This 5'HR was digested with Apa1 and SalI, and ligated into PL451.Puro^R-ΔTK-em7-neo^R to generate PL451.5'HR-CreER.Puro^R-ΔTK-em7-neo^R. A 3'HR targeting 436 bp of *Neurog3* coding sequence, starting from the ATG, was amplified:

(3'HR2a:GCGGCCGC**ATG**GCGCCTCATCCCTTGGATGCGCTCACCATCCAAGTGTCCCCAGAGACACAAC
AACCTTTTCCCGGAGCCTCGGACCACGAAGTGCTCAGTTCCAATTCCACCCCACCTAGCCCCACTCTCATA
CCTAGGGACTGCTCCGAAGCAGAAGTGGGTGACTGCCGAGGGACCTCGAGGAAGCTCCGCGCCCGACG
CGGAGGGCGCAACAGGCCCAAGAGCGAGTTGGCACTCAGCAAACAGCGAAGAAGCCGGCGCAAGAAG
GCCAATGATCGGGAGCGCAATCGCATGCACAACCTCAACTCGGCGCTGGATGCGCTGCGCGGTGTCCTG
CCCACCTTCCCGGATGACGCCAAACTTACAAAGATCGAGACCCTGCGCTTCGCCCACAACTACATCTGGG
CACTGACTCAGACGCTGCGCATAGCGGA)

This 3'HR was ligated into PL451.5'HR-CreER.Puro^R-ΔTK-em7-neo^R with Not1 to yield PL451.5'HR-CreER-3'HR.Puro^R-ΔTK-em7-neo^R. PL451.5'HR-CreER-3'HR.Puro^R-ΔTK-em7-neo^R was then linearized with Apa1 and SacII, gel purified, and electroporated into recombination competent *E. coli* carrying the RPCI-32-121F10 BAC molecule. Recombinants were selected for with amplicillin and kanamycin. This modified BAC (F10.5'HR-CreER-3'HR.Puro^R-ΔTK-em7-neo^R) contains a Lox2272 site 3' of the NeoR cassette. To generate a BAC transgene capable of undergoing RMCE, we placed a Lox71 site ~1.6 kb upstream of the original location of the Neurog3 start codon. 5' and 3'HRs were constructed:

(5'HRlox71:CAGGAAGGTCTACCCTTGCCTGCAGATTCAATTTCTCTGCAGTAGGGAAGGAATTCCCTCCT
CACTCTCGATCATTTTAGGGATAGTGTTATGCCCCCACCCAATCCTACCACCTCCCCTCCTGCTGAGTGCC
AAGCAAGCCATCCTCTGCCCAGGGGATTTTGTAGTGCTCCCTCCTCTTCCTTGCAGCCCAGGCGGCCAGT
GGTCATCATAGAGTCAAGTCACACACCTACCCCGACCCTGACTCTACGCCTTCAGCCTCCCAGCCAGGGT
ATGGTCCCTTCTACAATATCCAGGAGCTTCGGAGTTAGAGAACGTACTAGAAAGCTTAGAGTTACTGCC
AAGAATCTTTAACTCCCAGCCATAGCTTCCTCCCATGCACATCCTGACTAGAAAGCTGGGGGGGGGGGG
AGGGAGGGAGGGAGGGCAGGAGAGAGAGAGAGAGAGAGAGAGAGAGAGAGAGAGAGAGATCAGC
GGAAGCCACAACCCCTCACCCTGAG)

(3'HRlox71:TGACCGGAAACAGAAGACCACGGGGTGTCAGGGACAAGAAGGGCGGGTCTGCAGGGAA
GAAAGGACAATGTCTTAAGGCTCACAGGAAAGATTTCCAGATAGCTTAAGATAACCTCTTAAGAGGGAC
AAACTAGAAGTCTCCCTGCCCTGGGCTCACCCACAGTTCAGGAGTGATGGGGAGGGAGGGGGCGGGA
AGGAGTAGGACTAGGTGAAGCTGCTAGTCCTCTCTGGTCTGTGATTGGACAGGGGCACTAAAGGGGGC
AGAAAGTAGATCTGCTTTTCTCCCAGGGCCTGCACACGGAGGCATTGAAAAGACAAAAAAGGCTAGCA
GAGAACAAGTCCCTCCTTGACCTTTCCCTATCACCTGCCTCTCGGGTCAGGCCTTCCCGATAGCATCCATA
GTGGGGCGGGGCGTGATGAGATGCCCCCTCTGCACTCTCTCTACAACCACCCTCGCCTCCGGAATAGAA
CCCAATGTCTCGGATGAGGACTATGGTGGG)

And each inserted 5' (with Sal1 and EcoRV) and 3' (with Spe1 and Not1) of the galk ORF in pGALK. Homologous recombination into F10.5'HR-CreER-3'HR.Puro^{R}-ΔTK-em7-neo^{R} in *E. coli* with galk selection was performed, and recombinants verified by PCR and sequencing to generate GK-F10.5'HR-CreER-3'HR.Puro^{R}-ΔTK-em7-neo^{R}. To introduce Lox71 by galk replacement, Lox71 sequence was annealed, digested with Spe1 and EcoRV, an inserted to replace the galk ORF in pGALK. This construct was electroporated into recombination competent *E. coli* bearing GK-F10.5'HR-CreER-3'HR.Puro^{R}-ΔTK-em7-neo^{R}, and the resulting bacteria were galk-counterselected, grown and proper recombinants PCR and sequencing verified. This molecule is denoted Lox71-(F10.5'HR-CreER-3'HR.Puro^{R}-ΔTK-em7-neo^{R})-Lox2272, or hereafter Neurog3$^{BAC\text{-}CreER}$.

Preparation of BAC DNA for electroporation into mouse ES cells. Modified Neurog3$^{BAC\text{-}CreER}$ was purified using a QIAGEN Large-Construct Kit, linearized and separated from the BAC backbone

with Mlu1 and Pme1, and sent off to the Vanderbilt Transgenic ES Cell Core via established standards.

Single copy screening and qPCR: Single copy transgene estimation was performed using the standard curve method as described [201]. All PCR was run on a Bio-Rad CFX96 with SsoFast EvaGreen Supermix (Bio-Rad). Primers used were (PTK copy – F1 5'- CCACGCTACTGCGGGTTTAT-3') and (PTK copy – R1 5'- CAGTTGCGTGGTGGTGGTT-3') designed to amplify DNA internal within the Puro^{R} ORF.

Results

Targeted inactivation of RBPJ with Sox9^{CreER}

Canonical Notch signaling is proposed to act as a major determinant and feedback-effector of binary fate decisions in the developing pancreas, as it is in numerous other developing systems [34,183,184,185,186,187,188]. The transcription factor RBPJ is an obligatory cofactor for Notch mediated repression of pro-differentiation genes such as *Neurog3* [34], and a function for RBPJ in limiting differentiation in early pancreatic MPC has been long established [37,38,189,190]. To date, there has been no specific genetic intervention reported on Notch pathway function in the Sox9^{+} trunk epithelium during secondary transition. To address a function for *RBPJ* in limiting endocrine differentiation from the secondary transition trunk epithelium, we utilized a *Sox9*^{CreER} BAC transgene [15] to affect inducible Cre-mediated recombination of a floxed allele for *RBPJ* [191]. We focused our initial studies on targeting *RBPJ* ablation in large numbers of cells within the epithelium, in order to prospectively analyze a pronounced effect of broad RBPJ loss within the tissue.

To analyze the efficiency of *Sox9*^{CreER} in recombining floxed loci in response to tamoxifen (TAM), we paired *Sox9*^{CreER}-bearing mice with mates harboring a *ROSA*26-lox-STOP-lox-EYFP reporter allele (R26R-EYFP) [159], and administered persistent and high doses of TAM to the pregnant dam. Subsequent tracing of the resulting lineage labeled cells was used to assess the efficiency

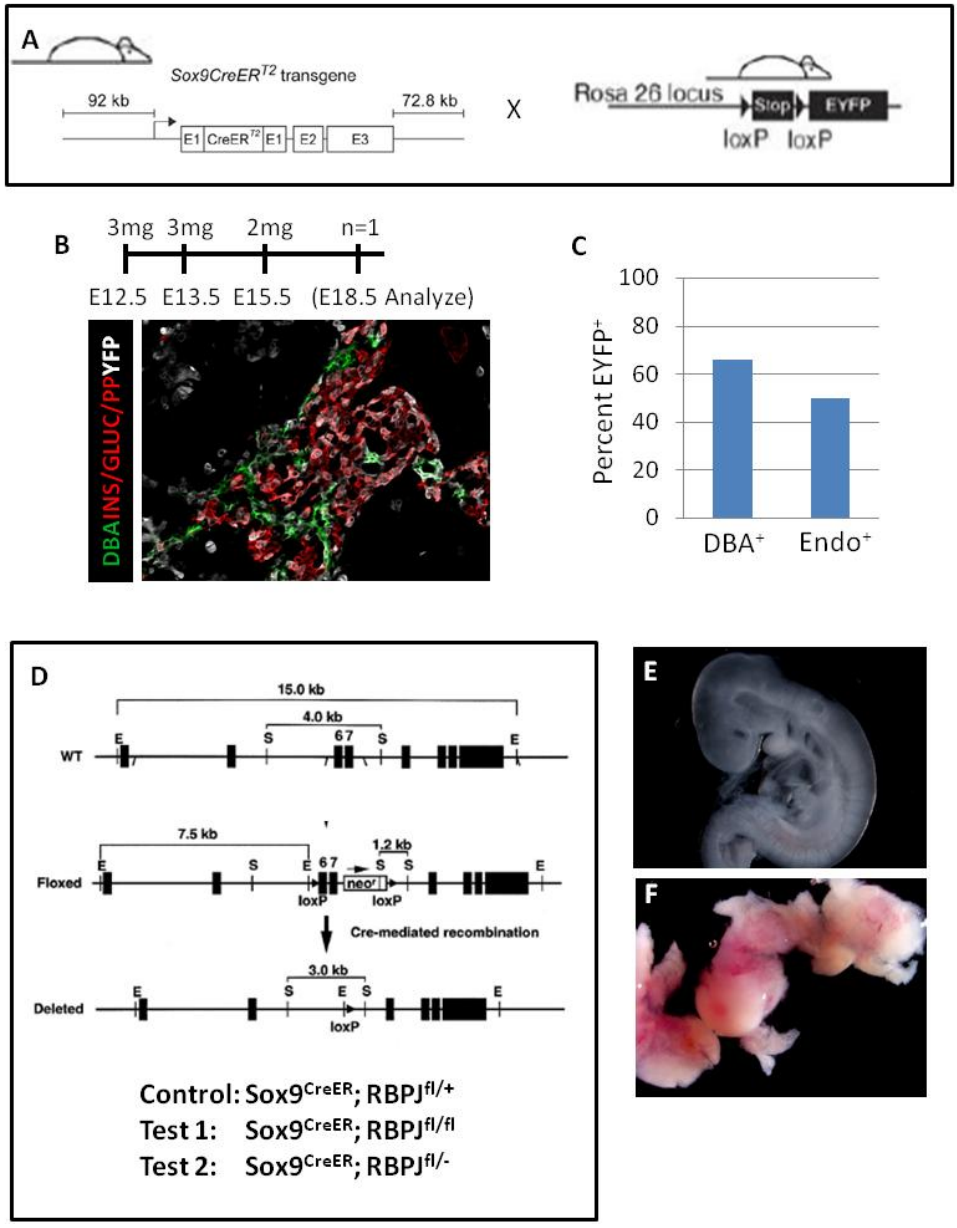

Figure 3.1. *Genetic systems used for conditional inactivation of RBPJ in the trunk. (A) Crossing Sox9^{CreER} and Rosa26^{EYFP} allele-bearing mice generates Sox9^{CreER};Rosa26$^{EYFP/+}$ embryos. (B) Tamoxifen-loading in pregnant dams causes conditional activation of lineage reporter. Distribution of EYFP^{+} cells in labeled endocrine and ductal lineages at E18.5 after tamoxifen administration. (C) Quantification of EYFP-positivity in endocrine and ductal lineages at E18.5, as determined by manual cell counting (66% DBA^{+}; 50% Endo^{+}; n = 1). (D) Design of RBPJ alleles used for conditional mosaic inactivation of RBPJ by Sox9^{CreER}. Control and experimental embryonic genotypes representing an allelic series are shown. (E,F) Selected embryos from a cross between RBPJ$^{+/-}$ mating pairs, where the RBPJ null allele was generated from the RBPJ^{floxed} allele using germline recombination with E2ACre [199]. The extraembryonic tissues are apparent at E9.5, but lack embryonic tissues in the most severe manifestation of the RBPJ null phenotype. This figure was adapted from [30,191].*

of CreER-mediated gene targeting in this system (Fig. 3.1A). For mice injected with 3 mg of TAM at E12.5 and E13.5, followed by an additional 2 mg dose at E15.5 (these doses were empirically determined as the most TAM a female could receive without termination of the pregnancy), there was a broad activation of lineage label throughout the pancreas at E18.5 (Fig. 3.1B). EYFP marked a large portion of the endocrine lineage, as marked by a cocktail of antibodies (Endo$^{C\text{-}TAIL}$) that bind to insulin, glucagon, and pancreatic polypeptide (PP). EYFP also marked a large portion of the ductal epithelium as demarcated by the lectin-binding protein DBA [192]. Quantification of the proportion of the DBA^{+} duct and Endo$^{C\text{-}TAIL+}$ endocrine compartments labeled by EYFP showed that over 60% of the duct cell population, and approaching 50% of the endocrine cell population, had undergone CreER-mediated activation of R26R-EYFP. We also observed that EYFP lineage reporter was activated in the acinar compartment of the pancreas, consistent with the notion that *Sox9*^{CreER} is not entirely specific for the trunk epithelium under these conditions. Notably, Sox9 protein is readily detectable, albeit at lower levels, in the pro-acinar tip domains at early stages of secondary transition [15]. These results are in line with previous studies suggesting that the bulk of the endocrine lineage is generated during the pancreatic secondary transition, and supports the notion that *Sox9*^{CreER} can be a useful tool to inactivate *RBPJ* broadly within the trunk domain.

To inactivate *RBPJ* within the *Sox9*-expressing trunk domain, we mated *Sox9*^{CreER};*RBPJ*$^{fl/+}$ mice with *RBPJ*$^{fl/fl}$ mice. Successful recombination of the *RBPJ* floxed allele results in a deletion of exons 6 and 7, which encode the DNA-binding domain of *RBPJ*, and generates a functional null allele [191]. We injected pregnant dams with 3 mg of TAM at E12.5 and E13.5, and analyzed the pancreas for loss of RBPJ protein by direct immunodetection at E15.5. Unfortunately, we were unable to obtain convincing nuclear signal for RBPJ on positive controls or experimental samples, with any of the immunodetection methods used in the lab, using three separate antibodies directed against RBPJ (data not shown) (See Fig. 3.9 for antibodies used). As another method to verify recombination of the *RBPJ* floxed allele, we isolated whole E15.5 pancreas and extracted and prepared DNA to attempt to detect allelic recombination by genotyping analysis. Genotyping primer sets that could detect and differentiate the intact the wild type allele, the intact floxed allele, and the recombined floxed allele were used to amplify PCR fragments from

whole pancreas DNA (See Fig. 4.9 for primers used). Tail DNA from wild type, *RBPJ*$^{fl/fl}$, and *RBPJ*$^{+/-}$mice in which the *RBPJ* floxed allele had been converted to an *RBPJ* null allele by using the germline deleter *E2A*.Cre (*RBPJ*$^{+/-}$) [199], were used as controls. While PCR amplicons representing wt and *RBPJ* floxed alleles were readily detected, we obtained no convincing evidence that there was recombination of the *RBPJ* floxed allele in our experimental mice. We ruled out the use of qRT-PCR or western blot as additional approaches to detecting a change in *RBPJ* expression, because *RBPJ* is a ubiquitously expressed gene [193], and we therefore did not expect to be able to detect a reduction in signal over what would be an already high basal signal. Finally, we ruled out the likelihood that we could detect a bias in the lineage allocation of *RBPJ*-mutant cells via lineage tracing, because the activation of EYFP lineage label is not linked to recombination of the *RBPJ*-floxed allele in a given cell. We had already, in collaboration with the Gu Lab, demonstrated that non-parallel recombination of non-linked genetic elements limits Cre-LoxP reporter systems as precise indicators of conditional genetic manipulations [194]. We next reasoned that the best way to proceed forward with the tools at hand would be to try and sensitize the genetic system to Cre-mediated recombination. To do this, we used a genetic condition in which one copy of the *RBPJ* floxed allele had been converted to a null condition (*RBPJ*$^{fl/-}$), thereby increasing the probability that the remaining *RBPJ* floxed allele would be recombined to generate a null genotype in response to TAM administration (Fig. 3.1D). This *Sox9*^{CreER};*RBPJ*$^{fl/-}$ genetic condition could then be analyzed in parallel with *Sox9*^{CreER};*RBPJ*$^{fl/fl}$, and *Sox9*^{CreER};*RBPJ*$^{fl/+}$ animals in order to assess a phenotypic spectrum. Matings of *RBPJ*$^{fl/fl}$ mice with *E2A*^{Cre} mice gave first generation pups in which the *RBPJ* floxed allele had been converted to a null allele based on genotyping analysis (data not shown). After breeding out *E2A*^{Cre} we crossed *RBPJ*$^{+/-}$ to *RBPJ*$^{+/-}$ mice to assess embryonic lethality before E10.5, which is the known consequence of complete RBPJ deficiency in mice [204]. Out of 30 E9.5 embryos generated from four separate matings, 6 exhibited severe growth retardation, and 8 showed complete embryonic absorption (Fig. 3.1E-F), consistent with the generation of a functional null allele for *RBPJ*. These alleles were used to generate an allelic series comprised of *Sox9*^{CreER};*RBPJ*$^{fl/+}$, *Sox9*^{CreER};*RBPJ*$^{fl/fl}$, and *Sox9*^{CreER};*RBPJ*$^{fl/-}$ mice. For analysis of a potential phenotype, we decided to focus on measuring changes in the ratio of Neurog3^{+} to

Sox9^{+} cells, alterations to the relative mass of duct and endocrine lineages, and effects on the gross morphology of in response to TAM exposure during development.

Sox9^{CreER};RBPJ$^{fl/fl}$ and Sox9^{CreER};RBPJ$^{fl/-}$ mice have altered ratios of Neurog3^{+} and Sox9^{+} cells after TAM administration

To assess and compare the consequences of TAM administration on the ratio of Neurog3^{+} and Sox9^{+} cells in *Sox9*^{CreER};*RBPJ*$^{fl/+}$, *Sox9*^{CreER};*RBPJ*$^{fl/fl}$, and *Sox9*^{CreER};*RBPJ*$^{fl/-}$ embryos, we crossed *Sox9*^{CreER};*RBPJ*$^{fl/+}$ mice with RBPJ$^{fl/-}$ mice, and administered TAM to the pregnant dam (Fig. 3.2.A). Sectional analysis of E15.5 pancreas from *Sox9*^{CreER};*RBPJ*$^{fl/+}$ and *Sox9*^{CreER};*RBPJ*$^{fl/fl}$ animals immunolabeled with Neurog3 and Sox9 showed an apparent increase in the number of

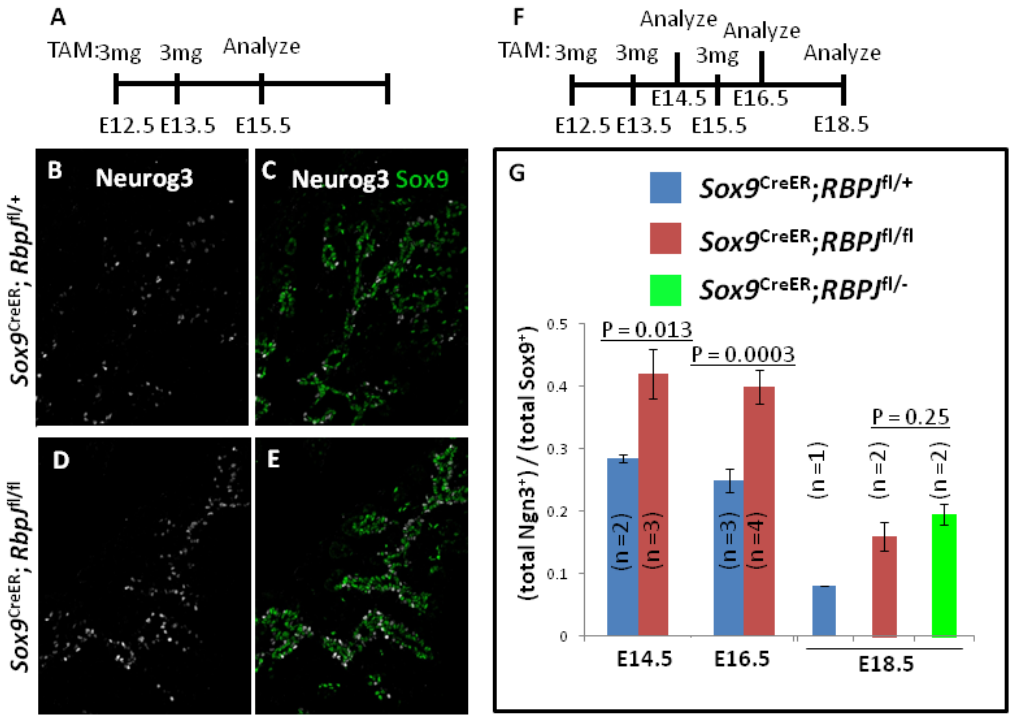

Figure 3.2. *The ratio of Neurog3^{+} and Sox9^{+} cells is altered in Sox9^{CreER};RBPJ$^{fl/fl}$ and Sox9^{CreER};RBPJ$^{fl/NULL}$ embryos after TAM administration. (A) Diagram for tamoxifen administration and analysis at E15.5. (B-E) Single and merged channels showing Sox9 and Neurog3 immunodetection at E15.5 in Sox9^{CreER};RBPJ$^{fl/+}$ and Sox9^{CreER};RBPJ$^{fl/fl}$ genotypes. (F) Diagram for tamoxifen administration and analysis of the RBPJ allelic series at E18.5. (G) Quantification of the Neurog3:Sox9 ratio (fractional representation) in Sox9^{CreER};RBPJ$^{fl/+}$, Sox9^{CreER};RBPJ$^{fl/fl}$, and Sox9^{CreER};RBPJ$^{fl/-}$ pancreata at various stages of secondary transition. Error bars are S.E.M. P values calculated by Student's t.*

Neurog3^{+} cells relative to Sox9^{+} cells (Fig. 3.2.B-E). Quantification of the change in (total Neurog3^{+}/total Sox9^{+}) at E14.5 (*Sox9*^{CreER};*RBPJ*$^{fl/+}$ = 0.285 ± 0.01, *Sox9*^{CreER};*RBPJ*$^{fl/fl}$ = 0.42 ± 0.04)

and E16.5 5 (*Sox9*^{CreER};*RBPJ*$^{fl/+}$ = 0.25 ± 0.02, *Sox9*^{CreER};*RBPJ*$^{fl/fl}$ = 0.40 ± 0.03) showed an approximate 25% increase in the number of Neurog3^{+} cells relative to Sox9^{+} cells. Quantification of (total Neurog3^{+}/total Sox9^{+}) at E18.5, with the addition of the *Sox9*^{CreER};*RBPJ*$^{fl/-}$ genotype, showed a correlative increase in (total Neurog3^{+}/total Sox9^{+}) as a function of whether *Sox9*^{CreER}-bearing embryos were *RBPJ*$^{fl/+}$ (~0.08 ± 0.0, n = 1), *RBPJ*$^{fl/fl}$ (~0.16 ± 0.023, n = 2), or *RBPJ*$^{fl/-}$ (~0.195 ± 0.02, n = 2) (Fig. 3.2.F,G). The statistical significance of these changes could not be definitively made with the number of samples analyzed. These alterations in (total Neurog3^{+}/total Sox9^{+}) did not appear to be due to increased cell death, because immunodetection of cleaved-caspase 3 did not label appreciable cell numbers in the experimental or control samples (Fig. 3.3). These results suggest that, relative to control, there is are alterations the relative numbers of Neurog3^{+} and Sox9^{+} cells in pancreata bearing conditional alleles for *RBPJ* and *Sox9*^{CreER}, and that have been injected with high and persistent doses of TAM.

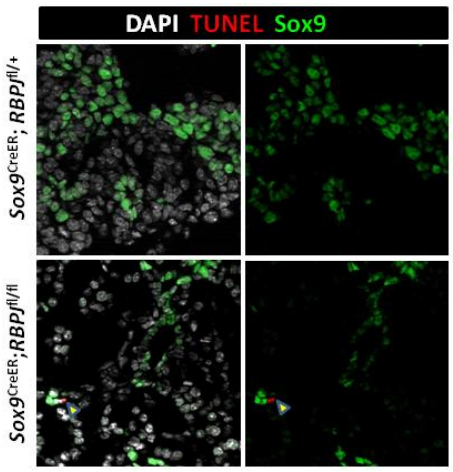

Figure 3.3. *Cell death is unchanged in Sox9*^{CreER}*:RBPJ*$^{fl/fl}$ *embryos exposed to TAM. Embryonic pancreata at E15.5 treated with 2 x 3 mg tamoxifen at E12.5 and E14.5, and labeled with DAPI, Sox9, and cleaved caspase-3 (n = 1).*

Alterations to epithelial morphology in Sox9^{CreER}*;RBPJ*$^{fl/fl}$ *and Sox9*^{CreER}*;RBPJ*$^{fl/-}$ *mice injected with TAM*

A previous study showed that increased endocrine differentiation caused by pharmacological inhibition of Notch resulted in thinning of Muc1^{+} epithelial lumens [72]. Because we were

observing changes to (total Neurog3^{+}/total Sox9^{+}) that were suggestive of increased endocrine differentiation, we hypothesized that this would result in alterations to epithelial morphology similar to what had been previously reported. We obtained thick frozen sections from E15.5 *Sox9*^{CreER};*RBPJ*$^{fl/+}$ and *Sox9*^{CreER};*RBPJ*$^{fl/fl}$ embryonic pancreas that had been exposed to TAM *in utero*, labeled them with Muc1, and rendered composite images of the whole dorsal pancreas. At E15.5, we observed no apparent difference in the gross anatomical morphology of the epithelium (Fig. 3.5A,B). Epithelial branch patterns appeared to be normal, and there was abundant and grossly normal web-like plexus epithelium in both conditions. There was no apparent thinning in the diameters of the epithelial lumens, as had been shown under conditions where Notch is pharmacologically inhibited *in vitro* [72]. There were also no apparent changes in the size or gross morphology of the pancreas as a whole (data not shown) at this stage. Inspection of the gross tissue morphology of the pancreas at E16.5, as shown using an anti-mouse secondary antibody that gives high background signal to reveal the general features of tissue architecture, showed alterations in the morphology of acinar clusters relative to control (Fig. 3.5C). The lumens of most, but not all, of the acinar clusters in *Sox9*^{CreER};*RBPJ*$^{fl/-}$ pancreata appeared to be enlarged or dilated relative to control (n = 1). At E18.5, however, even in the *Sox9*^{CreER};*RBPJ*$^{fl/-}$ condition there appeared to be little if any overt change to the gross morphology of the pancreas. In only one *Sox9*^{CreER};*RBPJ*$^{fl/-}$ pancreas out of numerous inspected (n > 3), there appeared to be some reduction in the size, and change in the gross morphology, of the pancreas (Fig. 5D). While, these data present instances where minor alterations in the morphology of the pancreas were documented, we conclude that there are no overt, reproducible phenotypes with respect to pancreas gross morphology observed in our experimental model.

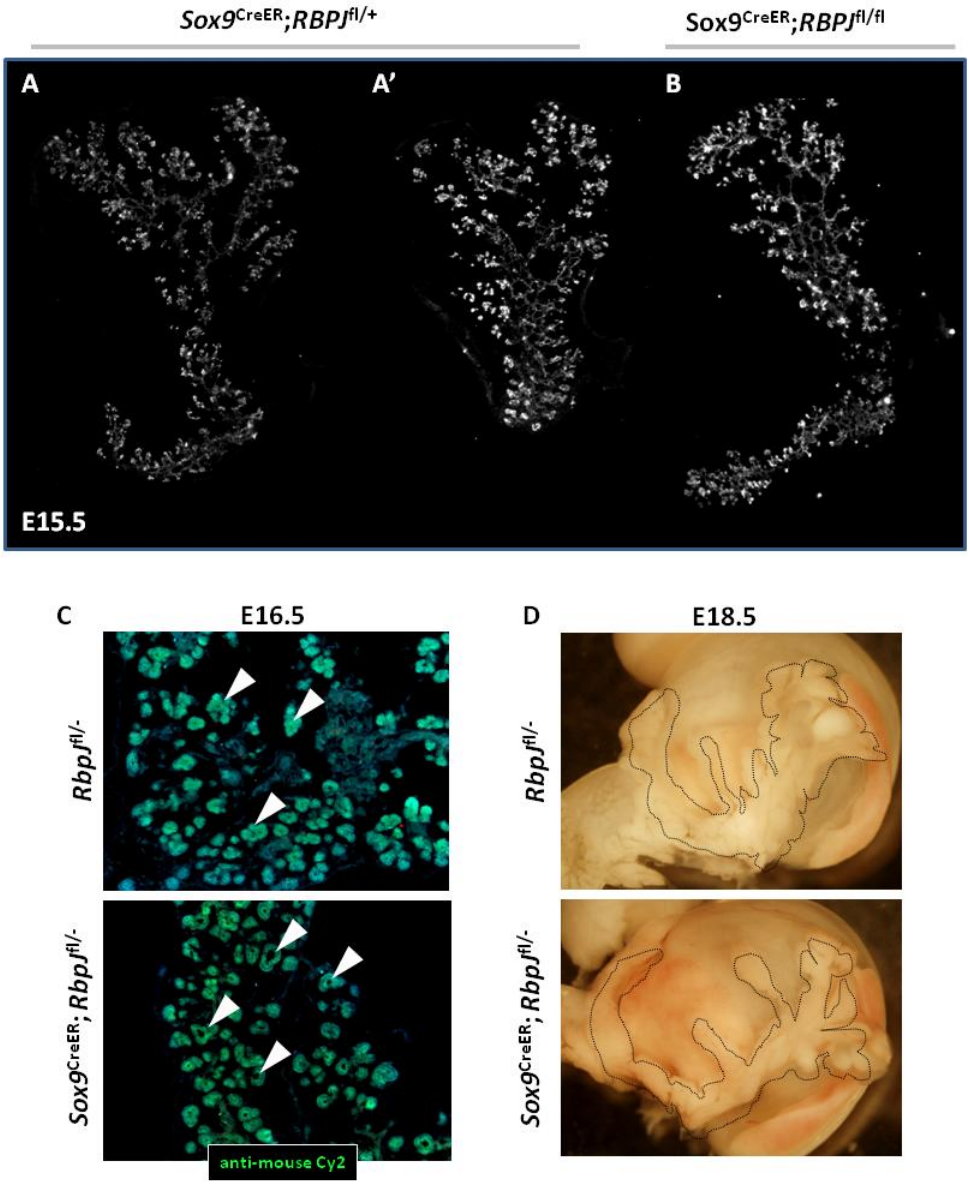

Figure 3.4. *Analysis of gross pancreatic epithelial morphology in Sox9^{CreER}:RBPJ$^{f/f}$ embryos exposed to TAM. (A-B) Composite 10x images of E15.5 Sox9^{CreER};RBPJ$^{fl/+}$ and Sox9^{CreER};RBPJ$^{fl/fl}$ pancreata treated with 2 x 3 mg tamoxifen at E12.5 and E14.5, and labeled in 30 μm thick sections with Muc1. (C) Background signal from Cy2-conjugated antibody used to highlight the gross architecture of the pancreatic epithelium at E16.5. Panels show RBPJ$^{fl/-}$ and Sox9^{CreER};RBPJ$^{fl/-}$ genotypes treated with 2 x 3 mg tamoxifen at E12.5 and E14.5, and an additional 2 mg at E15.5. White arrowheads point to dilated acinar lumens. (D) Illuminated stereomicroscopic images of RBPJ$^{fl/-}$ and Sox9^{CreER};RBPJ$^{fl/-}$ pancreata (dashed black line) treated with 2 x 3 mg tamoxifen at E12.5 and E14.5, and an additional 2 mg at E15.5.*

Altered duct and endocrine cell mass in Sox9^{CreER};RBPJ$^{fl/fl}$ and Sox9^{CreER};RBPJ$^{fl/-}$ mice injected with TAM

Lastly, we investigate whether or not the increased (total Neurog3^{+}/total Sox9^{+}) observed during multiple stages of development in *Sox9*^{CreER};*RBPJ*$^{fl/+}$ and *Sox9*^{CreER};*RBPJ*$^{fl/-}$ mice injected with TAM resulted in a change in the final relative sizes of the duct and endocrine pancreas. To do this, we sectioned E18.5 pancreas, labeled them with the Endo$^{C\text{-}TAIL}$ and DBA, and then measured and compared the relative pixel areas for the duct and endocrine tissues using ImageJ software. *Sox9*^{CreER};*RBPJ*$^{fl/-}$ embryos exposed to TAM showed an increase in the size of the endocrine pancreas relative to the duct (Fig. 3.6A). This increase was relatively minor (*Sox9*^{CreER};*RBPJ*$^{fl/+}$ = 60 ± 4.62% endocrine, *Sox9*^{CreER};*RBPJ*$^{fl/-}$ = 79.67 ± 6.08% endocrine), but was

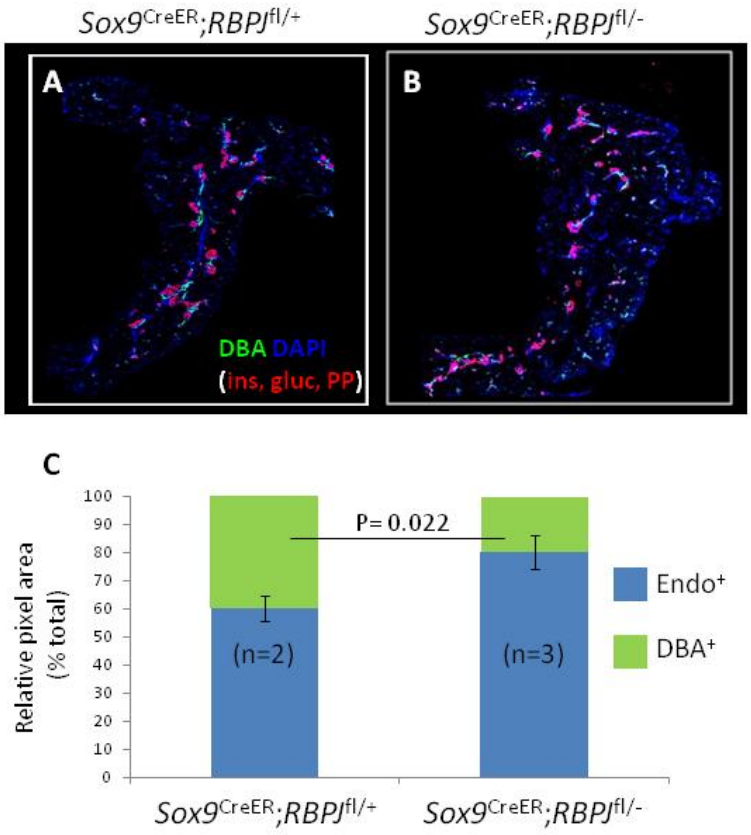

Figure 3.5. *Relative duct versus endocrine area is altered in Sox9^{CreER}:RBPJ$^{f/-}$ embryos injected with tamoxifen. (A, B) Composite 10x images of E18.5 Sox9^{CreER};RBPJ$^{fl/+}$ and Sox9CreER;RBPJ$^{fl/NULL}$ pancreata treated with 2 x 3 mg tamoxifen at E12.5 and E14.5, and an additional 2 mg at E15.5. Samples were sectioned, and labeled with DBA, DAPI and the endocrine-cocktail of antibodies. (C) Quantification of relative pixel area determined from samples in A & B; 30% of entire pancreas analyzed by serial section. Error bars are S.E.M. P values calculated by Student's t.*

significant (P= 0.022) when averaged across several samples. We did not normalize these measurements in a way that would allow for a conclusion to be made on whether the absolute sizes of the duct or endocrine pancreas were changed. We conclude that administration of TAM in *Sox9*^{CreER};*RBPJ*$^{fl/-}$ pancreata is associated with an increased relative size of the endocrine versus the duct pancreatic lineages.

Conditional genetic ablation of RBPJ with Sox9^{CreER} is not a suitable model for studying Notch and other endocrine-differentiation-dependent feedback influences on the trunk domain

The above experiments lead us to conclude that conditional genetic ablation of *RBPJ* with *Sox9*^{CreER} is not a suitable model for studying 1) studying the cell autonomous role of *RBPJ* in limiting endocrine differentiation, or 2) assessing non-cell autonomous endocrine-differentiation-dependent feedback influences on progenitor growth, differentiation, and morphogenesis in the trunk domain. In this model system, we could not definitively confirm that *Sox9*^{CreER} was causing genetic inactivation of *RBPJ*, we had no ability to directly trace the consequences of *RBPJ* loss in a cell or in populations of cells, and we had only minor and difficult-to-interpret changes in endocrine differentiation patterns during development. Thus, this was an insufficient experimental model given the questions we were trying to address. With these justifications, we discontinued this project, and sought other means to conditionally control endocrine differentiation during pancreas development.

Inducible ectopic Neurog3 expression to study endocrine-differentiation-dependent feedback on trunk progenitors

We reasoned that an alternative strategy for controlling endocrine differentiation from the trunk would be to ectopically express Neurog3, in a spatiotemporally controlled fashion, within the Sox9^{+} trunk. To do this, we developed a three allele system that permits 1) conditional mosaic activation of Neurog3 induction-competence via *Sox9*^{CreER}, 2) indelible and direct lineage tracing of control (uninduced) and experimental (Neurog3-induced) cells, and 3) and controlled ectopic expression of Neurog3. The first element of this three allele system (hereafter

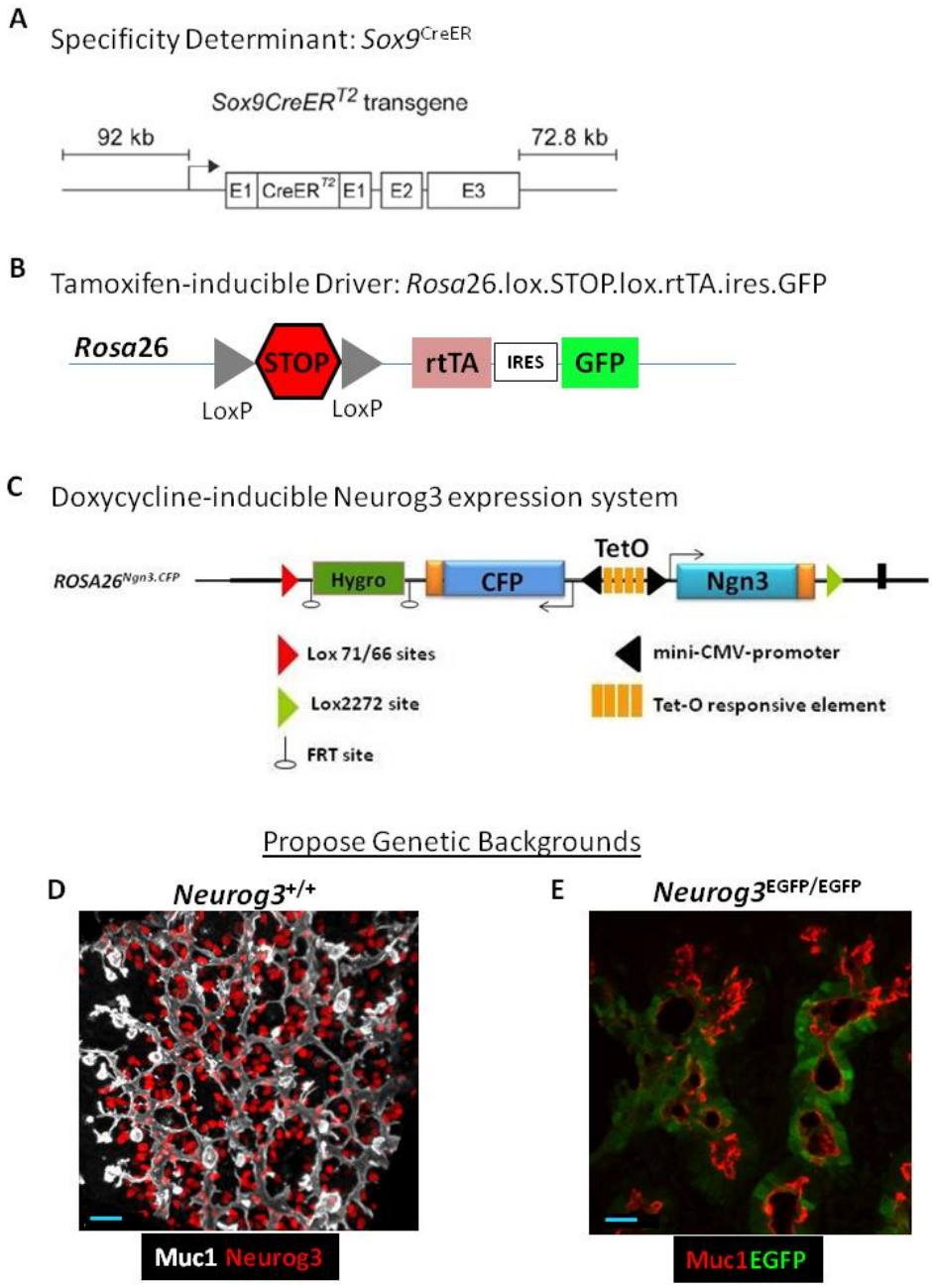

Figure 3.6. *Ectopic Neurog3 expression for controlled manipulation of endocrine flux from the trunk domain. (A) Sox9^{CreER}-based specificity determinant for targeting CreER-mediated recombination of lol.STOP.lox alleles knocked into the Rosa26 locus. (B) Tamoxifen-inducible driver allele for doxycyline-mediated overexpression of tet-responsive alleles knocked in to the Rosa26 locus. (C) Doxycycline-inducible system for controlled ectopic expression of Neurog3. (D,E) Proposed genetic backgrounds for analyses on the non-cell autonomous effects of ectopic Neurog3 expression on gene expression patterning, progenitor growth and differentiation, and epithelial morphogenesis in the trunk domain. The relative numbers of cells targeted for ectopic Neurog3-induction is controlled by the administered dose and timing of tamoxifen administration. This figure was adapted from schematics made in the M. Magnuson Lab.*

Neurog3^{OE}) is represented by the specificity determinant *Sox9*^{CreER} (Fig. 3.7A). As previously shown (Chapter II and Fig. 3.1B), administration of low or high doses of TAM recombines *Rosa*26.lox.STOP.lox alleles (such as R26R) in highly mosaic or broadly scattered populations of Sox9^{+} cells in the trunk. Different doses of TAM can be used to control the patterning of cells with recombined alleles within the *Sox9*$^{+}$ epithelium. The second element of *Neurog3*^{OE} is represented by a TAM-inducible *Rosa*26.lox.STOP.lox.rtTA.ires.GFP allele, which allows for conditional expression of a reverse tetracycline trans-activator (rtTA) [195] (which transcriptionally activates gene targets regulated by tetracycline responsive elements (TetO)) and tracing of recombined cells with a genetically coupled GFP fluorophore (Fig. 3.7B). The last element of Neurog3^{OE} is represented by a doxycycline responsive, bicistronic *Rosa*26.Neurog3.CFP allele [Mark Magnuson Lab, Vanderbilt, unpublished], which in response to doxycyline administration, is designed to express both Neurog3 and CFP proteins from a tetracycline responsive promoter (Fig. 3.7C). This proposed *Neurog3*^{OE} system could theoretically enable control over the patterning and timing of ectopic Neurog3 expression in the Sox9^{+} trunk domain, and thus represents a tractable model for mosaic studies on Neurog3-dependent cell non-autonomous feedback.

We next proposed that the Neurog3^{OE} system should be bred into two experimental backgrounds. The first model consists of *Neurog3*^{OE} bred into a 'normal' genetic background (Fig. 3.7D). The second experimental model consists of the *Neurog3*^{OE} system bred into a *Neurog3* nullizygous background [59] (Fig. 3.7E). With these experimental models in-hand, we propose that information can be gleaned about the nature and scale of the cell non-autonomous functions for Neurog3 in directing programs of progenitor growth and maintenance, gene expression patterning and cell differentiation, and patterns of epithelial morphogenesis in the trunk domain.

Neurog3^{OE} *allows for tight control over endocrine differentiation from the trunk*

We next carried out preliminary tests on the efficacy of the *Neurog3*^{OE} system as a model to conditionally control the entrance of Sox9^{+} epithelial cells into the endocrine lineage via ectopic Neurog3 expression. We bred the *Neurog3*^{OE} system into a normal genetic background, and

populated the epithelium with Neurog3 induction-competent cells via TAM injection at E13.5 and E14.5. We next compared the effects of doxycyline administration on Neurog3 induction in GFP-expressing cells in *Neurog3*^{OE} pancreata, and using a *Sox9*^{CreER};*ROSA*26-lox-STOP-lox-ires-GFP condition, which does not carry the *Rosa*26.Neurog3.CFP allele, as control. We injected doxycycline into pregnant dams at E15.5, and because we had previously shown that Sox9^{+}

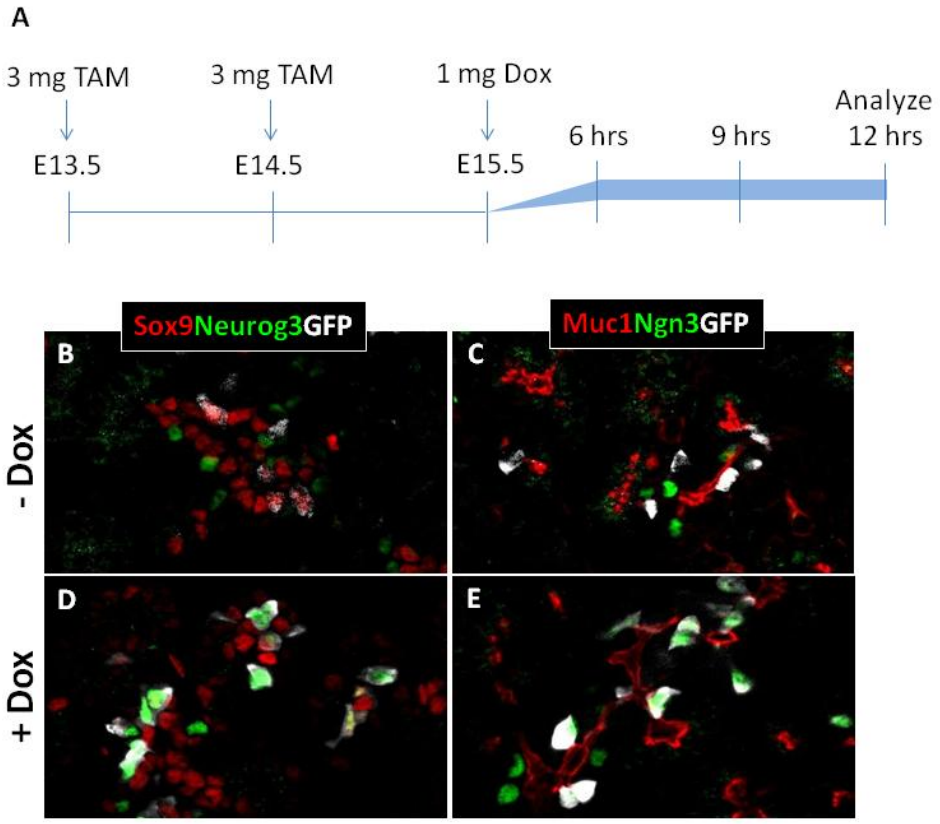

Figure 3.7. *Proof of efficacy of the Neurog3 ectopic expression system. (A) Experimental timeline for tamoxifen and doxycycline administration and analysis of resulting tissues in embryos harboring the Neurog3*^{OE} *system. (B-E) Analysis of the overlap between EGFP lineage label (coming from the tamoxifen-inducible driver allele) and Neurog3 protein in the presence or absence of doxycycline. Note the lack of overlap between EGFP and Neurog3 in the absence of doxycycline, and the near-full overlap in the presence of doxycycline. Muc1 and Sox9 are provided as markers for the trunk epithelium.*

epithelial cells normally activate Neurog3 and undergo differentiation over an estimated 12 hour period (Chapter II), analyzed embryonic pancreata 12 hours later (Fig. 3.8A). In control animals, we observed broad activation of GFP in the *Sox9*-expressing epithelium, indicating that *Sox9*^{CreER} had faithfully recombined and activated the *ROSA*26-lox-STOP-lox-ires-GFP allele in response to TAM administration. The vast majority of these GFP^{+} cells were not Neurog3

protein-positive (~10%, n = 1) at the twelve hour time point, consistent with the idea that only some *Sox9*-expressing cells activating GFP will "choose" to turn on Neurog3 within a given period of time (Fig. 3.8B,C). Most GFP cells were found in the epithelium and were $Sox9^{+}$. In contrast, in pancreata bearing *Neurog3*^{OE}, we observed a near complete coincidence (90%, n = 1) of GFP and Neurog3 protein expression. This result indicates that Neurog3 protein is faithfully induced in response to Dox-administration in cells that have undergone activation of the *ROSA*26-lox-STOP-lox-ires-GFP allele (Fig. 3.8D,E). Notably, these same cells were not positive for Sox9, indicating that similar to the normal endocrine differentiation process, Sox9 expression had been faithfully downregulated as a result of Neurog3 expression [31,80]. There were, as expected, $Neurog3^{+}$ cells that were not GFP^{+} in this condition, which is explained by the idea that cells that have not activated the *Neurog3*^{OE} system are still capable of entering into the endocrine differentiation program. Finally, analysis of these same expression patterns 24 hours after Dox-administration showed a much less pronounced overlap between GFP^{+} cells and those expressing Neurog3, suggesting that due to the short half-life of Dox in vivo (~ 170 min. [196]), cells that had previously ectopically expressed Neurog3 had since downregulated Neurog3 protein (data not shown, n = 1). Collectively, these data suggest that *Neurog3*^{OE} represents a faithful genetic system with which to control an ostensibly similar-to-normal process of *Neurog3* activation and endocrine differentiation from the pancreatic epithelium.

Neurog3^{CreER} *BAC transgene for tracing and manipulation of the Neurog3*^{LO} *state*

As an additional entry point into understanding the molecular and cellular mechanisms that function to balance endocrine differentiation and progenitor maintenance, we endeavored to generate new tools to study the proposed Neurog3^{LO} endocrine-biased state outlined in Chapter II. We reasoned that one useful avenue would be to generate a *Neurog3*^{CreER} BAC transgene, to conditionally lineage trace the progeny of cells expressing low levels of *Neurog3*. Several *Neurog3*^{Cre} lines have been generated, but these appear to mark mostly cells that have progressed into the Neurog3^{HI} state that is associated with endocrine commitment [16,63]. One *Neurog3*^{Cre} BAC transgene, however, has been shown to mark *Neurog3*-expressing cells of the pancreas and intestine that appear to maintain some degree of plastic lineage potency, and can

give rise to non-endocrine lineages [68]. We used this same BAC molecule to engineer a *Neurog3*^{CreER} BAC for generation of a new *Neurog3*$^{BAC\text{-}CreER}$ transgenic mouse line (Fig. 3.8A,B). This mouse would theoretically maintain the high sensitivity of lineage labeling necessary to track the Neurog3^{LO} condition [68], and would also evade phenotypes associated with Neurog3

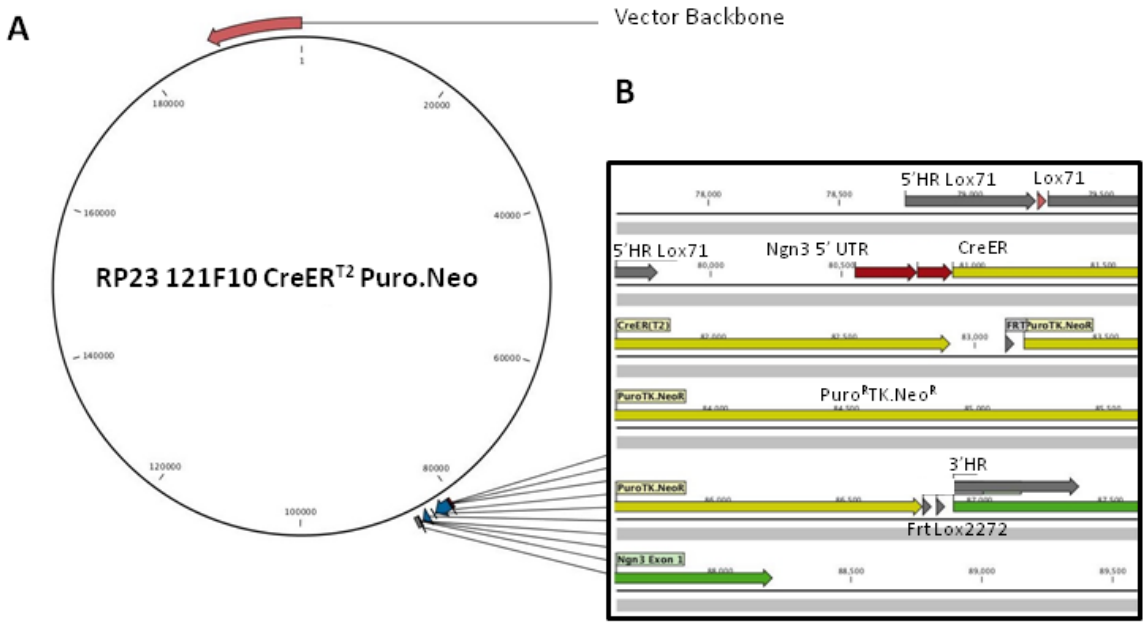

Figure 3.8. *Generation of the Neurog3*^{CreER} *BAC transgene. (A) Entire modified RP23-121F10 BAC harboring CreER(T2) and Puro*^{R}*.ΔtK.em7.Neo*^{R} *cassettes inserted in front of the Neurog3 start codon. BAC molecule is equipped with lox-cassette-acceptor (LCA) capability to provide for later exchanges of experimental constructs into the LCA by RMCE. See materials and methods for details.*

haploinsufficiency [69]. The final BAC construct featured a CreER-Puro^R-ΔTK-em7-neo^R cassette inserted in front of the endogenous *Neurog3* start codon. For later flexibility in exchanging other cassettes into this same allele via Recombinase Mediated Cassette Exchange (RMCE) in mouse embryonic stem cells (ESC), we inserted a Lox71 variant site [202] ~1.6 kb upstream of the CreER start codon, and a Lox2272 variant site [202] at the 3' end of the Puro^R-ΔTK-em7-neo^R cassette. The resulting *Neurog3*^{CreER} BAC molecule was released from the pBACe3.6 backbone by restriction enzyme digest (the backbone contains exogenous sequences necessary for BAC replication in bacteria, and includes unwanted variant loxP sites) and electroporated into TL1 [200] mESC (129/Sv background) at the Vanderbilt Transgenic ES Cell Core. The resulting mESC were selected by puromycin to isolate stable transgene integrations, mESC

colonies were grown, and DNA was prepped for a two-part screen to isolate single copy transgene insertions. It was vital that the transgene only be contained within the genome as a single copy, so that later exchange by RMCE could be predictably accomplished without undesirable recombinant products. The first round of screening was designed to use genomic PCR to screen for regions of the *Neurog3*^{CreER} BAC, including the *CreER* open reading frame (ORF), selection cassettes, and 5' and 3' junctions between inserted and endogenous DNA (see materials and methods), to verify successful insertion of the BAC. Genomic PCR was also used to find and to exclude mESC clones that had incorporated pBACe3.6 backbone DNA during electroporation. From this first screen were identified 14 out of 67 colonies screened that were qualified candidates for 'correct' transgenic insertions, without pBAC backbone insertions. For the next part of the screen, these 14 candidates were submitted to qPCR screening in order find single copy insertion events. Briefly, primers directed against the Puromycin ORF were generated. Then, qRTPCR was run on 2.5, 10, 20, 40 and 200 ng of DNA from a TL1 mouse line carrying *ROSA*26$^{Puro\Delta Tk}$ as a single copy of Puro^{R}-ΔTK-em7-neo^{R} to obtain a line of best fit for a standard Δ_{ct} curve reflecting increasing copy number. 20 ng of DNA from candidate single copy-bearing mESC clones was run in triplicate alongside this standard curve. Of the 14 clones tested, 2 clones showed estimated copy numbers of 1.0 (clone f5) and 1.6 (clone c10). Clones f5 and c10 were expanded, and subsequently prepped and injected into C57BL/6 blastocysts to generate chimeras. Two female and one male chimera were isolated. The two females were less than 10% TL1 as judged by brown coat color, while the male was ~50% TL1. Mating the chimeras with C57BL/6 mice showed no germline transmission of the 129/Sv (TL1) background with *Neurog3*^{CreER}. In sum, while animals were not successfully generated from these attempts, we have generated an RMCE-compatible Neurog3$^{BAC\text{-}CreER}$ for use in lineage tracing studies, and for generating additional mouse lines with experimental constructs inserted into the Neurog3 locus in a BAC by RMCE.

Discussion

Challenges and limitations of CreER-mediated deletion of RBPJ as a tool to control endocrine differentiation from the pancreatic epithelium

Our goals in achieving *Sox9*^{CreER}-mediated inactivation of *RBPJ* in the trunk were two-fold. First, we aimed to gain the first insight into a proposed cell-autonomous function for *RBPJ* in limiting *Neurog3* activation and endocrine differentiation within the *Sox9*$^{+}$ trunk. Second, we sought to use this conditional system as a tool to manipulate the magnitude of endocrine differentiation occurring from the trunk, as a basis to gain insights into the non-cell-autonomous regulation of growth, differentiation, and morphogenesis processes that occur in the trunk response to endocrine differentiation-dependent feedback. Due to a number of limitations in this experimental system, we were unable to achieve either of our goals. One main limitation in this model system was that we could not reliably detect, by any methods attempted, loss of *RBPJ* protein in *Sox9*-expressing progenitors. We propose that better methodologies and/or reagents will likely be needed in order to quantify and track the behaviors of *RBPJ*-deficient cells, at cellular resolution, in order to make definitive conclusions on the fate of *RBPJ*-deficient Sox9^{+} progenitor cells. A second limitation in this model system is that the lineage tracing methods, which in an ideal case would allow one to infer the fate of *RBPJ*-deficient cells by following EYFP positive lineage labeled cells, are flawed. We recently published a report, in collaboration with and led by the Gu Lab [194], which demonstrated that Cre-mediated activation of reporter alleles does not accurately predict recombination of another floxed allele in an individual cell. The degree of overlap between lineage-reporter activation and gene-inactivation appear to depend on a number of factors, including the levels of Cre-recombinase expressed in a given cell, the distance between loxP sites at a given floxed locus, the number of floxed loci that must be successfully targeted to achieve full genetic inactivation of a target gene, and perhaps even chromosome-localization effects that restrict the access of Cre-recombinase to a given floxed locus [194]. In the *Sox9*^{CreER};*RBPJ*-floxed system, we can invoke two of these factors as potentially detrimental to the efficacy of our lineage tracing capability. First, CreER-based systems are thought to be less efficient than Cre-based systems at recombining floxed alleles,

and the amount of Cre-recombinase translocated to the nucleus upon TAM-administration represents one important determinant of recombination frequency [194]. While we were successfully able to "hit" the lineage reporter allele in an appreciable number of *Sox9*-expressing cells through administration of high and persistent does of TAM (~50%), we expect there to be, even in an ideal case, as much as a 50% non-overlap between $EYFP^+$ cells that retain at least one intact floxed allele, and $EYFP^+$ cells that have undergone successful recombination. Second, the loxP sites that flank exons 6 and 7 in the *RBPJ* floxed allele are more widely spaced (~ 2.3 kb) [191], when compared to the Lox-STOP-Lox sequence in the lineage reporter allele (~ 1.9 kb) [194,195]. We suspect that a 400 bp increase in spacing between the loxP sites of the RBPJ floxed allele and the lineage reporter allele could contribute to the degree of non-parallel recombination in our system. Thus, multiple features of the *Sox9*^{CreER};*RBPJ*-floxed system call into question whether or not this model can be successfully utilized to target and analyze *RBPJ* function in the trunk domain.

The proposal that there may be an inefficient, or perhaps even non-existent, recombination of *RBPJ* in our system begs an important question. That is, how does one explain the observed changes in (total $Neurog3^+$/total $Sox9^+$), and the observed changes in relative endocrine versus duct compartment sizes which occur in the different genotypes in response to TAM administration? First, under the assumption that there is at least some deletion of *RBPJ* in response to TAM, and that *RBPJ* does in fact function to limit endocrine differentiation in *Sox9*-expressing cells, it could be the case that our genotyping methods used to detect recombined floxed alleles are not sensitive enough to detect a small number of recombination events. Indeed, the changes observed in our experimental animals a relatively minor. The ~25% increase in $Neurog3^+$ cell numbers relative to $Sox9^+$ cells is consistent with a 1 in 10 recombination rate for any given cell. The measured increase in endocrine 'mass' relative to the duct in *Sox9*^{CreER};*RBPJ*$^{fl/fl}$ animals at E18.5 could reflect the sum of these infrequent recombination events that occur over a 5-day period. The notion that the increase in (total $Neurog3^+$/total $Sox9^+$) is augmented at E18.5 (Fig. 3.3G) in the *Sox9*^{CreER};*RBPJ*$^{fl/-}$ condition (this condition should have hypothetically a higher frequency of *RBPJ* KO due to the presence of only one floxed allele) is consistent with the idea that *Sox9*^{CreER} is indeed able to recombine *RBPJ*

floxed alleles at some frequency. We propose that it might be useful to FACS isolate endocrine islets and DBA^+ duct cells from control and experimental animals at E18.5, and then assess the relative enrichment of recombined *RBPJ* floxed alleles in each tissue-fraction by genomic PCR. In this manner, it might be possible to show an enrichment of the recombined *RBPJ* floxed locus in the endocrine compartment versus the ductal compartment. We do not propose that these experiments convincingly argue for a cell autonomous function for *RBPJ* in limiting endocrine differentiation from the trunk domain during secondary transition.

Previous studies have shown that increased endocrine differentiation caused by pharmacological inhibition of Notch results in thinning of the trunk epithelial lumen [72]. We did not observe such changes in our experiments. We suspect that this could be due to either an inability to resolve small changes in epithelial lumen morphology using the relatively low-resolution analyses presented here. Conversely, there could be compensatory growth processes that become activated in the trunk in response to increased endocrine lineage differentiation. In this regard, it has been previously shown that the initial numbers of MPC allocated to the pancreas-specified bud determine the final size of the pancreas [17], suggesting that there are *not* compensatory growth mechanisms intrinsic to the pancreas growth program. However, these experiments [17] targeted primary MPC, and do not rule out that interventions in secondary transition progenitors might elicit compensatory growth at later-stages. We also documented observations that acinar lumens become enlarged or dilated in response to TAM exposure. This could be the result of *RBPJ*-loss in the acinar cells themselves (Sox9 is expressed at low levels in these cells) [31,80], or could be due to non-autonomous influences of RBPJ-loss in the trunk. A previous study showed that over-expression of a dominant negative form of the obligatory Notch transcriptional co-activator mastermind-like1 [46], or genetic deletion of the Notch-signal processing enzymes presinilin1/2 [197], caused Notch-pathway-deficient cells to adopt acinar status. Thus it is possible then that cells inactivating *RBPJ* adopt a pro-acinar fate, which leads to increasing numbers of cells moving into the acinar clusters, which then grow larger and become dilated as a result. If this altered cell-fate allocation depleted *Sox9*-expressing cells from the epithelium, without also depleting cells undergoing endocrine differentiation, it could explain how the relative sizes of the duct and endocrine pancreas

become skewed toward the endocrine compartment by late gestation. We suggest that gaining an understanding of the biology underlying these phenotypes will be much easier to accomplish in an experimental model that is more robust and not as hampered by the limitations and caveats intrinsic to the *Sox9*^{CreER};*RBPJ*$^{fl/fl}$ system.

The Neurog3^{OE} *system to study the cell-non-autonomous effects of endocrine differentiation on trunk progenitor function*

We find the *Neurog3*^{OE} system to be an attractive model for studying the non-autonomous effects of endocrine cell birth on the function and behavior of progenitor cells in the trunk epithelium, as it overcomes essentially all of the shortcomings of the *Sox9*^{CreER};*RBPJ*$^{fl/fl}$ system. This is especially true given the fact that cells experimentally induced to ectopically express Neurog3 move through a differentiation sequence that, in terms of timing and progress through different states of Neurog3 and Sox9-positivity, appears to be quite similar to that which is observed normally (Chapter II). Manipulations using *Neurog3*^{OE} should be informative in an otherwise "normal" genetic background. Such an experimental genotype allows for analysis of the consequences of 'over-production' of Neurog3^{+} cells from the trunk domain. For instance, one can assess the acute consequences of large-scale and abrupt endocrine lineage production on the patterning of *Neurog3* expression and endocrine differentiation within the trunk. We hypothesize that the controlled induction of large amounts of induced (and GFP-labeled) endocrine cells from the trunk will have a pronounced inhibitory effect on the numbers of un-induced (GFP-negative) cells entering into the Neurog3^{+} state. The power of the *Neurog3*^{OE} system should also become evident when it is bred into different genetic backgrounds. Breeding *Neurog3*^{OE} into the *Neurog3* nullizygous condition, for instance, would readily allow for two important levels of analysis. First, one could assess the acute consequences of broad induction of Neurog3 expressing cells on the altered state of the *Neurog3*-deficeint epithelium. These include documented alterations to the morphology of the epithelium, and alterations to *Neurog3* and Hes1 gene expression patterning within the epithelium [72]. At a second level of analysis, one can activate Neurog3 induction-competence in a highly mosaic or clonal fashion, and then assess the local effects that Neurog3 producing

cells have on, for instance, Hes1-expression in neighboring cells within the epithelium. In sum, the *Neurog3*^{OE} system could represent a powerful tool for studying the spatiotemporally defined and quantized influences that differentiating endocrine cells have in regulating the growth, morphogenesis, and differentiation properties of the epithelial progenitors.

Neurog3^{CreER} *BAC transgenic line for studying the behavior of the Neurog3*^{LO} *condition*

A previous study showed that *Neurog3*-expressing cells of the intestinal tract and pancreas exhibit a remarkable degree of plasticity with regards to their lineage potency [68]. All enteroendocrine cells in the intestine [68], and all endocrine cells of the pancreas are born from Neurog3^{+} cells [63]. However, a small fraction of *Neurog3*-expressing cells in the intestine can give rise to goblet and paneth cells [68], in the stomach to acid-producing cells [68], and in the pancreas to duct and acinar cells [63]. These studies suggest that a Neurog3^{LO} state in the pancreas could represent an important, and possibly stable, replicating intermediate progenitor cell that feeds the production of committed endocrine precursors during secondary transition. We have used the same BAC fragment used in the studies documenting the plastic lineage allocation behavior of *Neurog3*-expressing cells to generate our *Neurog3*$^{BAC\text{-}CreER}$ construct. This BAC molecule contains a large portion of the accessory genomic sequence comprised by the 5' and 3' DNA flanking the *Neurog3* locus, which has been shown to contain distal enhancer as well as promoter-proximal elements regulating *Neurog3* [59,198]. We suspect that the selection of this particular BAC molecule will improve the fidelity and sensitivity of lineage tracing in a manner that will benefit studies geared toward studying the Neurog3^{LO} condition. We propose that initial studies should focus on lineage tracing Neurog3^{LO} cells to assess whether they are maintained in the trunk epithelium for long periods of time, whether they can undergo several rounds of division, whether they are unipotent for hormone^{+} endocrine subtypes [16], and whether they exhibit a preferred mode of endocrine lineage allocation (via asymmetric division or terminal differentiation, for example) [163].

Acknowledgments

We thank M. Sander for the Sox9CreER transgenic line, and T. Honjo for RBPJ floxed. We thank members of the Wright and Gu labs, as well as Anna Means for helpful discussions. We thank M. Magnuson for the *ROSA26* and *Neurog3* ectopic expression alleles presented here.

CHAPTER IV

FEEDBACK CONTROL OF GROWTH, DIFFERENTIATION, AND MORPHOGENESIS OF PANCREATIC ENDOCRINE PROGENITORS IN AN EPITHELIAL-PLEXUS NICHE

Introduction

In the mammalian pancreas, endocrine cells undergo lineage allocation upon emergence from a bipotent duct/endocrine progenitor pool, which resides in the "trunk epithelium". Major questions remain regarding how niche environments are organized within this epithelium, to coordinate endocrine differentiation with programs of epithelial growth, maturation and morphogenesis. We used tissue-reconstruction approaches to analyze how endocrine progenitors, and their differentiating progeny, are assembled within the trunk as it undergoes remodeling from an irregular plexus of tubules to form the eventual mature, branched ductal arbor. The bulk of endocrine progenitors are maintained in an epithelial 'plexus state', which is a transient intermediate during epithelial maturation, and within which endocrine-cell differentiation is continually robust and surprisingly long-lived. Within the plexus, local feedback effects derived from the differentiating and delaminating endocrine cells non-autonomously regulate the flux of endocrine-cell birth, as well as proliferative growth of the bipotent cell population, using Notch-dependent and independent influences, respectively. These feedback effects, in turn, maintain the plexus state to ensure prolonged allocation of endocrine cells late into gestation. These findings begin to define a niche-like environment guiding the genesis of the endocrine pancreas, and advance current models for how differentiation is coordinated with the growth and morphogenesis of the developing pancreatic epithelium.

This chapter have been published as Bankaitis ED, Bechard ME, and Wright CV. 2015. Feedback control of growth, differentiation, and morphogenesis of pancreatic endocrine progenitors in an epithelial plexus niche. *Genes and Development* **29**, 2203-2216 [211].

Material and Methods

Mice. Neurog3^{EGFP} knock-in mice from Guoqiang Gu (Vanderbilt University) were genotyped as described [59]. *Neurog3*$^{EGFP/+}$ and Neurog3$^{EGFP/EGFP}$ embryos were phenotyped by EGFP fluorescence and lack of endocrine cells, or genotyped with primers *ngn3-1* 5'-ATACTCTGGTCCCCCGTG-3', *ngn3-2 5'-TGTTTGCTGAGTGCCAACTC-3', and EGFP 5'-GAACTTGTGGCCGTTTACGT-3' [59]*. Wild-type mice were of mixed genotype. All protocols were approved by Vanderbilt University IACUC.

*Immunodetection***.** Embryonic pancreas was paraformaldehyde-fixed (4%; 4^{o}C, 4-6 hours). For cryosectioning, samples were sucrose-equilibrated (30%; 4^{o}C overnight) and OCT-embedded (Tissue-Tek). Thick cryo-sections (30-45 μm) were obtained on a Leica CM3050 S. For whole-mounts, pancreata were manually divided into core and peripheral regions, and processed as described [166]. Antibodies used include hamster anti-Muc1 (NeoMarkers 1:1000), DBA (Vector Labs, 1:400), rabbit anti-CK19 (B. Stanger, U. Penn, 1:2000), rabbit anti-Sox9 (Millipore, 1:5000), goat anti-Neurog3 (Gu Lab, 1:40,000), guinea pig anti-Neurog3 (Sander Lab, 1:2000), guinea pig anti-Pdx1 (Wright Lab, 1:1000), rat anti-Ecad (AbCam, 1:1000), guinea pig anti-insulin (Dako, 1:1000), chicken anti-GFP (Aves, 1:2000), rabbit anti-amylase (Sigma, 1:1000), guinea pig anti-Hes1 (T. Sudo, Toray Industries, Japan, 1:4000).

qRTPCR. Total RNA was TRIzol-isolated from dorsal pancreata and cDNA synthesized with iScript cDNA Synthesis Kit (Bio-Rad) for PCR in a Bio-Rad CFX96 with SsoFast EvaGreen Supermix (Bio-Rad). Expression level was normalized to GAPDH by the ΔΔCt method. Primers include *GAPDH 1F* 5'-ACTTTGGCATTGTGGAAGG-3', *GAPDH 1R* 5'-GGATGCAGGGATGATGTTCT-3', *Hes1 RTf* 5'-TAGCCCACCTCTCTCTTCTGA-3', *Hes1 RTr* 5'-CAGTGCATGGTCAGTCACTTAAT-3', *Sox9 RT2for* 5'-CTCCCCCTTTTCTTTGTTGTTT-3', *Sox9 RT2rev* 5'-TCTGAAACCTCTCATTTGTCCA-3'.

DBZ and EdU administration and quantification. DBZ (Cayman Chemical) was resuspended finely in ME4M slow-delivery vehicle (Methocell^{TM}) using a motorized pestle, and injected I.P. EdU (Life Technologies) was given I.P. (10 mg/kg). EdU was detected by the Click-iT Plus EdU

Imaging Kit (Molecular Probes). S-phase indices and percent EdU incorporation were counted manually.

Image Acquisition and 3D reconstructions. Confocal images were from a Zeiss LSM 510 META (details in figure legends), and 3D reconstructions were rendered using Imaris Software.

Quantification and Statistical Analyses. Muc1$^+$ plexus and duct areas were traced manually as indicated in the figure legends. Pixel areas were obtained using ImageJ. All sectional analyses covered approx. 30% of the dorsal pancreas. For endocrine-yield measurements within plexus, duct, and DB states, the morphology types were based on the Muc1 lumen structure. Sox9$^+$ and Neurog3$^+$ cells were counted manually. Muc1$^+$ lumen that was not unambiguously scorable as plexus, duct, or DB was not analyzed. For Hes1-immunofluorescence, mean pixel intensity was determined using ImageJ. For Sox9 immunofluorescence, mean pixel intensity was determined using Imaris image-analysis software (Dots function, 4 μm nuclear sphere). Statistical analyses were performed using Graph Pad software.

Results

Neurog3$^+$ populations show non-random localization patterns within the trunk

To address if nascent endocrine cells arise preferentially in different locations within the secondary transition trunk, we evaluated the localization of Neurog3$^+$ cells relative to the Muc1$^+$ epithelial lumen. Because the bulk of the endocrine mass at birth lies relatively interiorly (data not shown), we compared core and peripheral regions to assess whether the later endocrine-mass distribution reflects an earlier bias in the location of newly born endocrine cells. As previously described, Neurog3$^+$ cells at E15.5 were broadly distributed in a salt-and-pepper pattern across the Muc1$^+$ lumen, both in the core and periphery, and were absent in Muc1$^+$Amylase$^+$ pro-acinar tips (Fig. 4.1A,C) [14]. At E17.5, significant portions of epithelium showed a reduction or lack of Neurog3$^+$ cells (Fig. 4.1B,D). Diminished Neurog3$^+$ cell numbers were evident in the core, especially where lumen diameters were large, and in the periphery where lumens joined with amylase$^+$ tips. There remained however, frequent instances along

the lumen where the density of Neurog3^{+} cells was comparable to the E15.5 stage. These data outline a non-random localization pattern of endocrine commitment from the trunk, and suggest that endocrine-cell birth might be coordinated with specific epithelial morphogenetic states.

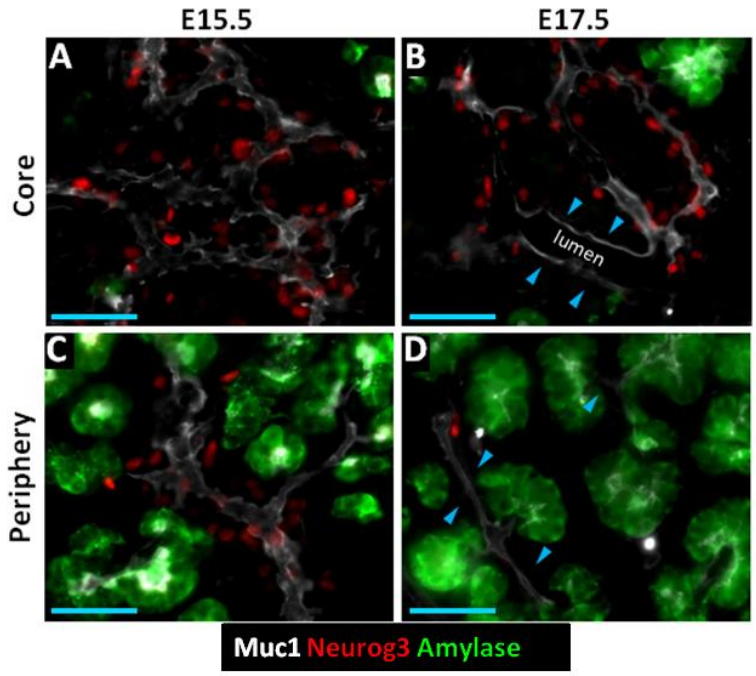

Figure 4.1. *Neurog3^{+} populations show non-random localization patterns within the trunk. (A-D) Epifluorescence images of core and peripheral regions, in 10 μm cryosections showing Muc1, Neurog3, amylase. (A,C) Neurog3^{+} cells distributed over Muc1^{+} lumen surface. (B,D) Regions of lumen where Neurog3^{+} cells are reduced in number. Blue arrowheads in B, enlarged lumen in the core; blue arrowheads in D, lumen interconnecting amylase^{+} tips. Scale bars 50 μm. This figure was adapted from [211].*

Plexus expansion and plexus-to-duct transformation in the organ core

As a first step toward analyzing relationships between endocrine differentiation and epithelial morphogenesis, we used a whole-mount and thick-section-based approach to categorize epithelial states (derived via lumen morphology) existing as the trunk remodels from the initial plexus to the arborized ductal system (Fig. 4.2A). At E14.5-15.5, consistent with a previous report [24], the majority of the core was composed of a complex, web-like plexus (Fig. 4.2B). Within the plexus, intersecting segments of epithelium varied in length and diameter (Fig.

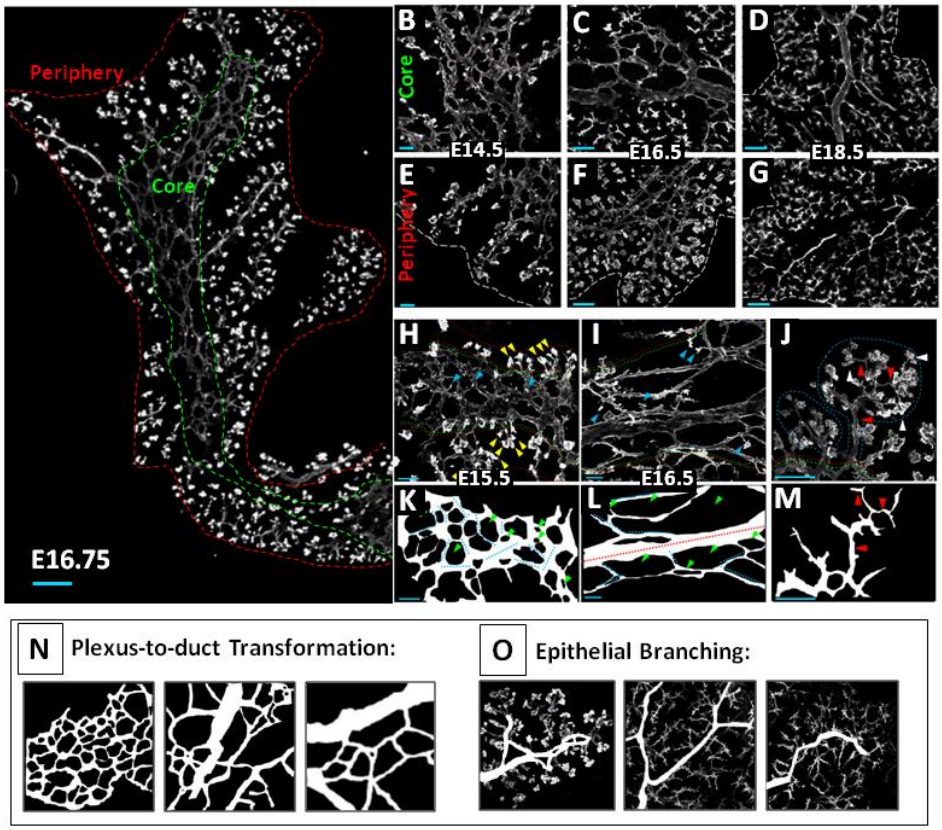

Figure 4.2. *Epithelial morphogenesis comprises plexus remodeling in the core and epithelial branching in the periphery. (A) Composite 10x images of 45 μm thick cryosectioned dorsal pancreas at E16.75. Green and red dashed lines bound the core and periphery, respectively.* ***(****B-D) Muc1-labeled 35 μm thick cryosections showing typical progression through plexus expansion and duct-transformation in the core. (E-G) Epithelial branching in the periphery. White dashed line, outer organ boundary. (G-L) Confocal z-stacks show features of plexus (H,K), duct (I,L), and DB (J,M) states. Core (green dashed line in I-J); periphery (red dashed line). Small, unclefted DBs in the core (blue arrowheads), clefted DBs in the periphery (yellow arrowheads in H), lobes of DBs (blue dashed line), Muc1^{+} lumen of pro-acinar tips (white arrowheads in J), and connecting lumen (red arrowheads in J). (K-M) Line traces of lumen from H-J. Individual segments of plexus (dotted light blue lines) and core duct-states (red dashed line). Note the increase in lumen diameter, and the continuous directionality across representative 40x field, of the duct-state in L relative to the plexus in K. Green arrowheads: unlabeled cell-fields (epithelial & parenchymal) bounded by Muc1 signal. (N,O) Traced representations of the processes of plexus-to-duct transformation in the core, and epithelial branching in the periphery. Scale bars 20 μm in B,E,H-J; 50 μm in C,F; 100 μm in A,D,G. This figure was adapted from [211].*

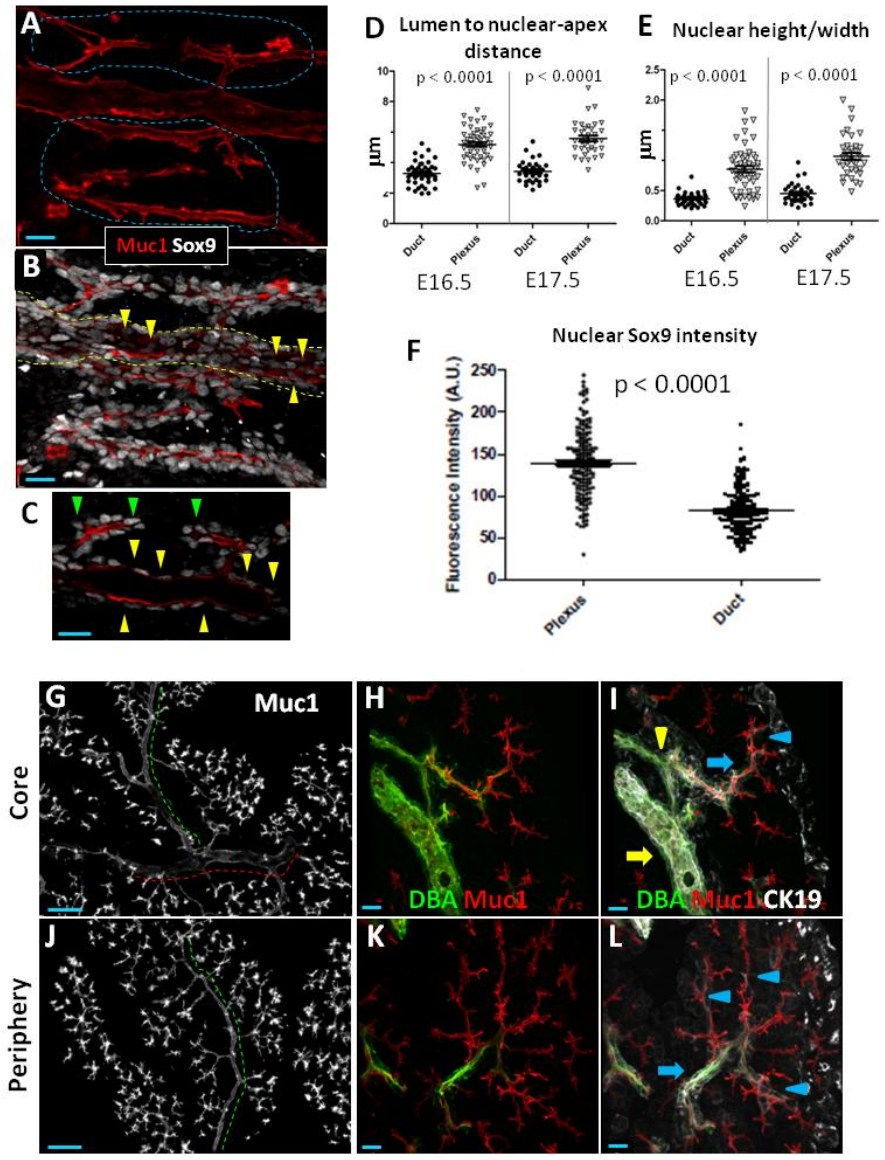

Figure 4.3. *Formation of the core-duct and ductal-branch states during late gestation. (A,B) Plexus-to-duct transformation (from Fig. 2I,L) showing plexus (blue dashed line in A) connected to duct (yellow dashed line in B). Sox9 in plexus and duct-states (C is sectional inset from B). (D,E) Analysis of nuclear position and shape in plexus versus core duct states. (F) Quantification of mean fluorescence intensities in Sox9$^+$ populations from plexus and duct states at E17.5 (G,J) Epifluorescence images of 30-40 µm-thick cryosections showing central (red dashed line) and interlobular ducts (green dashed line) at E17.5. (H,I,K,L) Fluorescence detection of DBA$^+$, Muc1$^+$, and CK19$^+$ epithelium at 40x magnification in ~35 µm confocal z-stacks. DBA marks the central (yellow arrow), interlobular (yellow arrowhead), and intralobular ducts (blue arrow). (L) CK19 marks the same, in addition to DBA$^-$ intercalating ducts (blue arrowhead). Scale bars are 15 µm in A-C, 100 µm in G,K; 20 µm in H,I,K,L. This figure was adapted from [211].*

4.2H). In traced representations, cell fields bounded by the Muc1$^+$ lumen (represented as "holes" in the plexus web) varied in size and shape, but showed a uniform heterogeneity across

the core (Fig. 4.2K). There was no evidence of an extensive arborized ductal structure at these stages. We found little evidence of multi-branched epithelia interconnecting pro-acinar tips, except at the outer edges of the plexus. Most pro-acinar tips (demarcated by a bulb-like morphology and intense Muc1-positivity) appeared as small, individual tips interspersed throughout the plexus. We conclude that the principal epithelial state in the core from E14-15.5 is plexus.

At E16.5, there was an expansion of the plexus state concomitant with the increase in organ size. This was accompanied by a transformation of the plexus into ductal states representing the beginnings of an arborized ductal system. Ductal states in the core were discernible by their increased lumen diameter and extended, continuous directional orientation compared to the web-like plexus (Fig. 4.2C,D). This "plexus-to-duct transformation" occurred asynchronously across the organ, and was evident first with appearance of the central duct (E16.5). Cells in the core ductal state showed measurably reduced Sox9 immunoreactivity, and a flattening of cells and their nuclei (Fig. 4.3A-F), consistent with an acquisition of a ductal phenotype [82]. At E17-18.5, connecting interlobular ducts were observed to form, oriented toward the periphery (Fig. 4.3G-I). This process remained incomplete even late into the secondary transition, and abundant plexus remained in scattered locations at E18.5 (Fig. 4.3). These analyses show that trunk morphogenesis in the core is dominated by an initial phase of growth and expansion in a plexus state, followed by plexus-to-duct transformation to generate the core of the ductal arbor (Fig. 4.2N).

Epithelial branch remodeling in the organ periphery

In contrast to the organ core, a pervasive epithelial branching process was evident in the periphery (Fig. 4.2A,E-G). From E14.5-E18.5, pro-acinar tips exhibited a variety of clefted morphologies, and appeared to grow and multiply progressively to generate lobes of interconnected ductal branches (hereafter "DB") linking multiple tips (Fig. 4.2J,M). Intervening DB-segments multiplied and lengthened over time, at late stages forming $CK19^{+}DBA^{+}$ intralobular ducts and distal $CK19^{+}DBA^{-}$ intercalating ducts (Fig. 4.3J-L) [167]. DBs were most

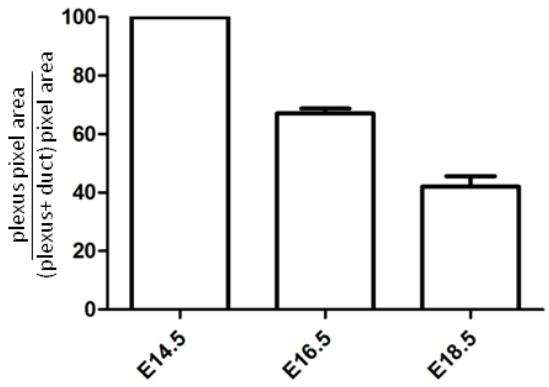

Figure 4.4. *Dynamics of plexus-to-duct transformation in the core. Measurement of relative pixel area for Muc1$^+$ plexus over the combined plexus and duct-state pixel area in the core. Measurements were taken from serial 30-40 μm thick sections covering whole dorsal pancreata. Measurements exclude Muc1$^+$ ductal branches and pro-acinar tips. Measurements were taken using ImageJ software. Error bars are S.E.M, n = 3 for each time point. This figure was adapted from [211].*

advanced in peripheral regions devoid of plexus, but less so in regions within or approaching the plexus. Taken together, we detect two disparate patterns of trunk morphogenesis during the secondary transition. There is a long-lived plexus expansion followed by plexus-to-duct transformation in the core, contrasted to pervasive epithelial branching in the periphery (Fig. 4.2N,O). These observations on the spatiotemporal and morphological features of plexus, duct, and branched (DB) epithelial states provide a basis to map correlations between endocrine-lineage flux and states of epithelial morphology.

Endocrine differentiation is enriched in the plexus

To ascertain if Neurog3$^+$ populations have specific localization patterns within the remodeling epithelium, we compared endocrine yield (as determined by the ratio of Neurog3-to-Sox9$^+$ cells; see Chapter II) between plexus, duct, and DB states from E14.5-E18.5. Epithelial cells in plexus, duct, and DB states showed similar Sox9 immuno-reactivity (Fig. 4.5A-F). Low Sox9 signal was observed in pro-acinar tip cells, which were excluded from our analysis. From E14.5-E18.5 endocrine yield was highest in the plexus, and significantly lower or absent in ducts and DBs (Fig. 4.6A-H). Endocrine yields measured selectively from samples of plexus consistently

exceeded those measured from bulk sectional analyses, indicating that endocrine yield is enriched in the plexus (Fig. 4.6I). At E18.5, there were scattered yet extensive remainders of plexus, which were invariably associated with large numbers of Neurog3^{+} cells, indicating that a high level of endocrine differentiation is consistently maintained in the plexus, independent of stage (Fig. 4.7A-D). Sharp boundaries demarcating high and low endocrine yields were

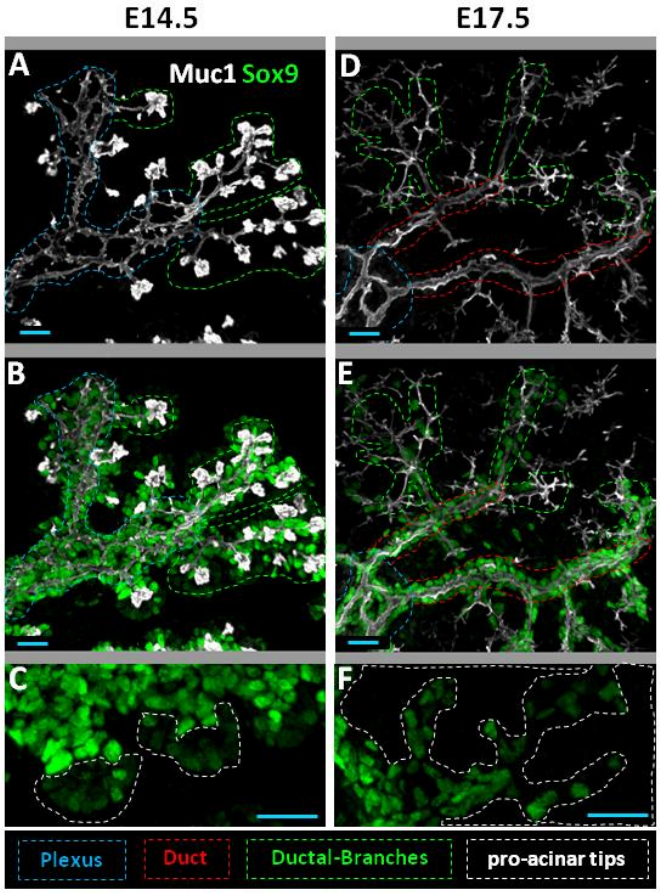

Figure 4.5. *Sox9^{+} populations mark plexus, duct, and ductal-branch states. (A-F) Whole mount z-stack reconstructions of Sox9 and Muc1-labeled epithelium in peripheral segments of wild-type dorsal pancreas at E14.5 and E17.5. Blue, red, and green boundaries demarcate plexus, duct, and ductal-branch states, respectively. (C,F) Pro-acinar tips are demarcated by intense Muc1 signal, a bulb-like morphology that becomes clefted and elongated over time, and a low nuclear Sox9 signal that diminishes over time. Scale bars are 20 μm. This figure was adapted from [211].*

commonly observed at the interface between plexus and duct or DB states, respectively, suggesting a rapid cessation of endocrine-cell birth concomitant with loss of plexus morphology. These data put forth the view that endocrine differentiation is robust and

enriched within the plexus during the entire secondary transition, and is rapidly downregulated upon plexus-to-duct transformation in the core, or engagement of epithelial branching in the periphery.

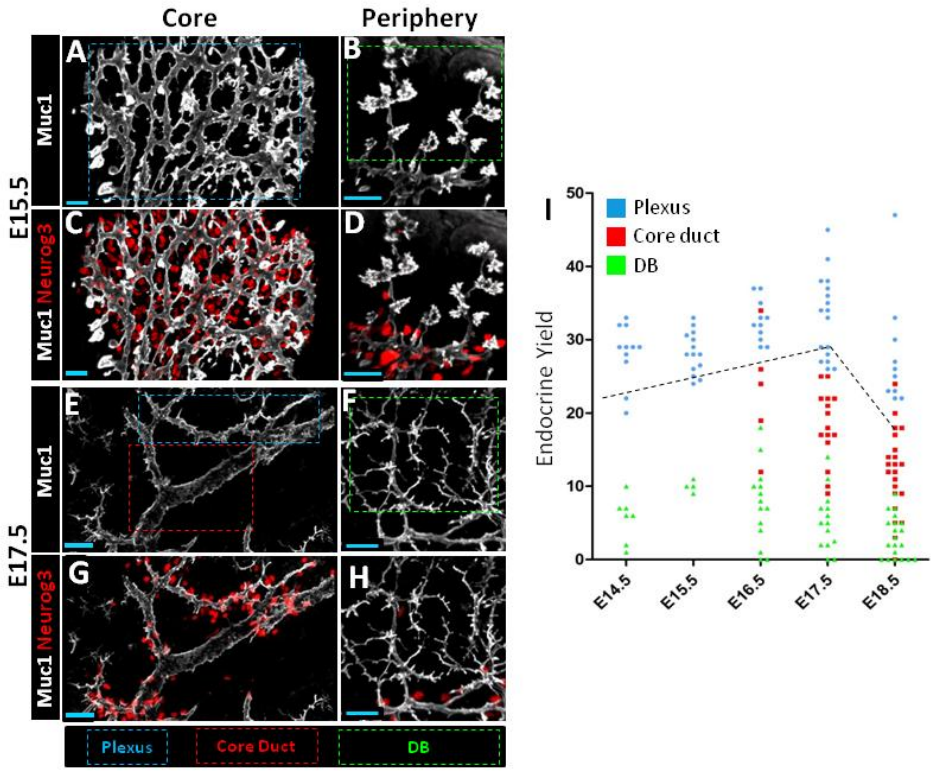

Figure 4.6. *Endocrine differentiation is enriched in the plexus-state. (A-H) Representative images of Neurog3^{+} cells in relation to plexus (blue dashed box), duct (red dashed box), and DB (green dashed box) states. Scale bars 20 μm. (I) Comparison of endocrine yield in plexus, duct, and DB states. Each point represents endocrine yield summed from individual 35-50 μm thick 40x z-stacks. E14.5-E18.5 plexus vs DB, $p < 0.0001$. E17.5 and E18.5 plexus vs duct, $p < 0.0001$. E16.5 plexus vs duct $p = 0.0019$. Error bars are S.E.M, Student's t-test. Bulk endocrine yield determined in A (black dashed line). This figure was adapted from [211].*

Notch-responsive endocrine progenitors are enriched in the plexus

Consistent with a proposed model for lateral Notch-pathway activation by Neurog3-expressing cells [32,168,169], genetic ablation of Neurog3, as reported previously [72], caused loss of Hes1 (a Notch transcriptional-effector) signal in Sox9^{+} epithelial cells, suggesting that Notch-pathway activity is Neurog3-dependent, and engaged locally in the plexus-state (Fig. 4.8A-D). Consistent with this notion, immunodetection of the Hes1 showed relatively pervasive expression in the

plexus compared to regions of fully-resolved core ducts and peripheral DBs, suggesting that Notch-responding cells are enriched within the plexus (Fig. 4.9A,B). Because Notch-Hes1 signaling blocks endocrine differentiation, we hypothesized that $Sox9^{+}$ populations in the plexus

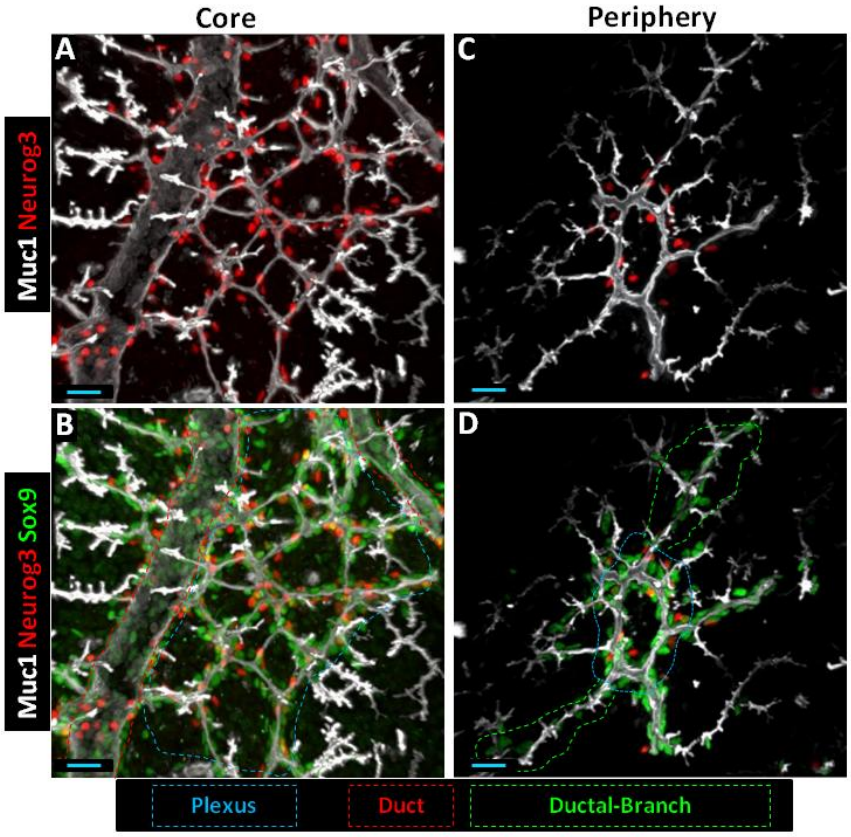

Figure 4.7. *Endocrine differentiation in the plexus-state persists late into secondary transition. (A-D) Muc1, Neurog3, and Sox9 whole-mount immunolabeling of core and peripheral regions of dorsal pancreas exhibiting plexus (blue dashed line), ductal-branch (green dashed line), and duct (red dashed line) states at E18.5. Note reduced Sox9 levels in duct compared to plexus in B. Scale bars are 20 μm. This figure was adapted from [211].*

would show an increased endocrine-differentiation response, compared to duct and DB states, under conditions where Notch is inhibited. To test this, we compared endocrine yield in E17.5 embryos from pregnant dams injected each day for two days with the gamma-secretase inhibitor DBZ, which blocks Notch signaling [170,171]. Similar to a previous report showing dose-dependent reductions in *Hes1* and *Sox9* expression in Notch-inhibited pancreatic explants [32], increasing DBZ doses elicited reproducible, progressive reductions in pancreatic *Hes1* and *Sox9* expression measured by qRT-PCR. *Hes1* decreased at a lower DBZ dose (0.15 ± 0.06 and 0.09 ± 0.07, at 12 and 20 μmol/kg DBZ relative to control, respectively) as compared to *Sox9*

(0.88 ± 0.18 and 0.43 ± 0.18, 12 and 20 μmol/kg DBZ relative to control) (Fig. 4.9H). We chose the 12 μmol/kg DBZ condition for analysis of endocrine yield, due to the minimal effect registered on *Sox9*. Endocrine yield from the plexus was robustly increased in response to DBZ

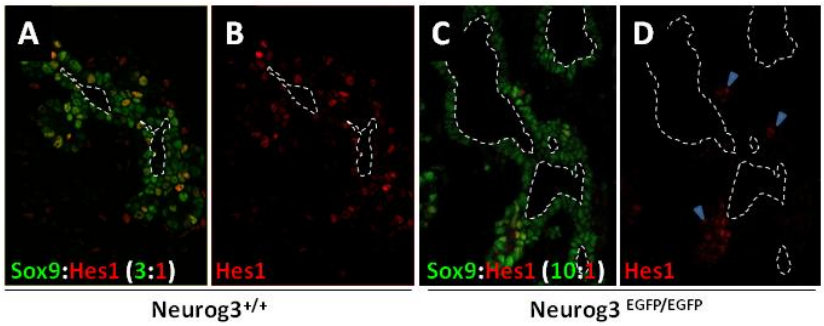

Figure 4.8. *Epithelial Hes1-expression is lost under Neurog3-deficient conditions. (A-D) Frozen section analysis of the ratios of Hes1^{+} and Sox9^{+} populations in the trunk domain of control and Neurog3-deficient animals. (D) Blue arrowheads indicate clusters of Hes1^{+} cells in the Neurog3$^{EGFP/EGFP}$ samples. This figure was adapted from [211].*

(Fig. 4.9C-F), and consistently approached a near three-fold increase relative to the vehicle-treated condition. Assuming the absence of a proliferation effect on Sox9^{+} cells, this increase indicates that approximately half of the plexus population (endocrine yield = 1 indicates 1:1 Neurog3:Sox9) defaults to the endocrine lineage under these conditions (Fig. 4.9G). In contrast, Sox9^{+} cells in duct and DB states showed marginal and variable responses to DBZ, indicating that Sox9^{+} cells in these states are largely refractory to endocrine differentiation. These expression data and inhibition studies suggest that the plexus-state is enriched for a Notch-responsive Sox9^{+} progenitor pool that is poised to adopt the endocrine lineage under normal conditions.

Sox9^{+} cell replication is uncoupled from Neurog3-dependent Notch-inhibition of endocrine differentiation

Notch signaling has been linked to the regulation of mitogenic cell-cycle progression [41,172,173]. We analyzed whether the Notch function in maintaining the undifferentiated progenitor state is coupled with the maintenance of proliferative growth in Sox9^{+} cells. We

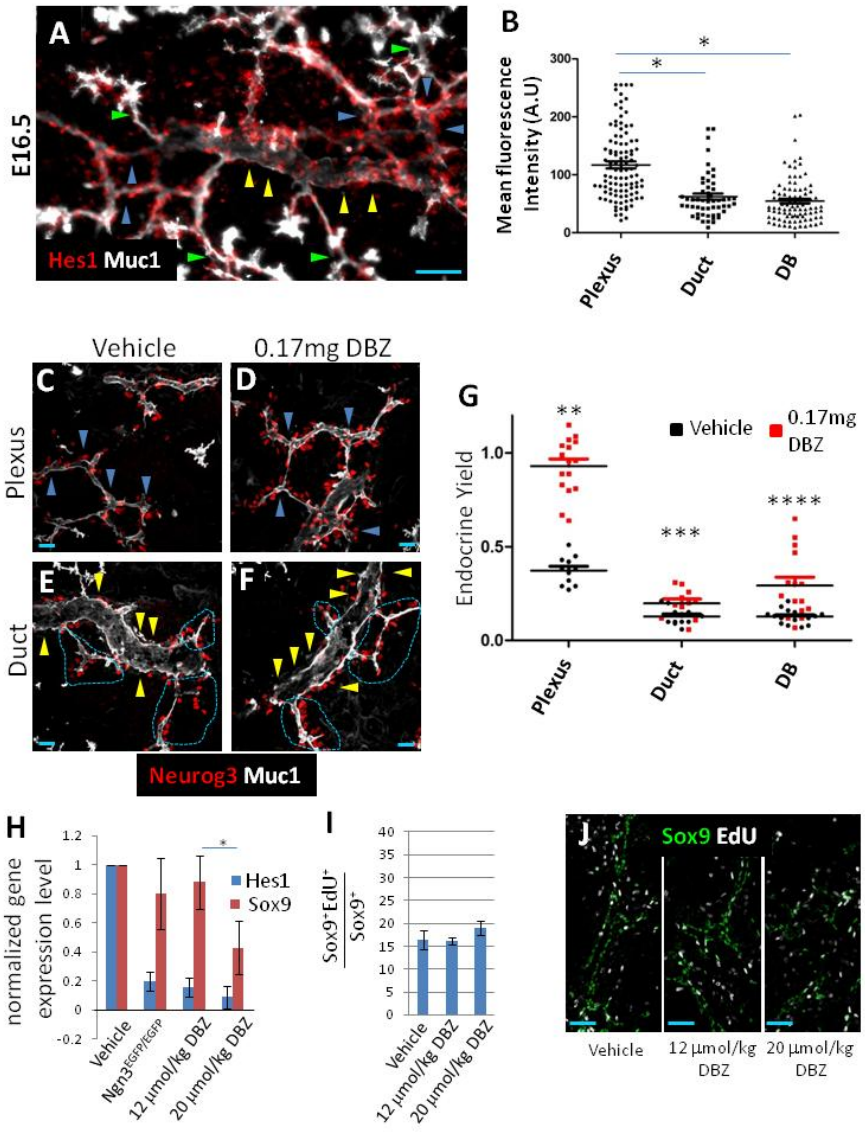

Figure 4.9. *Notch-responsive progenitors are enriched in the plexus-state. (A) Detection of Hes1 relative to the Muc1^{+} duct-state (yellow arrowheads), plexus-state (blue arrowheads), and DBs (green arrowheads). Scale bar 50 µm. (B) Mean nuclear intensity of Hes1 signal in individual Sox9^{+} cells. N=102 plexus, N=91 DB (*) (p < 0.0001), N=52 duct (p < 0.0001) from three separate z-stack volumes. Error bars: S.E.M, Student's t-test. (C-F) Representative images of Muc1 and Neurog3 in plexus and duct-states under vehicle or DBZ treatment. Blue arrowheads delineate plexus in C,D; yellow arrowheads indicate the surface of ductal states in E,F; dashed magenta lines delineate locations where Neurog3-rich plexus intersects with the duct state. Scale bar 20 µm. (G) Endocrine yield in plexus, duct, and DB states under vehicle or DBZ treatment. Each point represents endocrine yields summed from individual 40x z-stack volumes (~35-50 µm thick). N=11, N=12, N=15 for plexus, duct, and DB in vehicle control. N=16, N=11, N=15 for plexus, duct, and DB in DBZ-treated group. n=3 for both conditions. Error bars are S.E.M, (**) p < 0.0001, (***) p=0.0149, (****) p=0.0013, Student's t-test. (H) Normalized gene expression for Sox9 and Hes1 under control, Neurog3-deficient, and DBZ-treated conditions. Error bars are S.E.M, n ≥ 3 for each condition, (*) p=0.0373. (I,J) One-hour EdU indices in Sox9^{+} populations under control or DBZ treatment. Error bars S.E.M., n = 3. This figure was adapted from [211].*

evaluated EdU uptake in embryonic pancreata taken from DBZ-treated dams. For both 12 and 20 μmol/kg doses, we observed no change in the proportion of $Sox9^+$ cells replicating DNA after two days DBZ administration (Fig. 4.9I,J). Because these DBZ doses reduced Notch activity by an amount similar to or beyond that caused by Neurog3-deficiency (Fig. 4.9H), we conclude that bulk epithelial proliferation behaviors are not significantly affected by reduced Notch activity under these conditions.

Neurog3-deficiency causes reduced $Sox9^+$ progenitor replication and precocious remodeling of the plexus

To evaluate cell-non-autonomous functions for Neurog3 in regulating the growth of the epithelial progenitor pool, we compared cell replication behaviors in $Neurog3^{EGFP/+}$ and $Neurog3^{EGFP/EGFP}$ pancreata. Analysis of S-phase indices indicated a 50% decrease in EdU-labeling of $Sox9^+$ progenitors when *Neurog3* is lost. This decrease was evident at E13.5, when the vast majority of the trunk is in the plexus-state, and also at E16.5 when plexus-to-duct transformation begins in the organ core (Fig. 4.10A-C). This reduction in EdU-labeling was not a general feature of all pancreatic epithelial cells. S-phase indices in pro-acinar cells were unchanged, and because they represent the major cell type during mid-to-late gestation, no gross organ hypoplasia was evident at any stage (Fig. 4.11A-C, and data not shown). These results demonstrate a previously unreported function for Neurog3 in supporting robust replication in the $Sox9^+$ trunk that is, based on the DBZ treatment results above, largely independent of Notch-pathway activity.

Given the reduction in progenitor replication observed under *Neurog3* deficiency, we assessed potential defects in maintenance of the plexus by comparing the time-course for Neurog3-deficient plexus remodeling into duct and DB states. Analyses at E14.5 confirmed previously reported increases in lumen diameters, and moderate decreases in peripheral branching [72] (Fig. 4.10D,E). Surprisingly, we also found frequent DB-like structures emerging in peripheral locations normally comprised of plexus at this stage, indicating a precocious remodeling of plexus morphology into non-plexus states under Neurog3-deficient conditions. At E16.0, a time point just before the plexus normally undergoes transformation into core-duct and peripheral-

DB states, we observed multiple regions where plexus-morphology was diminished or completely lost relative to control (Fig. 4.10G-M). Consistent with this, the relative area of plexus compared to duct-like-states was significantly decreased at E14.5, 16.5 and 18.5 in *Neurog3* null tissue (Fig. 4.10F). These results indicate that Neurog3 functions not only to determine a normal plexus morphology, but also to maintain and propagate the plexus by limiting its remodeling into non-plexus states.

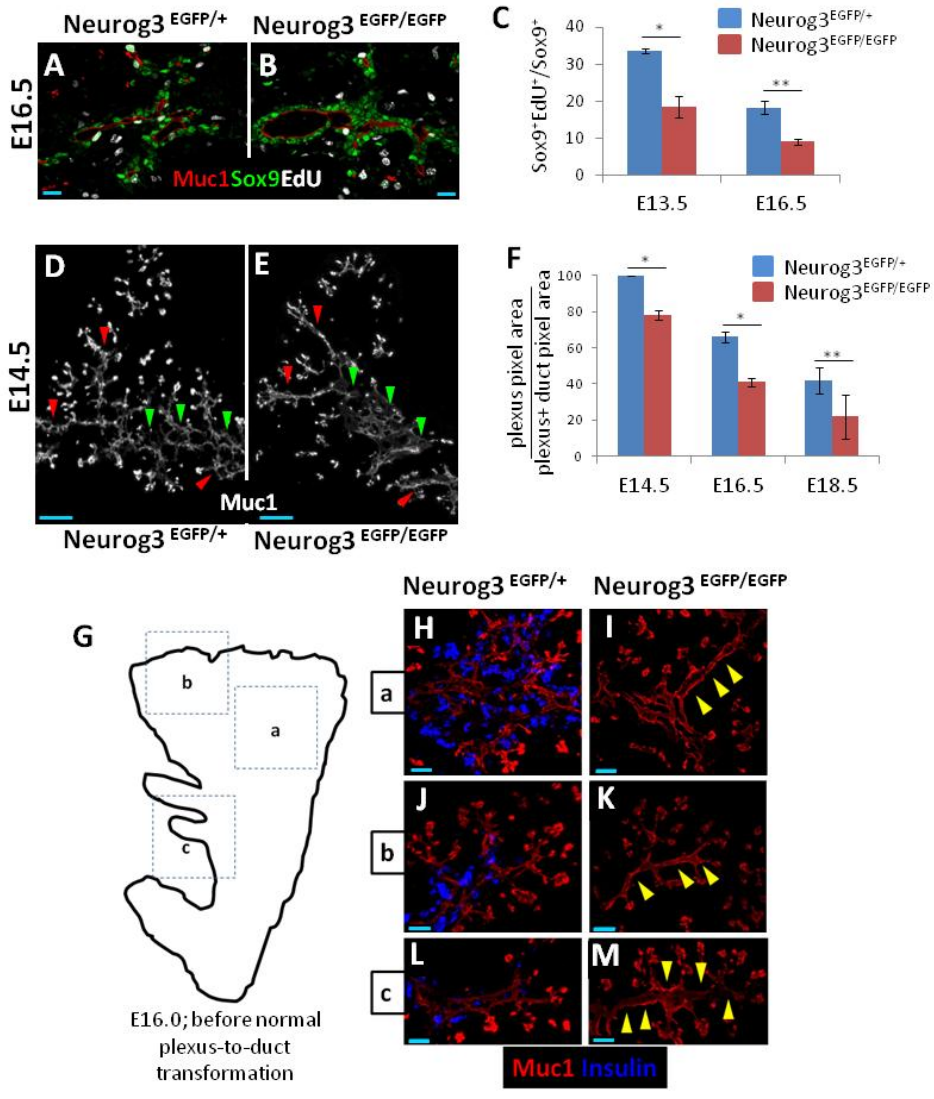

Figure 4.10. *Neurog3 deficiency causes reduced cell replication and precocious loss of the plexus-state. (A,B) S-phase indices in Sox9^{+} cells from Neurog3$^{EGPF/+}$ and Neurog3$^{EGFP/EGFP}$ samples. (C) Quantification of A & B (E16.5), plus measurements at E13.5. Error bars are S.E.M, n=2 E13.5 (*) p=0.0277, n=3 E16.5 (**) p=0.0048 with 30% of dorsal pancreas scored; Student's t-test. (D,E) Dorsal pancreas from E14.5 Neurog3$^{EGFP/+}$ and Neurog3$^{EGFP/EGFP}$*

samples at E14.5. Red arrowheads, regions where plexus is lost in the Neurog3$^{EGFP/EGFP}$ compared to control. Green arrowheads, core locations where plexus becomes dysmorphic in the Neurog3$^{EGFP/EGFP}$ animal compared to control. (F) Quantification of plexus-to-duct transformation in core Neurog3$^{EGFP/+}$ and Neurog3$^{EGFP/EGFP}$ pancreata. Error bars are S.E.M, n=3 all stages, (*) p<0.01, (**) p=0.119. The entire dorsal pancreas core was analyzed in serial thick sections (40 μm). (G) Analysis of precocious loss of plexus at E16.0. (G) Regions a, b and c in cartoon correspond to images in H-M. (H-M) Muc1 and insulin immune-detection in similar locations in Neurog3$^{EGFP/+}$ and Neurog3$^{EGFP/EGFP}$ littermates. Scale bars: A,B 20 μm; D,E 50 μm; H-M 40 μm. This figure was adapted from [211].

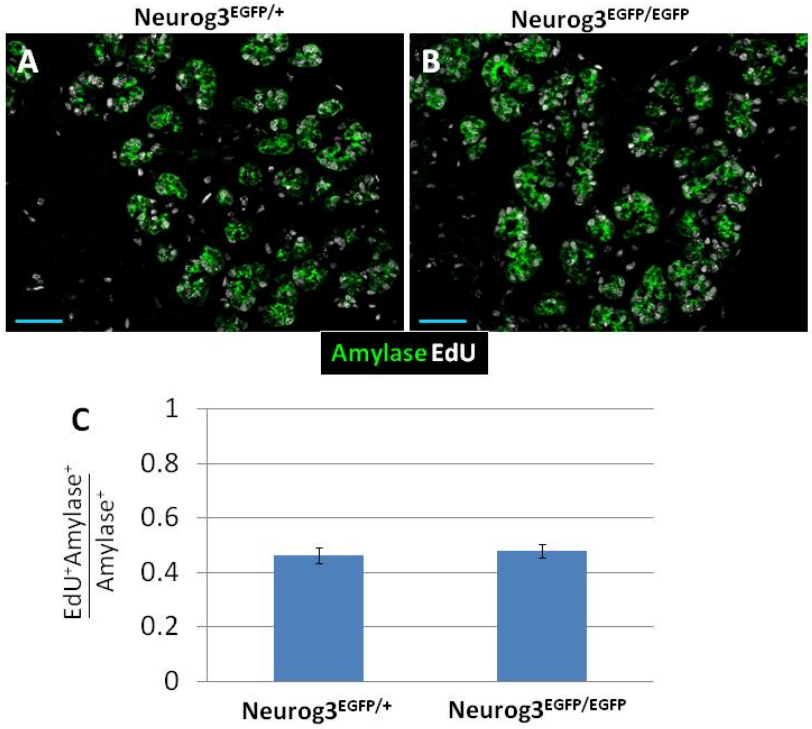

Figure 4.11. *S-phase indices in acinar cells are unchanged in Neurog3-deficient pancreata. (A) Representative 20x image of EdU incorporation at 1 hour post-injection in amylase^{+} acinar clusters of Neurog3$^{EGFP/+}$ and Neurog3$^{EGFP/EGFP}$ dorsal pancreas. (B) Quantification of the EdU-incorporation index. Scale bars are 50 μm. Error bars are S.E.M. N = 1673 Neurog3$^{EGFP/+}$ and N = 1436 Neurog3$^{EGFP/EGFP}$ amylase^{+} cells counted from five sections spanning n = 2 dorsal pancreas for each genotype. This figure was adapted from [211].*

Late-stage autonomous epithelial remodeling in the Neurog3-deficient plexus

While a limited amount of precocious remodeling and alteration of the Neurog3-null plexus morphology was observed at mid-gestation, there was no grossly aberrant phenotype at late gestation, suggesting that the mechanisms guiding epithelial remodeling could eventually over-ride the earlier defect. Consistent with this, Muc1 and insulin (to label the endocrine-cell mass

derived from the epithelium) detection in equivalent organ regions from E14.5-17.5 showed a progressive normalization of the Neurog3-null epithelium (Fig. 4.12A-F). Specifically, the

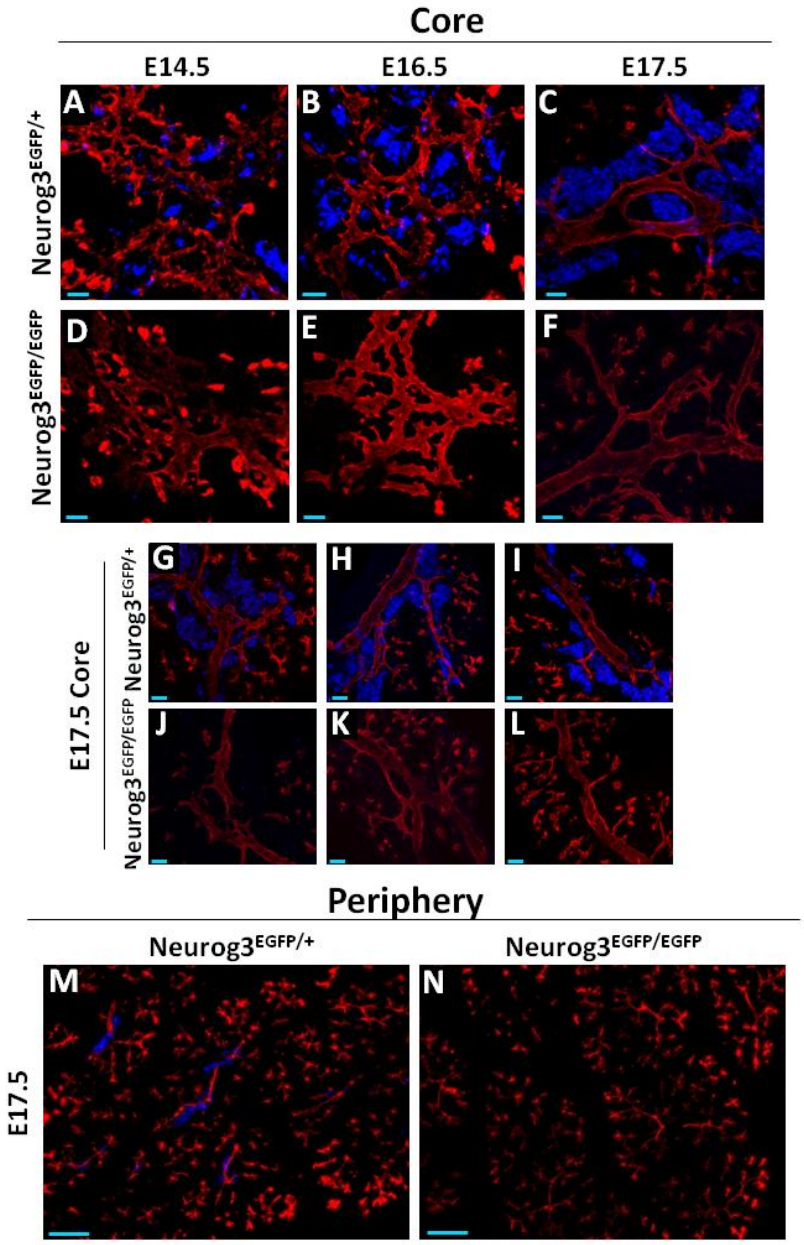

Figure 4.12. *Late-stage corrective remodeling in Neurog3-deficient epithelium. Muc1 and insulin labeling in 40 μm thick sections showing representative core (A-L) and peripheral (M & N) regions of Neurog3$^{EGFP/+}$ and Neurog3$^{EGFP/EGFP}$ pancreata at stages indicated. Scale bars are 30 μm in A,D,G-L; 20 μm in B,E; 50 μm in C,F; 100 μm in M,N. This figure was adapted from [211].*

expansive enlargements of Neurog3$^{EGFP/EGFP}$ plexus lumens seen at E14.5 underwent remodeling toward a morphology largely indistinguishable from control by E17.5. Furthermore, the

previously reported moderate reduction in peripheral branching in Neurog3-nulls [72] were also corrected (Fig. 4.12M,N). The plexus morphology at E12.5 was similar between Neurog3$^{EGFP/+}$ and Neurog3$^{EGFP/EGFP}$ (data not shown), indicating that the perturbed morphology of the Neurog3-deficient plexus manifests most severely during the peak of endocrine (β-cell) birth [57]. These analyses show a late-stage process of autonomous epithelial remodeling occurs in the absence of Neurog3-dependent differentiation, delamination, and Notch-regulated processes.

Discussion

Understanding how niche environments direct progenitor activities is fundamental to uncovering the basic principles underlying complex organ formation and function, and predisposition to disease. In studying endocrine-progenitor activity during the secondary transition of pancreatic organogenesis, we discovered that endocrine progenitors are largely constrained within an epithelial plexus-state. Although the plexus is transient, it is maintained through all stages of the secondary transition, and is as productive at generating endocrine cells during late gestation as it is at earlier stages. Genetic and pharmacological interference tests indicate that endocrine-progenitor expansion, differentiation and morphogenesis processes are coordinated by local feedback effects within the plexus. These effects derive largely from differentiating Neurog3^{+} cells, but can be uncoupled on the basis of Neurog3-dependent differentiation/delamination functions supporting progenitor replication, and Notch-dependent functions in maintaining an undifferentiated progenitor state. Together, these feedback interactions serve to propagate the plexus, and the large numbers of endocrine progenitor cells maintained therein, late into gestation. Ultimately, as the plexus remodels into duct and DB states, endocrine differentiation and progenitor maintenance behaviors are reduced then lost. We propose that the epithelial plexus functions as a niche environment, where endocrine progenitors are assembled and maintained, and where local differentiation-dependent feedback interactions are deployed to direct the genesis of the endocrine pancreas (Fig. 4.13).

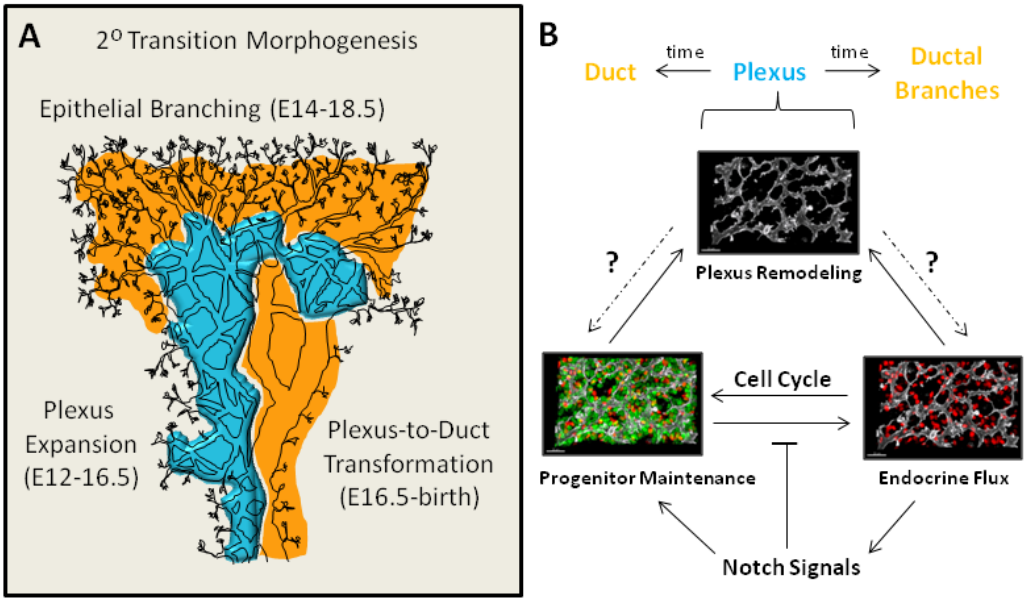

Figure 4.13. *Feedback control of endocrine progenitor growth, differentiation, and morphogenesis in the plexus niche. (A) Diagrammatic representation of the principle morphogenetic processes comprising trunk epithelial morphogenesis during 2° transition. Regions of the organ enriched for Notch-responsive endocrine progenitors are demarcated in blue, whereas regions reduced or absent in this respect are orange. (B) Diagrammatic representation of the local feedback interactions operating in the plexus-state. This figure was adapted from [211].*

Distinct processes of plexus-to-duct remodeling and epithelial branching in the trunk

Our characterization of pancreatic epithelial remodeling indicates distinct modes of morphogenesis in largely separate zones of the organ. In the core, plexus expansion and growth from E12.5-E15.5, accompanied by plexus-to-duct transformation from E16.5-E18.5, represents the principal mode by which ductal tissues analogous to the trunk and main limbs of a tree are generated. In the periphery, however, an "epithelial branching" mode remodels the epithelium, apparently by a clefting and outgrowth process, to eventually generate tightly-packed peripheral lobules of interconnected DB structures. This dual-mode program, especially the major contribution from plexus expansion and resolution, diverges greatly from the classical and more stereotypically defined branching morphogenesis involved in the growth of other endodermal organs [26,174,175].

Because the plexus-remodeling process occurs asynchronously across the organ, it will be important to determine what influences (cellular or otherwise) cause some plexus regions to undertake expansion while remaining unresolved (and in a high endocrine-yield state), while others begin transformation toward the mature duct-like states. We do not find evidence, at any stage of plexus resolution, which would suggest that remodeling is accomplished through breakage and regression of epithelial segments, as reported for vascular plexus remodeling [176]. Rather, we observe an apparent progressive consolidation of epithelial plexus segments that effectively reduces the complexity of, and eventually eliminates, the plexus-web, to generate the final ductal tree. Our analysis of Neurog3$^{-/-}$ pancreata allows us to rule out a model whereby plexus remodeling is primarily driven by epithelial-cell departure (delamination) of Neurog3^{+} endocrine precursors. While Neurog3-dependent processes are clearly important for regulating and propagating a "normal" plexus state, the observation of the late-stage corrective remodeling demonstrates that the epithelial remodeling program, albeit with substantial delay, eventually enforces a relatively normal morphogenesis even in the absence of Neurog3. Therefore, in normal tissue, we propose that the function of Neurog3 in maintaining and propagating the progenitor-rich plexus is balanced with an opposing, and apparently self-organizing epithelial morphogenesis process, that eliminates the plexus intermediate in favor of the typical ductal structures of the mature epithelium. It remains to be determined how other known regulators of pancreatic epithelial morphogenesis and growth, especially those derived from epithelium-extrinsic sources such as the mesenchyme [177,178,179] and vasculature [24,72], contribute to localized epithelial remodeling patterns during plexus growth, plexus-to-duct transformation, and epithelial branch specification and outgrowth. We propose that the detailed analysis of the dual-mode morphogenesis program reported here should enable future connection of such extrinsic cues to specific epithelial-remodeling outcomes.

Notch and endocrine-differentiation-mediated feedback effects regulate distinct endocrine-progenitor behaviors

Our finding that *Hes1* expression is maintained locally within the plexus, even at late gestational stages, leads to interesting questions regarding how duct vs. endocrine cell-fate allocation might be dynamically influenced by Notch activity. Our data showing that Hes1, similar to Neurog3, is enriched in the plexus, and that Notch inhibition by DBZ increases the portion of the plexus cell population activating Neurog3, fit a model whereby Notch-based signals derived locally from Neurog3^{+} cells maintain epithelial cells in an undifferentiated and Notch-responsive state. Ultimately, Sox9^{+} cells of the duct-state epithelium – that is, in the core ducts and peripheral DB – downregulate Hes1 and Sox9, and become a poor source of Neurog3^{+} cells, both normally and under Notch-inhibited conditions, consistent with the idea that non-plexus-state cells have truly entered a ductal differentiation program. Our observations thus begin to outline spatial variations in the level of Notch pathway activity, and the differentiation response to perturbing Notch, which are correlated with distinct states of epithelial morphology arising during organogenesis. Identifying markers that distinguish states of pro-duct specification versus undifferentiated bipotent-progenitor will likely aid in defining the non-cell-autonomous cues that instruct duct specification or maintain the bipotent pool, perhaps as obligatory features of developmental coordination in the plexus.

We observe profound reductions in progenitor replication under conditions where Neurog3 is inactivated, but not when Notch signal processing is inhibited. While spatiotemporally more precise Notch perturbation may uncover roles in regulating the replicative amplification of endocrine progenitors in mice, our results raise the possibility that a delamination function for Neurog3 may determine replication rates in the epithelial population. Indeed, studies in *Drosophila* demonstrate that cell delamination limits tissue overcrowding and promotes epithelial growth [127], suggesting that biomechanical mechanisms and/or pathways regulating cell-shape or density-dependent growth [180] could be critical determinants of pancreatic progenitor growth and replication.

Intrinsic versus feedback-based regulation of endocrine lineage allocation, progenitor maintenance, and plexus morphogenesis during the secondary transition

In contrast to growth-compensation programs in the liver, the pancreatic growth program is regulated intrinsically by the number of MPC initially allocated to the pancreatic anlagen [17]. We speculate that an internally regulated, feedback-rich process of plexus morphogenesis, from its initial establishment to maturation as a ductal arbor, could explain how endocrine lineage output is "pre-determined" by founder MPC number. Our data are consistent with a highly processive plexus state from which endocrine cells are continuously born. Endocrine yield is robust within the plexus at all stages, but is rapidly reduced upon its transformation into non-plexus states. The initial number of MPC allocated to the initial plexus-state could influence how long the plexus is maintained, and thereby prolong or shorten the period of endocrine-lineage allocation. Of relevance is the effect of ectopic *Nkx6.1* expression in pancreatic MPC. During stages concomitant with plexus formation, *Nkx6.1* antagonizes the pro-tip gene *Ptf1a*, diverting MPC toward bipotent trunk progenitors [43]. This transcriptional-antagonism effect on tissue-compartment allocation is Notch-regulated, providing a potential link between the timing and/or levels of Notch in the Nkx6.1^{+} MPC during *initial* plexus formation and the final endocrine-cell output [169,181]. Current translational objectives regarding the differentiation of pluripotent cells toward the endocrine cell fate *in vitro* could benefit from investigating how the size of the "initiating plexus" and duration of its maintenance impact the final size and composition of the endocrine pancreas, and if these parameters can be controlled by modulation of Notch, Nkx6.1, and Ptf1a.

Our data put forward the possibility that endocrine-differentiation dynamics, in terms of the rate of endocrine flux and/or the specific type of endocrine cells produced, could be guided by epithelium-intrinsic morphogenetic influences. Of particular interest to endocrine sub-type specification, a previous study [57] showed that competence windows for the differentiation of endocrine-cell sub-types are regulated by factors intrinsic to the pancreatic epithelium. Such windows of competence could be connected to specific tissue-level or cell-biological alterations associated with plexus formation, expansion, and remodeling phases. [The α-cell competence

window could correlate with initial plexus formation (E9.5-E12.5), β-cell birth more with the mid-gestation plexus-expansion phase (E12.5-E15.5), and the later production of δ/ε/PP cells with plexus-to-duct transformation (E16.5-E18.5)]. We envisage the future testing of the idea that specific, and perhaps relatively subtle perturbations to the plexus morphogenesis program might alter the epithelial environment in ways that influence the number and type of endocrine cells born.

Linked programs of endocrine progenitor maintenance, differentiation, and morphogenesis

Emerging reports suggest that some aspects of endocrine-progenitor differentiation and proliferative expansion are dependent on molecular determinants of cell and tissue morphology. For instance, a requirement for Cdc42-mediated apicobasal polarization has already been linked to the generation of an endocrine-differentiation-competent progenitor pool [71], and could thus be considered as a central contributor to the generation of the plexus. Additionally, ablation of Strad13, a RhoA-ROCK-nmMyoII negative regulator, reduces the size and replicative activity of pancreatic MPC [182], and defects in planar cell polarity are associated with reduced Neurog3^{+} cell numbers [85]. While the detailed mechanistic underpinnings causing defective endocrine-lineage development in these cases remain unclear, the picture emerging is that insights into how endocrine progenitors and committed endocrine precursors are efficiently maintained and generated, respectively, may be gleaned from characterizing, with increased spatiotemporal resolution, how cytoskeletal dynamics, cell polarity, actomyosin contractility, and/or the trafficking and distribution of receptors such as Notch, functionally link cell and tissue morphogenesis processes with cell-fate determination.

Acknowledgements

We thank Tetsuo Sudo (Toray Industries) for the gift of Hes1 antibody, the Vanderbilt Cell Imaging Shared Resource for training and access to equipment and image-processing software. Imaging scholarships were from the VUMC DDRC, DRTC and VICC [supported by NIH grants CA68485, DK20593, DK58404, DK59637]. We thank Anna Means, Guoqiang Gu, and members

of the Wright/Gu labs for discussions. This study was supported by the National Institutes of Health (1UO1DK089570-01).

CHAPTER V

A ROCK-nmMYOII, NOTCH, AND NEUROG3 GENE DOSAGE CIRCUIT LINK EPITHELIAL MORPHOGENESIS AND CELL FATE IN THE PANCREATIC ENDOCRINE PROGENITOR NICHE

Introduction

How cell differentiation and morphogenesis are coordinated during organogenesis remains a central question in biology. During pancreas development, endocrine cells are allocated from a bipotent duct/endocrine progenitor pool located within an epithelial “plexus state”. We find that upregulation of the endocrine lineage determinant *Neurog3* occurs in the plexus upstream of Neurog3 protein function and concomitant with initiation of cell-delamination, suggesting that endocrine commitment is directed by a epithelium-intrinsic morphogenetic program. Progression through delamination is characterized by initial apical-narrowing and focalization, and increased migratory activity at the basal cell surface, with the latter being *Neurog3*-dependent. Mechanistically, the ROCK-nmMyoII pathway mediates *Neurog3*-independent and dependent steps in delamination to guide endocrine cell birth. NmMyoII is necessary for apical narrowing and basal migratory activity, and its inhibition results in an early block in *Neurog3* upregulation. ROCK activity gates the transition from low to high *Neurog3* expression by limiting apical narrowing and basal migratory activity, and its inhibition can rescue defects in *Neurog3* upregulation observed in *Neurog3*-hypomorphs. Finally, *Neurog3* gene dosage, ROCK/nmMyoII, and Notch pathways comprise a self-organizing feedback circuit that optimizes endocrine lineage commitment from the plexus state. These studies demonstrate linked programs of differentiation and morphogenesis in the plexus, and provide insights into principles underlying the formation of complex organs.

Material and Methods

Mice

Neurog3^{EGFP} knock-in and Neurog3^{Flox} mice were from Guoqiang Gu (Vanderbilt University). Ngn3$^{EGFP/EGFP}$ embryos were phenotyped by EGFP fluorescence and lack of endocrine cells. Wild-type mice were of mixed genotype. The *Neurog3*^{RG} line was generated as described [Matt Bechard, Wright Lab, submitted). All protocols were approved by Vanderbilt University IACUC. Genotyping primers for the EGFP allele were *ngn3*-1 5'-ATACTCTGGTCCCCCGTG-3', *ngn3*-2 5'-TGTTTGCTGAGTGCCAACTC-3', and EGFP 5'-GAACTTGTGGCCGTTTACGT-3' [59]. Genotyping primers for Neurog3 floxed allele were 5'HRsFr-ccttctcttccagagacttc and 5'HRsH-ctctggtcagagatacctgg, or 722: 5'-CTATCCACTGCTGCTTGTCACTG-3', 723: 5'-TGTGTCTCTGGGGACACTTGGAT-3', jv45: 5'-TTCCGGTTATTCAACTTGCACC-3' [52]. The nmMyoIIC-GFP line was a kind gift from Dr. Adelstein [212], and nmMyoIIC-GFP+ embryos were phenotyped under a fluorescence microscope.

Immunodetection

Embryonic pancreas paraformaldehyde fixed (4%, 4^{o}C for 4-6 hours). For cryosectioning, samples were sucrose-equilibrated (30%, 4^{o}C overnight), and embedded in OCT (Tissue-Tek, Sakura). Thick sections were obtained on a Leica CM3050 S in the range of 30-40 μm; thin sections at 10 μm. Protein detection reagents used include chicken anti-GFP (Aves), hamster anti-Muc1 (NeoMarkers), rabbit anti-Sox9 (Millipore), goat anti-Neurog3 (Gu lab), DAPI (Life Technologies), mouse anti-Ecad (AbCam), rabbit anti-gamma-tubulin (AbCam), rabbit anti-Prox1 (AngioBio Co), guinea pig anti-Pdx1 (Wright Lab), phalloidin (Molecular Probes), rabbit anti-ZO1 (AbCam), rabbit anti-aPKC (Santa Cruz), rabbit anti-phospho-nmMyoII (AbCam), rabbit anti-nmMyoIIa (Covance), rabbit anti-nmMyoIIb (Cell Signaling).

Image Acquisition and Data Collection

Confocal images were obtained using Zeiss LSM 510 META upright scope or a Zeiss Apotome. Z-stack volumes were acquired in the 20-30 μm range at 40X magnifications. 3D reconstructions were rendered using Imaris software.

Quantification and Statistical Analyses

Method to distinguish plexus from non-plexus states was performed as described [211]. Fluorescence intensity measurements were performed by mean pixel intensity using ImageJ. Sox9 and Ngn3 ratios were determined by manual counting. Measurements of all morphological structures and nuclear densities were acquired using line or polygon-trace functions in IMARIS.

Explants and Drug Treatments

Explants were manually dissected and culture at the air liquid interface on transwell permeable supports (Costar, 3422). Incubator conditions were 37^{o}C and 5% CO_2. S(-) Blebbistatin (Abcam), Y27632 (Selleckchem), and DBZ (Cayman Chemical) were administered in the culture medium (10% FBS, 1% Pen/Strep, 1% L-glut). After harvesting, explants were fixed for 2 hours in 4% paraformaldehyde.

EdU incorporation studies

EdU (Life Technologies) was given I.P. (10 mg/kg). EdU was detected by the Click-iT Plus EdU Imaging Kit (Molecular Probes).

Live Imaging

Neurog3^{RG+} pancreata were isolated at E12.5 and phenotyped under a fluorescence microscope. These were grown on fibronectin, cultured in DMEM (10% FBS, 37^{O} C, 5% CO_2) in an incubator overnight to promote attachment to the matrix, and imaged on a LSM 780 two-photon microscope.

Results

Morphological transitions at the F-actin^{+} apical cell cortex are associated with cell-fate allocation

In polarized epithelial cells, a prominent feature of the cytoskeleton is a belt of bundled filamentous actin (F-actin) that circumscribes the subapical cell cortex [112]. These belt-like structures (hereafter F-actin^{BELT}) are closely apposed to tight and adherens junctions, and play important roles in mediating cell and tissue remodeling processes such as apical constriction, tissue folding, cell intercalation, and delamination or extrusion [210]. To gain insight into whether specific cell-shape changes may be involved in mediating duct and endocrine lineage allocation, we compared the shape of the F-actin^{BELT} in cells residing within the progenitor-rich plexus-state, in cells expressing *Neurog3*, and in cells within the endocrine-progenitor-poor duct-state. In confocal z-stack reconstructions of the plexus, a multicellular meshwork of cortical F-actin could be visualized by a relatively intense phalloidin signal closely associated with the Muc1^{+} epithelial apical lumen surface (Fig. 5.1A). This meshwork of F-actin was apposed to apical ZO1^{+} tight junctions, and located apically with respect to the basolateral Ecad^{+} adherens junctions (Fig. 5.2A-H'), as defined for F-actin^{BELT} in numerous epithelia. Plotting the measured F-actin^{BELT} aspect ratio against F-actin^{BELT} perimeter from individual cells (as a surrogate for apical domain shape (Fig. 5.3A-B)) showed a broad spectrum of apical domain shapes in the plexus (Fig. 5.1D). The domain and range of this spectrum was similar in the plexus throughout the secondary transition, indicating that the characteristics of the plexus at both tissue and cellular levels are maintained during the course of development. In addition, we consistently observed at all stages numerous distinct puncta of intense F-actin signal, located directly at the lumen, that were associated with the focalized Muc1^{+}aPKC^{+} apical surface-to-lumen contact (hereafter F-actin^{FOCAL}) of delaminating *Neurog3*-expressing cells, as shown using the *Neurog*^{EGFP} knock-in mouse strain (Fig. 5.1B,C, Fig. 5.4A-D) [58]. Essentially all cells reporting high levels of EGFP (EGFP^{HI}) exhibited a measurably narrowed or focalized F-actin^{BELT} (Fig. 5.1F). In contrast, the F-actin^{BELT} of cells in the duct-state showed measurable increases in perimeter and aspect ratio reflecting enlargements of the apical domain (Fig. 5.1G-

J). Consistent with our previous findings using direct immune-detection of Neurog3, the numbers of *Neurog3*-reporting cells were greatly diminished in ductal states, and accordingly, F-actin^{FOCAL} structures were significantly reduced or absent. Comparisons of cell morphologies using E-cad as an additional indicator of cell shape suggested similar increases in apical domain size in the duct versus plexus (Fig. 5.5A-D), and a cell-flattening phenotype indicative of cell differentiation toward a duct-cell-like state [82,211]. These analyses on the morphological features of the apical domain in the plexus, *Neurog3*-expressing, and ductal-states suggest that within the plexus, F-actin^{BELT} narrowing and F-actin^{FOCAL} formation are associated with endocrine differentiation, while F-actin^{BELT} expansion is associated with duct-cell differentiation.

Apical narrowing and F-actin^{FOCAL} formation mediate endocrine commitment in the plexus upstream of Neurog3 *protein*

Genetic inactivation of *Neurog3* results in a morphologically abnormal plexus state at E14.5 [72], and a complete absence of EGFP^{HI} cells. To test whether the defect in *Neurog3* upregulation could be the result of defective apical narrowing or F-actin^{FOCAL} formation in this condition, we compared the cortical F-actin^{BELT} meshwork in *Neurog3*$^{EGFP/+}$ and *Neurog3*$^{EGFP/EGFP}$ epithelia. Indeed, the relatively broad spectrum of F-actin^{BELT} observed in the *Neurog3*$^{EGFP/+}$ shifted toward a more uniformly circular morphology in the *Neurog*$^{EGFP/EGFP}$ plexus (Fig. 5.6A-D, I). There was no evidence for F-actin^{FOCAL} structures in the *Neurog3*$^{EGFP/EGFP}$ plexus, suggesting that F-actin^{FOCAL} formation does not occur in the *Neurog3*-deficient plexus at this stage. *Neurog3*-reporter expression was expanded but reduced (EGFP^{LO}) across essentially the whole dysmorphic plexus. Consistent with a previous report, we observed a broad expansion of the epithelial lumen diameter [72] in the *Neurog3*-defiecient condition. There was also a measureable increase in the number of Sox9^{+} cells over the Muc1^{+} lumen surface distance, suggesting a cell crowding effect caused by the lack of endocrine cell delamination (Fig. 5.7A,B). Collectively, these data are consistent with previously-proposed functions for *Neurog3* in non-autonomously limiting its own expression domain, and in regulating epithelial morphology

[80,169], but do not rule out the possibility that the alterations in *Neurog3* expression may occur as a consequence of dysregulated epithelial morphogenesis.

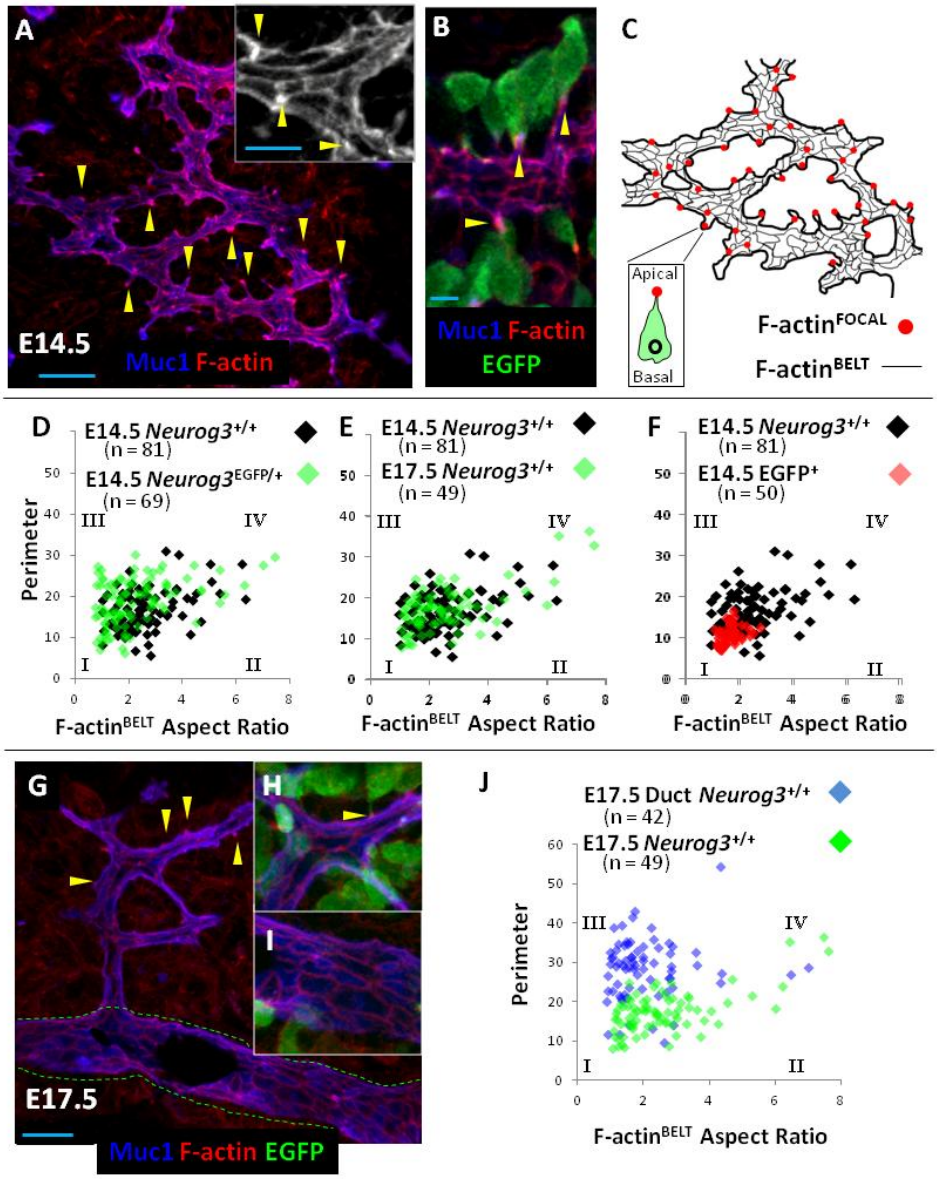

Figure 5.1. *Duct versus endocrine differentiation is associated with apical expansion or narrowing of the F-actin^{+} epithelial cell cortex. (A) Confocal z-stack (30 μm depth) of E14.5 dorsal pancreas showing the plexus web labeled with Muc1 and F-actin. Inset shows F-actin channel, with intense cortical F-actin signal marking F-actin^{BELT} circumscribing the apical domain of individual epithelial cells. Yellow arrowheads show Muc1^{+} F-actin^{FOCAL} structures. (B) F-actin^{FOCAL} structures mark the apical-lumen contacts of delaminating Ngn3$^{EGFP/+}$ reporter^{+} cells. (C) Manual trace of the F-actin^{BELT} meshwork (thin black lines) from A, F-actin^{FOCAL} structures (red dots), and representative Neurog3-expressing cells (inset). (D) Dot-plots of cortical F-actin^{BELT} dimensions (aspect ratio/perimeter) from individual cells superimposed for control or Neurog3$^{EGFP/+}$ cells in the E14.5 plexus. (E)*

Superimposed F-actin^{BELT} dot-plots from E14.5 and E17.5 control plexus. (F) Superimposed F-actin^{BELT} dot-plots from E14.5 plexus and in Neurog3-expressing cells. (G) Confocal z-stack (30 μm depth) of representative plexus and duct-states at E17.5. Duct state is demarcated by green dashed line. Yellow arrowheads indicate F-actin^{FOCAL} structures. (G,H) Zoomed insets from plexus and duct-state in F. Note the expansion of F-actin^{BELT} and dearth of F-actin^{FOCAL} in the duct state. (I) Superimposed F-actin^{BELT} dot-plots from E17.5 plexus and duct states. Scale bars are 20 μm in A,F, 5 μm in B.

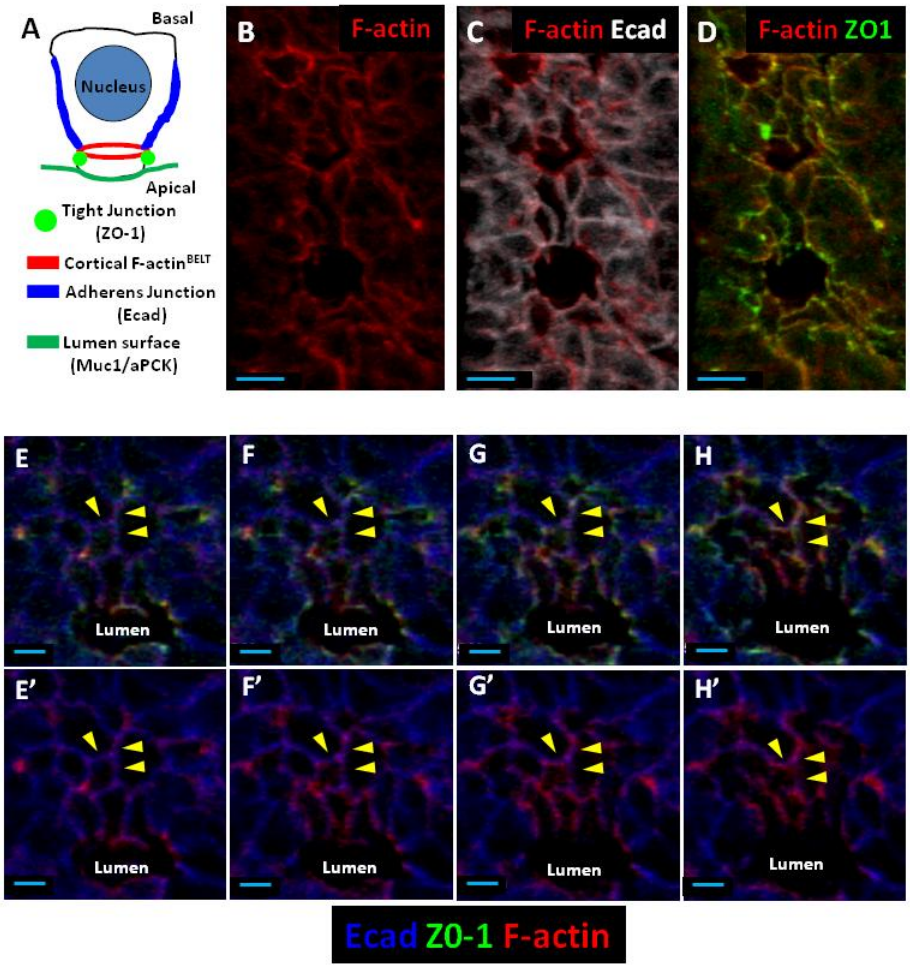

Figure 5.2. *Adherens and tight-junction markers demarcate a multicellular F-actin^{BELT} meshwork. (A) Schematic showing the localization of the cortical F-actin^{BELT} with respect to apical-surface (Muc1), tight junction (ZO1), and adherens-junction (Ecad). (B-D) Representative en fasse images of Ecad and ZO1 in relation to the F-actin^{BELT} network. (E-H') Confocal steps (z-direction, 1.0 μm/step) through a plane of representative epithelial cells. Note the progression from Ecad (blue) through to intense F-actin signal and ZO1. Scale Bars in B, C, & D are 10 μm, and 5 μm in E-H'.*

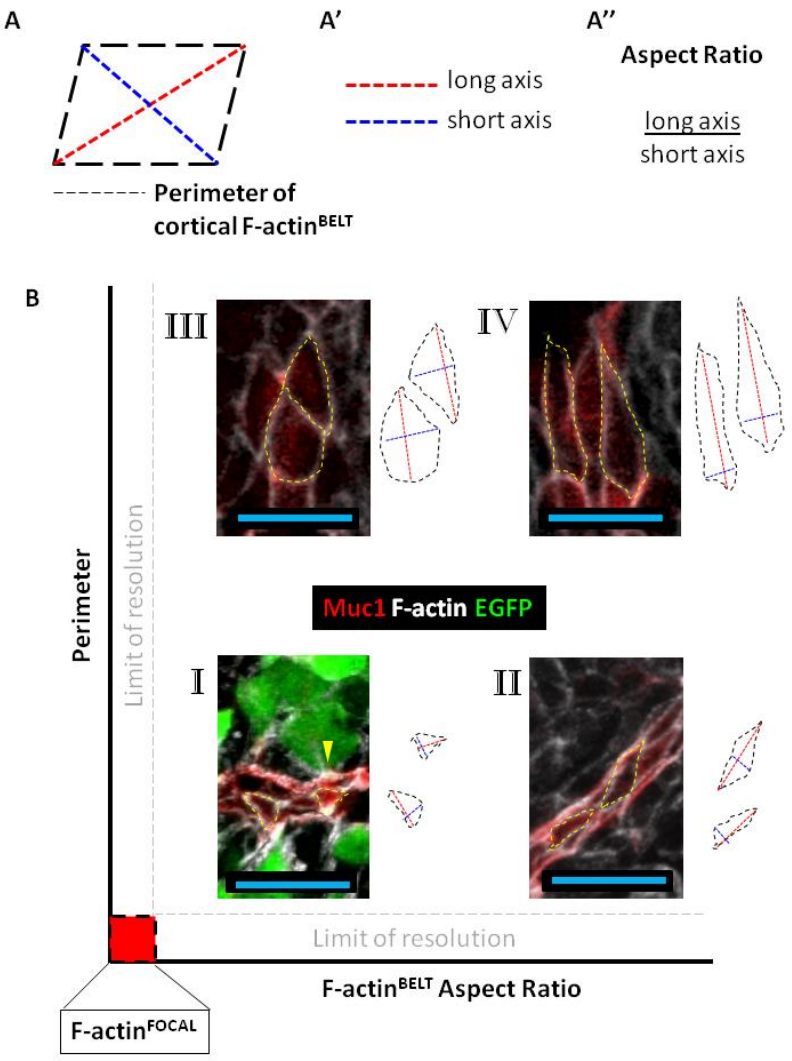

Figure 5.3. *F-actin^{BELT} aspect ratio versus perimeter defines the spectrum of F-actin^{BELT} sizes in epithelial populations. (A) Schematic of a typical cortical F-actin^{BELT} near apical surface an epithelial cell. Perimeter (black line) demarcates the F-actin^{BELT}. (A') Long axis (red dashed line) and short axis (blue dashed line) defines perpendicular axial dimensions of the F-actin^{BELT}. (A'') Aspect ratio is defined by the divisional product of the long and short axis. (B) Schematic with examples of the extremes in possible F-actin^{BELT} (white) dimensions (F-actin^{BELT} traced in yellow dashed line) obtained from measurements as described. Roman numeral I indicates narrowed apical cortex. Roman numeral II indicates elongated F-actin^{BELT}. Roman numeral III indicates expanded F-actin^{BELT}. Roman numeral IV indicates expanded and elongated F-actin^{BELT}. Grey dashed line demarcates minimum of resolution in x and y for accurate measurements by these methods (~2.0 μm). F-actin^{FOCAL} perimeter and aspect ratio are below minimum resolution or at the origin (red box). Yellow arrowhead marks typical F-actin^{FOCAL} structure at the apical surface of a delaminating Neurog3$^{EGFP/+}$ reporting^{+} cell. Scale bars are 20 μm.*

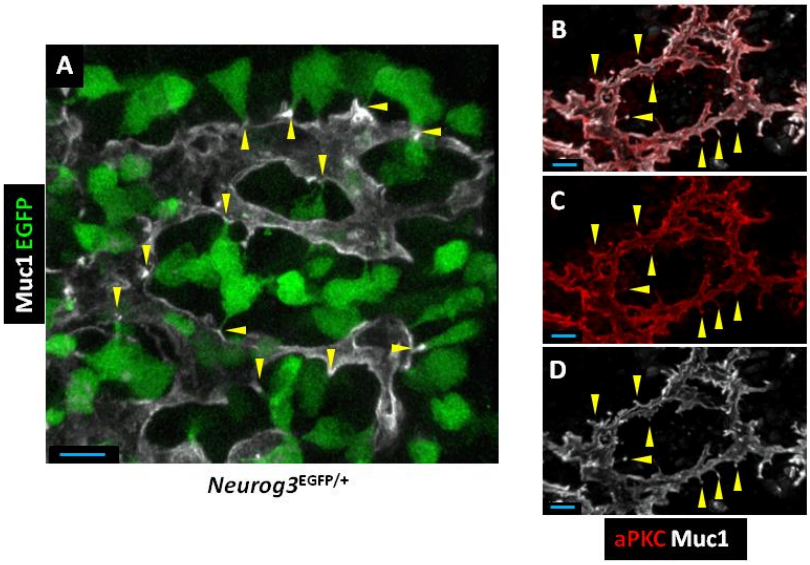

Figure 5.4. *Delaminating endocrine cells maintain contact with a narrow apical lumen-surface contact. (A) Representative 40x confocal z-stack of E14.5 Ngn3$^{EGFP/+}$ plexus showing apical lumen-surface contact of delaminating EGFP-reporting cells. (B-D) Immuno-detection of aPKC and Muc1 showing the localization of each at representative Muc1^{+} F-actin^{FOCAL} structures (yellow arrowheads). Scale Bars are 10 μm in A-D.*

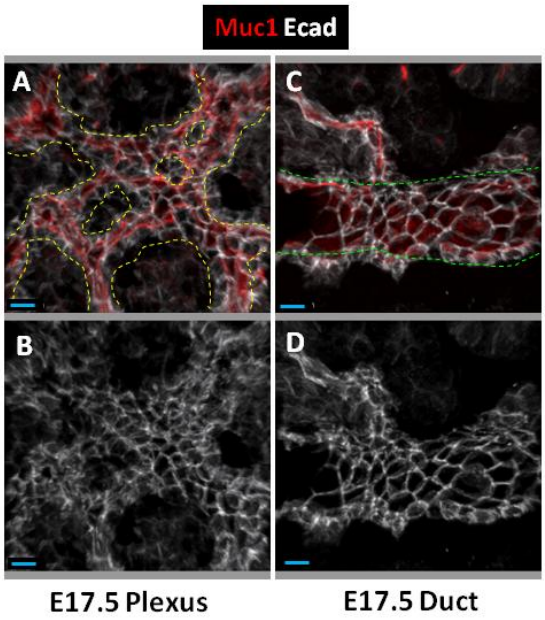

Figure 5.5. *Ecad immunolabeling shows enlargements in cell shape in the duct-state compared to the plexus. (A,B) Confocal z-stack of Muc1 and Ecad markers showing cell morphologies in the plexus at E17.5 (plexus traced by yellow dashed line). (C,D) Confocal z-stack of cell dimensions and shapes in the duct at E17.5 (duct traced by green dashed line). Scale bars are 10 μm.*

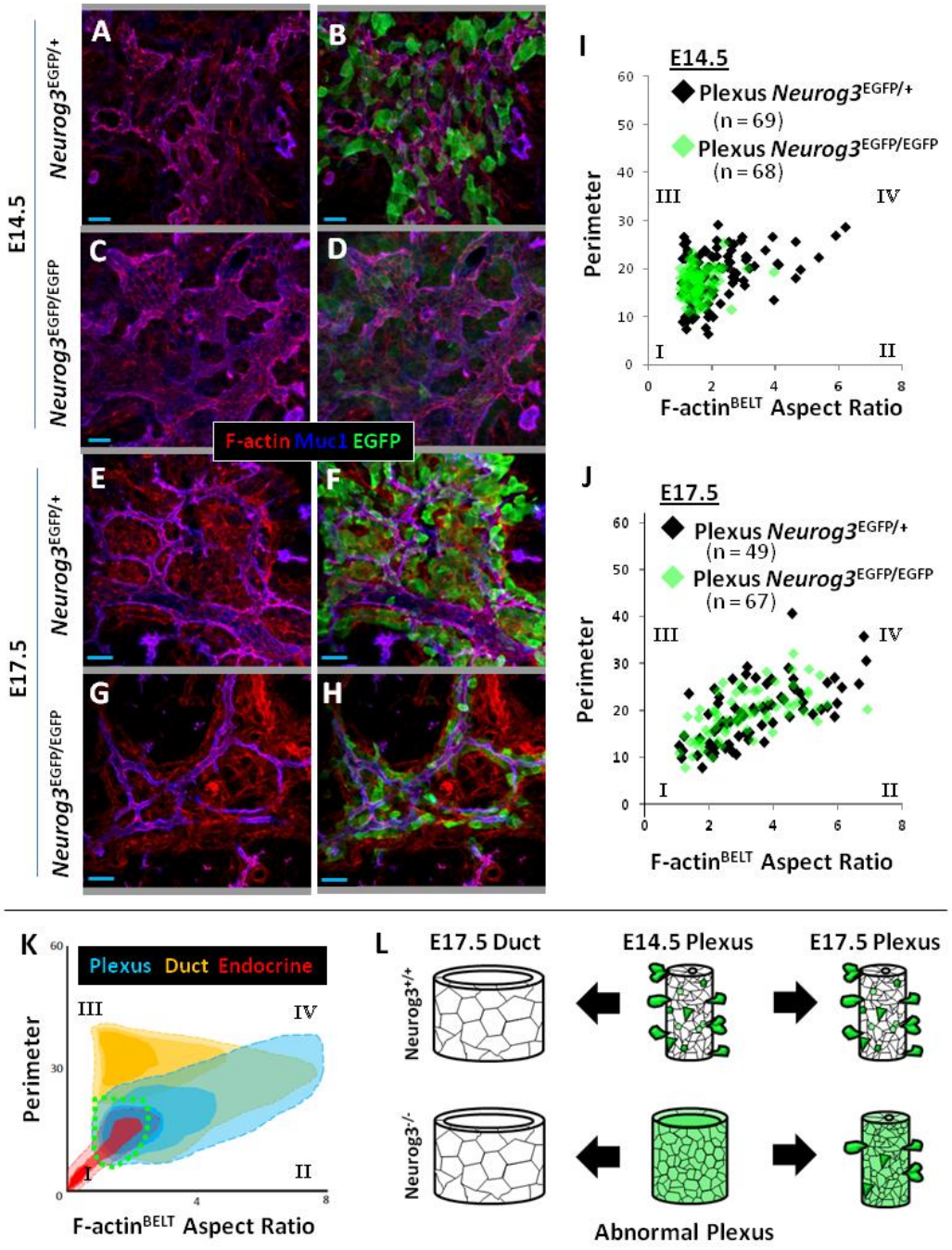

Figure 5.6. *Plexus-state morphogenesis is associated with upstream activation of Neurog3. Representative Neurog3$^{EGFP/+}$ plexus (A,B) versus Neurog3$^{EGFP/EGFP}$ plexus (C,D) with EGFP^{HI}-reporting cells distributed within the cortical F-actin^{BELT} meshwork at E14.5. Note the dilations of the Muc1^{+} lumens, alterations to the F-actin^{BELT} network, and expansion of EGFP^{LO}-reporting cells throughout the epithelium of Neurog3$^{EGFP/EGFP}$ compared to Neurog3$^{EGFP/+}$ plexus. Representative Neurog3$^{EGFP/+}$ plexus (E,F) versus Neurog3$^{EGFP/EGFP}$ plexus (G,H) with EGFP-reporting cells distributed within the cortical F-actin^{BELT} meshwork at E17.5. Note the re-activation of EGFP reporter to high levels in the Neurog3$^{EGFP/EGFP}$ plexus. (I,J) Superimposed F-actin^{BELT} dot-plots from Neurog3$^{EGFP/+}$ and Neurog3$^{EGFP/EGFP}$ plexus at E14.5 and E17.5, respectively. Note that the abnormalities observed in the*

Neurog3$^{EGFP/EGFP}$ plexus at E14.5 are largely corrected within the plexus by E17.5. (K) Schematic representation of the general patterns of F-actin^{BELT} shape-change as normal epithelial cells transition from the plexus (blue), to the duct (orange) or Neurog3-expressing states. Green dashed line demarcates the spectrum of F-actin^{BELT} in the Neurog3$^{EGFP/EGFP}$ plexus at E14.5. (L) Schematic representation of the morphological alterations associated with states of Neurog3-activation in Neurog3$^{EGFP/+}$ and Neurog3$^{EGFP/EGFP}$ epithelium during the secondary transition. Scale bars are 15 μm in A-D, 20 μm in E-H.

We have recently reported that the abnormal *Neurog3*$^{EGFP/EGFP}$ epithelium remodels during late gestation (E16.5-18.5) to a morphological state essentially indistinguishable from the wild type condition [211]. This "corrective epithelial remodeling" process suggests that the pancreatic epithelial morphogenesis program can over-ride early morphological defects caused by the absence of *Neurog3*-dependent differentiation, delamination, and Notch-regulated processes. The *Neurog3*$^{EGFP/EGFP}$ condition thus provides a stringent model to assess the activation dynamics of *Neurog3* in the complete absence of Neurog3 protein, as an initially "abnormal" plexus-state undergoes corrective remodeling toward a "normal" plexus-state. Numerous inspections of thick-sectioned and Muc1-labeled late-stage (E16.5-onward) embryonic pancreata confirmed a pervasive corrective remodeling of the epithelium to generate grossly normal plexus, duct, and branched states by E17.5 (Fig. 5.6A-D). In contrast to the increased cell densities observed in the plexus at E14.5, the number of Sox9^{+} cells over Muc1^{+} lumen surface distance was comparable in the plexus between control and mutant samples by E17.5 (Fig. 5.7A-H). Moreover, the spectrum of F-actin^{BELT} shapes within the corrected plexus was essentially indistinguishable from the spectrum observed in stage-matched controls.

Surprisingly, we observed periodic F-actin^{FOCAL} structures within the corrected plexus which demarcated, as in control samples, the narrowed or focalized apical domains of individual EGFP^{HI} cells (Fig. 5.6E-H,J). While the relative number of EGFP^{HI} cells in the late-stage *Neurog3*$^{EGFP/EGFP}$ plexus was reduced compared to control, these data indicate an appreciable rescue of *Neurog3*-promoter upregulation, up-stream and in the complete absence of Neurog3 protein function, within the correctively remodeled *Neurog3*-deficient epithelium. Rescue of

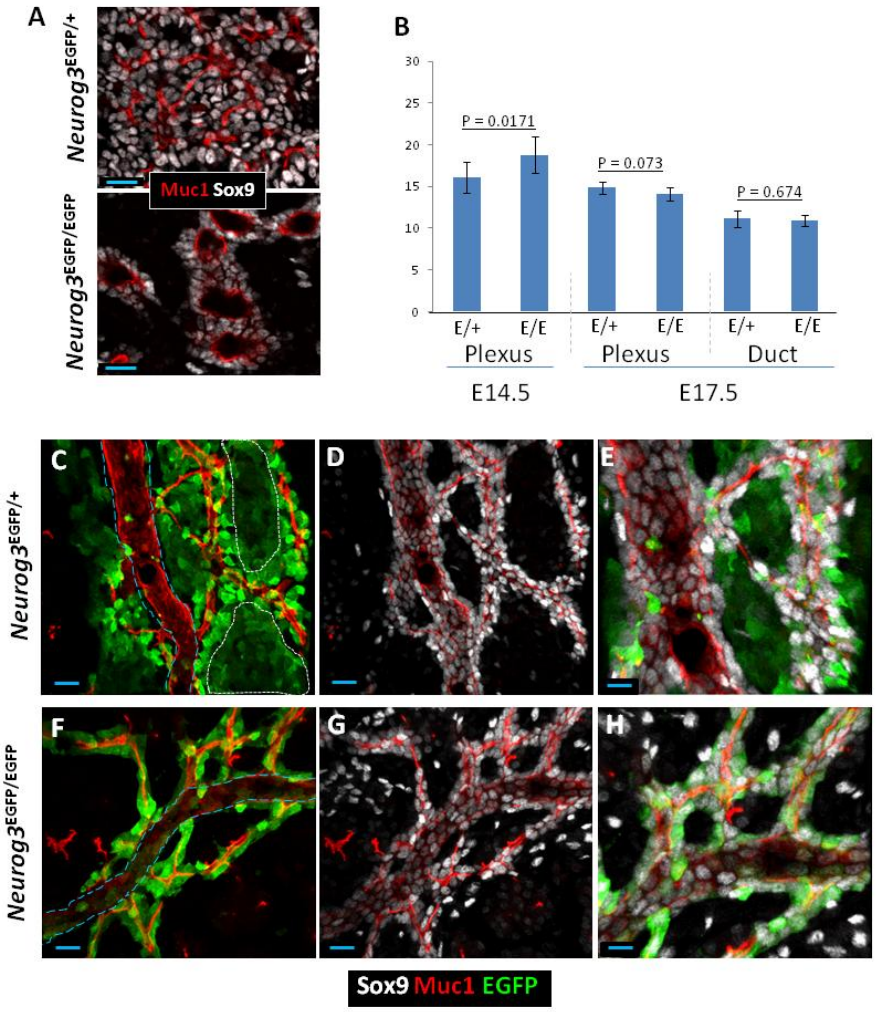

Figure 5.7. *Alterations in Sox9^{+} cell-densities in the Neurog3-deficient epithelium are corrected by late gestation. (A,B) Measurements on the number of Sox9^{+} nuclei along the length of Muc1^{+} lumen Neurog3$^{EGFP/+}$ versus Neurog3$^{EGFP/EGFP}$ epithelium at E14.5 and E17.5, respectively. (C-H) Representative thick sections of Muc1, Sox9 and EGFP in duct and plexus states at E17.5. Cyan dashed lines in C and F demarcate the duct from the plexus-state, and white trace marks low EGFP expression in the forming endocrine islets. Scale bars are 20 μm in C,D,F,G; 10 μm in E,H.*

Neurog3 upregulation was tightly associated with plexus morphology, because non-plexus ductal and branched states, as in control samples, did not exhibit appreciable numbers of EGFP^{HI} cells (Fig. 5.8A-D). Taken together these data suggest that there are tight morphological and tissue-architectural constraints imposed within the plexus that are necessary to direct the initiating step in endocrine commitment, and that deviations from these constraints can preclude efficient engagement of the endocrine lineage commitment process (Fig. 5.6K,L).

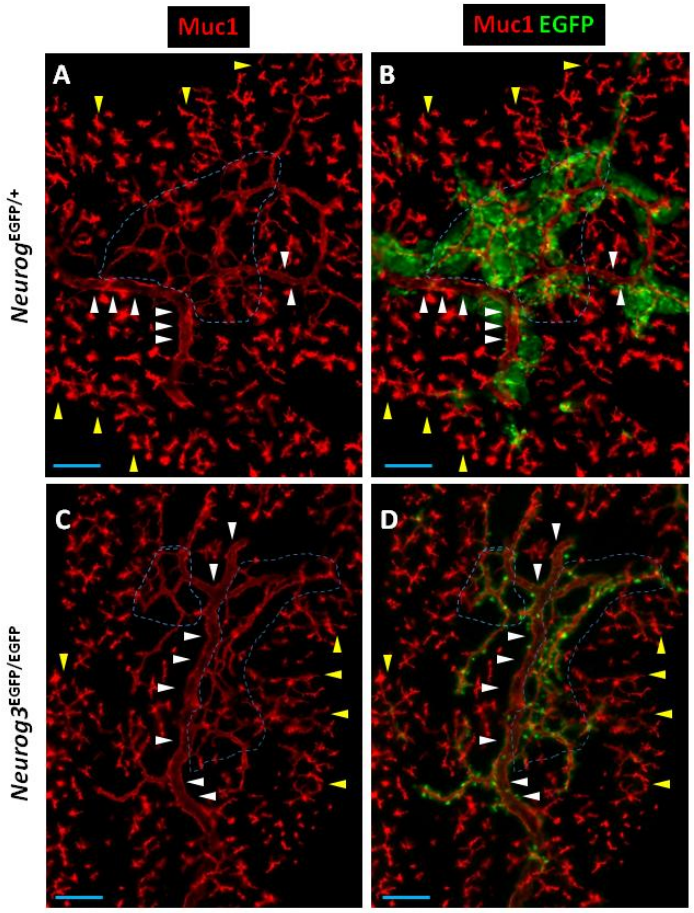

Figure 5.8. *Neurog3 is broadly upregulated in cells within the Neurog3-deficeint plexus at late gestation. (A-D) Wide-field 10x epifluorescent images of thick-sectioned pancreas (30 μm) showing Neurog3-expressing cells in the plexus (blue dashed line), duct (white arrowheads), and peripheral ductal-branches (yellow arrowheads) in Neurog3$^{EGFP/+}$ and Neurog3$^{EGFP/EGFP}$ epithelium at E18.5. Scale bars are 100 μm.*

Apical narrowing and increased migratory activity at the basal cell-surface demarcate the Neurog3^{LO-HI} *transition*

To better understand how specific morphogenetic inputs might mediate endocrine commitment within the plexus, we focused on the precise cell-morphological alterations that occur as *Neurog3*-reporter becomes activated (EGFP^{LO}) and then upregulated (EGFP^{HI}) during endocrine cell specification and commitment. Using the *Neurog3*$^{EGFP/+}$ reporter line, we found at E14.5 a rare population of EGFP^{LO} cells (6.5%; n = 95; Fig. 5.10A) that did not exhibit a highly-narrowed apical domain (as judged by the size of the F-actin^{BELT} relative to the basal surface),

nor any evidence for delamination-type migratory behavior at the basal cell surface (Fig. 5.9A-A'). A significant portion of the total $EGFP^{+}$ population showed a narrowed apical domain (19.3%), and exhibited an $EGFP^{HI}$ state (Fig. 5.9B-B'). The remainder of $EGFP^{HI}$ cells (and the largest portion of the total $EGFP^{+}$ population at 74.2%) exhibited a fully-formed and elongated F-$actin^{FOCAL}$ structure, as well as prevalent migratory activity at the basal cell-surface (Fig. 5.9C-C'; Fig. 5.10A,B). Measurements of mean EGFP intensity in non apically-narrowed, apically narrowed, and migrating (cells with protrusions at the basal leading edge) cell-states were consistent with a sequence whereby the *Neurog*3 is rapidly upregulated in association with the initiation and then progression of a cell delamination process (Fig. 5.9E; Fig. 5.10C). The delamination process was finalized upon rear detachment of the apical surface-to-lumen contact (Fig. 5.9D-D'). To independently confirm these observations, we employed a *Neurog3*^{BAC} transgenic dual-reporter line (hereafter referred to as *Neurog3*^{RG}), which features chromatin-localized H2B-mCherry and membrane-localized GPI-GFP fluorophores, and can be used to precisely monitor the cell-morphological transitions occurring during *Neurog3*-activation and upregulation (Matt Bechard, Wright Lab, submitted). Focusing on the membrane-linked EGFP component of the *Neurog3*^{RG} reporter, and consistent with the *Neurog3*^{EGFP} line, at both E14.5 and E17.5 only a rare population $EGFP^{RG-LO}$ cells we found (4.7% at E14.5, n = 295; 2.3% at E17.5, n = 84), and these exhibited a non apically-narrowed shape (Fig. 5.9G,G'; Fig. 5.10D,D'). $EGFP^{RG-HI}$ cells, however, consistently were apically-narrowed (17% at E14.5, 17.9% at E17.5), or were associated with an F-$actin^{FOCAL}$ structure and displaying prevalent migratory activity at the basal surface (~75%) (Fig. 5.9H-I'). Fully delaminated $EGFP^{RG+}$ endocrine precursors were rounded in morphology, and exhibited full apical-detachment from the $Muc1^{+}$ lumen surface (Fig. 5.9J,J'). Thus, *Neurog3*^{EGFP} and *Neurog3*^{RG} reporter lines independently confirm that *Neurog3* transcriptional upregulation occurs concomitant with an initial step in apical-narrowing (*Neurog3*^{LO}), followed by formation of an F-$actin^{FOCAL}$ structure and increased migratory activity at the basal cell surface (*Neurog3*^{HI}) (Fig. 5.9L).

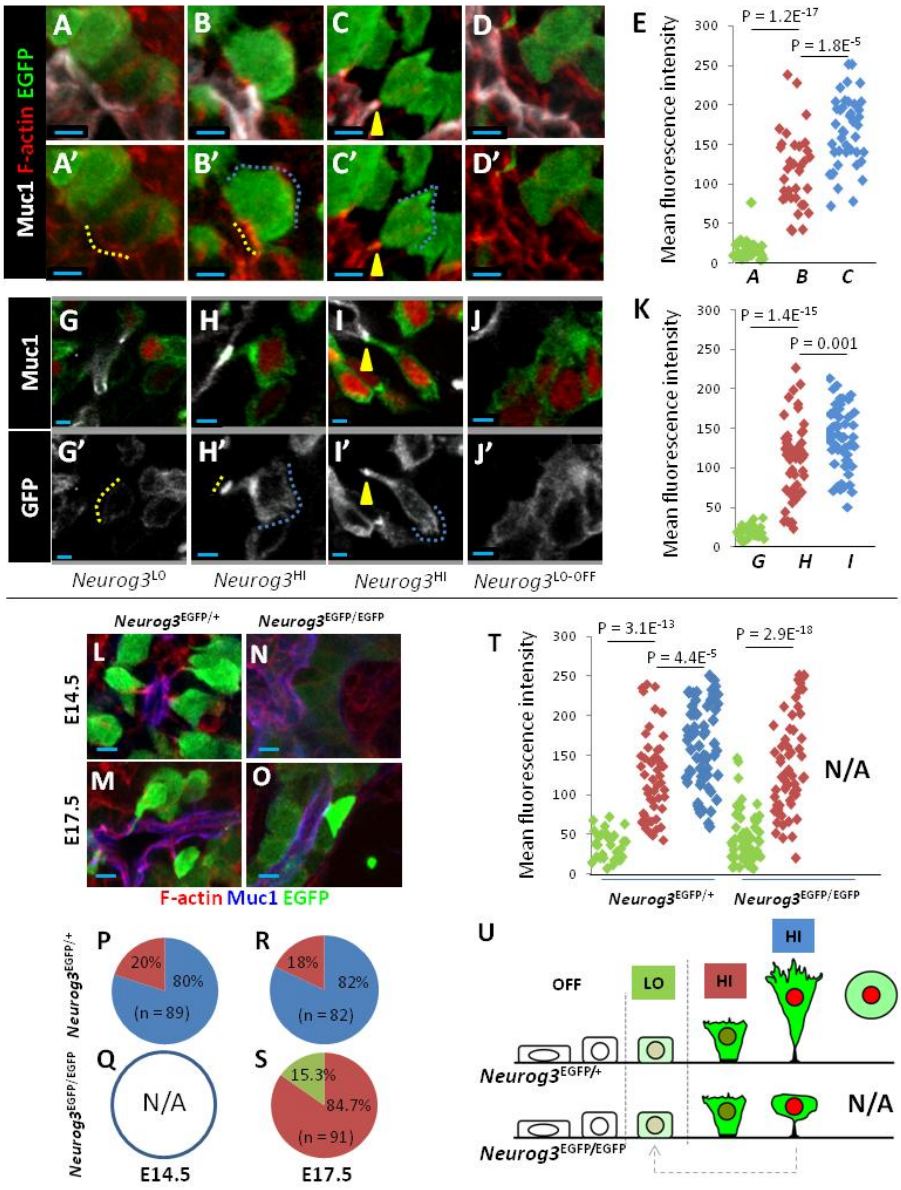

Figure 5.9. *Neurog3-independent apical narrowing and Neurog3-dependent basal migration guide endocrine cell birth. (A-D') Neurog3$^{EGFP/+}$ reporter-expressing cells showing step-wise progression from a non-apically-narrowed and non-delaminating Neurog3^{LO} state, to an apically-narrowed (yellow dashed line) Neurog3^{HI} state, an F-actin^{FOCAL}-associated migrating (blue dashed line) Neurog3^{HI} state, and finally an apically detached delaminated state. (E) Mean fluorescence intensity measurements (arbitrary units) in typical cells in non-apically-narrowed, apically-narrowed, or migrating states. (G-J') Neurog3^{RG} reporter-expressing cells showing similar progression as A-D'. (K) Mean fluorescence intensity measurements in typical cells in non-apically-narrowed (green), apically-narrowed (red), or migrating (blue) states. (L,M) Neurog3-expressing cells in the Neurog3$^{EGFP/+}$ plexus at E14.5 and E17.5. (N,O) Neurog3-expressing cells in the Neurog3$^{EGFP/EGFP}$ plexus at E14.5 and E17.5. (P-S) Percentage of Neurog3^{HI} cells in non-apically-narrowed, apically-narrowed, and migrating states at E14.5 and E17.5. (T) Mean fluorescence intensities from non-apically-narrowed (green), apically-narrowed (red), and migrating (blue) Neurog3-reporting states in Neurog3$^{EGFP/+}$ and Neurog3$^{EGFP/EGFP}$ epithelium at E17.5. (U) Schematic showing*

Neurog3-independedt and Neurog3-dependent steps in the process of Neurog3-upregulation during cell delamination from the plexus. Scale bars are 5 μm in A-D' and L-M, 3 μm in G-J'.

Endocrine-cell birth proceeds through Neurog3-independent and Neurog3-dependent steps

Neurog3-deficient cells are incapable of undergoing endocrine differentiation and delamination, but during corrective remodeling of the plexus can upregulate *Neurog3*. To understand when during the endocrine commitment process Neurog3 protein function becomes required, we analyzed the progression of control (*Neurog3*$^{EGFP/+}$) and Neurog3 protein-deficient (*Neurog3*$^{EGFP/EGFP}$) EGPF-producing cells as they moved through the step-wise process of apical-narrowing, F-actin^{FOCAL} formation, and basal migration during cell delamination. In the E17.5 *Neurog3*-deficient plexus, most EGFP^{HI} exhibited an apically-narrowed shape (84.7% versus 18% in control; n = 90) (Fig. 5.9L-S, Fig. 5.11A). A significant portion of EGFP^{HI} cells were associated with and apical F-actin^{FOCAL} structure (41.6%), but these were reduced in number (41.5% of total EGFP^{HI} cells versus 81.7% in control), and the length of the F-actin^{FOCAL} structures was reduced compared to control (Fig. 5.11A-D). Importantly, the F-actin^{FOCAL}-associated EGFP^{HI} cells did not display prevalent migratory activity at the basal cell surface, suggesting that the migratory stages of delamination are dependent on Neurog3 protein function. Notably, a portion of the EGFP^{HI} population at this stage exhibited a non-delaminating phenotype (15.3% in *Neurog3*$^{EGFP/EGFP}$ versus 2.3% in *Neurog3*$^{EGFP/+}$; Fig. 5.9S-U), which we interpret as cells that have likely previously entered the initial stages of cell delamination, have upregulated *Neurog3*, but have failed to retract the cell rear and then returned to an epithelial-resident state upon delamination failure [80,164]. These data support a model whereby *Neurog3* upregulation is controlled by morphogenetic factors that regulate apical narrowing and F-actin^{FOCAL} formation in the plexus, and suggest that later stages of cell migration and rear retraction require Neurog3 protein function (Fig. 5.9U).

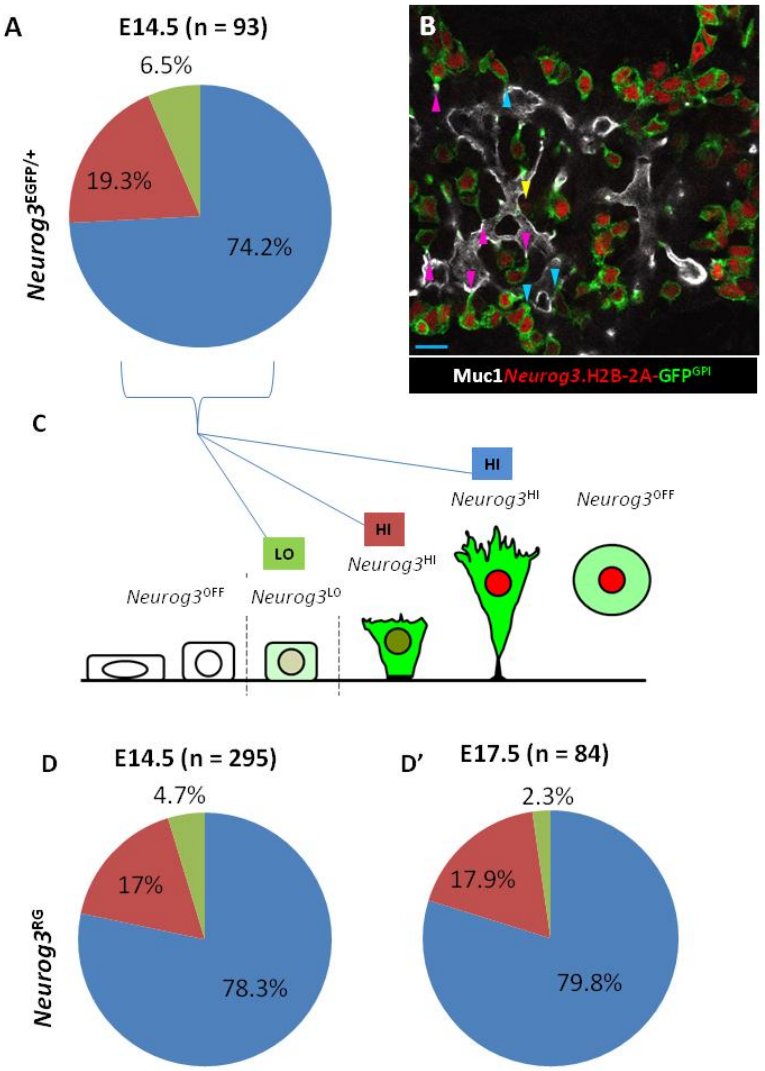

Figure 5.10. *Quantification of Neurog3-expressing states using Neurog3 knock-in and BAC-transgenic reporter alleles. (A) Quantification of the proportions of non-apically narrowed (green), apically narrowed (red), and migrating (blue) Neurog3$^{EGFP/+}$ cells at E14.5. (B) Neurog3^{RG+} cells in a representative z-stack labeled with Muc1 at E14.5. Yellow arrowhead marks non-apically narrowed EGFP^{LO} cell, cyan arrowheads mark apically narrowed EGFP^{HI} cells, pink arrowheads mark EGFP^{HI} cells associated with fully formed F-actin^{FOCAL} structures. Scale bar is 20 μm. (C,C') Percentage of non-apically narrowed (green), apically narrowed (red), and F-actin^{FOCAL}-associated migrating (blue) Neurog3^{RG+} cells at E14.5 and E17.5. (D) Diagram of the principle cell-morphological states associated with Neurog3^{OFF}, Neurog3^{LO}, and Neurog3^{HI} populations, color coded to match A-C'.*

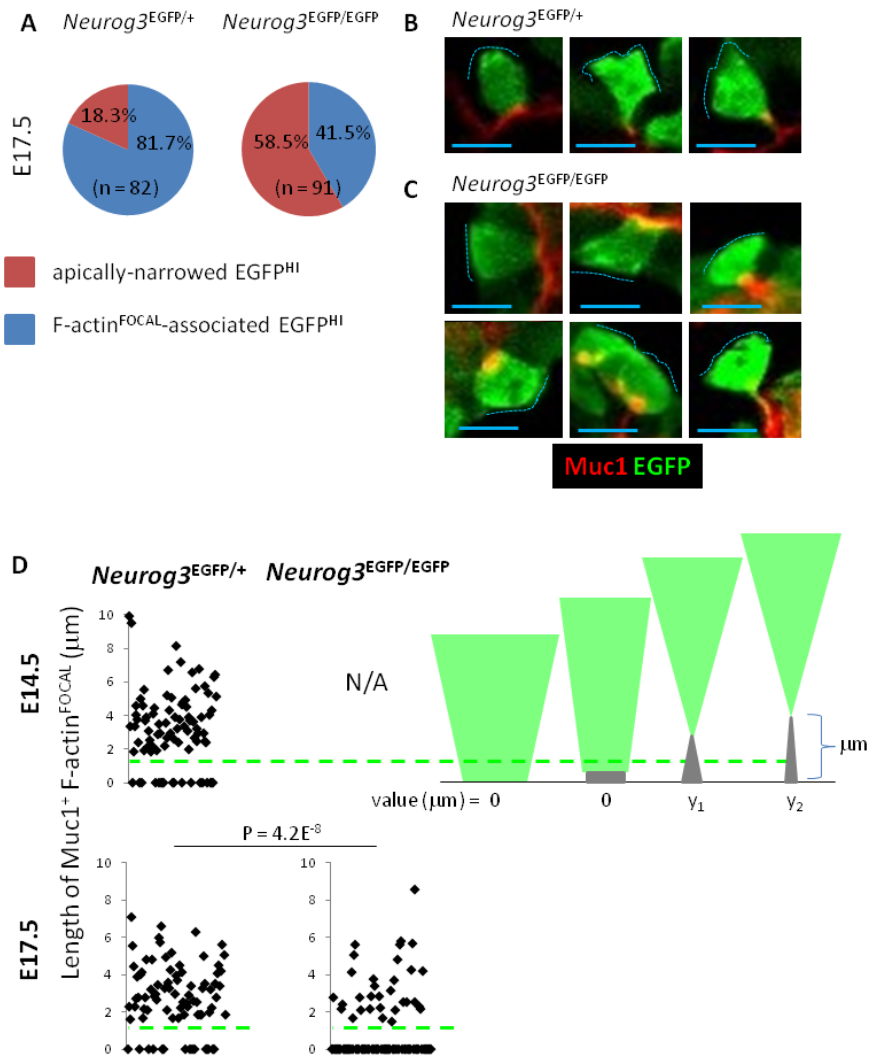

Figure 5.11. *Neurog3-deficeint Neurog3^{HI} cells become apically narrowed and form F-actin^{FOCAL} structures, but do not migrate from the epithelium. (A) Proportion of Neurog3^{HI} cells that exhibit a narrowed apical surface versus a fully formed F-actin^{FOCAL} structure in Neurog3$^{EGFP/+}$ and Neurog3$^{EGFP/+}$ plexus at E17.5. (B) Images of Neurog3^{HI} cells in Neurog3$^{EGFP/+}$ pancreata undergoing Neurog3 upregulation during apical narrowing and F-actin^{FOCAL}-formation. Note the migratory protrusions at the basal cell surface (dashed cyan lines). (C) Images of Neurog3^{HI} cells in Neurog3$^{EGFP/EGFP}$ pancreata undergoing Neurog3 upregulation during apical narrowing and F-actin^{FOCAL}-formation. (D) Measurements of the lengths of typical F-actin^{FOCAL} structures associated with Neurog3^{HI} cells in Neurog3$^{EGFP/+}$ and Neurog3$^{EGFP/EGFP}$ epithelium at E14.5 and E17.5. Green dashed line indicates the distinction between an apically-narrowed surface (below line; apically narrowed length ~ 0.0 μm) versus a fully formed F-actin^{FOCAL} structure (above line). Scale bars are 7 μm in B,C.*

Evidence for nmMyoII as a regulator of plexus morphogenesis

The molecular motor nmMyoII, which is expressed in IIa, IIb, and IIc isoforms in mammals, has known functions in acting on F-actin substrates to drive processes such as apical constriction and cell delamination, among others [112]. A high immunofluorescence signal for the active, phosphorylated nmMyoII light chain (p-nmMyoII, non-isoform-specific) was enriched at the apical aspect of epithelial cells, in a pattern consistent with localization along the F-actin^{BELT} meshwork (Fig. 5.12A,B). P-nmMyoII was detected on most Muc1^{+} F-actin^{FOCAL} structures, but showed significant variation in signal intensity (Fig. 5.12C,D), suggesting a dynamic localization during the delamination process. High levels of p-nmMyoII were also observed in the large blood vessels of the pancreas (data not shown), and relatively lower levels were observed throughout the parenchyma. NmMyoIIa and IIb isoforms showed high signal in the large blood vessels of the pancreas, and was seen at lower levels throughout the mesenchyme (Fig. 5.12K,L). We were unable to detect IIa and IIb isoforms in the epithelium or in EGFP-expressing populations using the available reagents. Analysis of nmMyoIIC using a GFP-fusion line [212], however, showed surprisingly selective and intense expression throughout the epithelium at E14.5. This pattern became largely restricted to the non-acinar epithelium by E17.5 (Fig. 5.12E-H), though there was a relatively low level of expression in differentiating endocrine cells (data not shown). These data are consistent with roles for nmMyoII activity in mediating epithelial morphogenesis and cell differentiation in the plexus.

NmMyoII activity limits plexus-to-duct remodeling and promotes endocrine differentiation

To evaluate potential functions for nmMyoII in regulating plexus morphogenesis, we isolated and explanted plexus-enriched segments of E15.5 dorsal pancreata (Fig. 5.13A), and cultured them in the presence or absence of the nmMyoII inhibitor blebbistatin (BBS) [213]. In control samples, the plexus maintained gross morphological features indistinguishable from those observed *in vivo* over 36 hours of culture (data not shown). Conversely, under nmMyoII-inhibited conditions we observed a broad, rapid, and reproducible, albeit abnormal,

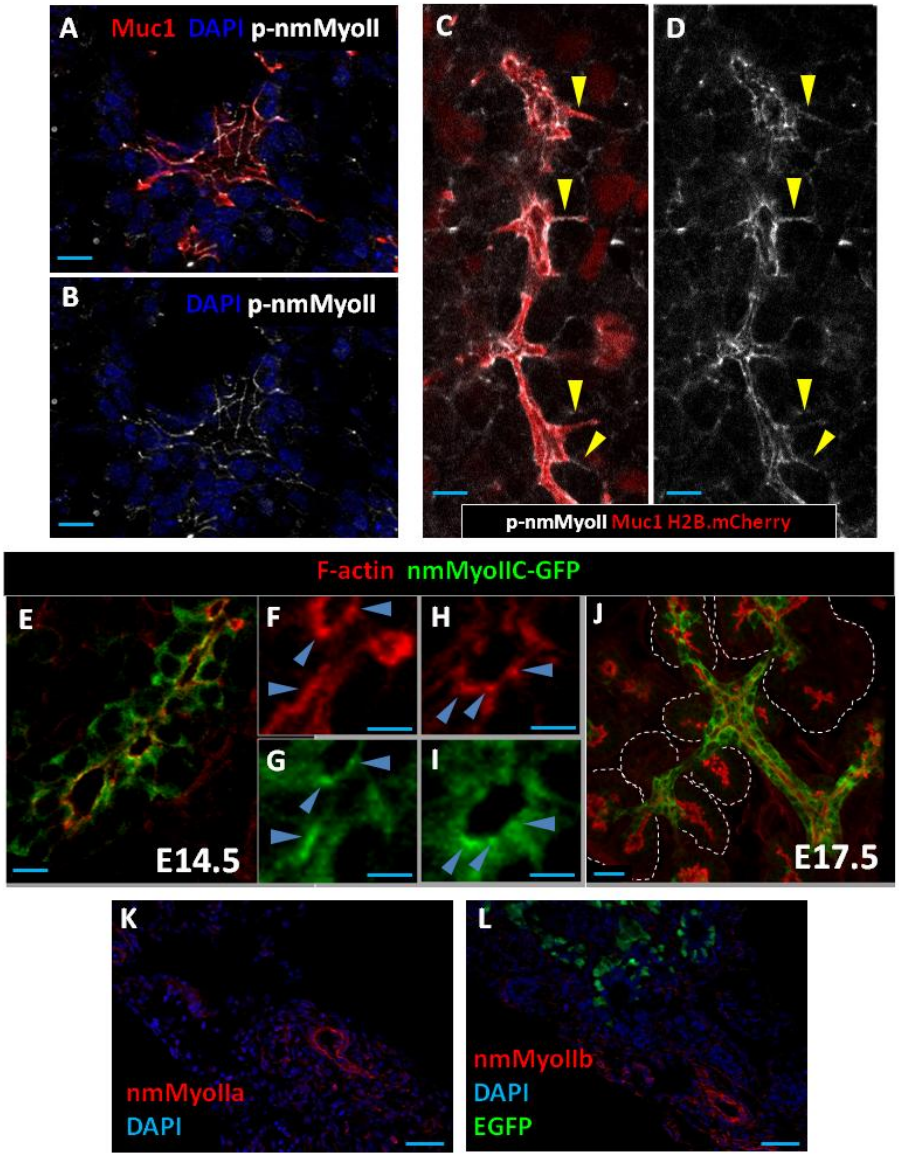

Figure 5.12. *NmMyoII isoforms and are expressed and activated in the embryonic pancreas. (A,B) Split channels of p-nmMyoII along the Muc1^{+} lumen surface at E14.5. (C,D) P-nmMyoII localization along F-actin^{FOCAL} structures (yellow arrowheads) in the Neurog3^{RG} line. Muc1 and nuclear H2B-mCherry are shown in red, to indicate the lumen surface of Neurog3-expressing cells. (E) Localization of nmMyoIIC-GFP fusion in epithelial cells at E14.5. (F-I) Evidence for enriched co-localization of nmMyoIIC-GFP signal with intense phalloidin signal near the apical surface. (J) NmMyoIIC-GFP signal becomes enriched in the non-acinar epithelium by E17.5 (white dashed line demarcates acinar clusters). (K-L) nmMyoIIa and b isofoms detected in the parenchyma (main blood vessels and mesenchyme) of the embryonic pancreas. EGFP signal is from the Neurog3$^{EGFP/+}$ knock-in strain. Scale bars are 10 μm in A,B,E, 5 μm in C,D,F-I, 20 μm in J, and 100 μm in K,L.*

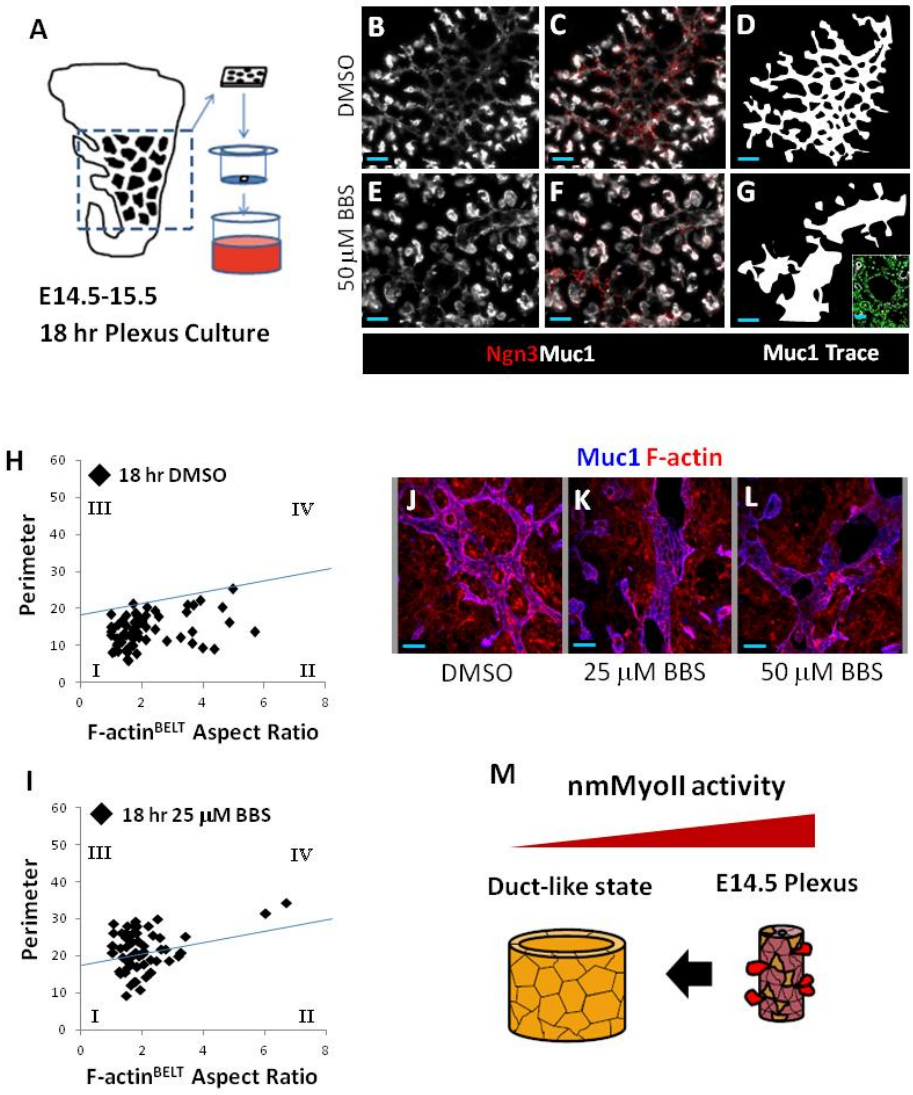

Figure 5.13. *NmMyoII activity limits apical expansion and plexus-to-duct transformation. (A) Diagram of plexus explant culture on microporous filters at the air-liquid interface. (B-G) Muc1 and Neurog3 immuno-detection in plexus explant cultured for 18 hours under vehicle-treated or BBS-treated conditions with manual traces of the epithelium in D and G. Inset shows a sectional plane from G at higher magnification, with DAPI to indicate position of nuclei around the duct-like structure. (H,I) Dimensions of F-actin^{BELT} in plexus treated with vehicle or BBS. Blue line indicates the maximum on the y-axis for F-actin^{BELT} dimensions measured in the plexus in vivo. (J-L) Muc1 and F-actin in explants treated with increasing doses of BBS. (M) Diagram showing morphological transformation of the plexus-state into a duct-like state under conditions where nmMyoII is inhibited. Scale bars are 50 μm in B-G, 30 μm in inset of G, 20 μm in J-L.*

transformation of the plexus into a duct-like state (Fig. 5.13B-G). Within the transformed duct-like-states, the F-actin^{BELT} meshwork became dilated compared to the untreated plexus (Fig. 5.13H-L), consistent with known roles for nmMyoII in regulating apical domain shape [112].

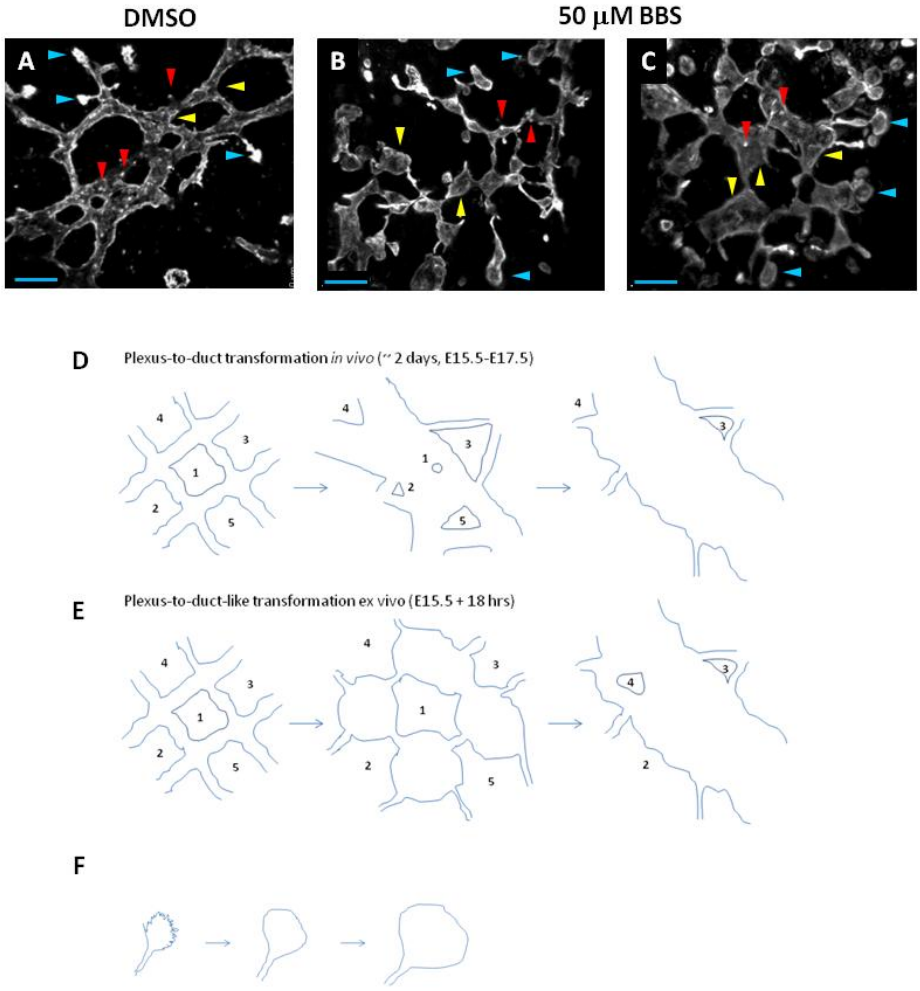

Figure 5.14. *NmMyoII-inhibition causes an abnormal plexus-to-duct-like transformation. (A) Qualities of the normal plexus-state in un-treated explants. (B-C) Representative images of abnormal plexus observed in BBS-treated explants. Qualities of the abnormal plexus state include localized sphere-like dilations of the epithelium (yellow arrowheads), malformations of the terminal acinar lumens (cyan arrowheads), and diminished numbers of F-actin^{FOCAL} structures (red arrowheads). Scale bars are 20μm. (D) Proposed diagram depicting the plexus-to-duct transformations observed under normal (in vivo) and (E) nmMyoII-inhibited conditions. Note the difference in time scales. (F) Depiction of the process of acinar lumen dilation observed under nmMyoII-inhibited conditions.*

Much of any remaining plexus exhibited abnormal morphological characteristics, such as dilation of the acinar lumens, luminal distensions at epithelial intersections within the plexus web (Fig. 5.14A-F). These BBS-mediated effects on the plexus were dose dependent and

reversible, because an 18 hour washout of the drug resulted in restoration of normal F-actin^{BELT} morphology, except in locations where plexus had become fully transformed into duct-like

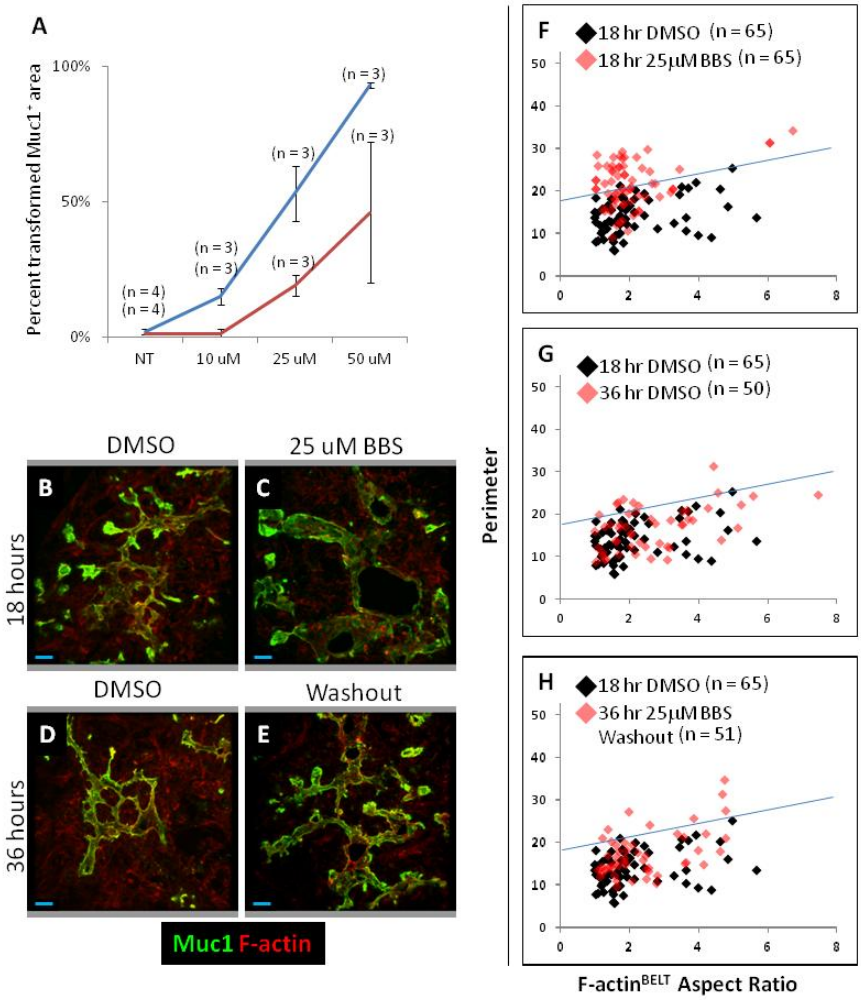

Figure 5.15. *Effects of BBS treatment on the plexus are dose-dependent and reversible. (A) Measurements of the relative Muc1^{+} pixel area exhibiting full duct-like transformation (red line), or typical abnormalities in plexus state morphology (blue line). Muc1 and F-actin localization in explants grown for 18 hr in DMSO (B), 18 hrs in 25 μM BBS (C), 36 hrs in DMSO (D), or 18 hrs in 25 μM BBS with a subsequent washout and 18 hr culture in DMSO (D). (F) Dimensions of F-actin^{BELT} in plexus treated with DMSO for 18 hrs (black dots F,G,H) or 25 μM BBS for 18 hrs (red dots) used as reference for G,H. (G) Dimensions of F-actin^{BELT} in plexus treated with DMSO for 36 hrs (red dots). (H) Dimensions of F-actin^{BELT} in plexus treated with 25 μM BBS for 18 hrs, with a subsequent washout and 18 hr culture in DMSO (red dots). Blue line indicates the maximum on the y-axis for F-actin^{BELT} dimensions measured in the plexus in vivo. Scale bars are 20 μm.*

states (Fig. 5.15A-H). The effect of nmMyoII inhibition on plexus morphology was not due to loss of epithelial cell polarity or epithelial cell-cell contact, as aPKC, the primary cilium marker gamma-tubulin, and Ecad maintained localization at their respective apical and basal-lateral cell membranes during these experimental time-frames (Fig. 5.16A-F). Interestingly, along the Muc1^{+} lumen of transformed duct-like-states in BBS treated explants there was a marked

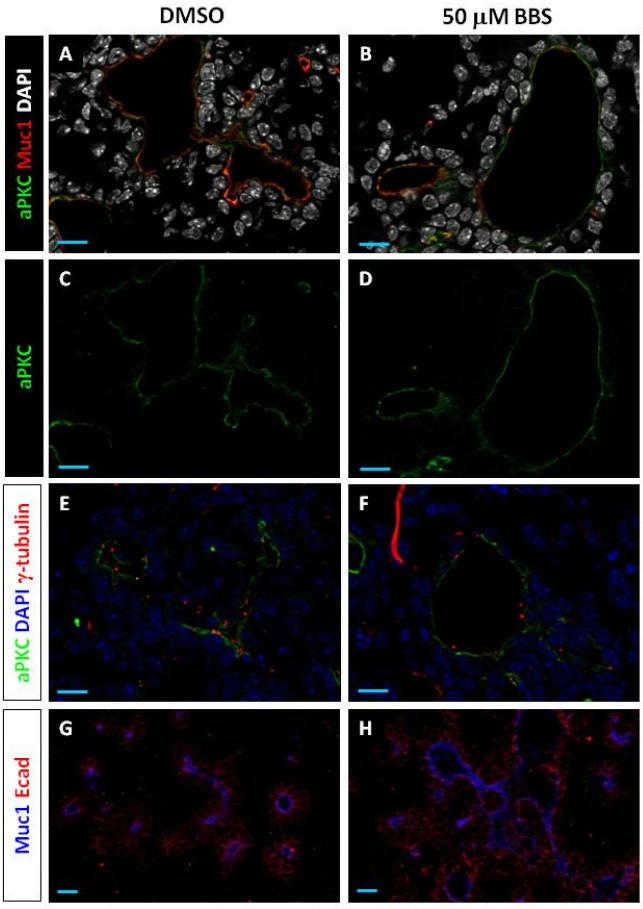

Figure 5.16. *Apical polarity and cell contact are maintained under nmMyoII-inhibited conditions. (A-D) Representative images of E14.5 plexus explants treated for 18 hr with DMSO or 50 μM BBS and labeled with the apical markers Muc1, and aPKC. (E,F) Untreated and treated samples labeled with the ciliary basal-body marker gamma tubulin, which is normally localized near the aPKC^{+} apical surface of epithelial cells. (G,H) Ecad localization in epithelial cells from treated and untreated explants. Scale bars are 10 μm.*

decrease in the number of Neurog3^{+} cells (Fig. 5.13C,F). In these same samples, epithelium remaining in the plexus-state remained associated with large numbers of Neurog3^{+} cells. While Sox9 expression was reduced in the treated condition, there was no change in the epithelial expression pattern of Pdx1, suggesting that the changes in Neurog3 production were not the

result of loss of pancreatic identity. Moreover, the transcription factor Prox1, which represents an epithelial cell marker with known functions in regulating epithelial identity, was unchanged (Fig. 5.17A-H) [76]. These experiments show that nmMyoII inhibition causes acute morphological alterations to the plexus and a block in Neurog3 protein production, suggesting functions for nmMyoII in limiting plexus-to-duct remodeling and promoting endocrine differentiation within the plexus (Fig. 5.13M).

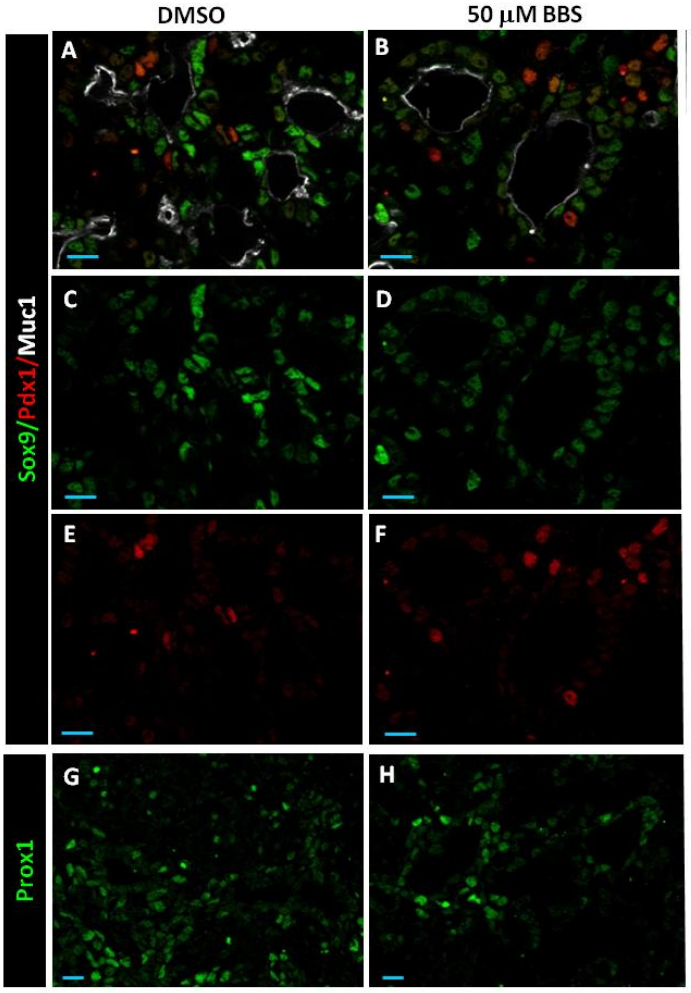

Figure 5.17. *Selective alterations in epithelial transcription factor expression under nmMyoII-inhibited conditions. (A-F) Immunodetection of Sox9 and Pdx1 in plexus explants treated with DMSO or 50 μM BBS for 18 hrs. (G,H) Expression of Prox1 in plexus explants treated with DMSO or 50 μM BBS for 18 hrs. Scale bars are 10 μm.*

ROCK-nmMyoII pathway activity mediates apical narrowing, leading edge migration, and cell rear retraction in Neurog3-expressing populations

To address how cell morphogenesis influences endocrine cell-fate allocation, we next studied the effects of two small molecule inhibitors (BBS and Y-27632) on the cell delamination and *Neurog3*-activation. BBS inhibits nmMyoII directly by interfering with intrinsic GTPase motor activity [214], and can thus inhibit all nmMyoII-dependent processes. Y-27632 inhibits ROCK [215], which is known to limit cell migration (depending on the cell type) by modulating actin filament stabilization and nmMyoII activity [146], and is also required for cell rear retraction [153]. Using the *Ngn3*^{RG}-reporter line, explants treated with BBS showed reductions in *Neurog3*$^{RG+}$ populations along the Muc1^{+} lumen, consistent with the reductions of Neurog3^{+} cells observed in wild-type explants by immunodetection (Fig. 5.18A-D;Fig. 5.19A-F). In epithelium where *Neurog3*$^{RG+}$ cells remained (likely due to reporter-protein purdurance in cells that had already begun the *Neurog3*-upregulation process), quantification of the proportion of non-apically narrowed, apically-narrowed, and migrating RG^{+} cells indicated a shift toward a non-apically narrowed state, and a flattened cell shape, with little to no migratory activity at the basal cell surface (Fig. 5.18G,G'). There was also a reduction in Muc1^{+} F-actin^{FOCAL} structures, and the lengths of those remaining were decreased relative to control (Fig. 5.18H,H'). These results are consistent with a requirement for nmMyoII activity in mediating apical-narrowing, F-actin^{FOCAL} formation, and basal migration steps during cell delamination and *Neurog3* upregulation.

ROCK-inhibition, like nmMyoII inhibition, had several effects on tissue and cell morphology in the plexus. Contrary to BBS, Y27632-treated explants showed no evidence of plexus-to-duct-like transformation, or any apparent decrease in *Neurog3*$^{RG+}$ cells along the Muc1^{+} lumen (Fig. 5.18E,F,G"). Rather, the plexus was maintained in association with numerous delaminating Neurog3^{RG+} cells. The morphology of the Neurog3^{RG+} cells themselves, however, was altered.

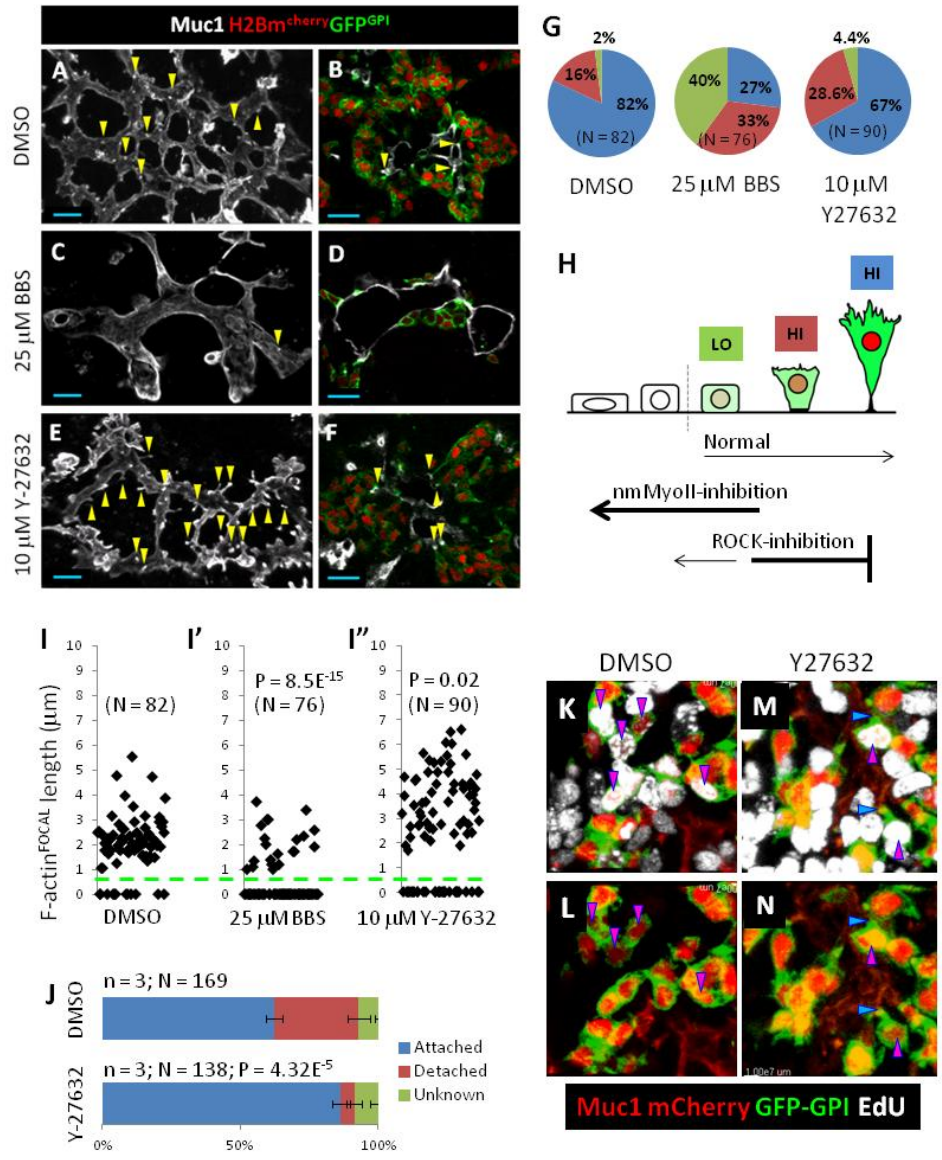

Figure 5.18. *ROCK-nmMyoII pathway activity mediates steps in endocrine cell birth. (A-F) Muc1^{+} and Neurog3^{RG+} cells in plexus explants treated with DMSO, BBS, or Y-27632 for 18 hrs. Muc1^{+} F-actin^{FOCAL} structures are shown by yellow arrowheads. Note the reductions in apically-narrowed and migrating populations in the BBS treated condition. (G) Proportions of non-apically-narrowed, apically-narrowed, and migrating Neurog3-expressing populations in explants treated with DMSO, BBS, or Y27632. (H) Diagram of non-apically-narrowed, apically-narrowed, and migrating Neurog3-expressing cells shown in G, and outlining the effects of nmMyoII versus ROCK inhibition on the endocrine cell birth process. (I-I") Measurements of the lengths of typical F-actin^{FOCAL} structures in explants treated with DMSO, BBS, or Y27632. Green dashed line indicates the distinction between an apically-narrowed surface (below line; F-actin^{FOCAL} length ~ 0.0 µm) versus a fully formed and lengthened F-actin^{FOCAL} structure (above line). (J) Quantification of the defect in tail retraction observed in Y-27632- treated explants by*

EdU pulse-chase. (K-N) Representative images of EdU-labeled RG^+ cells exhibiting attached (blue arrowheads) or detached (pink arrowheads) cell rears. Scale bars are 20 μm.

Consistent with known functions for ROCK in limiting protrusive migratory activity at the leading edge of migrating cells, most ROCK-inhibited $Neurog3^{RG+}$ cells were elongated in shape, and displayed augmented protrusions at their basal cell surface (Fig. 5.19A-I). Live imaging of pancreatic explants cultured on fibronectin, in the presence or absence of BBS or Y27632, confirmed that nmMyoII inhibition reduced leading edge protrusive activity, while ROCK-inhibition augments leading edge protrusive activity (Fig. 5.20). ROCK-inhibition increased the number and lengths of $F\text{-}actin^{FOCAL}$ structures distributed across the plexus, suggestive of a known defect in cell rear-retraction caused by reduced ROCK activity [148]. We tested and confirmed defective cell rear-retraction using EdU pulse chase methodology. Briefly, replicating progenitor cells incorporate EdU at S-phase, and then differentiate into delaminated endocrine cells over an estimated 17-18 hour period on average [211, Chapter II]. After a one hour injection of EdU into pregnant dams, pancreas was harvested from E13.5 embryos and explants cultured in the presence or absence of ROCK-inhibitor for 18 hours. If ROCK-inhibition causes a defect in cell retraction, then we predict a relative accumulation of $Neurog3^{RG+}$ cells remaining attached to $Muc1^+$ lumen in the ROCK-inhibited condition, whereas EdU^+ $Neurog3^{RG+}$ cells in untreated explants should be able to retract their cell rear and complete epithelial delamination. Z-stack volumes (~ 20 μm thick) of EdU pulse-labeled RG^+ cells were acquired so that attached and detached states could be unambiguously scored. In DMSO treated explants, 63.4 ± 3.1% of RG^+ cells were attached to the lumen, 30.6 ± 3.9% were detached, and 7.0 ± 1.0% could not be definitively categorized as attached or detached (Fig. 5.18J-L). In Y-27632 treated explants, 86.6 ± 3.1% of RG^+ cells were attached to the lumen, 4.8 ± 2.9% were detached, and 8.6 ± 2.7% could not be definitively categorized as attached or detached (Fig. 5.18J-N). Collectively, these data indicate that ROCK has functions in limiting protrusive migration at the basal surface during the early stages of endocrine cell birth, and then functions to direct retraction of the cell rear from the apical lumen surface upon completion of delamination. Thus, ROCK-nmMyoII pathway dynamics mediate multiple steps in cell delamination during endocrine cell birth by regulating initial apical narrowing and $F\text{-}actin^{FOCAL}$ formation, basally directed cell migration, and cell rear retraction.

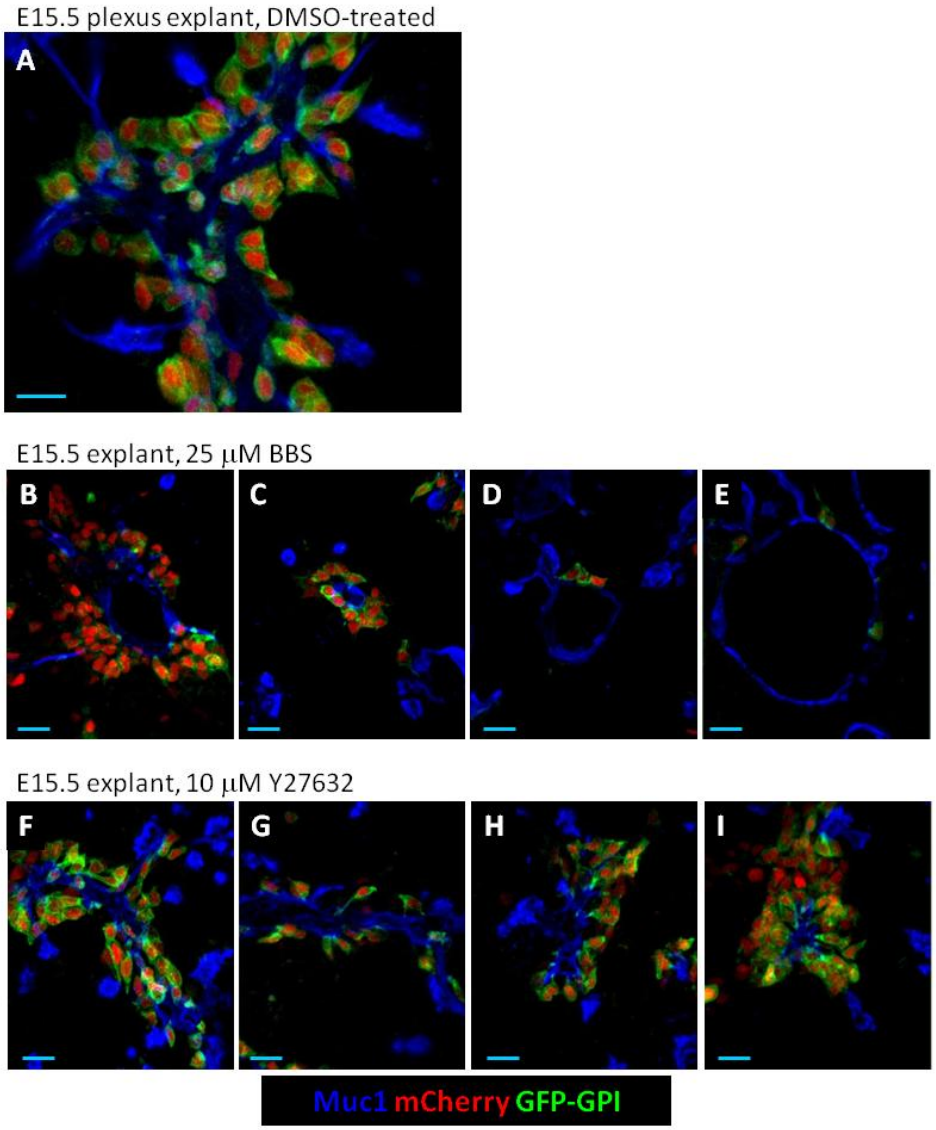

Figure 5.19. *ROCK-nmMyoII pathway inhibitors influence luminal expansion, apical narrowing, and basal migration processes during Neurog3 activation and upregulation. (A) Muc1^{+} lumen and Neurog3^{RG+} cell morphology in untreated, BBS-treated (B-E), and Y27632-treated (F-I) explants. Scale bars are 15 μm.*

nmMyoII activity mediates escape from Notch signaling

Comparison of the numbers of Neurog3^{+} over Neurog3^{-}Muc1^{+}DAPI^{+} cells in the epithelium of pancreatic explants treated with BBS or vehicle showed a near 50% reduction in Neurog3^{+} cells in the BBS-treated condition, indicating that *Neurog3* activation and upregulation is blunted under conditions where nmMyoII is inhibited (Fig. 5.21A-B',E). Because Notch signaling is also

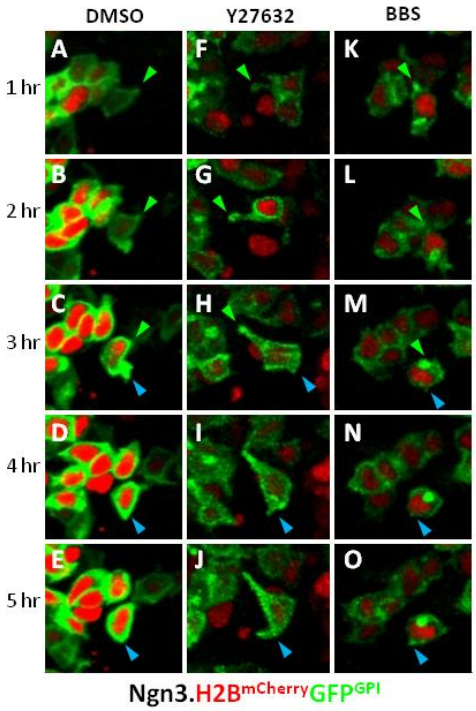

Figure 5.20 *Live imaging of explants treated with ROCK-nmMyoII pathway inhibitors confirms alterations to apical narrowing, basal migration, and Neurog3 upregulation. E12.5 Neurog3^{RG} pancreata were grown for 24 hours on fibronectin coated Met-Tek dishes. DMSO, 10 μM Y27632, and 10 μM BBS were applied for an additional 24 hour period, while explants were subjected to live imaging. (A-E) One hour snapshots from live imaging during delamination of Neurog3^{RG} cell in DMSO treated condition. (F-J) One hour snapshots from live imaging during delamination of Neurog3^{RG} cell in Y27632 treated condition. (K-O) One hour snapshots from live imaging during delamination of Neurog3^{RG} cell in BBS treated condition. Green arrowheads demarcate the apical domain, and blue arrowheads demarcate the basal leading edge, of individual Neurog3-expressing cells.*

known to block *Neurog3* activation, we hypothesized that nmMyoII might function, at least in part, to mediate escape from Notch. To test this, we cultured explanted plexus in the presence of the Notch inhibitor DBZ [170], or BBS and DBZ together (BBS was applied 6 hr before DBZ), and scored (total Neurog3^{+})/(total Neurog3^{-}Muc1^{+}DAPI^{+}) cells in each condition. Consistent with previous reports, pharmacological inhibition of Notch pathway activity in pancreatic explants caused much of the pancreatic epithelium to become Neurog3^{+} (Fig. 5.21C,C',E) [72,80]. In explants treated with both BBS and DBZ, Neurog3^{+} cells were increased relative to DMSO and BBS treated conditions (Fig. 5.21D-E. These results indicate that the block in Neurog3-activation observed in nmMyoII-inhibited conditions can be bypassed through

inhibition of Notch, and suggest that nmMyoII activity mediates escape from repressive Notch signals.

A ROCK-nmMyoII, Notch and Neurog3 gene-dosage circuit regulates cycles of endocrine cell birth

A previous study showed that the upregulation of Neurog3 to high levels is required for full commitment to the endocrine lineage [69]. Cells that are genetically hypomorphic for Neurog3 are more prone to being maintained in the Sox9 epithelium in a Neurog3^{LO} state than their wild type counterparts, which rapidly progress to a delaminating Neurog3^{HI} state. We thus utilized an allelic series comprised of *Neurog3* nullizygous (*Neurog3*$^{EGFP/EGFP}$), hypomorphic (*Neurog3*$^{EGFP/flox}$), and control (*Neurog3*$^{EGFP/+}$) conditions to dissect the relationship between ROCK-nmMyoII, Notch, and *Neurog3* gene dosage functions during the process of endocrine birth. To do this, we analyzed reporter activation (from the *Neurog3*^{EGFP} allele) in explants from each genetic condition, and that were treated with ROCK inhibitor, Notch inhibitor, or both in combination. In *Neurog3*$^{EGFP/EGFP}$ explants, where the vast majority of the plexus is EGFP^{LO}, neither ROCK inhibition, Notch inhibition, nor both in combination was sufficient to cause upregulation of *Neurog3* to high levels (Fig. 5.21F-I,Q,R). Because Notch signaling is already reduced in this genetic condition [72,211], these results are consistent with the notion that Neurog3^{LO} state is acquired in part through escape from Notch, but that escape from Notch is not sufficient to generate Neurog3^{HI} cells when Neurog3 protein is absent. In explants from *Neurog3* hypomorphs, there was a significant increase in the number of EGFP^{LO} cells in the Sox9^{+} epithelium, and a significant decrease in the numbers of Sox9^{-}EGFP^{HI} cells, similar to what has been previously shown [69]. In ROCK-inhibited hypomorphic explants, however, we observed a large increase in Sox9^{-}EGFP^{HI} cells, and a corresponding decrease in Sox9^{+}EGFP^{LO} cells (Fig. 5.21J,K,Q,R). This indicates that ROCK-inhibition can convert *Neurog3*^{LO} cells into *Neurog3*^{HI} cells when *Neurog3* gene dosage is limiting. DBZ treated hypomorphic explants also showed increased EGFP^{HI} cells relative to the DMSO-treated condition, indicating that if Neurog3 protein is present, escape from Notch results in upregulation of Neurog3 to high levels

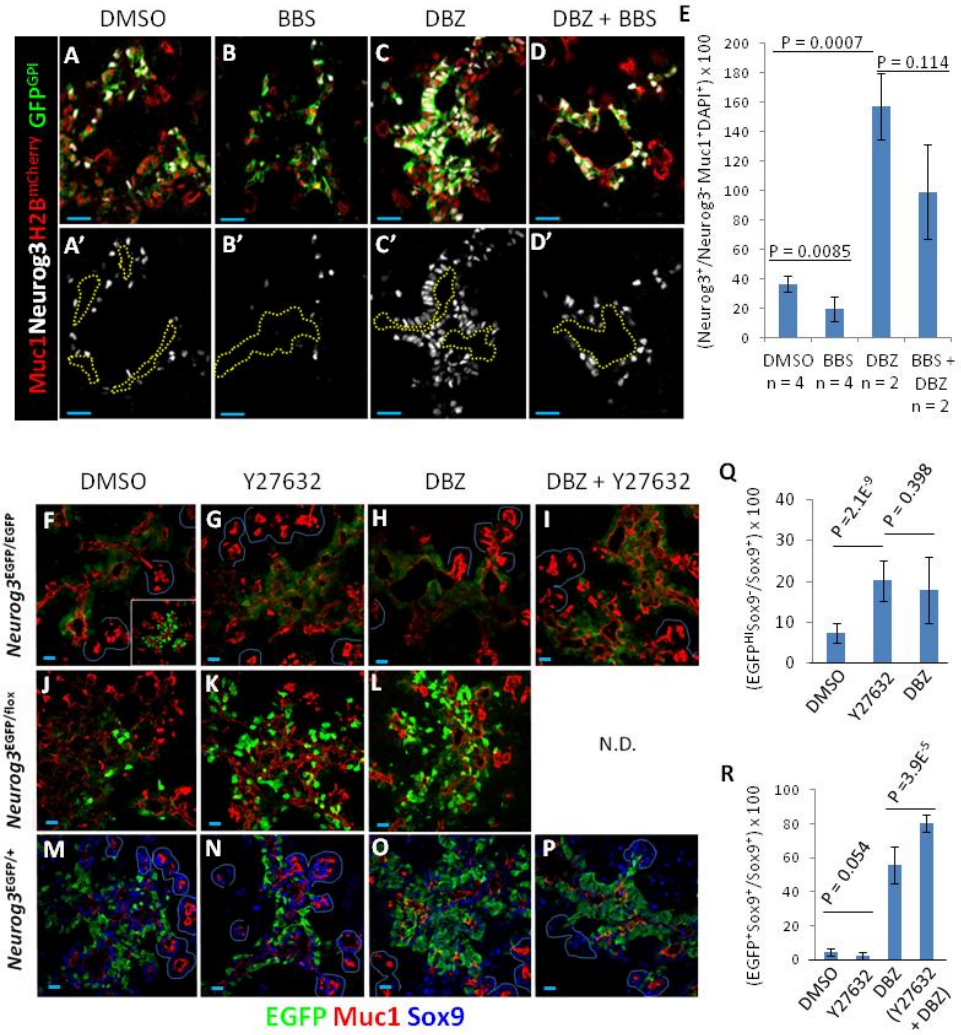

Figure 5.21. *ROCK-nmMyoII, Notch, and Neurog3 gene dosage regulate the progression of cells through Neurog3-expressing states.(A-D') Immunodetection of Muc1 and Neurog3 protein in E15.5 Neurog3^{RG+} pancreatic explants treated with DMSO, 25 μM BBS, 20nM DBZ, or BBS and DBZ. BBS was applied for an 18 hour period. DBZ was administered 6 hour into the culture period, for a total DBZ culture period of 12 hours. Quantification of the number of Muc1^{+}, DAPI^{+} (not shown) cells that are Neurog3^{+} in each condition (n = 3 for DMSO and BBS, n = 2 for DBZ and DBZ + BBS). Approximately 30% of each explants was scored for each condition, the numbers of each cell state were summed, and averaged between each explant for each condition. (F-I) Immunodetection of Muc1, EGFP, and Sox9 (not shown) in E13.5 Neurog3$^{EGFP/EGFP}$ explants treated with 10 mM Y27632, 20 nM DBZ, or Y27632 and DBZ for 18 hours. (J-L) E13.5 Neurog3$^{EGFP/flox}$ explants treated and analyzed according to F-H. (M-P) Immunodetection of Muc1, EGFP, and Sox9 in E13.5 Neurog3$^{EGFP/+}$ explants treated according to F-I. (Q) Quantification of endocrine-committed EGFP^{HI}Sox9- cells over total Sox9^{+} cells in 40x z-stack images (~20 μm thick) Neurog3$^{EGFP/flox}$ explants treated with DMSO, Y27632, or DBZ. (R) Quantification of the number of Sox9^{+} cells activating EGFP in Neurog3$^{EGFP/+}$ explants treated with DMSO, Y27632, DBZ, or DBZ and Y27632. For Q and R, three explants were imaged (~30% of total explants by serial thick sections), numbers of cells were scored and summed for each image, and individual images for each condition were averaged. Error bars are S.E.M. Scale bars are 20 μm for A-D', and 10 μm for F-P. Blue lines demarcate acinar clusters. N.D. No Data.*

(Fig. 5.21L,Q,R). Finally, in the *Neurog3*$^{EGFP/+}$ condition, explants treated with ROCK inhibitor showed only a minor increase in the number of EGFP^{HI} cells relative to the untreated condition (Fig. 5.21M,N,R), indicating that ROCK inhibition is not sufficient to increase endocrine differentiation under normal genetic conditions. This suggests that the effect of ROCK inhibition in pushing cells toward the Neurog3^{HI} state (observed in ROCK-inhibited *Neurog3* hypomorphs) might be limited by the number of Neurog3^{HI} cells. We thus hypothesized that the pro-endocrine effect of ROCK inhibition could be limited by Notch-inhibition from Neurgo3^{HI} cells. Consistent with this notion, administration of ROCK and DBZ together resulted in activation of *Neurog3* in the vast majority of the plexus (Fig. 5.21O-R). These collective results indicate that ROCK-nmMyoII, Notch and Neurog3 gene activities together orchestrate the progression of cells in the plexus through sequential *Neurog3* expressing states during endocrine-cell birth.

Adaptive self organization in the plexus confers a robust endocrine differentiation program

The data presented thus far indicate that *Neurog3* activity influences epithelial plexus morphogenesis, and that morphogenetic inputs within the plexus, such as ROCK-nmMyoII, influence *Neurog3* activity. We therefore hypothesized that, together, endocrine differentiation and plexus morphogenesis processes feed-forward to confer robustness on the endocrine lineage allocation program. To test this, we quantified and compared the relative numbers of EGFP^{HI} cells being born from the plexus (by measuring total EGFP^{HI}/Sox9^{+} cells), during a time course (E13.5, E16.5, and E18.5) for normal plexus remodeling (Neurog3$^{EGFP/+}$), for *Neurog3*-deficeint corrective plexus remodeling (Neurog3$^{EGFP/EGFP}$), and for an experimental condition wherein the plexus is supplemented with a sub-commitment dose of *Neurog3* (*Neurog3*$^{EGFP/flox}$) [69]. In *Neurog3*$^{EGFP/+}$ pancreata, endocrine differentiation was robust and prolonged during the entire course of secondary transition. In *Neurog3*$^{EGFP/EGFP}$ pancreata, the early and pervasive defects in *Neurog3* upregulation became progressively, but only partially rescued by E16.5 and E18.5, confirming that Neurog3 dependent processes are necessary for a full restoration of *Neurog3* upregulation in the plexus. In *Neurog3*$^{EGFP/flox}$ pancreata, the early and pervasive defects in *Neurog3* upregulation became progressively, and then completely rescued to normal levels by E18.5. These results indicate that in addition to the feed-back functions for Neurgo3 in

limiting its own expression domain via Notch, there are also feed-forward functions for Neurog3 that promote endocrine differentiation from within the remodeling plexus-state.

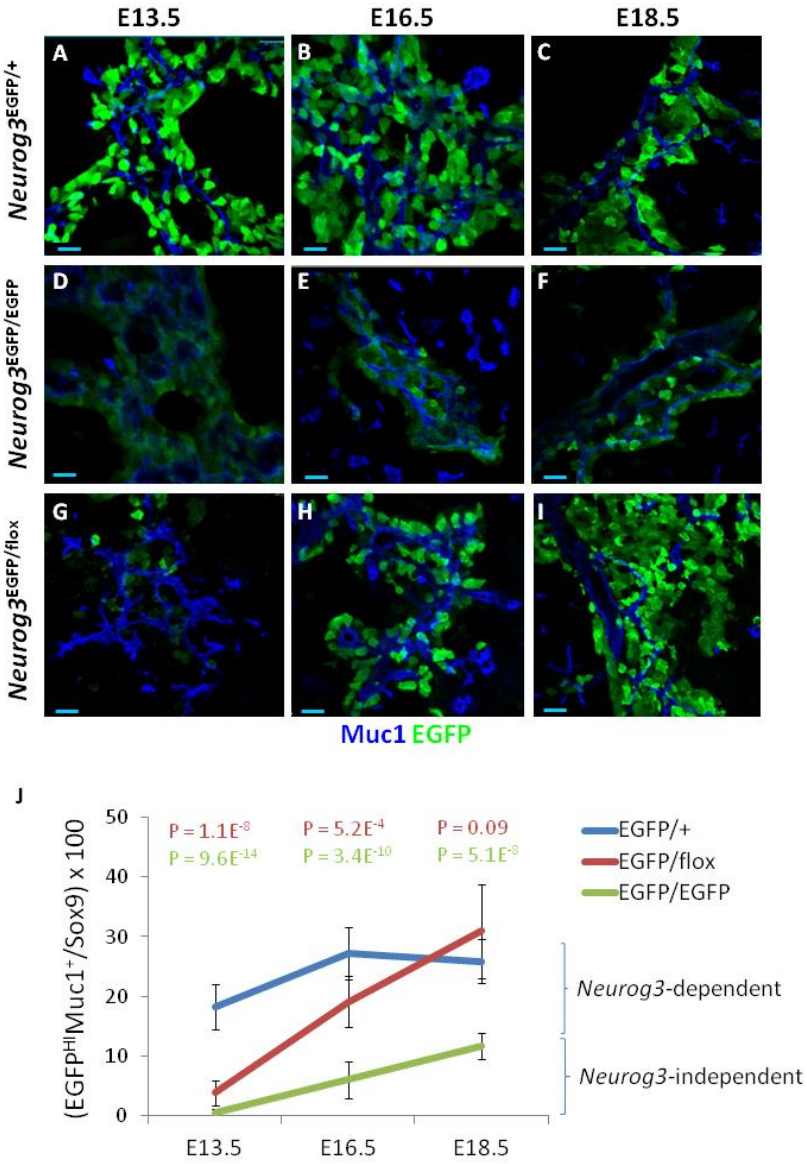

Figure 5.22. *Adaptive self organization in the plexus confers a robust endocrine differentiation program. Immunodetection of Muc1, EGFP, and Sox9 (not shown) during a time-course for plexus remodeling in thick-sectioned (30 μm) Neurog3$^{EGFP/+}$, Neurog3$^{EGFP/EGFP}$, and Neurog3$^{EGFP/flox}$ pancreata. (J) Quantification of delaminating endocrine committed EGFP^{HI}Muc1^{+}Sox9^{-} cells over total Sox9^{+}EGFP^{-} cells at each stage. Images of plexus were taken from n = 3 pancreata at each stage (Neurog3$^{EGFP/+}$ = 11, 10, and 9 images for E13.5, E16,5 and E18.5; Neurog3$^{EGFP/EGFP}$ = 12, 10, and 9 images for E13.5, E16,5 and E18.5; Neurog3$^{EGFP/flox}$ = 9, 11, and 14 images for E13.5, E16,5 and E18.5, respectively). Error bars are S.E.M. Scale bars are 15 μm in A-I.*

Discussion

In studying the molecular and genetic control of epithelial-plexus remodeling and *Neurog3* activation during the pancreatic secondary transition, we arrive at a new model for how epithelial morphogenesis, progenitor maintenance, and lineage differentiation are integrated to direct the allocation of pancreatic duct/endocrine tissues. In the absence of *Neurog3*-dependent differentiation, delamination, and Notch-pathway activities, essentially all progenitors in the plexus are maintained in an 'equivalent' state of low *Neurog3* expression. This *Neurog3*^{LO} plexus-state is dependent on nmMyoII activity, because in normal tissue nmMyoII inhibition results in an epithelial transformation into non-plexus duct-like states, and causes an acute and early block in *Neurog3* activation. The transition from the *Neurog3*^{LO} to a *Neurog3*^{HI} state is controlled by an nmMyoII-dependent narrowing of the apical cell-surface, which represents the initial step in a cell-delamination program that is specified within the plexus upstream of Neurog3. Later steps in delamination include basal migration and epithelial exit, which are nmMyoII-dependent, *Neurog3*-dependent, and limited by ROCK. ROCK activity gates the transition of the Neurog3^{LO} to the Neurog3^{HI} state, because its inhibition can promote both basal migration and Neurog3 upregulation under conditions where Neurog3 is limiting. Finally, differentiating endocrine cells exert multiple feedback effects on the epithelium to locally repress endocrine differentiation, but also to augment endocrine lineage allocation from the plexus as a whole. We propose endocrine differentiation and plexus morphogenesis programs cross-regulate one another to both achieve and maintain a physiologically optimized rate for the allocation of duct and endocrine tissues. In this manner, progenitors assembled and maintained in the plexus can make enough cells, the right type of cell, and place these cells in the right place and at the right time during organ formation.

Tissue morphogenesis mediates acquisition of states of Neurog3 activation

Our data suggest that states of *Neurog3* activation are controlled within the plexus, at least in part, through regulated changes in cell morphology. In the absence of *Neurog3*, the normally heterogeneous spectrum of cells' apical domain shapes observed within the plexus becomes misconfigured toward a relatively homogeneous and uniformly 'circular' state. This

reorganization of epithelial structure is associated with a broad acquisition of the *Neurog3*^{LO} state, and a loss of both the *Neurog3*^{HI} and *Neurog3*^{OFF} states (E12.5-E15.5). During late-stage 'corrective remodeling' of the dysmorphic *Neurog3*-deficeint epithelium (E16.5-E18.5), the spectrum of apical domain shapes is observed to progressively reconfigure toward a more normal configuration. As this occurs, cells moving into the *Neurog3*^{HI} state are observed throughout the plexus, and appear to form in association with a process of apical narrowing and basal displacement.

Apical narrowing or basal displacements have been previously proposed mechanisms for how epithelial progenitor populations escape from repressive Notch signals [218,245,246]. Our data showing that Notch inhibition does not induce *Neurog3*^{HI} cells in the dysmorphic *Neurog3*-deficient plexus explants at E13.5, however, combined with our data showing that *Nuerog3*^{HI} cells form in the correctively remodeled *Neurog3*-deficient plexus from E16.5-E18.5 *in vivo*, rule out that Notch or Neurog3 are required for the conversion of the *Neurog3*^{LO} state to *Neurog3*^{HI}. We suspect, rather, that an nmMyoII-dependent process of apical narrowing and basal displacement, which is specified periodically within the normal plexus state, mediates (in addition to escape from Notch) the exposure of individual progenitor cells to a pro-endocrine cue(s) located at or near the basal ECM. NmMyoII inhibition blocks Neurog3 activation in normal explants, and consistent with a role for nmMyoII in mediating escape from Notch, administration of the Notch-inhibitor DBZ to nmMyoII-inhibited explants results in activation of Neurog3. The degree of Neurog3 activation, however, is reduced in comparison to explants treated with DBZ alone, suggesting that nmMyoII also mediates access to a pro-endocrine cue(s). The idea that states of Neurog3 activation might be mediated by apical versus basal positioning within the epithelium, is in line with a previous study showing that the cell polarity determinant Cdc42 plays important roles in regulating epithelial tubulogenesis as well as endocrine differentiation in the pancreas [25]. We envision that further investigations in the polarity regulators such as Rho and Rac, which have known functions in regulating actomyosin contractility [109-125], actin dynamics [128,132-134], and apical versus basal polarization in numerous cell types [146,147], could provide new entry points into dissecting the morphogenetic regulation of endocrine cell birth. The idea that ROCK, which is activated by Rho

and has been shown in some cell types to inhibit cell migration [140,146,150-154], limits the conversion of *Neurog3*^{LO} to *Neurog3*^{HI} cells in Neurog3 hypomorphs, is consistent with the notion that cell polarity pathways represents important mediators of endocrine fate allocation in the pancreas [25,259,260,261]. Collectively, these data support the concept that provided the right environmental conditions, small molecule manipulations on the activity of morphogenetic determinants could be a productive avenue toward guiding cell fate transitions during the artificial directed differentiation of embryonic stem cells toward the endocrine lineage.

Transcriptional determinants of cell fate regulate tissue and cellular morphogenesis

Tissue-specific inactivation of transcriptional regulators – such as HNF1b [74], HNF6 [73], Prox1 [75,76] Neurog3 [72,211], and Pdx1 [13,258] – in the pancreatic epithelium all cause epithelial malformations concurrent with defects in endocrine cell lineage allocation. While the interpretations of these phenotypes have been based largely on direct transcriptional effects at promoter targets such as *Neurog3*, they are equally consistent with the idea that alterations to epithelial morphology can preclude efficient engagement of the endocrine-differentiation program. In animals deficient for Pdx1, which is a master regulator of pancreas formation and lineage specification, early dorsal evagination from the foregut, cell polarization, and microlumen-formation all occur [24,258], but there is a complete failure in pancreas-specified cells to subsequently assemble into a plexus. Thus, transcriptional regulators of cell fate are likely to have both direct and indirect roles in building and regulating precise states of tissue architecture, which in turn mediate the placement of the right types and numbers of organ specific lineages. In the future, a movement toward building increasingly integrated network models linking epithelial morphogenesis, gene transcription, and intracellular signaling as obligatory principle components of a larger “niche-framework” will improve our understanding of how specificity, robustness, and heterogeneity in multicellular behaviors are achieved during organ self-assembly.

Feedback control of progenitor maintenance, differentiation, and morphogenesis within a transient niche during organogenesis

While the structure and function of stem-cell niches in homeostatic and regenerative systems [2,3,4,5,6] are becoming relatively well understood, the transient nature of organ-specific progenitors, and the complexity underlying the process of organ formation itself, has hindered our ability to build niche-based paradigms for how organ progenitors are regulated. Our data suggest that the epithelial plexus represents a niche for differentiating endocrine cells, and that differentiating endocrine cells represent a type niche 'support cell' for the epithelial plexus. In line with this, our studies and others have shown that Neurog3 functions not only as an endocrine lineage determinant and effector of Notch [34]. Rather, Neurog3 has broad functions in influencing multiple developmental programs in the plexus. These include supporting robust progenitor replication, regulating gene expression patterning, maintaining undifferentiated progenitors, shaping and maintaining a precise multicellular architecture of the plexus state, and stimulating endocrine differentiation [72,80,211]. While the mechanisms that directly or indirectly link these multiple processes together remain to be defined, it appears they are all guided by, or responding to, the *Neurog3*-dependent process of endocrine cell birth. Thus, *Neurog3* represents an executive feedback-determinant that instructs multiple developmental processes within the plexus.

Within the plexus, we proved evidence that a feedback-control circuit comprised of ROCK/nmMyoII, Notch, and *Neurog3* gene dosage integrates differentiation, growth, and epithelial morphogenesis. This circuit functions to regulate the timely progression of cells from the plexus into a delaminating endocrine-committed state, and directs an appropriate growth, gene expression patterning, and morphogenesis in the plexus progenitor pool. We suspect that the process of cell delamination itself may represent a major contributor to the feedback effects than *Neurog3* expressing cells exert on the epithelial environment. Conceivably, cell delamination could influence the developmental properties of the plexus through the transmission of mechanical cues [223-231,242-244], through the regulation of density dependent growth [232-234], the cell-cycle dependent regulation of transcription factor

stability [235-238], and/or through the sub-cellular trafficking of signaling molecules such as Notch ligands/receptors [216,217], among others. Another particular point relevant to feedback-control in the plexus is our observation that a *Neurog3*-dependent and pro-endocrine 'community effect' [79] appears to promote a sustained and robust population-level flux toward the endocrine lineage. This suggests that the feedback mechanisms regulating endocrine progenitor growth, differentiation, and morphogenesis, are carefully metered to run at an optimal rate, and are capable of adaptively self organizing within the plexus to achieve and maintain a necessary level of productivity [240,241]. Understanding the minimum requirements necessary to stimulate this intrinsic property of self-organization within a multicellular context could be critical in moving forward artificial directed differentiation protocols for the study and treatment of diabetes.

Acknowledgements

We thank Dr. M Adelstein for the kind gift of the nmMyoIIC-GFP mouse strain, M. Tyska for helpful conversations, scholarship funding from the Vanderbilt Cell Imaging Shared Resource [CA68485, DK20593, DK58404, DK59637], and 1UO1DK089570-01.

CHAPTER VI

SUMMARY OF MAIN FINDINGS AND CONCLUSIONS

The plexus is an epithelial niche for pancreatic endocrine progenitors

Our mapping and kinetic analyses on endocrine-progenitor dynamics showed that endocrine cells are continually born from a transient, but long-lived, epithelial intermediate comprised by the plexus state. Our measurements indicate that the bulk of the endocrine lineage is born from the plexus, that the plexus allocates roughly one-quarter to one-third of its cell mass toward the endocrine lineage every twelve hours, and that this endocrine differentiation 'flux' is balanced by a roughly twelve-hour cell cycle in the $Sox9^{+}$ progenitors that remain behind in the growing, remodeling epithelium. Our *in utero* Notch-inhibition studies indicate that cells in the plexus are maintained in a Notch-responsive state and are, as a population, poised to activate *Neurog3* upon escape from Notch-mediated repression. As the plexus undergoes its later-stage maturation and becomes remodeled into non-plexus states – that is, ducts and ductal branches – the window for endocrine lineage allocation becomes closed. Thus, the plexus represents a highly dynamic epithelial niche wherein endocrine progenitors are assembled and maintained, and where their growth and differentiation properties are regulated, during the process of pancreas organogenesis.

Newly born endocrine cells are 'support cells' for the plexus niche

Our studies on the manifold consequences of *Neurog3* deficiency on progenitor growth, gene expression patterning, and epithelial morphogenesis in the plexus suggest that *Neurog3* is not simply an endocrine fate determinant and effector of Notch signaling. Rather, our data suggest that *Neurog3* functions broadly as a feedback determinant whose expression is tightly responsive to, but at the same time also instructive in, multiple aspects of the developmental programs that occur within the plexus. *Neurog3*-dependent processes support robust replication in the $Sox9^{+}$ epithelium, diversify gene expression (which includes non-autonomous regulation of the $Neurog3^{OFF}$, $Neurog3^{LO}$, and $Neurog3^{HI}$ states), and shapes, maintains, and propagates the plexus tissue from which duct and endocrine tissues are derived. Consequently,

when *Neurog3* is removed from the system, developmental programs of morphogenesis, differentiation and growth become mis-regulated, the diversity of cellular states within the epithelium is lost, and the plexus regresses into what appears to be a relatively inert 'ground state'. Therefore, we propose that the differentiating endocrine cell represents a type of niche 'support cell' for the plexus. We believe this is consistent with the concept that during development, transient 'support cells' regulate organ-specific progenitor states that are assembled, maintained, and regulated within interim niche environments.

Endocrine cell-fate allocation is guided by the plexus morphogenesis program

We have shown that at both tissue and cellular scales, specific states of epithelial cell morphology are associated with specific states of *Neurog3* activity. We find that the transition along the spectrum of Neurog3 OFF-LO-HI is associated with a progressive apical narrowing and focalization of the cell's apical domain, which represents the first phase in an epithelial delamination process that is specified within the plexus. Possibly our most interesting finding in this respect is that, even in the absence of Neurog3 protein, cells in the plexus that undergo this initial step in cell delamination activate *Neurog3* gene expression to high levels. This suggests a new model where endocrine cell-birth is initiated by morphogenetic transitions that are encoded intrinsically within, and possibly patterned by, the plexus morphogenesis program. We propose that an optimum efficiency rate for endocrine-cell production from the epithelium requires that tight epithelial and cell-morphological constraints be imposed and maintained within the plexus.

Cycles of endocrine-cell birth are governed by a ROCK-nmMyoII, Notch, and Neurog3 gene dosage circuit

We have used an allelic series for Neurog3 gene dosage, comprised of *Neurog3*$^{EGFP/EGFP}$ (null), Neurog3$^{EGFP/fl}$ (hypomorph), and Neurog3$^{EGFP/+}$ (heterozygous) conditions, to demonstrate the sequential requirements for ROCK-nmMyoII, Notch, and activity thresholds of Neurog3 in guiding the process of endocrine cell birth. We show that ROCK-nmMyoII, Notch, and Neurog3 represent three principal components in a regulatory circuit governing the step-wise and re-iterative progression of cells through Neurog3^{OFF}, Neurog3^{LO}, Neurog3^{HI}, and delaminated

endocrine precursor states. Importantly, we show that at every transition point along this progression (OFF-LO, LO-HI, HI-delaminated), each of these principle components requires a change in the activity of one or both of the other components. Briefly, Neurog3^{OFF-LO} and Neurog3^{LO-HI} require nmMyoII-activity and escape from Notch, but do not require Neurog3. Escape from Notch is sufficient to cause Neurog3^{LO-HI} only in the presence of Neurog3, and nmMyoII activity is largely dispensable in this context. ROCK inhibition can cause the Neurog3^{LO-HI} conversion in the presence of even low doses of Neurog3, but like Notch, cannot do so in the complete absence of Neurog3. ROCK activity is required again at the *Neurog3*$^{HI-delaminated}$ transition to regulate retraction and detachment of the cell's rear from the apical surface, which similarly requires Neurog3. Finally, we provide evidence that successful completion of rear-surface retraction is important for disengaging Notch-mediated repression from the Neurog3^{HI} state. Thus, ROCK-nmMyoII, Notch, and Neurog3 threshold-based functions are mechanistically coupled to, first, guide the cell-autonomous process of endocrine cell birth and, second, to mediate the deployment of *Neurog3*-dependent feedback influences that regulate both the form and function of the plexus niche.

Adaptive self-organization of organ growth, morphogenesis, and differentiation in the plexus

According to Jamie A. Davies' Mechanisms of Morphogenesis [240]:

"The addition of feedback to a self-assembling system gives it a property far more powerful than mere self-assembly. This property is referred to as 'adaptive self-organization'. Systems that show adaptive self-organization can arrange their structures in ways not simply dictated by the properties of the structures' subunits, but also according to the unpredictable environment in which they find themselves [240]."

Our investigations suggest that differentiation, morphogenesis, and progenitor growth processes are coupled through feedback-control mechanisms to regulate the self-assembly of the duct and endocrine pancreas. Our analyses on *Neurog3* gene activation and expression upregulation (OFF-LO-HI) as a function of normal (E13-E18.5; *Neurog3*$^{EGFP/+}$), abnormal (E13.5-E15.5; *Neurog3* $^{EGFP/flox\ \&\ EGFP/EGFP}$), or "corrective" plexus remodeling (E16.5-E18.5; *Neurog3* $^{EGFP/flox\ \&\ EGFP/EGFP}$), indicate that there are cross-regulatory interactions administered between

the plexus morphogenesis program and the endocrine differentiation program, that are designed to both achieve and maintain a physiologically optimized 'run rate' for the developmental processes that result in the proper allocation of duct and endocrine tissues. While the molecular and cell-biological details of these feedback mechanisms remain to be investigated (discussed below), we propose that the tight integration between plexus form and plexus function reflect a genetically encoded, robust, and adaptive organ 'self-assembly' program that is deployed within the confines of a highly organized niche. In this manner, the developmental program of the pancreas ensures that enough cells, and of the right types, are distributed at the correct place and time as duct and endocrine tissues are generated.

CHAPTER VII

FUTURE DIRECTIONS

A working model for duct/endocrine pancreas formation

In studying the regulation of the expansion of the endocrine-progenitor population, its differentiation, and morphogenesis during the secondary transition, we have arrived at a new working model for how pancreatic duct and endocrine tissues are formed from a plexus niche during pancreas organogenesis. In the absence of *Neurog3*-dependent feedback, essentially the whole plexus assumes an abnormal 'ground state' where essentially all progenitors exhibit sub-commitment levels of transcriptional activity at the *Neurog3* promoter (*Neurog3*^{LO}). Alterations to the morphology of cells within this 'ground state' result in changes in *Neurog3* transcriptional activity. Cells which are instructed to initiate basally directed delamination will activate *Neurog3* to high levels, whereas cells that undergo flattening and apical expansion will turn off *Neurog3* and adopt a duct cell fate. In the *Neurog3*-deficient plexus, upregulation of *Neurog3* only occurs during late-gestation when the plexus has moved well into a phase of autonomous 'corrective remodeling' to form a more 'normal' epithelial architecture. While Neurog3 protein is not required for cells to initiate the first part of the delamination program and to upregulate *Neurog3* in this context, later steps in leading-edge protrusive/exploratory behavior, rear retraction, and epithelial exit require Neurog3. Neurog3 functions cell-autonomously to drive the process of endocrine cell birth from the plexus, and non-cell-autonomously to regulate tissue morphogenesis, progenitor growth, and gene expression patterning within the plexus. The collective functions for *Neurog3* ensure that a 'normal' plexus state is assembled, maintained and propagated over time, and as the organ grows substantially in size, to ensure a processive allocation of endocrine cells for the duration of the secondary transition.

On the fundamental unit(s) of endocrine cell birth

In his book *Self-Organization in Biological Systems* [241], Scott Camazine writes: "In biological systems self-organization is a process in which global patterns in a system emerge solely from

numerous interactions among the lower-level components of the system. The rules specifying interactions among the system's components are executed using only local information, without reference to the global pattern."

The concept of self-organization (in terms of what one defines as 'global patterns,' 'lower-level components of a system,' and 'local information') is directly relevant to how we will need to approach future investigations into the cell-biological regulatory mechanisms and networks of regulatory mechanisms that function within the plexus niche. A central tenet of our "Niche Framework" model was that the developmental programs guiding organ formation must be coupled by feedback mechanisms that are deployed within *organized "units" of cells*. In an ideal case, each organized "unit" of cells would comprise a "fundamental unit" of endocrine-cell birth. Our data suggest that, by a relatively loose definition, the plexus as a whole can be considered a 'fundamental unit' of endocrine-cell birth. This definition, however, does not account for the possibility that there may be 'sub-units' of cells tiled within the plexus that themselves can function independently as niche-environments for endocrine progenitors. Below, I propose several lines of investigation that could shed light on what are the basic, minimum requirements for a functional "fundamental unit" that can drive cycles of endocrine-cell birth. First, I discuss how we might come to understand what collections of factors lead to specification of a single *Neurog3*^{HI} state in the plexus when Neurog3 is absent (endocrine-cell birth initiation). Second, I focus on how we might move towards a better definition of the nature and scale of the intra-epithelial feedback that individual endocrine-cell birth events exert on the surrounding microenvironment. Last, I discuss how it might be incorrect to conceive of a 'fundamental unit' of endocrine-cell birth as a stable (or perhaps metastable), long lived, and independently functioning group of cells that is patterned in neat units throughout the epithelium. Rather, we propose that the 'fundamental unit' of endocrine-cell birth might be best represented as an interconnected multi-cellular field of somewhat interdependent subunits. In this case, morphogenesis, growth, and differentiation signals are relayed and sensed between subunits by a precisely geared and extensive 'community effect' [79] within the tissue, which is designed to achieve and maintain an efficient and optimized rate of endocrine birth and progenitor growth.

Initiation of Neurog3^{LO-HI} in the Neurog3-deficient condition

In the absence of Neurog3 and all *Neurog3*-dependent feedback effects on the epithelium, the plexus assumes a 'ground state' (discussed above) wherein essentially all cells have become more phenotypically 'equivalent' (for instance, all cells become *Neurog3*^{LO}). Although this 'ground state' is an abnormal condition, it represents an extremely powerful system for interrogating how pro-endocrine niche environments are built, and how they operate, within the plexus. We showed that numerous and scattered populations of cells can upregulate *Neurog3* to high levels in the absence of Neurog3 protein function, but that this process appears to require the initially morphologically abnormal 'ground state' to undergo 'corrective remodeling', and a process of apical-narrowing and basally-directed epithelial displacement. Thus, in both a local and global sense, there appear to be precise morphological constraints imposed within the plexus that are important for moving cells from *Neurog3*^{LO} through to *Neurog3*^{HI} states. A major point of interest here centers on understanding what causes a cell within the 'ground state' to decide to initiate apical-narrowing, basal displacement, and *Neurog3*^{HI}. We have shown that Notch inhibition is not in and of itself sufficient to drive this process in the absence of Neurog3 (Chapter V). We suspect, rather, that there are specific types of *Neurog3*-independent cellular re-arrangements that precede and then guide the transition to the *Neurog3*^{HI} state. One important future direction will be to understand the patterns of cell movements, especially with respect to one another, in cells upregulating *Neurog3* and their neighbors. We propose that the *Neurog3*-deficient epithelium represents a useful platform for such studies, because changes in *Neurog3* activity can be monitored as a function of both abnormal (E13.5-E15.5) and 'normal' (E16.5-E18.5) plexus morphogenesis. In these settings, one could use a membrane-localized fluorescence reporter (for instance *Sox9* driving GPI-linked mCherry) to label the membranes of epithelial cells in the *Neurog3*$^{EGFP/EGFP}$ condition, and then visualize using live imaging and 3-dimensional reconstructions the patterns of cell movement that presage a *Neurog3* upregulation event. Interestingly, the precise localization of nmMyoII along the sub-apical cell cortices of groups of cells, at least in some experimental systems, is proposed to reflect, if not precede (and thus predict), generic types of cellular re-arrangements occurring in an epithelium [111,242,243]. Our data showing that the nmMyoIIC isoform is

relatively selectively expressed in the epithelium suggests that live imaging of nmMyoIIC-GFP pancreatic epithelium, in combination with reporter alleles for *Neurog3*, could be a productive avenue to observe the patterns of group-cell morphogenesis that underlie the generation of a Neurog3^{HI} cell. Lastly, a more detailed mapping of precisely where within the plexus *Neurog3* becomes activated could be informative. For instance, destabilized short half-life reporters for *Neurog3* could enable a better resolution on whether *Neurog3* activation occurs preferentially close to or far from the epithelial 'nodes' of the plexus (where multiple segments of epithelium intersect), within 'inter-node' segments of epithelium, and at specific distances away from other cells activating *Neurog3*. By these methods, we might gain important insights, especially when coupled with functional interventions, on how candidate 'units' of cells in the epithelium coordinate patterns of local cell re-arrangements to mediate endocrine commitment.

One very important remaining question is what cue(s) actually cause(s) *Neurog3* to become upregulated? We have shown that a morphogenetic process of delamination initiation, and basal-ward displacement of the cell body, mediates movement into the *Neurog3*^{HI} condition (this occurs upstream of Neurog3 protein function). However, we still do not know the identity of the extrinsic signaling factor(s) that stimulate the *Neurog3* promoter. We also do not know whether the process of delamination initiation is regulated upstream by epithelium-extrinsic factors, whether it is controlled <u>*solely*</u> by such processes, or whether the morphogenetic events that lead to *Neurog3*^{HI} are mechanistically coupled to the factors that instruct the cell to turn on *Neurog3*. We discuss these topics in more detail below, in sections entitled "*The plexus as an asymmetric niche"* and *"Identifying biochemical regulators of endocrine differentiation".* In sum, a major point of investigation on the 'fundamental unit' of endocrine cell birth will be to try and understand the minimum cellular components and signaling processes required to drive initiation of *Neurog3*^{HI} within the plexus.

Local feedback from the delaminating Neurog3^{HI} state

Another angle from which to study a proposed 'fundamental unit' of endocrine-cell birth will be to try and understand the nature and scale of the local feedback effects individual Neurog3^{+} cells exert on their surrounding epithelial neighbors, the detailed molecular mechanisms of

such feedback, and how temporal control is achieved with respect to those cells that must wait their turn to differentiate. We have shown that the absence of delaminating endocrine cells, and in some cases simple reductions in their numbers (as is the case for the *Neurog3* hypomorphs), causes alterations in gene expression, replication, and cell and tissue morphology. Future investigations could focus on understanding how individual delaminating endocrine cells influence gene expression, replication behaviors, and morphogenesis in neighboring cells, or even in cells at a distance. We designed the Neurog3^{OE} model (Chapter II) specifically for getting at questions such as these. As discussed previously, especially when done in a *Neurog3*-deficient genetic condition, the *Neurog3*^{OE} model (or similar models) should enable clonal-type analyses on how a single delaminating endocrine cell influences its surrounding environment during the process of endocrine cell birth. One could use this system (*Neurog3*^{OE} in the *Neurog3*-deficient 'ground-state' plexus) to document, for instance, whether single delaminating endocrine cells cause Hes1 protein to become expressed in surrounding cells, and if so, how many. Does Hes1 become activated in non-neighboring cells? One could use similar approaches to ask: How do Neurog3^{+} cells alter the morphology of surrounding cells as they undergo, and then complete, delamination? Do Neurog3^{+} cells influence the cycling properties of surrounding cells? It should be possible to understand when and how, and how robustly, Neurog3^{+} cells influence programs of morphogenesis, differentiation and progenitor growth in the epithelium.

We suspect that biomechanical influences (discussed below) will represent a major mediator of feedback influences emanating from Neurog3^{+} cells –an attractive subject for a number of reasons. For instance, the effective communication of Notch signals between cells is proposed to involve endocytosis-driven tension-dependent cleavage of Notch ligands as a critical step in Notch signal transduction to the cell nucleus [244]. Thus, as a cell begins to delaminate from the epithelium, it could 'pull' on neighboring cells in a manner that generates tension, which could be linked to Notch signal processing and lateral inhibition to repress *Neurog3*. In addition, our data show that *Neurog3*-dependent processes also stimulate Neurog3$^{LO\text{-}HI}$ transitions in the plexus. Does this non-autonomous stimulatory effect modulation or direct instruction by biomechanical mechanisms (discussed in more detail later)? It will be important to use models

such as *Neurog3*^{OE} to study and gain control over this previously undocumented stimulatory effect, and to bring in interventions targeting the activity of biomechanical mediators such as nmMyoII, or tension-sensitive signaling pathways such as Hippo, to study the mechanistic basis of *Neurog3*-dependent feedback [223-228,230,231].

Adaptive self-assembly and 'community effect' in the niche

An appealing way to think about a 'fundamental unit' of endocrine-cell birth is to ask, what are the minimum molecular and cellular requirements necessary to generate a system that can: 1) feed-forward to drive endocrine cell birth; 2) feed-back to ensure progenitors are maintained; 3) establish an optimum balance, over significant lengths of time, between differentiation and maintenance. As previously discussed, a very important finding from our studies is that Neurog3^{+} cells do not function simply to repress *Neurog3* activation in surrounding progenitors via Notch, but that they also have functions in stimulating continued endocrine differentiation from the epithelium. Thus, while *Neurog3*-dependent Notch-mediated lateral inhibition is a simple model that explains how endocrine differentiation might be balanced with progenitor growth in local 'units' of neighboring cells, this model does not explain the stimulatory effects of *Neurog3*. A different way of looking at this issue is to propose that the 'fundamental unit' of endocrine-cell birth might actually comprise a much larger 'fundamental network' of interconnected cells (or cell groups), rather than a collection of spatially distributed clusters of independently operating cells similar to that seen, for instance, in the developing notum of *Drosophila* [217]. Our data argue that a major role for Neurog3 protein is to generate a 'community effect' within the epithelium. This community effect appears to be comprised of very carefully metered feedback and feed-forward interactions, which determine a physiologically optimized rate at which endocrine cells are differentiated, and progenitor cells are replicated. It is unclear at this time how large or small of a population of cells is needed to generate and maintain this community effect, but it is interesting to imagine how a critical mass of committing endocrine cells (although one should remember that this could even work with a relatively small number) within the epithelium could set in motion, and progressively amplify, a much more robust endocrine differentiation program. It will be important in the future to

understand the nature, scale, and mechanistic underpinnings of this proposed community effect, as a basis to define 'fundamental unit(s)' of endocrine-cell birth.

Cellular components in the plexus that regulate endocrine lineage differentiation

While we have presented coherent arguments that the plexus represents a niche for endocrine progenitors, and that *Neurog3*-expressing cells represent support cells for the niche, there are still many unknowns regarding what signaling factors regulate states of *Neurog3* activation. We note that in the *Neurog3*-deficient condition, there is a very broad expression of low level *Neurog3*, but a focalized distribution of a subset of these cells that activate *Neurog3* to high levels. This suggests that the signals activating low levels of *Neurog3* are distributed broadly throughout the plexus, but that the signals activating *Neurog3* to high levels appear to be either administered or interpreted in a more scattered and dispersed pattern. It will be important to determine the degree to which these observations on a mutant, perturbed condition are transferable to the normal developmental context. And to address these issues: if there are distinct extrinsic signals that regulate the Neurog3^{LO} and Neurog3^{HI} states, or whether each state is controlled by a quantized exposure to the same signal(s). As I describe next, there are several interesting avenues of investigation to be pursued in this regard.

The plexus as an asymmetric niche

A common feature of the stem-cell niche in invertebrates and mammals is one of structurally asymmetry [1]. For example, factors that maintain the stem cell in an undifferentiated state could be localized near the apical surface of the stem cell, while factors that promote differentiation could be localized more basally. By this design, any process that regulates the exposure of the stem cell to apical or basal cues (by delamination or ACD, for instance) could potentially determine the stem-cell phenotype. One interpretation of our studies on the morphogenetic control of endocrine commitment is that the plexus is a niche environment where pro-maintenance and pro-differentiation cues are localized at or near the apical and basal surfaces of the epithelium, respectively. Our data suggest that the architecture of the plexus aligns progenitors at a balance point between epithelial maintenance versus differentiation outcomes (the *Neurog3*^{LO} expression state is the default state in the plexus

when Neurog3 protein is removed). Upon *Neurog3*-upregulation and delamination initiation by apical narrowing (which occurs in a relatively scattered pattern), *Neurog3*^{HI} cells become basally displaced, suggesting that apical versus basal positioning might mediate responses to oppositely localized cues. Studies in the zebrafish retina have shown, for instance, that neurogenesis is substantially controlled by the regulation of interkinetic nuclear migration along an apical-to-basal Notch signaling gradient [245]. Moreover, with respect to apically localized maintenance cues, studies in vertebrate neuroepithelium indicate that regulation of apical domain size and polarity modulates the strength of Notch activity [218,245,246]. Similar mechanisms could influence pancreas cell-fates, because high, medium, and low levels of Notch are known to influence duct, bipotent progenitor, or endocrine cell fates [41, 80], which we have shown are each associated with large, intermediate, or reduced apical domain sizes, respectively. Lastly, ROCK has been implicated as a regulator of transitions in cell migration and cell polarity [129,146], and so its downregulation within the plexus may represent a key symmetry-breaking step in the decision to be maintained as an undifferentiated progenitor, or to acquire an endocrine fate through basally directed migration. This is consistent with our data showing that ROCK inhibition can convert low *Neurog3*-expressers into high *Neurog3*-expressers under conditions where *Neurog3* gene dosage is limiting. Ongoing investigations into how polarity molecules such a Cdc42, Rac, and RhoA function, in concert with their downstream regulators and effectors, to establish and maintain a properly apically and basally 'tuned' epithelium, will be vital in defining if asymmetric distribution of developmental cues is used within the plexus niche.

Identifying biochemical regulators of endocrine-cell birth

While our field has been very successful in identifying the function of the transcription factors that control lineage allocation, to date there is no extrinsic cue that has been identified as a direct positive regulator of endocrine commitment. Because we have found that *Neurog3* upregulation can occur in the absence of Neurog3 protein function, we propose that it should be possible to identify the biochemical signals that cause *Neurog3* upregulation to occur. One line of investigation, arguably significantly under-developed in the "pancreas developmental

biology" community, centers on identifying the signaling pathways that become activated within the cell during *Neurog3* upregulation. It will be beneficial to evaluate the phosphorylation states of molecules downstream of, for example, receptor tyrosine kinase, integrin, Wnt, and TGF-beta signaling pathways, as a basis to name and test candidate inputs that direct the initial step in endocrine birth. Such investigations could focus on proteomics-based approaches, in sorted cells or in intact tissue, to analyze the active signaling pathways in Neurog3^{LO} and Neurog3^{HI} populations in *Neurog3*$^{EGFP/+}$, *Neurog3*$^{EGFP/flox}$, and *Neurog3*$^{EGFP/EGFP}$ pancreata. Ideally, such approaches will fill in a number of gaps in our understanding of the biochemical mechanisms regulating states of *Neurog3* activation, and how they converge on the *Neurog3* promoter to regulate a seemingly very rapid process of transcriptional upregulation. We suspect that a potentially fruitful direction will be to understand the molecular composition and function of signals embedded within the basal ECM, as a potential source for pro-endocrine cues regulating both the Neurog3^{LO} and Neurog3^{HI} states.

The cell biology of delamination: a conserved process linking epithelial niche form and function?

The process of cellular delamination from an epithelium is associated with the acquisition of cell fate during numerous developmental processes distributed across many phyla [248-255]. Our studies on endocrine-cell birth from the plexus argue for two important functions for cell delamination in the pancreas. First, sequential steps in cell delamination are vital for cell-autonomously pushing progenitors into and through distinct states of *Neurog3* activation. Second, the process of cell delamination is mechanistically coupled to the deployment of feedback signals emanating from Neurog3^{+} cells. These data together suggest the cell-autonomous function for cell delamination in driving cell-fate acquisition, and its connection back to the regulation of the form and function of the epithelial niche from which these cells are derived, could represent a conserved mechanism through which organ formation is coordinated, and through which increasing complex organ systems have evolved. We propose that a major unexplored territory in pancreas development is to understand how the cellular mechanisms regulating distinct transitions in the cell delamination process are linked to the transmission of regulatory signals that guide different cell behaviors in the epithelium.

Cell delamination coupled to Notch Signaling

It will be important to understand whether and how Notch ligands and receptors are shuttled to different cellular compartments of the cell during cell delamination. In *Drosophila* sensory-organ precursors, Notch is trafficked during cytokinesis from the basal cell cortex to sub-apical endosomes [216]. In this subcellular location, Notch-receptor recycling becomes inhibited, and the cell escapes from Notch to differentiate. Studies in the *Drosophila* notum suggest that dynamic basal actin-based filopodial protrusions are important for sending transient Notch signals through membrane-bound Delta to refine bristle patterning [217]. These reports and others suggest that the regulated trafficking and sub-cellular localization of Notch/Notch ligands is important for mediating activation or inactivation of Notch pathway signaling [218,219]. In the pancreas, it remains unclear where Notch signal components localize within the plexus epithelium, or within cells that are undergoing commitment toward the endocrine lineage. As discussed previously, one interesting subcellular structure to investigate is the narrowed apical domain of differentiating endocrine cells. Our ROCK-inhibition studies argue that, in normal explants, blockade of the cell-rear retraction step in delamination appears to block entry of additional cells into the Neurog3^{HI} condition. This suggests that timely rear retraction might be connected to how Notch-inhibitory signals are turned off, so that additional rounds of endocrine specification can occur. Initial entry points into such studies could focus on whether the Notch ligands produced by *Neurog3*-expressing cells become concentrated at the narrowed apical domain of these cells. Later investigations might be geared toward understanding if Notch signals deployed during delamination contribute to the periodicity or amplitude of Neurog3 or Hes1 oscillations [262]. Such knowledge will provide a foundation on which to dissect the mechanistic connections between Notch signaling and cell delamination, but will likely require the generation of new tools such as EGFP-fusions to Notch pathway components and good antibodies that target these proteins.

Cell delamination couples tissue morphogenesis and differentiation

One interesting idea is that the *Neurog3*-dependent cell-morphological changes that occur during cell delamination (basal migration, elongation of the F-actin^{FOCAL} apical lumen contact,

and epithelial exit) result in the transmission of intraepithelial forces that can be sensed and interpreted by cells that are adjacent and even at a distance. A growing body of evidence has shown that contraction of the actomyosin cytoskeleton in relatively small numbers of cells, for instance, can transmit forces across cell-cell adhesion sites [223] to non-autonomously control large-scale tissue-morphogenetic processes [229]. Also, the control of cell-shape change, or the modulation of tensile properties in a cell's environment, has also long been known to influence cell proliferation and fate [220,221,222]. While these biological principles are becoming firmly established from work in simple systems and in culture, their participation in regulating much more complex processes such as organogenesis in mammals remains unclear. With the identification of the plexus as an endocrine-progenitor niche, and the documentation of numerous influences that delaminating endocrine cells have on the surrounding tissue environment, we propose that a movement in the direction of biomechanics and mechanotransduction could yield fundamental insights into how organ systems build themselves during development. While there are numerous challenges currently in obtaining useful tools to study biomechanical mechanisms regulating endocrine progenitors, there are a few ready entry points. The activity of YAP (Yes-associated protein) and TAZ (transcriptional co-activator with PDZ-binding motif) have been extensively linked to the transmission of mechanical signals to the nucleus [224,225,226]. YAP and TAZ are transcription factors that, in response to mechanical signals, shuttle between nuclear or cytoplasmic compartments to regulate gene expression [227,228]. YAP and TAZ associate primarily with the TEAD (TEA domain family member) transcription factors to regulate genes involved in proliferation, survival, differentiation, and organ size determination [223]. It was recently found that TEAD binding motifs represent a core component of *cis*-regulatory elements in certain pancreatic-progenitor-defining genes, where they function in early pancreas development to regulate the growth program of the MPC [230]. Moreover, these authors and others were able to show that YAP-TEAD becomes inactivated upon differentiation, and that YAP protein is lost from the nucleus in Neurog3^{+} cells [231]. Therefore, there is evidence to suggest that factors with known functions in sensing and transmitting mechanical cues are present during differentiation transitions in the pancreas. While pancreas-specific deletions of the kinases Mst1 and Mst2,

which regulate YAP activity, early in development result in reductions in pancreas size, and lineage-allocation/differentiation defects throughout the organ, new highly pertinent and more specific information will likely be gained from studying YAP and TAZ activity specifically in the plexus. Genetic interventions might be enabled through the use of *Sox9*^{CreER} or other trunk-selective CreER-driver alleles. Analysis of YAP/TAZ expression and function in the *Neurog3* null condition, as well as in a *Neurog3*-null condition where cells can be induced to ectopically express Neurog3 protein (such as described for *Neurog3*^{OE}, in Chapter III), could shed light on how *Neurog3*-dependent processes such as cell delamination drive tension-dependent changes in gene expression and activity within the niche.

Cell delamination coupled to progenitor growth

It has been demonstrated in the fly notum that live-cell delamination counterbalances epithelial growth to limit tissue overcrowding [232]. The induction of forced cell delamination or cell-extrusion in over-crowded tissues [233], are proposed mechanisms that tightly balance epithelial growth in order to ensure the well-ordered cell packing during development. This function for cell delamination in limiting tissue overcrowding is likely to impact proliferation rates in epithelia as well, and it has been successfully demonstrated that spatial constraints imposed on epithelial cells via experimental alterations in boundary conditions, stretching, and compression, have acute effects on cell proliferation [234]. Thus, consistent with the findings reported in Chapter IV, we propose that *Neurog3*-dependent cell delamination could have functions in directly or indirectly supporting robust mitotic states in the plexus. One implication is that the Neurog3^{LO} state, as a prospective replicating intermediate progenitor state, could be regulated by indirect influences from cell-delaminating cells that confer a precise duration for the cell cycle in these cells. The length of time that cells spend in the G1 phase of the cell cycle has been linked to the likelihood that a cell will be maintained in an undifferentiated state or will undergo differentiation [235,236,237,238]. Cell cycle progression in neural progenitors has been linked as well to the regulation of Neurog2 stability, which has important functions in regulating neuronal differentiation, apparently through cell-cycle regulated and level-dependent binding (or binding ON-OFF rates) to different ‘suites’ of pre- or pro-lineage-

commitment genes [239,263]. This suggests that Neurog3 may be similarly regulated by cell cycle properties during pancreas development. It is interesting to think about how Neurog3 deficiency (where there is no cell delamination) causes reduced replication rates in $Sox9^{+}$ cells, and whether this change in replication status is connected to the spatial spreading of the $Neurog3^{LO}$ state within the epithelium. Thus, future investigations into the direct and indirect roles, and Notch-dependent and independent roles, for cell delamination in mediating replication rates in the progenitor epithelium as a prospective mechanism to non-cell autonomously control the levels of *Neurog3* gene expression in neighboring cells should be pursued.

REFERENCES

[1] Li L, Xie T. 2005. Stem cell niche: structure and function. *Annu. Rev. Cell Dev. Biol.* **21,** 605–31.

[2] Xie T, Spradling AC. 2000. A niche maintaining germ line stem cells in the Drosophila ovary. *Science* **290**:328–30.

[3] Kawase E, Wong MD, Ding BC, Xie T. 2004. Gbb/Bmp signaling is essential for maintaining germline stem cells and for repressing bam transcription in the Drosophila testis. *Development* 131:1365–75.

[4] Kiger AA, Jones DL, Schulz C, Rogers MB, Fuller MT. 2001. Stem cell self-renewal specified by JAK-STAT activation in response to a support cell cue. *Science* 294:2542–45.

[5] Shivdasani AA, Ingham PW. 2003. Regulation of stem cell maintenance and transit amplifyingcell proliferation by tgf-beta signaling in Drosophila spermatogenesis. *Curr. Biol.* 13:2065–72.

[6] Tulina N, Matunis E. 2001. Control of stem cell self-renewal in Drosophila spermatogenesis by JAK-STAT signaling. *Science* 294:2546–49.

[7] Calvi LM, Adams GB, Weibrecht KW, Weber JM, Olson DP, et al. 2003. Osteoblastic cells regulate the haematopoietic stem cell niche. *Nature* 425:841–46.

[8] Zhang J, Niu C, Ye L, Huang H, He X, et al. 2003. Identification of the haematopoietic stem cell niche and control of the niche size. *Nature* 425:836–41.

[9] Fuchs E, Segre JA. 2000. Stem cells: a new lease on life. *Cell* 100:143–55.

[10] Fuchs E, Tumbar T, Guasch G. 2004. Socializing with the neighbors: stem cells and their niche. *Cell* 116:769–78.

[11] Mills JC, Gordon JI. 2001. The intestinal stem cell niche: there grows the neighborhood. *Proc. Natl. Acad. Sci. USA* 98:12334–36.

[12] Weissman IL. 2000. Stem Cells: Units of Development, Units of Regeneration, and Units of Evolution. *Cell* 1000:157-168.

[13] Pan FC, Wright C. 2011. Pancreas organogenesis: From bud to plexus to gland. *Dev. Dyn.* 240, 530–565.

[14] Zhou Q, Law AC, Rajagopal J, Anderson WJ, Gray PA, Melton DA. 2007. A Multipotent Progenitor Domain Guides Pancreatic Organogenesis. *Developmental Cell* 13:103-114.

[15] Kopp JL, Dubois C, Schaffer AE, Hao E, Shih HP, Seymour P, Ma J, Sander M. 2011. Sox9^{+} ductal cells are multipotent progenitors throughout development but do not produce new endocrine cells in the normal or injured adult pancreas. *Development* 138:653–665.

[16] Desgraz R, Herrera PL. 2009. Pancreatic Neurogenin3-expressing cells are unipotent islet precursors. *Development* 136:3567–3574.

[17] Stanger BZ, Akemi J, Melton D. 2007. Organ size is limited by the number of embryonic progenitor cells in the pancreas but not the liver. *Nature* 445:886-891.

[18] Slack JM. 1995. Developmental biology of the pancreas. *Development* 121:1569-1580.

[19] Lioubinski O, Muller M, Wegner M, Sander M. 2003. Expression of Sox transcription factors in the developing mouse pancreas. *Dev Dyn* 227:402–408.

[20] Eberhard D, Lammert E. 2009. The pancreatic b-cell in the islet and organ community. *Curr Opin Genet Dev* 19:469-475.

[21] Sherwood IR, Chen TA, Melton DA. 2009. Transcriptional Dynamics of Endodermal Organ Formation. *Developmental Dynamics* 238:29-42.

[22] Kawaguchi Y, Cooper B, Gannon M, Ray M, MacDonald RJ, Wright CV. 2002. The role of the transcriptional regulator Ptf1a in converting intestinal to pancreatic progenitors. *Nature Genetics* 32:128-134.

[23] Pan FC, Bankaitis ED, Boyer D, Xu X, Van de Casteele M, Magnuson MA, Heimberg H, Wright CV. 2013. Spatiotemporal patterns of multipotentiality in *Ptf1a*-expressing cells during pancreas organogenesis and injury-induced facultative restoration. *Development* 140:751-764.

[24] Villasenor A, Chong DC, Henkemeyer M, Cleaver O. 2010. Epithelial dynamics of pancreatic branching morphogenesis. *Development* 137:4295-4305.

[25] Kesavan G, Sand FW,Greiner TU, Johansson JK, Kobberup S, Xunwei W, Brakebusch C, Semb H. 2009. Cdc42-Mediated Tubulogenesis Controls Cell Specification. *Cell* 139:791–801.

[26] Hick AC, van Eyll JM, Sabine C, Forez C, Passante L, Kohara H, Nagasawa T, Vanderhaeghen P, Courtoy P, Rousseau G, et. al. 2009. Mechanism of primitive duct formation in the pancreas and submandibular glands: a role for SDF-1. *BMC Dev. Biol.* 9:66.

[27] Vidal VP, Chaboissier MC, Lutzkendorf S, Cotsarelis G, Mill P, Hui CC, Ortonne N, Ortonne JP, Schedl A. 2005. Sox9 is essential for outer root sheath differentiation and the formation of the hair stem cell compartment. *Curr Biol* 15:1340–1351.

[28] Cheung M, Briscoe J. 2003. Neural crest development is regulated by the transcription factor Sox9. *Development* 130:5681–5693.

[29] Blache P, van de Wetering M, Duluc I, Domon C, Berta P, Freund JN, Clevers H, Jay P. 2004. SOX9 is an intestine crypt transcription factor, is regulated by the Wnt pathway, and represses the CDX2 and MUC2 genes. *J Cell Biol* 166:37–47.

[30] Kopp JL, Dubois C, Schaffer AE, Hao E, Shih HP, Seymour P, Ma J, Sander M. 2011. $Sox9^{+}$ ductal cells are multipotent progenitors throughout development but do not produce new endocrine cells in the normal or injured adult pancreas. *Development* 138:653–665.

[31] Seymour PA, Freude KK., Tran MN, Mayes EE, Jensen J, Kist R, Scherer G, Sander M. 2007. SOX9 is required for maintenance of the pancreatic progenitor cell pool. *Proc Natl Acad Sci USA* 104:1865–1870.

[32] Shih HP, Kopp J, Sandhu M, Dubois C, Seymour P, Grapin-Botton A, Sander M. 2012. A Notch-dependent molecular circuitry initiates pancreatic endocrine and ductal cell differentiation. *Development* 139:2488-2499.

[33] Simpson P. 1997. Notch signalling in development: on equivalence groups and asymmetric developmental potential. Current Opinion in Genetics and Development 7:537-542.

[34] Serup P. 2012. Signaling pathways regulating murine pancreas development. *Seminars in Cell and Developmental Biology* 23:663-672.

[35] Lammert E, Brown J, Melton DA. 2000. Notch gene expression during pancreatic organogenesis. *Mech Dev* 94:199–203.

[36] Jensen J, Pedersen EE, Galante P, Hald J, Heller RS, Ishibashi M, Kageyama R, Guillemot F, Serup P, Madsen OD. 2000b. Control of endodermal endocrine development by Hes-1. *Nature Genetics*, 24:36–44.

[37] Apelqvist A, Li H, Sommer L, Beatus P, Anderson DJ, Honjo T, Hrabe de Angelis M, Lendahl U, Edlund H. 1999. Notch signalling controls pancreatic cell differentiation. *Nature* 400:877–881.

[38] Fujikura J, Hosoda K, Iwakura H, Tomita T, Noguchi M, Masuzaki H, Tanigaki K, Yabe D, Honjo T, Nakao K. 2006. Notch/Rbp-j signaling prevents premature endocrine and ductal cell differentiation in the pancreas. *Cell Metabolism* 3:59–65.

[39] Hald J, Hjorth JP, German MS, Madsen OD, Serup P, Jensen J. 2003. Activated Notch1 prevents differentiation of pancreatic acinar cells and attenuate endocrine development. *Developmental Biology* 260:426–437.

[40] Murtaugh LC, Stanger BZ, Kwan KM, Melton DA. 2003. Notch signaling controls multiple steps of pancreatic differentiation. *Proc Natl Acad Sci USA* 100:14920–14925.

[41] Ninov N, Borius M, Stainier DY. 2012. Different levels of Notch signaling regulate quiescence, renewal, and differentiation in pancreatic endocrine progenitors. *Development* **139**, 1557-67.

[42] Afelik S, Qu X, Hasrouni E, Bukys M, Deering T, Nieuwoudt S, Rogers W, MacDonald R, Jensen J. 2012. Notch-mediate patterning and cell fate allocation of pancreatic progenitor cells. *Development* **139**, 1744-1753.

[43] Schaffer AE, Freude K, Nelson S, Sander M. 2010. Nkx6 transcription factors and Ptf1a function as antagonistic lineage determinants in multipotent pancreatic progenitors. *Developmental Cell* **18**, 1022-1029.

[44] Masui T, Long Q, Beres TM, Magnuson MA, MacDonald RJ. 2007. Early pancreatic development requires the vertebrate Suppressor of Hairless (RBPJ) in the PTF1 bHLH complex. *Genes Dev* **21**, 2629–2643.

[45] Apelqvist A, Li H, Sommer L, Beatus P, Anderson DJ, Honjo T, Hrabe de Angelis M, Lendahl U, Edlund H. 1999. Notch signalling controls pancreatic cell differentiation. *Nature* **400**, 877–881.

[46] Kopinke D, Brailsford M, Shea JE, Leavitt R, Scaife CL, Murtaugh LC. 2011. Lineage tracing reveals the dynamic contribution of Hes1+ cells to the developing and adult pancreas. *Development* **138**, 431–441.

[47] Solar M, Cardala C, Houbracken I, Martin M, Maestro MA, De Medts N, Xu X, Grau V, Heimberg H, Bouwens L, Ferrer J. 2009. Pancreatic exocrine duct cells give rise to insulin-producing β cells during embryogenesis but not after birth. *Dev. Cell* **17,** 849–860.

[48] Huang HP, Liu M, El-Hodiri HM, Chu K, Jamrich M, Tsai MJ. 2000. Regulation of the pancreatic islet-specific gene BETA2 (neuroD) by neurogenin 3. *Mol Cell Biol* **20**, 3292–3307.

[49] Smith SB, Qu HQ, Taleb N, Kishimoto NY, Scheel DW, Lu Y, Patch AM, Grabs R, Wang J, Lynn FC, Miyatsuka T, Mitchell J, Seerke R, Desir J, Eijnden SV, Abramowicz M, Kacet N, Weill J, Renard ME, Gentile M, Hansen I, Dewar K, Hattersley AT, Wang R, Wilson ME, Johnson JD, Polychronakos C, German MS. 2010. Rfx6 directs islet formation and insulin production in mice and humans. *Nature* **463**, 775–780.

[50] Smith SB, Gasa R, Watada H, Wang J, Griffen SC, German MS. 2003. Neurogenin3 and hepatic nuclear factor 1 cooperate in activating pancreatic expression of Pax4. *J Biol Chem* **278**, 38254–38259.

[51] Watada H, Scheel DW, Leung J, German MS. 2003. Distinct gene expression programs function in progenitor and mature islet cells. *J Biol Chem* **278**, 17130–17140.

[52] Wang S, Zhang J, Zhao A, Hipkens S, Magnuson MA, Gu G. 2007. Loss of Myt1 function partially compromises endocrine islet cell differentiation and pancreatic physiological function in the mouse. *Mech Dev* **124**, 898–910.

[53] Soyer J, Flasse L, RaffelsbergerW, Beucher A, Orvain C, Peers B, Ravassard P, Vermot J, Voz ML, Mellitzer G, Gradwohl G. 2010. Rfx6 is an Ngn3-dependent winged helix transcription factor required for pancreatic islet cell development. *Development* **137**, 203–212.

[54] Mellitzer G, Bonne S, Luco RF, Van De Casteele M, Lenne-Samuel N, Collombat P, Mansouri A, Lee J, Lan M, Pipeleers D, Nielsen FC, Ferrer J, Gradwohl G, Heimberg H. 2006. IA1 is NGN3-dependent and essential for differentiation of the endocrine pancreas. *EMBO J* **25**, 1344–1352.

[55] Gradwohl G, Dierich A, LeMeur M, Guillemot F. 2000. Neurogenin3 is required for the development of the four endocrine cell lineages of the pancreas. *Proc Natl Acad Sci USA* **97**, 1607–1611.

[56] Gouzhi M, Kim Y, Katsumoto K, Johansson K, Grapin-Botton A. 2011. Neurogenin3 initiates stepwise delamination of differentiating endocrine cells during pancreas development. *Developmental Dynamics* **240**, 589-604.

[57] Johansson KA, Dursun U, Jordan N, Gu G, Beermann F, Gradwohl G, Grapin-Botton A. 2007. Temporal Control of Neurogenin3 Activity in Pancreas Progenitors Reveals Competence Windows for the Generation of Different Endocrine Cell Types. *Dev. Cell* **12,** 457–465.

[58] Lee CS, Sund NJ, Behr R, Herrera PL, Kaestner KH. 2005. Foxa2 is required for the differentiation of pancreatic alpha-cells. *Dev Biol* **278**, 484–495.

[59] Lee JC, Smith SB, Watada H, Lin J, Scheel D, Wang J, Mirmira RG., German MS. 2001. Regulation of the pancreatic pro-endocrine gene neurogenin3. *Diabetes* **50**, 928–936.

[60] Lynn FC, Smith SB, Wilson ME, Yang KY, Nekrep N, German MS. 2007. Sox9 coordinates a transcriptional network in pancreatic progenitor cells. *Proc Natl Acad Sci USA* **104**, 10500–10505.

[61] Oliver-Krasinski JM, Stoffers DA. 2008. On the origin of the beta cell. *Genes Dev* **22**, 1998–2021.

[62] Jensen J, Heller RS, Funder-Nielsen T, Pedersen EE, Lindsell C, Weinmaster G, Madsen OD, Serup P. 2000. Independent development of pancreatic alpha- and beta-cells from neurogenin3-expressing precursors: A role for the notch pathway in repression of premature differentiation. *Diabetes* **49**:163–176

[63] G. Gu, J. Dubauskaite, D. Melton. 2002. Direct evidence for the pancreatic lineage: $Ngn3^{+}$ cells are islet progenitors and are distinct from duct progenitors. *Development* **129**, 2447-57.

[64] Sander M, Sussel L, Conners J, Scheel D, Kalamaras J, Dela Cruz F, Schwitzgebel V, Hayes-Jordan A, Germa M. 2000. Homeobox gene Nkx6.1 lies downstream of Nkx2.2 in the major pathway of beta-cell formation in the pancreas. *Development* **127**:5533–5540.

[65] Rukstalis JM, Habener JF. 2007. Snail2, a mediator of epithelial-mesenchymal transitions, expressed in progenitor cells of the developing endocrine pancreas. *Gene Expr Patterns* **7**, 471–479.

[66] Morales AV, Acloque H, Ocana OH, de Frutos CA, Gold V, Nieto MA. 2007. Snail genes at the crossroads of symmetric and asymmetric processes in the developing mesoderm. *EMBO Rep* **8**, 104–109.

[67] Kim YH, Larsen HL, Rué P, Lemaire LA, Ferrer J, Grapin-Botton A. 2015. Cell cycle-dependent differentiation balances growth and endocrine differentiation in the pancreas. *PLOS Biology* **13**, 1-25.

[68] Schonhoff SE, Giel-Moloney M, Leiter AB. 2004. Neurogenin 3-expressing progenitor cells in the gastrointestinal tract differentiate into both endocrine and non-endocrine cell types. *Dev Biol* **15**, 443-454.

[69] Wang S, Yan J, Anderson D, Xu Y, Maneesh K, Zheng C, Wright C, Gu G. 2010. Neurog3 gene dosage regulates allocation of endocrine and exocrine cell fates in the developing mouse pancreas. *Developmental Biology* **339,** 26-37.

[70] Wang S, Hecksher-Sorensen J, Xu Y, Zhao A, Dor Y, Rosenberg L, Serup P, Gu G. Myt1 and Ngn3 form a feed-forward expression loop to promote endocrine islet cell differentiation. *Dev Biol* **317**, 531-540.

[71] Kesavan G, Sand FW,Greiner TU, Johansson JK, Kobberup S, Xunwei W, Brakebusch C, Semb H. 2009. Cdc42-Mediated Tubulogenesis Controls Cell Specification. *Cell* **139,** 791–801.

[72] Magenhiem J*,* Klein AM, Stanger BZ, Ashery-Padan R, Sosa-Pineda B, Gu G, Dor Y. 2011. $Ngn3^{+}$ endocrine progenitor cells control the fate and morphogenesis of pancreatic ductal epithelium. *Dev. Biol.* **359,** 26–36.

[73] Pierreux CE, Poll AV, Kemp CR, Clotman F, Maestro MA, Cordi S, Ferrer J, Leyns L, Rousseau GG, Lemaigre FP. 2006. The Transcription Factor Hepatocyte Nuclear Factor-6 Controls the Development of Pancreatic Ducts in the Mouse. *Gastroenterology* **130,** 532–541.

[74] De Vas MG, Kopp J, Heliot C, Sander M, Cereghini S, Haumaitre C. 2015. Hnf1b controls pancreas morphogenesis and the generation of $Ngn3^{+}$ endocrine progenitors. Development **142**, 871-882.

[75] Wang J, Kilic G, Aydin M, Burke Z, Oliver G, Sosa-Pineda B. 2005. Prox1 activity controls pancreas morphogenesis and participates in the production of “secondary transition” pancreatic endocrine cells. *Dev. Biol.* **286,** 182–194.

[76] Westmoreland JJ, Kilic G, Sartain C, Sirma S, Blain J, Rehg J, Harvey N, Sosa-Pineda B. 2012. Pancreas-specific deletion of Prox1 affects development and disrupts homeostasis of the exocrine pancreas. *Gastroenterology* **142**, 999-1009.

[77] Jacquemin P, Durviaux SM, Jensen J, Godfraind C, Gradwohl G, Guillemot F, Madsen OD, Carmeliet P, Dewerchin M, Collen D, Rousseau GG, Lemaigre FP. 2000. Transcription factor hepatocyte nuclear factor 6 regulates pancreatic endocrine cell differentiation and controls expression of the proendocrine gene ngn3. *Mol. Cell Biol.* **20**, 4445-4454.

[78] Villasenor A, Chong DC, Cleaver O. 2008. Biphasic Ngn3 expression in the developing pancreas. *Dev. Dyn.* **237,** 3270–3279.

[79] Gurdon JB. 1988. A community effect in animal development. *Nature* **336**, 772-774.

[80] Shih HP, Kopp J, Sandhu M, Dubois C, Seymour P, Grapin-Botton A, Sander M. 2012. A Notch-dependent molecular circuitry initiates pancreatic endocrine and ductal cell differentiation. *Development* **139**, 2488-2499.

[81] Serup P. 2012. Signaling pathways regulating murine pancreas development. *Seminars in Cell and Developmental Biology* 23, 663-672.

[82] Grapin-Botton A. 2005. Ductal Cells of the pancreas. *International Journal of Biochemistry & Cell Biology* **37**, 504-510.

[83] Miyatsuka T, Kosaka Y, Kim H, German MS. 2011. Neurogenin3 inhibits proliferation in endocrine progenitors by inducing Cdkn1a. *Proc Natl Acad Sci* **108**: 185–190.

[84] Petzold KM, Naumann H, Spagnoli FM. 2013. Rho signalling restriction by the RhoGAP Stard13 integrates growth and morphogenesis in the pancreas. *Development* **140,** 126–135.

[85] Cortijo C, Gouzi M, Tissir F, Grapin-Botton A. 2012 Planar Cell Polarity Controls Pancreatic Beta Cell Differentiation and Glucose Homeostasis. *Cell Reports* **2**, 1593-1606.

[86] Han H, Tanagaki K, Yamamoto N, Kuroda K, Yoshimoto M, Nakahata T, Ikuta K, Honjo T. 2002. Inducible gene knockout of transcription factor recombination signal binding protein-J reveals its essential role in T versus B lineage decision. *Int. Immunology* **14**, 637-645.

[87] Davidson L. 2012. Epithelial machines that shape the embryo. *Trends in Cell Biology* **22**, 82-87.

[88] Schock F, Perrimon N. 2002. Molecular Mechanisms of Epithelial Morphogenesis. Annual *Reviews in Cell Biology* **18**, 463-493.

[89] Hartstock A, Nelson JW. 2008. Adherens and Tight Junictions: Structure, Function and Connections to the Actin Cytoskeleton. *Biochim Biophys Acta* **1778**, 660-669.

[90] Gumbiner BM. 2005. Regulation of cadherin-mediated adhesion in morphogenesis. *Nat Rev Mol Cell Biol* **6**, 622-634.

[91] Yamada S, Pokutta S, Drees F, Weis WI, Nelson WJ. 2005. Deconstructing the cadherin-catenin-actin complex. *Cell* **123**, 889-901.

[92] Drees F, Pokutta S, Yamada S, Nelson WJ, Weis WI. 2005. Alpha-catenin is a molecular switch that binds E-cadherin-beta-catenin and regulates actin filament assembly. *Cell* **123**, 903-915.

[93] Perez-Moreno M, Fuchs E. 2006. Catenins: keeping cells from getting their signals crossed. *Developmental Cell* **11**, 601-612.

[94] Reynold AB, Herbert L, Cleveland JL, Berg ST, Gaut JR. 1992. p120, a novel substrate of protein tyrosine kinase receptors and of p60v, is related to cadherin-binding factors beta-catenin, plakoglobin and armadillo. *Oncogene* **7**, 2439-2445.

[95] Yanagisawa M, Anastasiadis PZ. 2006. p120 catenin is essential for mesenchymal cadherin-mediated regulation of cell motility and invasiveness. *J Cell Biol* **174**, 1087-1096.

[96] Furuse M, Fujita K, Hiiragi T, Fujimoto K, Tsukita S. 1998. Claudin-1 and -2: novel integral membrane proteins localizing at tight junctions with no sequence similarity to occluding. *J Cell Biol* **141**, 1539-1550.

[97] Hou J, Shan Q, Wang T, Gomes AS, Yan Q, Paul DL, Bleich M, Goodenough DA. Transgenic RNAi Depletion of Claudin-16 and the Renal Handling of Magnesium. *J Biol Chem* **282**, 17114–17122.

[98] Funke L, Dakoji S, Bredt DS.2005 Membrane-associated guanylate kinases regulate adhesion and plasticity at cell junctions. *Annu Rev Biochem* **74**, 219–245.

[99] Itoh M, Nagafuchi A, Moroi S, Tsukita S. 1997. Involvement of ZO-1 in cadherin-based cell adhesion through its direct binding to alpha catenin and actin filaments. *J Cell Biol* **138**, 181–192.

[100]. Muller SL, Portwich M, Schmidt A, Utepbergenov DI, Huber O, Blasig IE, Krause G. 2005 The tight junction protein occludin and the adherens junction protein alpha-catenin share a common interaction mechanism with ZO-1. *J Biol Chem* **280**, 3747–3756.

[101] Rajasekaran AK, Hojo M, Huima T, Rodriguez-Boulan E. 1996. Catenins and zonula occludens-1 form a complex during early stages in the assembly of tight junctions. *J Cell Biol* **132**, 451–463.

[102] Itoh M, Morita K, Tsukita S. 1999. Characterization of ZO-2 as a MAGUK family member associated with tight as well as adherens junctions with a binding affinity to occludin and alpha catenin. *J Biol Chem* **274**, 5981–5986.

[103] Wittchen ES, Haskins J, Stevenson BR. 2003. NZO-3 expression causes global changes to actin cytoskeleton in Madin-Darby canine kidney cells: linking a tight junction protein to Rho GTPases. *Mol Biol Cell* **14**, 1757–1768.

[104] Fanning AS, Jameson BJ, Jesaitis LA, Anderson JM. 1998. The tight junction protein ZO-1 establishes a link between the transmembrane protein occludin and the actin cytoskeleton. *J Biol Chem* **273**, 29745–29753.

[105] Mattagajasingh SN, Huang SC, Hartenstein JS, Benz EJ Jr. 2000. Characterization of the interaction between protein 4.1R and ZO-2. A possible link between the tight junction and the actin cytoskeleton. *J Biol Chem* **275**, 30573–30585.

[106] Stricker J, Falzone T, Gardel ML. 2010. Mechanics of the F-actin cytoskeleton. *Journal of Biomechanics* **43**, 9-14.

[107] Le Clainche, C., Carlier, M.-F., 2008. Regulation of actin assembly associated with protrusion and adhesion in cell migration. *Physiol. Rev.* **88**, 489–513.

[108] Naumanen, P., Lappalainen, P., Hotulainen, P., 2008. Mechanisms of actin stress fibre assembly. *J. Microsc.* **231**, 446–454.

[109] St Johnston D, Sanson B. 2011. Epithelial polarity and morphogenesis. *Current Opinion in Cell Biology* **23**, 540-546.

[110] Sawyer JM, Harrell JR, Shemer G, Sullivan-Brown J, Roh-Johnson M, Goldstein B. 2010. Apical constriction: a cell shape change that can drive morphogenesis. *Dev Biol* **341**, 5-19.

[111] Gorfinkiel N, Blanchard GB. 2011. Dynamics of actomyosin contractile activity during epithelial morphogenesis. *Current Opinion in Cell Biology* **23**, 531-539.

[112] Martin AC, Goldstein G. Apical constriction: themes and variations on a cellular mechanism driving morphogenesis. *Development* **141**, 1987-1998.

[113] Baker PC, Schroeder TE. 1967. Cytoplasmic filaments and morphogenetic movement in the amphibian neural tube. *Dev. Biol.* **15**, 432-450.

[114] Burnside B. 1973. Microtubules and microfilaments in amphibian neurulation. *Amer. Zool.* **13**, 989-1006.

[115] Chung MI, Nascone-Yoder NM, Grover SA, Drysdale T A, Wallingford JB. 2010. Direct activation of Shroom3 transcription by Pitx proteins drives epithelial morphogenesis in the developing gut. *Development* **137**, 1339-1349.

[116] Ernst S, Liu K, Agarwala S, Moratscheck N, Avci ME, Dalle Nogare D, Chitnis AB, Ronneberger O, Lecaudey V. 2012. Shroom3 is required downstream of FGF signalling to mediate proneuromast assembly in zebrafish. *Development* **139**, 4571-4581

[117] Plageman T F, Jr Chauhan BK, Yang C, Jaudon F, Shang X, Zheng Y, Lou M, Debant A, Hildebrand JD, Lang R A. 2011. A Trio-RhoA-Shroom3 pathway is required for apical constriction and epithelial invagination. *Development* **138**, 5177-5188.

[118] Hildebrand JD. 2005. Shroom regulates epithelial cell shape via the apical positioning of an actomyosin network. *J. Cell. Sci*. **118**, 5191-5203.

[119] Hildebrand JD, Soriano P. 1999. Shroom, a PDZ domain-containing actin binding protein, is required for neural tube morphogenesis in mice. *Cell* **99**,485-497.

[120] Nishimura T, Takeichi M. 2008. Shroom3-mediated recruitment of Rho kinases to the apical cell junctions regulates epithelial and neuroepithelial planar remodeling. *Development* **135**, 1493-1502.

[121] Anstrom JA. 1992. Microfilaments, cell shape changes, and the formation of primary mesenchyme in sea urchin embryos. *J. Exp. Zool*. **264**, 312-322.

[122] Nance J, Priess JR. 2002. Cell polarity and gastrulation in C. elegans. *Development* **129**, 387-397.

[123] Harrell JR, Goldstein B. 2011. Internalization of multiple cells during C. elegans gastrulation depends on common cytoskeletal mechanisms but different cell polarity and cell fate regulators. *Dev. Biol*. **350**, 1-12.

[124] Williams M, Burdsal C, Periasamy A, Lewandoski M, Sutherland A. 2012. Mouse primitive streak forms in situ by initiation of epithelial to mesenchymal transition without migration of a cell population. *Dev. Dyn*. **241**, 270-283.

[125] Toyama Y, Peralta XG,Wells AR, Kiehart DP, Edwards GS. 2008. Apoptotic force and tissue dynamics during Drosophila embryogenesis. *Science* **321**, 1683-1686.

[126] Slattum G, McGee KM, Rosenblatt J. 2009. P115 RhoGEF and microtubules decide the direction apoptotic cells extrude from an epithelium. *J. Cell Biol*. **186**, 693-702.

[127] Marinari, E, Mehonic A, Curran S, Gale J, Duke T, Baum B. 2012. Live-cell delamination counterbalances epithelial growth to limit tissue overcrowding. *Nature* **484**, 542-545.

[128] Jaffe AB, Hall A. 2005. Rho GTPases: biochemistry and biology. *Annu. Rev. Cell Dev. Biol*. **21**, 247-269.

[129] Amano M, Ito M, Kimura K, Fukata Y, Chihara K, Nakano T, Matsuura Y, Kiabuchi K. 1996. Phosphorylation and Activation of Myosin by Rho-associated Kinase (Rho-kinase). *Journal of Biological Chemistry* **34**, 20246-20249.

[130] Kimura K, Ito M, Amano M, Chihara K, Kukata Y, Nakafuku M, Yamamori B, Feng J, Nakano T, Okawa K, Iwamatsu A, Kiabuchi K. 1996. Regulation of myosin phosphatase by Rho and Rho-associated kinase (Rho-kinase). *Science* **12**, 245-248.

[131] Bresnick AR. 1999. Molecular mechanisms of nonmuscle myosin-II regulation. *Curr. Opin. Cell Biol*. **11**, 26-33.

[132] Dawes-Hoang RE, Parmar KM, Christiansen AE, Phelps CB, Brand AH, Wieschaus EF. 2005. Folded gastrulation, cell shape change and the control of myosin localization. *Development* **132**, 4165-4178.

[133] Homem CF, Peifer, M. 2008. Diaphanous regulates myosin and adherens junctions to control cell contractility and protrusive behavior during morphogenesis. Development 135, 1005-1018.

[134] Goode BL, Eck MJ. 2007. Mechanism and function of formins in the control of actin assembly. *Annu. Rev. Biochem*. **76**, 593-627.

[135] Heasman SJ, Ridley AJ. 2008. Mammalian Rho GTPases: new insights into their functions from *in vivo* studies. *Nature* **9**, 690-701.

[136] Watanabe N, Kato T, Fujita A, Ishizaki T, Narumiya S. 1999. Cooperation between mDia1 and ROCK in Rho-induced actin reorganization. *Nature Cell Biology* **1**, 136–143.

[137] Kosako H, Yoshida T, Matsumura F, Ishizaki T, Narumiya S, Inagaki M. 2000. Rho kinase/ROCK is involved in cytokinesis through the phosphorylation of myosin light chain and not ezrin/ radixin/moesin proteins at the cleavage furrow. *Oncogene* **19**, 6059–6064.

[138] Watanabe S, Ando Y, Yasuda S, Hosoya H, Watanabe N, Ishizaki T, Narumiya S. 2008. mDia2 Induces the Actin Scaffold for the Contractile Ring and Stabilizes Its Position during Cytokinesis in NIH 3T3 Cells. *Molecular Biology of the Cell* **19**, 2328–2338.

[139] Ridley AJ, Schwartz MA, Burridge K, Firtel RA, Ginsberg MH, Borisy G, Parsons JT, Horwitz AR. 2003. Cell migration: integrating signals from front to back. *Science* **302**, 1704– 1709.

[140] Narumiya S, Tanji M, Ishizaki T. 2009. Rho signaling, ROCK and mDia1, in transformation, metastasis and invasion. *Cancer Metastasis Reviews* **28**, 65-76.

[141] Nobes CD, Hall A. 1999. Rho GTPases control polarity, protrusion, and adhesion during cell movement. *Journal of Cell Biology* **144**, 1235–1244.

[142] Allen WE, Zicha D, Ridley AJ, Jones GE. 1998. A role for Cdc42 in macrophage chemotaxis. *Journal of Cell Biology* **141**, 1147–1157.

[143] Itoh RE, Kurokawa K, Ohba Y, Yoshizaki H, Mochizuki N, Matsuda M. 2002. Activation of rac and cdc42 video imaged by fluorescent resonance energy transfer-based single molecule probes in the membrane of living cells. *Molecular and Cellular Biology* **22**, 6582–6591.

[144] Gomes ER, Jani S, Gundersen GG. 2005. Nuclear movement regulated by Cdc42, MRCK, myosin, and actin flow establishes MTOC polarization in migrating cells. *Cell* **121**, 451–463.

[145] Cory GO, Ridley AJ. 2002. Cell motility: braking WAVEs. *Nature* **418**, 732–733.

[146] Riento K, Ridley AJ. 2003. Rocks: multifunctional kinases in cell behavior. *Nature* **4**, 446-456.

[147] Amano M, Nakayama M, Kaibuchi K. 2010. Rho-Kinase/ROCK: A key regulator of the cytoskeleton and cell polarity. *Cytoskeleton* **67**, 545-554.

[148] Worthylake RA, Burridge K. 2003. RhoA and ROCK promote migration by limiting membrane protrusions. *J Biol. Chem.* **278**, 13578-13584.

[149] Tsuji T, Ishizaki T, Okamoto M, Higashida C, Kimura K, Furuyashiki T, Arakawa Y, Birge RB, Nakamoto T, Hirai H, Narumiya S. 2002. ROCK and mDia antagonize in Rho-dependent Rac activation in Swiss 3T3 fibroblasts. *J. Cell Biol*. **157**, 819-830.

[150] Groysman M, Shoval I, Kalcheim C. 2008. A negative modulatory role for rho and rho-associated kinase signaling in delamination of neural crest cells. *Neural Development* **22**, 3-27.

[151] Totsukawa G, Wu Y, Sasaki Y, Hartshorne DJ, Yamakita Y, Yamashiro S, Matsumura F. 2004. Distinct roles of MLCK and ROCK in the regulation of membrane protrusions and focal adhesion dynamics during cell migration of fibroblasts. *J Cell Biol* **164**, 427–439.

[152] Magdalena J, Millard TH, Machesky LM. 2003. Microtubule involvement in NIH 3T3 Golgi and MTOC polarity establishment. *J Cell Sci* **116**, 743–756.

[153] Worthylake RA, Lemoine S, Watson JM, Burridge K. 2001. RhoA is required for monocyte tail retraction during transendothelial migration. *J Cell Biol* **154**, 147-160.

[154] Yoshinaga-Ohara N, Takahashi A, Uchiyama T, Sasada M. 2002. Spatiotemporal regulation of moesin phosphorylation and rear release by Rho and serine/threonine phosphatase during neutrophil migration. *Experimental Cell Research* **278**, 112–122.

[155] Salic A, Mitchison TJ. 2008. A chemical method for fast and sensitive detection of DNA synthesis in vivo. *Proc. Natl. Acad. Sci. USA* **105**, 2415-2420.

[156] Fox P, Vought V, Hanazawa MH, Lee M, Maine E, Schedl T. 2011. Cyclin E and CDK-2 regulate proliferative cell fate and cell cycle progression in the C. Elegans germline. *Development* **138**, 2223-2234.

[157] Cheraghali A, Knaus E, Wiebe L. 1994. Bioavailability and pharmacokinetic parameter for 5-ethyl-2'-deoxyuridine. Antiviral Research, **3-4**, 259-67.

[158] Schwitzgebel VM, Scheel DW, Conners JR, Kalamaras J, Lee JE, Anderson DJ, Sussel L, Johnson JD, German MS. 2000. Expression of neurogenin3 reveals an islet cell precursor population in the pancreas. *Development* **127,** 3533–3542.

[159] Srinivas S, Watanabe T, Lin CS, William CM, Tanabe Y, Jessell TM, Costantini F. 2001. Cre reporter strains produced by targeted insertion of EYFP and ECFP into the ROSA26 locus. BMC *Developmental Biology* **1**, Epub March 27.

[160] Niwa Y, Masamizu T, Liu R, Nakayama C, Deng X, Kageyama R. 2007. The initiation and propagation of Hes7 oscillation are cooperatively regulated by Fgf and Notch signaling in the somite segmentation clock. *Developmental Cell* **13**, 298-304.

[161] Shimojo H, Ohtsuka T, Kageyama R. 2008. Oscillations in Notch signaling regulate maintenance of neural progenitors. *Neuron* **58**, 52-64.

[162] Kageyama R, Niwa Y, Shimojo H, Kobayashi T, Ohtsuka T. 2010. Ultradian Oscillations in Notch Signaling Regulate Dynamic Biological Events. *Current Topics in Developmental Biology* **92**, 311-331.

[163] Kim YH, Larsen HL, Rué P, Lemaire LA, Ferrer J, Grapin-Botton A. 2015. Cell cycle-dependent differentiation balances growth and endocrine differentiation in the pancreas. *PLOS Biology* 13, 1-25.

[164] Beucher A, MartinM, Spenle C, Poulet M, Collin C, Gradwohl G. 2013. Competence of failed endocrine progenitors to give rise to acinar but not ductal cells is restricted to early pancreas development. *Developmental Biology* **361(2)**, 277-285.

[165] Miyatsuka T, Li Z, German MS. 2009. Chronology of islet differentiation revealed by temporal cell labeling. *Diabetes* **58**:1863–1868.

[166] Ahnfelt-Ronne J, Jorgensen MC, Hald J, Madsen OD, Serup P, Hecksher-Sorensen J. 2007. An improved method for three-dimensional reconstruction of protein expression patterns in intact mouse and chicken embryos and organs. *J Histochem Cytochem* **55,** 925–930.

[167] Reichert M, Rustgi AK. 2011. Pancreatic ductal cells in development, regeneration, and neoplasia. *J Clin Invest*. **121,** 4572-4578.

[168] Metzger DE, Gasperowicz M, Otto F, Cross JC, Gradwohl G, Zaret KS. 2012. The transcriptional co-repressor Grg3/Tle3 promotes pancreatic endocrine progenitor delamination and □-cell differentiation. *Development* **139**, 1447-1456.

[169] Qu X, Afelik S, Jensen JN, Bukys MA, Kobberup S, Schmerr M, Xiao F, Nyeng P, Veronica Albertoni M, et al. 2013. Notch-mediated post-translational control of Neurog3 protein stability regulates pancreatic patterning and cell fate commitment. *Dev. Biol.* **376,** 1–12.

[170] Milano J, McKay J, Dagenais C, Foster-Brown L, Pognan F, Gradient R, Jacobs R, Zacco A, Greenberg B, Ciacco P. 2004. Modulation of Notch Processing by □-secretase inhibitors causes intestinal goblet cell metaplasia and induction of genes known to specify gut secretory lineage differentiation. *Toxicological Science* **82**, 341-358.

[171] van Es J, van Gijn M, Riccio O, van den Born M, Vooijs M, Begthel H, CozijnsenM, Robine S, Winton D, Radtke F, et al. 2005. Notch/□-secretase inhibition turns proliferative cells in intestinal crypts and adenomas into goblet cells. *Nature* **435**. 959-963.

[172] Kageyama R, Ohtsuka T, Shimojo H, Imayoshi I. 2008. Dynamic Notch signaling in neural progenitors and a revised view of lateral inhibition. *Nature Neuroscience* **11**, 1247-1251.

[173] Pierfelice T, Alberi L, Gaiano N. 2011. Notch in the vertebrate nervous system: an old dog with new tricks. *Neuron* **69**, 840-855.

[174] Hogan, Brigid. 1999. Morphogenesis. *Cell* **96**, 225-233.

[175] Metzger RJ, Klein OD, Martin GR, Krasnow MA. 2008. The branching programme of mouse lung development. *Nature* **453**, 745-750.

[176] Franco CA, Jones ML, Bernabeu MO, Geudens I, Mathivet T, Rosa A, Lopes FM, Lima AP, Ragab A, Collins RT, et al. 2015. Dynamic endothelial cell rearrangements drive developmental vessel regression. *PLOS Biology* **13**, 1-19.

[177] Hart A, Papadopoulou S, Edlund H. 2003. Fgf10 Maintains Notch Activation, Stimulates Proliferation, and Blocks Differentiation of Pancreatic Epithelial Cells. *Dev. Dyn.* 185–193.

[178] Kobberup S, Schmerr M, Dang ML, Nyeng P, Jensen JN, MacDonald RJ, Jensen J. 2010. Conditional control of the differentiation competence of pancreatic endocrine and ductal cells by Fgf10. *Mech. Dev.* **127,** 220–234.

[179] Landsman L, Nijagal A, Whitchurch TJ, VanderLaan RL, Zimmer WE, MacKenzie TC, Hebrok M. 2011. Pancreatic mesenchyme regulates epithelial organogenesis throughout development. *PLoS Biol.* **9,** e1001143.

[180] Huang S and Ingber DE. 1999. The structural and mechanical complexity of cell-growth control. *Nature Cell Biology* **1**, 131-138.

[181] Afelik S, Jensen J. 2032. Notch signaling in the pancreas: patterning and cell fate specification. *WIREs Dev Biol* **2**, 531-544.

[182] Petzold KM, Naumann H, Spagnoli FM. 2013. Rho signalling restriction by the RhoGAP Stard13 integrates growth and morphogenesis in the pancreas. *Development* **140,** 126–135.

[183] Huppert SS, Jacobsen TL, Muskavitch MA. 1997. Feedback regulation is central to Delta-Notch signaling required for *Drosophila* wing vein morphogenesis. *Development* **124**, 3283-3291.

[184] Kageyama R, Ohtsuka T, Shimojo H, Imayoshi I. 2008. Dynamic Notch signaling in neural progenitor cells and a revised view of lateral inhibition. *Nature Neuroscience* **11**, 1247-1251.

[185] Cornall RA, Eisen JS. 2005. Notch in the pathway: The roles of Notch signaling in neural crest development. *Seminars in Cell & Developmental Biology* **16**, 633-672.

[186] Simpson P. 1997. Notch signaling in development: on equivalence groups and asymmetric developmental potential. *Current Opinion in Genetics and Development* **7**, 537-542.

[187] Hofmann JJ, Iruela-Arispe ML. 2007. Notch Signaling in Blood Vessels: Who is talking to whom about what? *Circulation Research* **100**, 1556-1568.

[188] S. Artavanis-Tsakonas, M. Rand, and R. Lake. 1999. Notch Signaling: cell fate control and signal integration in development. *Science* **284**, 770-776.

[189] J. Jensen, Pedersen EE, Galante P, Hald J, Heller RS, Ishibashi M, Kageyama R, Guillemot F, Serup P, Madsen OD. 2000 Control of endodermal endocrine development Hes1. *Nature Genetics* **24**, 36-44.

[190] H. Nakhai, J. Slveke, B. Klein, Mendoza-Torres L, Mazur PK, Alqul H, Radtke F, Strobl L, Zimber-Srobl U, Schmid RM. 2008. Conditional ablation of Notch signaling in pancreatic development. *Development* **135**, 2757-2765.

[191] Tanigaki Kenji, Han H, Yamamoto N, Tashiro K, Ikegawa M, Kuroda K, Suzuki A, Nakano T, Honjo T. 2002. Notch-RBPJ signaling is involved in cell fate determination of marginal zone B cells. *Nature Immunology* **3**, 443-450.

[192] Kobayashi H, Spilde TL, Li Z, Marosky JK, Bhatia AM, Hembree MJ, Prasadan K, Preuett BL, Gittes GK. 2002. Lectin as a marker for staining and purification of embryonic pancreatic epithelium. *Biochem Biophys Res Commun* **293**, 691-7.

[193] Hamaguchi Y, Yamamoto Y, Iwanari H, Maruyama S, Furukawa T, Matsunami N, Honjo T. 1992. Biochemical and Immunological Characterization of the DNA Binding Protein (RBPJx) to Mouse Jx Recombination Signal Sequence. *Journal of Biochemistry* **112**, 314-320.

[194] Liu J, Willet SG, Bankaitis ED, Xu Y, Wright CV, Gu G. 2013. Non-parallel recombination limits Cre-LoxP-based reporters as precise indicators of conditional genetic manipulation. *Genesis* **51**, 436-442.

[195] Belteki G, Haigh J, Kabacs N, Haigh K, Sison K, Costantini F, Whitsett J, Quaggin SE, Nagy A. 2005. Conditional and inducible transgene expression in mice through the combinatorial use of Cre-mediated recombination and tetracycline induction. *Nucleic Acids Research* **33**, e51.

[196] Bocker R, Estler CJ, Maywald M, Weber D. 1981. Comparison of distribution of doxycycline in mice after oral and intravenous application measured by a high-performance liquid chromatographic method. *Arzneimittelforschung* **31**, 2116-2117.

[197] Cras-Meneur C, Li L, Kopan R, Permutt MA. 2009. Presinilins, Notch dose contol the fate of pancreatic endocrine progenitors during a narrow developmental window. *Genes and Development* **23**, 2088-2101.

[198] Ejarque M, Cervantes S, Pujadas G, Tutusaus A, Sanchez L, Gasa R. 2013. Neurogenin3 cooperates with Foxa2 to autoactivate its own expression. *J Biol Chem* **288**: 11705–11717.

[199] Lasko M, Pichel JG, Gorman JR, Sauer B, Okamoto Y, Lee E, Alt FW, Westphal H. 1996. Efficient in vivo manipulation of mouse genomic sequences at the zygote state. *Proc Natl Acad Sci USA* **93**, 5860-5865.

[200] Labosky PA, Barlow DP, Hogan BL. 1994. Mouse embryonic germ (EG) cell lines: transmission through the germline and differences in the methylation imprint of insulin-like growth factor 2 receptor (Igf2r) gene compared with embryonic (ES) cell lines. *Development* **120**, 3197-3204.

[201] Chandler KJ, Chandler RL, Broeckelmann EM, Hou Y, Southard-Smith ME, Mortlock DP. 2007. Relevance of BAC transgene copy number in mice: transgene copy number variation across multiple transgenic lines and correlations with transgene integrity and expression. *Mammalian Genome* **18**, 693-708.

[202] Branda CS, Dymecki SM. 2004. Talking about a Revolution: The Impact of Site-Specific Recombinases on Genetic Analysis in Mice. *Developmental Cell* **6**. 7-28.

[203] Liu P, Jenkins NA, Copeland NG. 2003. A Highly Efficient Recombineering-Based Method for Generating Conditional Knockout Mutations. *Genome Research* **13**, 467-484.

[204] Oka C, Nakano T, Wakeham A, de la Pompa JL, Mori C, SakaiT, Okazaki S, Kawaichi M, Shiota K, Mak TW, Honjo T. 1995. Disruption of the mouse RBPJ kappa gene results in early embryonic death. *Development* **121**, 3291-3301.

[205] Kawaguchi Y, Cooper B, Gannon M, Ray M, MacDonald R Wright CV. 2002. The role of the transcriptional regulator Ptf1a in converting intestinal to pancreatic progenitors. *Nature Genetics* **32**, 128-134.

[206] Masui T, Long Q, Beres TM, Magnuson MA, MacDonald RJ. 2007. Early pancreatic development requires the vertebrate suppressor of hairless (RBPJ) in the PTF1 bHLH complex. *Genes and Development* **21**, 2629-2643.

[207] Jonsson J, Carlsson L, Edlund T, Edlund H. 1994. Insulin-promoter-factor 1 is required for pancreas development in mice. *Nature* **371**, 606-609.

[208] Offield MF, Jetton TL, Labosky PA, Ray M, Stein RW, Magnuson MA, Hogan BL, Wright CV. 1996. PDX-1 is required for pancreatic outgrowth and differentiation in the rostral duodenum. *Development* **122**, 983-995.

[209] Masui T, Swift GH, Deering T, Shen C, Coats WS, Long Q, Elasser HP, Magnuson MA, MacDonald RJ. 2010. Replacement of Rbpj with Rbpjl in the PTF1 complex controls the final maturation of pancreatic acinar cells. *Gastroenterology* **139**, 270-280.

[210] Heisenberg CP, Bellaiche Y. Forces in Tissue Morphogenesis and Patterning. 2013. *Cell* **153**, 948-962.

[211] Bankaitis ED, Bechard ME, Wright CV. 2015. Feedback control of growth, differentiation, and morphogenesis of pancreatic endocrine progenitors in an epithelial plexus niche. *Genes and Development* **29**, 2203-2216.

[212] Ebrahim S, Fujita T, Millis BA, Kozin E, Ma X, Kawamoto S, Baird MA, Davidson M, Yonemura S, Hisa Y. 2013. NMII form a Contractile Transcellular Sarcomeric Network to Regulate Apical Cell Junctions and Tissue Geometry. *Current Biology* **23**, 731-736.

[213] Straight AF, Cheung A, Limouze J, Chen I, Westwood NJ, Sellers JR, Mitchison TJ. 2003. Dissecting temporal and spatial control of cytokinesis with a myosin II inhibitor. *Science* **14**, 1743-1747.

[214] Kovacs Mihaly, Toth J, Hetensyi C, Malnasi-Csizmadia A, Sellers JR. 2004. Mechanism of Blebbistatin inhibition of Myosin II. *Journal of Biological Chemistry* **279**, 35557-35563.

[215] Uehata M, Ishizaki T, Satoh H, Ono T, Kawahara T, Morishita T, Tamakawa H, Yamagami K, Inui J, Maekawa M et al. Calcium sensitization of smooth muscle mediated by a Rho-associated kinase in hypertension. *Nature* **389**, 990-994.

[216] Couturier L, Mazouni K, Schweisguth F. 2013. Numb localizes at endosomes and controls the endosomal sorting of Notch after asymmetric division in *Drosophila. Current Biology* **23**, 588-593.

[217] Cohen M, Georgiou M, Stevenson NL, Miodownik M, Baum B. 2010. Dynamic Filopodia Transmit Intermittent Delta-Notch Signaling to Drive Pattern Refinement during Lateral Inhibition. *Developmental Cell* **19**, 78-89.

[218] Ossipova O, Sokol SY. 2010. Cell polarity, Notch signaling, and neurogenesis. *Cell Cycle* **9**, 1-2.

[219] Bultje RS, Castaneda-Castellanos DR, Jan LY, Jan YN, Kriegstein AR, Shi SH. 2009. Mammalian Par3 Regulates Progenitor Cell Asymmetric Division via Notch Signaling in the Developing Neocortex. *Neuron* **63**, 189-202.

[220] Wozniak MA, Chen CS. 2009. Mechanotransduction in development: a growing role for contractility. *Molecular Cell Biology* **10**, 34-43.

[221] Mammoto A, Ingber DE. 2009. Cytoskeletal control of growth and cell fate switching. *Current Opinion in Cell Biology* **21**, 864-870.

[222] Discher DE, Mooney DJ, Zandstra PW. 2009. Growth factors, matrices, and forces combine and control stem cells. *Science* **324**, 1673-1677.

[223] Halder G, Dupont S, Piccolo S. 2012. Transduction of mechanical and cytoskeletal cues by YAP and TAZ. *Nat Rev Mol Cell Biol*. **9**, 591-600.

[224] Wada KI, Itoga K, Okano T Yonemura S, Sasaki H. 2011. Hippo pathway regulation by cell morphology and stress fibers. *Development* **138**, 3907-3914.

[225] Sansores-Garcia L, Bossuyt W, Wada K, Yonemura S, Tao C, Sasaki H, Halder G. 2011. Modulating F-actin organization induces organ growth by effecting the Hippo pathway. *EMBO J*. **30**, 2325-2335.

[226] Fernandez BG, Gaspar P, Bras-Pereira C, Jezowska B, Rebelo SR, Janody F. 2011. Actin capping protein and the Hippo pathway regulates F-actin and tissue growth in *Drosophila*. *Development* **138**, 2337-2346.

[227] Pan D. 2010. The Hippo signaling pathway in development and cancer. *Developmental Cell* **19**, 491-505.

[228] Zhao B, Li L, Lei Qm Guan KL. 2010. The Hippo-YAP pathway in organ size control and tumorigenesis: an updated version. *Genes & Development* **24**, 862-874.

[229] Monier B, Gettings M, Gay G, Mangeat T, Schott S, Guarner A, Suzanne M. 2015. Apico-basal forces exerted by apoptotic cells drive epithelium folding. *Nature* **518**, 245-248.

[230] Cebola I, Rodriguez-Segui SA, Cho CH, Bessa J, Rovira M, Luengo M, Chhatriwala M, Berry A, Ponsa-Cobas J, Maestro MA, Jennings RE, Pasquali L, Moran I, Castro N, Hanley NA, Gomez-Skarmeta JL, Vallier L, Ferrer J. 2015. TEAD and YAP regulate the enhancer network of human embryonic pancreatic progenitors. *Nature Cell Biology* **17**, 615-626.

[231] George NM, Day CE, Boerner BP, Johnson RL, Sarvetnick NE. 2012. Hippo Signaling Regulates Pancreas Development through Inactivation of YAP. *Mol. Cell Biol.* **32**, 5116-5128.

[232] Marinari E, Mehonic A, Curran S, Gale J, Duke T, Baum B. 2012. Live-cell delamination counterbalances epithelial growth to limit tissue overcrowding. *Nature* **484**, 542-545.

[233] Eisenhoffer GT, Loftus PD, Yoshigi M, Otsuna H, Chien CB, Morcos PA, Rosenblatt J. 2012. Crowding induces live cell extrusion to maintain homeostatic cell numbers in epithelia. *Nature* **484**, 546-549.

[234] Streichan SJ, Hoerner CR, Schneidt T, Holzer D, Hufnagel L. 2014. Spatial constraints control cell proliferation in tissues. *PNAS* **111**, 5586-5591.

[235] Calegari F. 2005. Selective Lengthening of the Cell Cycle in the Neurogenic Subpopulation of Neural Progenitor Cells during Mouse Brain Development. *J Neurosci* **25**: 6533–6538.

[236] Hardwick LJ a, Ali FR, Azzarelli R, Philpott A. 2015. Cell cycle regulation of proliferation versus differentiation in the central nervous system. *Cell Tissue Res* **359**: 187–200.

[237] Hindley C, Ali F, McDowell G, Cheng K, Jones a., Guillemot F, Philpott a. 2012. Post-translational modification of Ngn2 differentially affects transcription of distinct targets to regulate the balance between progenitor maintenance and differentiation. *Development* **139**: 1718–1723.

[238] Pauklin S, Vallier L. 2013. The Cell-Cycle State of Stem Cells Determines Cell Fate Propensity. *Cell* **155**: 135–147.

[239] Ali F, Hindley C, McDowell G, Deibler R, Jones A, Kirschner M, Guillemot F, Philpott A. 2011. Cell cycle-regulated multi-site phosphorylation of Neurogenin 2 coordinates cell cycling with differentiation during neurogenesis. *Development* **138**: 4267–4277.

[240] Davies JA. *Mechanisms of Morphogenesis: Second Addition*. London: Academic Press. 2013. Print.

[241] Camazine, Deneubourg, Franks, Sneyd, Theraulaz, Bonabeau. *Self-Organization in Biological Systems*. Princeton: Princeton University Press. 2003. Print.

[242] Ebrahim S, Kachar B. 2013. Myosin transcellular networks regulate epithelial apical geometry. *Cell Cycle* **12**, 2931-2932.

[243] Munjal A, Philippe JM, Munro E, Lecuit T. 2015. A self-organized biomechanical network drives shape changes during tissue morphogenesis. *Nature* **524**, 351-368.

[244] Meloty-Kapella L, Shergill B, Kuon J, Botvinick E, Weinmaster G. 2012. Notch Ligand Endocytosis Generates Mechanical Pulling Forge Dependent on Dynamin, Epsins, and Actin. *Developmental Cell* **22**, 1299-1312.

[245] Del Bene F, Wehman AM, Link BA, Baier H. 2008. Regulation of Neurogenesis by interkinetic nuclear migration through an apical-basal notch gradient. *Cell* **134**, 1055-1065.

[246] Clark BS, Cui S, Miesfeld JB, Klezovitch O, Vasioukhin V, Link BA. 2012. Loss of Llgl in retinal neuroepithelia reveals links between apical domain size, Notch activity and neurogenesis. *Development* **139**, 1599-1610.

[247] Thiery JP, Acloque A, Huang RY, Nieto MA. 2009. Eptihelial-Mesenchymal Transitions in Development and Disease. *Cell* **139**, 871-890.

[248] Ciruna B, Rossant J. 2001. FGF signaling regulates mesoderm cell fate specification and morphogenetic movement at the primitive streak. *Cell* **1**, 37-49.

[249] Dale JK, Malapert P, Chal J, Vilhais-Neto G, Maroto M, Johnson T, Jayasinghe S, Trainor P, Herrmann B, Pourquie O. 2006. Oscillations of the snail genes in the presomitic mesoderm coordinate segmental patterning and morphogenesis in vertebrate somitogenesis. *Developmental Cell* **10**, 355-366.

[250] Eastham AM, Spencer H, Soncin F, Ritson S, Merry CL, Stern PL, Ward CM. 2007. Epithelial-mesenchymal transition events during human embryonic stem cell differentiation. *Cancer Res.* **67**, 11254–11262.

[251] del Barrio MG, Nieto MA. 2002. Overexpression of Snail family members highlights their ability to promote chick neural crest formation. *Development* **129**, 1583-1593.

[252] Heisenberg CP, Solnica Krezel L. 2008. Back and forth between cell fate specification and movement during vertebrate gastrulation. *Curr. Opin. Genet. Dev.* **18**, 311-316.

[253] Tanimizu N, Miyajima A. 2007. Molecular mechanisms of liver development and regeneration. *Int. Rev. Cytol.* **259**, 1-48.

[254] Yang J, Weinberg RA. 2008. Epithelial-mesenchymal transition: at the crossroads of development and tumor metastasis. *Developmental Cell* **14**, 818-829.

[255] Wu SY, Yang YP, McClay DR. 2008. Twist is an essential regulator of the skeletogenic gene regulatory network in the sea urchin embryo. *Dev. Biol.* **319**, 406-415.

[256] Coffinier C, Gresh L, Fiette L, Tronche F, Schutz G, Babinet C, Pontoglio M, Yaniv M, Barra J. 2002. Bile system morphogenesis defects and liver dysfunction upon targeted deletion of HNF1beta. *Development* **129**, 1829-1838.

[257] Clissold RL, Hamilton AJ, Hattersley AT, Ellard S, Bingham C. 2015. HNF1B-associated renal and extra-renal disease-an expanding clinical spectrum. *Nat. Rev. Nephrol.* **11**, 102-112.

[258] Marty-Santos L, Cleaver O. 2016. Pdx1 regulates pancreas tubulogeneis and E-cadherin expression. *Development* **143**, 101-112.

[259] Sordella R, Jiang W, Chen GC, Curto M, Settleman J. 2003. Modulation of Rho GTPase signaling regulates a switch between adipogenesis and myogenesis. *Cell.* **113**, 147-158.

[260] McBeath R, Pirone DM, Nelson CM, Chen CS. 2004. Cell shape, cytoskeletal tension, and RhoA regulate stem cell lineage commitment. *Dev. Cell.* **6**, 483-495.

[261] Kim K, Ossipova O, Sokol SY. 2015. Neural crest specification by inhibition of the ROCK/Myosin II pathway. *Stem Cells* **33**, 674-685.

[262] Shimojo H, Ohtsuka T, Kageyama R. 2008. Oscillations in Notch Signaling Regulate Maintenance of Neural Progenitors. Neuron **58**, 52-64.

[263] Vosper JM, McDowell GS, Hindley CJ, Fiore-Heriche CS, Kucerova R, Horan I, Philpott A. 2009. Ubiquitylation on canonical and non-canonical sites targets the transcription factor neurogenin for ubiquitin-mediated proteolysis. *J Biol Chem* **284**, 15458-15468.